NEW POLYOLEFIN ARCHITECTURES THROUGH THE DEVELOPMENT OF LIVING AND STEREOSELECTIVE GROUP IV PHENOXYKETIMINE AND PHENOXYAMINE OLEFIN POLYMERIZATION CATALYSTS

A Dissertation

Presented to the Faculty of the Graduate School

of Cornell University

In Partial Fulfillment of the Requirements for the Degree of

Doctor of Philosophy

by

Joseph B. Edson

August 2009

NEW POLYOLEFIN ARCHITECTURES THROUGH THE DEVELOPMENT OF LIVING AND STEREOSELECTIVE GROUP IV PHENOXYKETIMINE AND PHENOXYAMINE OLEFIN POLYMERIZATION CATALYSTS

Joseph B. Edson, Ph.D.

Cornell University 2009

Since the pioneering work by Ziegler and Natta in the 1950s on metal-catalyzed olefin polymerization, decades of research have led to the development of catalysts capable of furnishing a wide variety of polymers. Early work focused on heterogeneous catalysts, but the later development of homogeneous catalysts provided mechanistic insights that have allowed researchers to develop catalysts that provide access and control over specific polymer microstructures. The majority of commercial polyolefins has traditionally been limited to homopolymers, random copolymers, or blends thereof. In the past decade however, the development of olefin polymerization catalysts that are living have now allowed access to virtually a limitless number of new polyolefin architectures. Despite the fact that a living polymerization system is capable of producing only one polymer chain per metal center, the real advantage lies in the ability to synthesize well-defined block copolymers and identify new materials with promising properties.

Our efforts have focused on C_2-symmetric bis(phenoxyketimine) titanium dichloride complexes and C_1-symmetric phenoxyamine zirconium and hafnium dibenzyl complexes supported by an sp^3-C donor. We have shown that upon activation, these complexes can catalyze the living and isoselective polymerization of α-olefins. Using these, the synthesis of a number of new block copolymers featuring semicrystalline isotactic

polypropylene segments and amorphous poly(ethylene-*co*-propylene) segments was accomplished. The resultant block copolymers displayed elastomeric behavior and excellent mechanical properties. We have further shown that catalysts derived from the C_1-symmetric phenoxyamine zirconium and hafnium dibenzyl complexes are capable of the cyclopolymerization of 1,5-hexadiene. The resultant polymers were shown to have a previously unreported *cis*-isotactic microstructure.

BIOGRAPHICAL SKETCH

Joseph Burton Edson was born on September 21st, 1981, the last of three brothers, in Greeley, Colorado to parents James Burton and Judith Ann. He was raised in Fort Morgan, Colorado; living the "country" life until 1st grade where his family moved into the "city" bolstering a population of 10,000.

From an early age, Joe was fascinated with all areas of science. Throughout his early childhood the thought of becoming a marine biologist captured his daily imagination, mainly because he enjoyed pictures of exotic ocean life while browsing magazines at the dental office. When he finally realized that such a profession would involve deep sea diving, and his fear of being trapped underneath a pressure filled body of water with only a small air tank for survival, he turned his attention to more lab-oriented professions. Upon entering Fort Morgan High School, he began taking classes in science, math, and computer programming that quickly gathered his attention. He especially enjoyed the chemistry course his junior year, but was unable to take the Advanced Placement course the following year due to lack of interest from his fellow classmates. He was, however, able to take the Advanced Placement courses in physics and calculus that further propelled his interest in science and math.

Joe started his college career in the fall of 2000 at Colorado School of Mines in Golden. With his affection for chemistry as well as physics and math, he decided to enroll as a chemical engineering major thinking that it would be the best combination of all his interests. While it looked good on paper, he quickly learned his sophomore year that chemical engineering really didn't have a lot to do with actual chemistry. It was while taking Dr. Daniel Knauss' organic chemistry course that Joe decided that working with small molecules

would be more enjoyable than working with the Carnot cycle. After completing the organic chemistry course, Dr. Knauss was gracious enough to allow Joe to work in his laboratory beginning that summer for the next two years. It was in Dr. Knauss' lab where Joe was introduced to the world of large molecules (polymers). While he initially enjoyed small molecule organic synthesis, the ability to make a polymer product from the same chemistry that you could actually hold in your hand truly fascinated Joe.

Joe graduated from Colorado School of Mines in 2004 and moved to Ithaca, NY later that summer to start his graduate studies at Cornell University. In late 2004, he joined the research group of Professor Geoffrey W. Coates and began work on the development of group IV olefin-polymerization catalysts. Specifically, Joe was charged with the task of developing highly isoselective and living catalysts for α-olefin polymerization with the ultimate goal of using the catalysts he developed to prepare polyolefin-based block copolymers that behaved as thermoplastic elastomers. Through this work, he was introduced to the beneficial world of collaboration where Professor Edward J. Kramer at the University of California, Santa Barbara corroborated results on properties of the block copolymers Joe synthesized.

After finishing at Cornell in June of 2009, Joe will head back west to start a governmental postdoctoral position at Los Alamos National Laboratory in New Mexico under the guidance of Dr. James Boncella. He hopes that successful collaboration and research continue to follow him on his journey where he hopes to someday begin a career in research academics or industry.

Dedicated to my friends and family.

ACKNOWLEDGMENTS

Without the support and guidance of a number of people on both a professional and personal level, I would have never endured the past five years of graduate school and be where I am today. First and foremost, I must thank my advisor, Proffesor Geoff Coates, who provided unlimited resources and boundless knowledge for my development as a chemist. Geoff has provided me with a great deal of freedom in the lab to explore the field of olefin polymerization catalysts that captured my interest. While embarking on new catalyst development in a field with more than 60 years of research was initially somewhat daunting, the support and guidance of Geoff allowed me to pursue this work to ensure my success. The self-gratitude in developing new and exciting catalysts was well worth all the effort. I must also thank Professor Peter Wolczanski and Professor Jón Njarðarson for serving on my committee. Despite not taking full advantage of their expertise, they have helped my development as chemist through challenging coursework and asking insightful questions during my admission to candidacy examination. Additionally, I must thank the entire Department of Chemistry and Chemical Biology from the staff members, who keep the department running, to the rest of the entire faculty, who serve as a source for inspiration in continuing to excel and set standards for high quality research.

It is crucial that I acknowledge the generous funding support by a number of sources and collaborators throughout my graduate career. The Department of Chemistry and Chemical Biology provided funding in my early graduate career through a teaching assistantship. In my later years, the Mitsubishi Chemical Group continued my funding and also provided valuable insight into my research. Specifically I would like to thank Dr.

Fumihiko Shimizu, Dr. Akio Tanna, Mr. Hisashi Ohtaki, and Mr. Toshihiko Sugano. Through biannual meetings they have shown a great interest in my research and provided additional and fresh ideas. It is also through these meetings that I have been able to dine at some of the finer establishments in Ithaca (i.e. John Thomas Steakhouse), and for that I'm very grateful. I am especially grateful for help given by Professor Ed Kramer (University of California, Santa Barbara) for collaboration on materials testing on polymers that I synthesized during my stay at Cornell.

The people who initially inspired me to pursue a career in chemistry also deserve my sincerest thanks. The guidance of the faculty of Colorado School of Mines Chemistry Department and the individual attention I received as a student there helped in my decision to pursue graduate school. Specifically, I owe a great deal of thanks to Dr. Daniel Knauss for allowing me to join his research group in the summer following my sophomore year to the summer before I came to Cornell. Dan spent a great deal of time in the laboratory with me honing my skills as an organic chemist. He also introduced me to the world of polymers, a field that I continue to thoroughly enjoy all aspects of. Furthermore, Dan was one of those bosses that you could genuinely call a friend and every time I make a trip back to Colorado I try to go out of my way to visit him.

The people who I have worked with in the Coates group over the past five years deserve my thanks and acknowledgement for their contribution to my graduate education. Between all the past members and new ones I have learned that the Coates group is definitely not devoid of talent. Specifically I must thank Dr. Greg Domski and Dr. Jeff Rose for acting as my mentors during the early years of my graduate education. Despite being only one year

my senior in the lab, both Greg and Jeff immensely helped my development as a chemist and were always there when I had questions. Greg has always impressed me with his ability to fully grasp and understand a problem before embarking on it in the lab or presenting it to the group. His great personality, corky humor, and somewhat inappropriate comments (albeit usually pretty funny) have been truly missed this past year. Jeff has always been a role model for what success can come from a truly hard working individual. Jeff is also one of the nicest individuals I have ever met and was always willing to go out of his way to help someone. I developed a strong friendship with both Greg and Jeff and truly miss our Saturday lunches, the occasion BBQ on the weekend and great conversations. I count Greg and Jeff as some of my closest friends that I've met at Cornell and I will go out of my way to remain friends with them in the face of geographical separation.

Nick Robertson has been an ideal labmate the past couple years since moving over from the CO_2 lab. Nick and I entered into graduate school in the same year and he is refreshing in that we generally do not talk much about chemistry. He is also a genuinely nice person and someone who I have never seen upset, despite my repeated attempts at "pushing his buttons." Nick will be taking a position at Northland College where I'm sure he will have success.

The Coates group is never devoid of talented visiting scientists or postdoctoral researchers who are willing to share their knowledge with some of the younger group members. I want to sincerely thank Dr. Timothy Clark and Dr. Kevin Noonan for extremely helpful discussions on practical matters and advice in navigating the job search during a time of economic turmoil.

I have also had the pleasure of really getting to know some of the younger scientists of the Coates Group. Amelia Anderson joined the olefin

subgroup a year after me and I've enjoyed our time together both in and out of the lab. I often joke that when Greg and Jeff left that she had no other choice than to become the person I talk to most in the lab. Thus, she reluctantly took over Greg and Jeff's prior held position of Saturday lunches with me and in return I have accepted wine tasting on Thursdays with her. She is a very hard working scientist and I'm eager to see how her last year plays out. Pasquale Iacono joined the olefin subgroup and my lab in the fall of 2008. He has impressed me in his resolve to embark on the field of new catalyst development in addition to putting up with a sometimes cantankerous fifth year graduate student trying to finish up.

A number of people outside the Coates group deserve special thanks as well. Dr. Ryan Trovitch was a fellow classmate of mine and since entering graduate school he has been one of my closest friends. From day one Ryan has been there for Wolczanski homework sessions on Saturdays, various intramural athletics and Friday night bowling, the occasional trip to Turning Stone Casino, showing up on my doorstep one weekend telling me we're driving to Philadelphia to eat cheesesteaks, and lastly bestowing the nickname of "RiverJoe" on me. We should have plenty of more time to bond, as Ryan is currently a postdoctoral researcher at Los Alamos National Labs where I'll be heading in June. Mike Airola and Mahendra (Chris) Orilall were also fellow classmates of mine and generally accompanied us on these endeavors. I specifically want to thank Mike for golf outings and Chris for organizing our Cornell fantasy football league every year and always being there to discuss everything football.

Last, but certainly not least, I need to acknowledge the tremendous love and support from my family. My parents have always been supportive of the

decisions I have made and never pushed me in any one direction. My mothers decision to go back to school and pursue her nursing degree while I was still in high school engrained in me the importance of education and following your dreams, even if you get sidetracked for awhile (like having three children). My father has always been a model for hard work and he instilled upon me a work ethic that has gotten me to where I'm at today. I only hope that someday I can say that I've worked half as hard as he has. My brother Mark has, and still is, an amazing role model for me in all aspects of life. Throughout our childhood I was always in awe of his intellect, which has served him well as he is currently in an M.D.-Ph.D. program at Baylor University in Texas where he lives with his wife, Janel. My other brother, Chris, inherited a lot of traits from my father. His determination and work ethic continue to inspire me to do the best work I can. Along with his wife, Emily, they have made me a proud uncle of two nephews, Logan and Cooper. I'm especially thankful of the time I get to spend with them every time I return to Colorado. My family has remained close by during my graduate career, never claiming to actual understand any of the work I was doing, but always there to share in my accomplishment.

TABLE OF CONTENTS

LIST OF FIGURES

LIST OF SCHEMES

LIST OF TABLES

Chapter 1

Living Transition Metal Catalyzed Alkene Polymerization: Polyolefin Synthesis and New Polymer Architectures

1.1 Introduction

One of the ultimate challenges in polymer chemistry is the development of new synthetic methods for the polymerization of a wide range of monomers with well-defined stereochemistry[1] while controlling molecular weight and molecular weight distribution.[2,3] A primary goal of synthetic polymer chemistry over the last half century has been the development of chain-growth polymerization methods that enable consecutive enchainment of monomer units without termination. Known as living polymerizations,[4] these systems allow both precise molecular weight control as well as the synthesis of a wide array of polymer architectures.[5] Living polymerization methods also allow the synthesis of end-functionalized polymers in addition to the creation of virtually limitless types of new materials from a basic set of monomers.

Polyolefins are by far the largest volume class and most important commercial synthetic polymers in use today.[6] Since the initial discoveries of Ziegler[7] and Natta,[8] remarkable advances have been reported concerning the control of comonomer incorporation as well as dramatic improvements in activity. Homogeneous olefin polymerization catalysts now exist that are unparalleled in all of polymer chemistry concerning the detailed control of macromolecular stereochemistry.[9] However, olefin polymerization catalysts have traditionally been inferior to their other chain-growth counterparts in one respect. While extraordinary advances in living/controlled polymerization have been discovered using anionic,[10] cationic,[11] and radical-based polymerization,[12-15] until very recently there existed a comparative lack of living olefin polymerization systems. The main reason for this is that alkene polymerization catalysts often undergo irreversible chain transfer to metal

alkyls and β-elimination reactions that result in the initiation of new polymer chains by the catalyst (Scheme 4.1). However, systems are now available that have acceptable rates of propagation with negligible rates of termination that allow the truly living polymerization of alkenes such that block copolymer synthesis via sequential monomer addition methods are now possible.

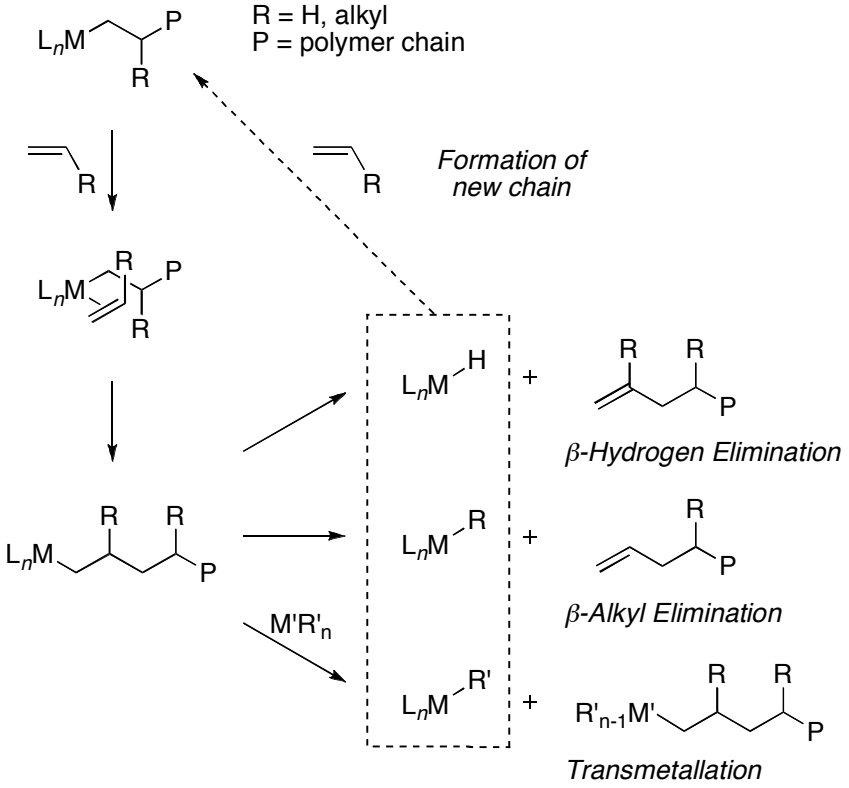

Scheme 1.1. Mechanisms of propagation and chain transfer in transition-metal catalyzed olefin polymerization.

This review is a comprehensive account of living alkene polymerization systems with special attention paid to systems developed in the past couple of years focusing on the polymer types and architectures as in our previous review.[3] This review will primarily focus on living polymerization of terminal-alkenes with some coverage of non-conjugated

dienes and cyclic olefins. The homopolymerization of the aforementioned alkenes will be initially discussed with an order of early metal to late metal catalyzed polymerizations followed by a section discussing new polymer architectures with special emphasis paid to block copolymers. Note that in this review, we refer to living species for alkene polymerization as catalysts, not initiators, to emphasize the fundamental catalytic event of monomer enchainment, not polymer chain formation. There are seven generally accepted criteria for a living polymerization: (1) polymerization proceeds to complete monomer conversion, and chain growth continues upon further monomer addition; (2) number average molecular weight (M_n) of the polymer increases linearly as a function of conversion; (3) the number of active centers remains constant for the duration of the polymerization; (4) molecular weight can be precisely controlled through stoichiometry; (5) polymers display narrow molecular weight distributions, described quantitatively by the ratio of the weight average molecular weight to the number average molecular weight ($M_w/M_n \sim 1$); (6) block copolymers can be prepared by sequential monomer addition; and (7) end-functionalized polymers can be synthesized.[16] Few polymerization systems, whether ionic, radical, or metal mediated, that are claimed to proceed by a living mechanism have been shown to meet all of these criteria. This review will therefore include all systems that claim living alkene polymerization, providing that a number of the key criteria have been met.

1.2 Living α-Olefin Polymerization

1-Hexene is the most commonly employed monomer for detailed studies of living olefin polymerization due to the fact that it is an easily

handled liquid, and molecular weight determination of its polymers are easily accomplished at or slightly above room temperature employing low boiling GPC eluents (Figure 1.1). However, due to their poor mechanical properties, poly(1-hexene) (PH) and homopolymers derived from higher a-olefins (with the exception of poly(4-methyl-1-pentene)) are of little commercial significance. One application of amorphous poly(a-olefin)s are as impact strength modifiers when blended with polypropylenes.[6]

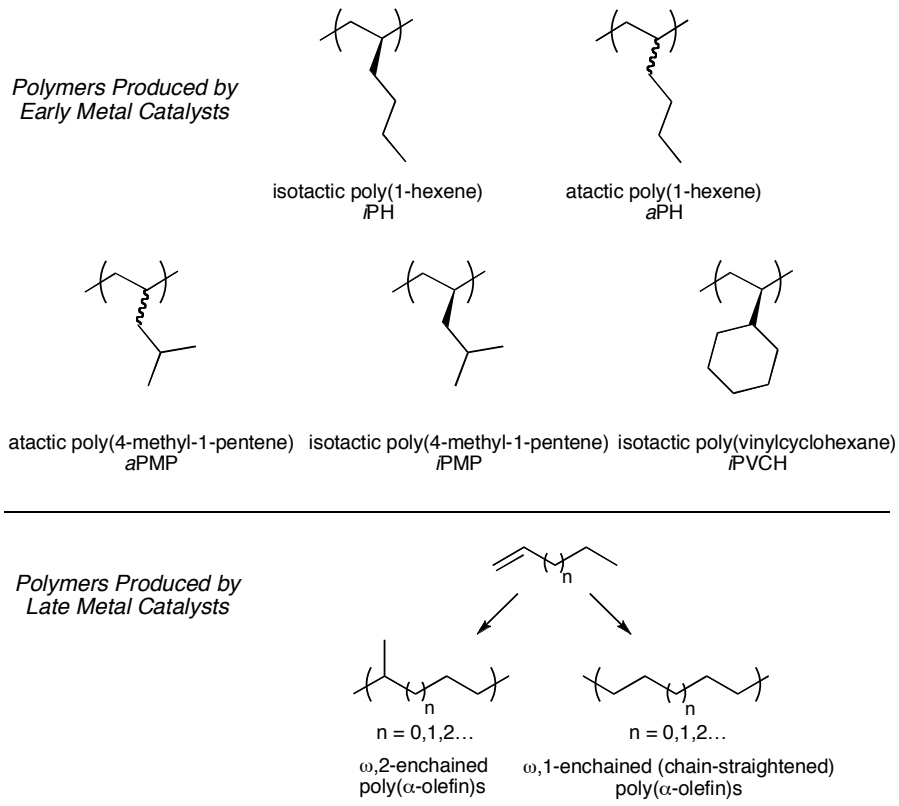

Figure 1.1 Homopolymers of higher 1-alkenes.

1.2.1 Metallocene Based Catalysts

Since the discovery of their catalytic activity, Group 4 metallocene complexes have found extensive use as olefin polymerization catalysts.[1] Due

to their high propensity toward termination via chain-transfer (e.g. β-H elimination/transfer, transfer to alkylaluminum species) there have been few examples of living olefin polymerization using metallocene-based catalysts. However, several groups have shown that by employing well-defined boron-based activators[17] at low reaction temperatures these termination pathways can be suppressed. For example, Fukui reported the living polymerization of 1-hexene with a *rac*-(Et)Ind_2ZrMe_2 (**1**, Figure 1.2) activated with $B(C_6F_5)_3$ at -78 °C in which Al(*n*Oct)$_3$ was used as a scavenging agent to furnish isotactic poly(1-hexene)s with a narrow molecular weight distributions (M_w/M_n = 1.22 – 1.29).[18] While the molecular weights were relatively low ($M_n \leq$ 5,400 g/mol), the M_n was shown to increase linearly with reaction time. Titanium complexes bearing a linked monocyclopentadienyl-amido ligand, such as **2** (Figure 1.2), have also been shown to polymerize 1-hexene in a living fashion when activated with $B(C_6F_5)_3$ in the presence of Al(*n*Oct)$_3$ at -50 °C.[19] The poly(1-hexene) formed was syndio-enriched ([*rr*] = 0.49) with M_n up to 26,000 g/mol and M_w/M_n = 1.07 – 1.12. A linear relationship between M_n and polymer yield was also demonstrated. In a subsequent report, **2**/($B(C_6F_5)_3$/Al(*n*Oct)$_3$ was also shown to polymerize 1-octene and 1-butene in a living fashion.[20]

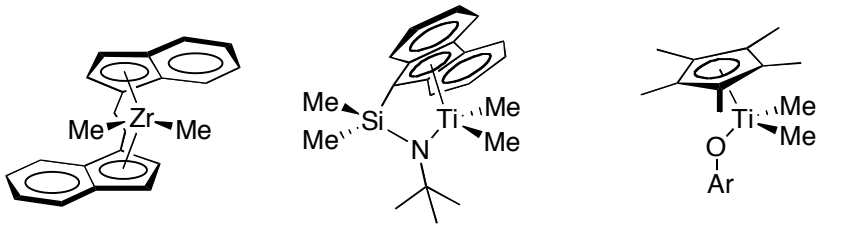

1 **2** **3** Ar = 2,6-*i*Pr$_2$C$_6$H$_3$

Figure 1.2. Metallocene and mono-cyclopentadienyl catalyst precursors for living 1-hexene polymerization.

Nomura and Fudo demonstrated that an unbridged half-metallocene complex bearing a phenoxide donor (**3**, Figure 1.2) was capable of polymerizing 1-hexene in a living fashion.[21] When activated with $[Ph_3C][B(C_6F_5)_4]$ in the presence of Al(*i*Bu)$_3$ at -30 °C, **3** furnished poly(1-hexene)s with narrow polydispersities (M_w/M_n = 1.27 – 1.64) and high molecular weight (M_n up to 1,865,000 g/mol). The M_n was shown to increase linearly with turn over number (TON).

1.2.2 Catalysts Bearing Diamido Ligands

While Group 4 metallocene-based olefin polymerization catalysts have dominated the field of homogenous olefin polymerization catalysis since the late 1950s,[1] the development of complexes bearing non-Cp ligands as potential olefin polymerization catalysts has become a rapidly expanding area over the last 15 years.[22,23] McConville and Scollard reported that titanium complexes bearing diamide ligands, compounds **4a**,**b** (Figure 1.3), polymerized 1-hexene, 1-octene, and 1-decene to high molecular weight (M_n = 121,500 – 164,200 g/mol) and narrow polydispersity index (PDI) (M_w/M_n = 1.07) upon activation with $B(C_6F_3)_3$ at room temperature.[24] Polymerization of 1-hexene by **4b**/$B(C_6F_5)_3$ exhibited a linear increase of M_n with time. Kim and co-workers later reported the living polymerization of 1-hexene catalyzed by a structurally similar zirconium diamide with an ethylene bridging unit.[25] When activated with $B(C_6F_5)_3$ at -10 °C, **5** (Figure 1.3) furnished poly(1-hexene)s with M_n = ca. 30,000 – 175,000 g/mol and M_w/M_n = 1.18 – 1.27. It was also shown that the M_n increased linearly with increasing monomer loading.

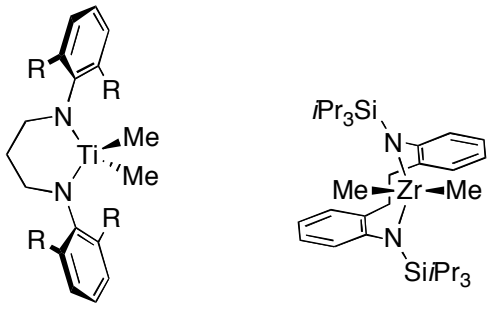

4a R = *i*Pr
4b R = Me

5

Figure 1.3. Diamido-ligated catalyst precursors for living alkene polymerization.

1.2.3 Catalysts Bearing Diamido Ligands with Neutral Donors

Schrock and co-workers reported on the olefin polymerization behavior of tridentate diamido group IV complexes bearing a central oxygen donor that was postulated to enhance stability of the corresponding cationic alkyl active species.[26,27] Upon activation with $[PhNMe_2H][B(C_6F_5)_4]$ at 0 °C the zirconium complex, **6a** (Figure 1.4), furnished atactic poly(1-hexene) (*a*PH) with M_n = ca. 4,000 – 40,000 g/mol and M_w/M_n = 1.02 – 1.14. A linear increase in M_n with increasing monomer conversion was exhibited. Upon activation with $[PhNMe_2H][B(C_6F_5)_4]$, the titanium congener (**6b**) decomposed to unidentifiable species which were not active for 1-hexene polymerization. The analogous hafnium complex (**6c**) furnished poly(1-hexene) with broadened molecular weight distribution (M_w/M_n = 1.19 – 1.53) and anomalous M_n-values when activated with $[PhNMe_2H][B(C_6F_5)_4]$.

A second class of catalysts developed by Schrock and co-workers bearing diamidopyridine ligands were shown to be effective living olefin polymerization catalysts.[28] The diamidopyridine zirconium complexes **7a,b** (Figure 1.4) when activated with $[Ph_3C][B(C_6F_5)_4]$ produce poly(1-hexene)s

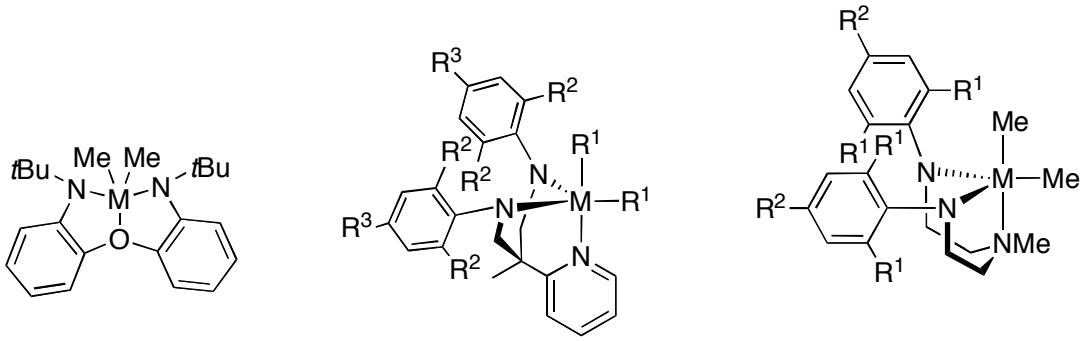

6a M = Zr
6b M = Ti
6c M = Hf

	M	R^1	R^2	R^3
7a	Zr	Me	Me	Me
7b	Zr	*i*Bu	Me	Me
8	Hf	*i*Bu	Me	Me
9	Hf	*i*Bu	Cl	H

	M	R^1	R^2
10a	Zr	Me	Me
10b	Zr	Cl	H
10c	Hf	Cl	H

Figure 1.4. Amido-donor-amido ligated catalyst precursors.

with narrow polydispersities ($M_w/M_n < 1.08$). The identity of the alkyl group bound to zirconium was shown to greatly effect the polymerization behavior. Upon activation, **7a** reacts with 1-hexene to a significant extent by 2,1-insertion into the initial Zr-Me bond to give a 3-heptyl complex that undergoes β-H elimination to yield 2-heptenes; only a fraction that undergoes 1,2-insertion gives a stable propagating species. No 2,1-insertion into the Zr-*i*Bu bond is observed upon activation of **7b** which gives rise to a relatively well-behaved polymerization system in which M_n values are three times higher than those expected based on the assumption of one polymer chain per metal center (M_n^{theo}). The diisobutyl hafnium analogue (**8**) was also shown to polymerize 1-hexene in a living fashion at 0 °C upon activation with $[Ph_3C][B(C_6F_5)_4]$ to furnish poly(1-hexene)s with $M_w/M_n = 1.02 – 1.05$ and M_n = 10,000 – 50,000 g/mol that matches M_n^{theo}.[29,30] The apparent difference in polymerization behavior is attributed to greater stability toward β-H elimination in this system. Upon replacing the mesityl groups with 2,6-$C_6H_3Cl_2$ within the ligand framework of **8**, Schrock and co-workers found that

the living character of 1-hexene polymerization catalyzed by **9**/[Ph_3C][$B(C_6F_3)_4$] was slightly diminished with evidence of β-H elimination.[31] Despite the fact that β-H elimination was observed, the resultant polymers still displayed narrow polydispersities (M_w/M_n = 1.01 – 1.05) and the M_n values were about 90 % of those expected.

A third class of compounds for olefin polymerization introduced by Schrock and co-workers was the diamidoamine complexes of zirconium and hafnium.[32-34] When activated with [Ph_3C][$B(C_6F_5)_4$], **10a** (R^1 = R^2 = Me, Figure 1.4) was shown to be active for 1-hexene polymerization furnishing poly(1-hexene)s that possessed M_w/M_n = 1.1 – 2.1 and M_n = 19,200 – 45,000 g/mol that deviated from the expected values.[32] Subsequent studies showed that **10a** undergoes deactivation via an intramolecular C-H activation of the *ortho*-Me on the mesityl group upon methide abstraction. Replacing the *ortho*-Me with *ortho*-Cl (**10b**) and subsequent activation with [$PhNMe_2H$][$B(C_6F_5)_4$] at 0 °C gives rise to a catalyst that is living for 1-hexene polymerization.[33] The resultant polymer exhibited narrow polydispersity (M_w/M_n = 1.01 – 1.04) and M_n values that were in good agreement with M_n^{theo}. When activated with [Ph_3C][$B(C_6F_5)_4$] or $B(C_6F_5)_3$ the hafnium analogue of **10b** (**10c**) exhibited significant termination via β-H elimination.[34]

1.2.4 Amine-phenolate and Amine-diol Titanium and Zirconium Catalysts

In 2000 Kol and co-workers reported on the synthesis and olefin polymerization behavior of a titanium complex bearing an amine bis(phenolate) ligand into which was incorporated an additional amino side-arm donor (**11a**, Figure 1.5).[35] When activated with $B(C_6F_5)_3$ at room temperature, **11a** furnished atactic poly(1-hexene)s with narrow molecular

distributions (M_w/M_n = 1.09 – 1.18) and the M_n was shown to increase linearly with time. When the amino side-arm donor was omitted (**12**) only low molecular weight poly(1-hexene) (M_n = ca. 2,000 g/mol) with M_w/M_n = 1.92 – 2.43 was obtained. Replacing the bulky *t*Bu groups with sterically less demanding chlorides (**11b**) allowed the living polymerization of 4-methyl-1-pentene to furnish atactic poly(4-methyl-1-pentene).[36]

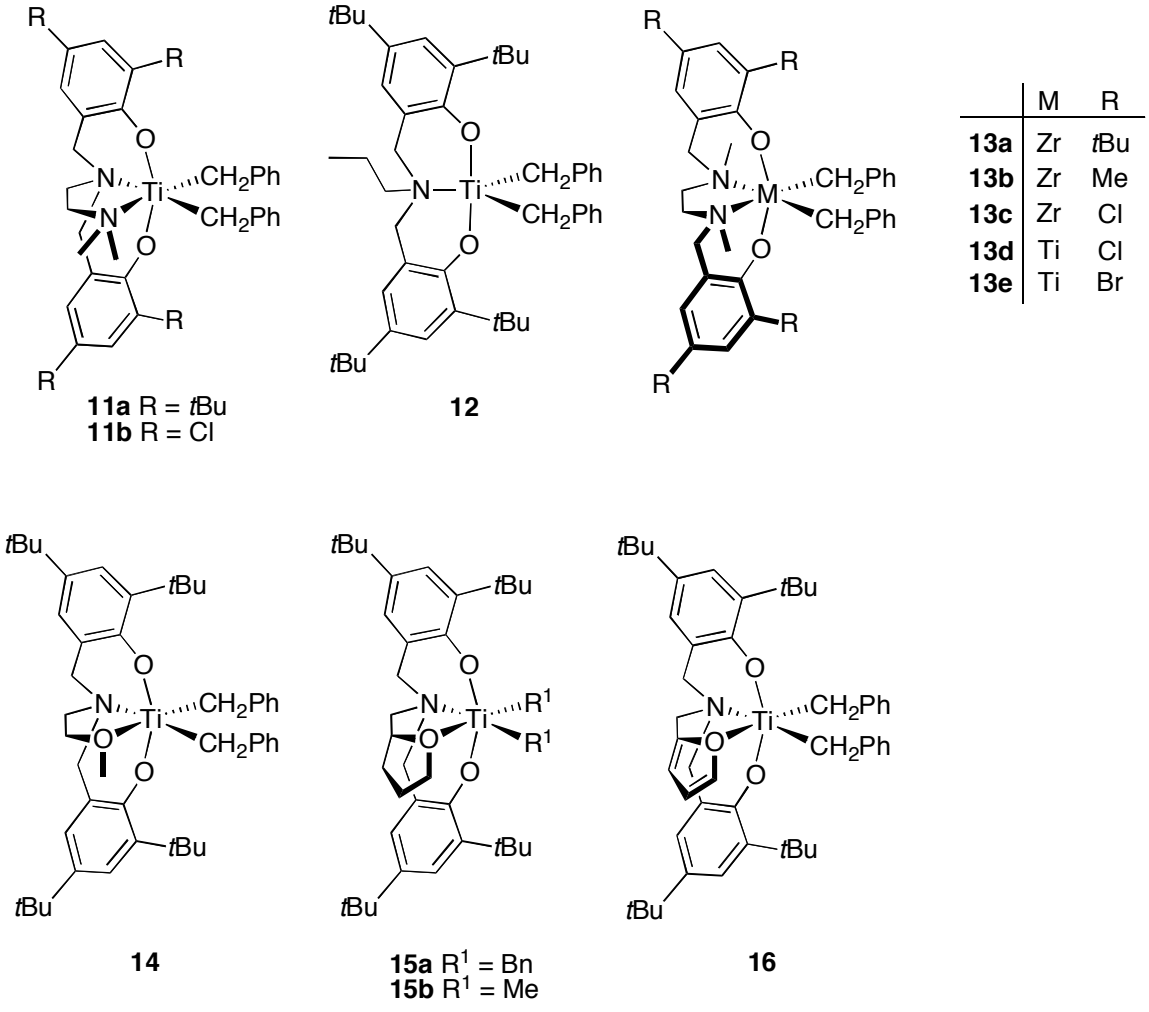

Figure 1.5. [ONNO], [ONO] and [ONOO] Complexes of titanium and zirconium.

In 2000 Kol and co-workers reported on the synthesis and polymerization behavior of the C_2-symmetric, ethylene-bridged zirconium analogue of **11a** (**13a**, Figure 1.5).[37] When activated with $B(C_6F_5)_3$ at room temperature, **13a** furnished highly isotactic poly(1-hexene) and poly(1-octene). The poly(1-hexene)s exhibited narrow polydispersities (M_w/M_n = 1.11 – 1.15) with M_n = ca. 4,000 – 12,000 g/mol; the M_n was shown to increase linearly with monomer consumption. Reducing the substituent size on the phenoxide moiety (**13b**) furnished atactic poly(1-hexene) with a broadened molecular weight distribution (M_w/M_n = 1.57). In a subsequent report it was shown that replacing the *ortho*- and *para-tert*-butyl substituents of **13a** with chlorides (**13c**) resulted in greatly diminished living behavior.[38] Importantly, the titanium congener (**13d**) and the analogous 2,4-dibromophenol-bearing complex (**13e**) polymerized 1-hexene in a living manner for a period of 40 to 75 minutes when activated with $B(C_6F_5)_3$. The poly(1-hexene)s exhibited extremely high molecular weights (M_n up to 1,750,000 g/mol, $M_w/M_n \leq 1.2$) and moderate degrees of isotacticity (**13d**: [*mm*] = 0.60, **13e**: [*mm*] = 0.80).

In 2001 Kol and co-workers introduced a third class of novel olefin polymerization catalysts featuring [ONOO] Group 4 metal complexes bearing a methoxy side-arm donor.[39] Upon activation with $B(C_6F_5)_3$ at room temperature, **14** (Figure 1.5) furnished poly(1-hexene)s with narrow polydispersities (M_w/M_n = 1.07 – 1.12) and high molecular weights (M_n up to 445,000 g/mol). A linear increase in M_n with increasing reaction time was observed for up to 31 hours. The living character of the polymerization was maintained upon heating to 65 °C for one hour as evidenced by the narrow polydispersity of the resultant polymer (M_w/M_n = 1.30). Introduction of the 2,4-dimethyl or 2,4-dichloro phenoxide moiety led to a loss of living

character.[40] The zirconium and hafnium analogues of **14** also deviated from living behavior (M_w/M_n = 1.4 – 3.0).[41]

The effect of the neutral oxygen donor's identity on the polymerization behavior of the [ONOO] titanium complexes has also been investigated. Replacing the methoxy donor of **14** with a THF-moiety (**15a**, Figure 1.5) gave similar results, however, replacing the benzyl ligands with methyl ligands (**15b**) results in a dramatic increase in the duration of the living period for up to 6 days at room temperature upon activation with $B(C_6F_5)_3$. The resultant atactic poly(1-hexene) had a M_n up to 816,000 g/mol and M_w/M_n = 1.04 – 1.12.[42] Introduction of a furan donor (**16**, Figure 1.5) into the ligand framework led to a ten-fold increase in polymerization activity relative to **15a**/$B(C_6F_5)_3$ furnishing poly(1-hexene)s of high molecular weight (M_n up to 500,000 g/mol, $M_w/M_n \leq 1.37$).[43] The increase in activity of **16**/$B(C_6F_5)_3$ resulted in diminished living character of the 1-hexene polymerization exhibiting a linear increase in M_n over the course of only two hours.

The importance of neutral donors in the ligand framework of living olefin polymerization catalysts was also demonstrated recently by Sundararajan and co-workers.[44,45] In 2002 the authors reported titanium dichloride complexes of tridentate aminodiol ligands (***rac*** and ***meso*-17**, Figure 1.6) treated with MAO furnished poly(1-hexene)s possessing relatively narrow polydispersities (M_w/M_n = 1.07 – 2.9) with a range of tacticities depending on the symmetry of the catalyst precursor.[44] Incorporation of a pendent methoxy donor into the aminodiol ligand framework gave rise to catalysts that were capable of living 1-hexene polymerization.[45] When activated with MAO at temperatures between -10 – 30 °C both **18a** and **18c** furnished poly(1-hexene)s with low polydispersities (M_w/M_n = 1.06 – 1.11)

and M_n = 73,000 – 424,000 g/mol. The highest degree of isotacticity ([*mmmm*] = 0.85) was obtained for polymer produced by **18a** at -10 °C. At -10 °C a linear dependence of M_n on reaction time was observed. The zirconium congeners of **18a** and **18c** (**18b** and **18d**, Figure 1.6) have been prepared by Sudhakar and upon activation with MAO gave similar results for 1-hexene polymerization.[46] A linear relationship between M_n and reaction time was observed at 28 °C.

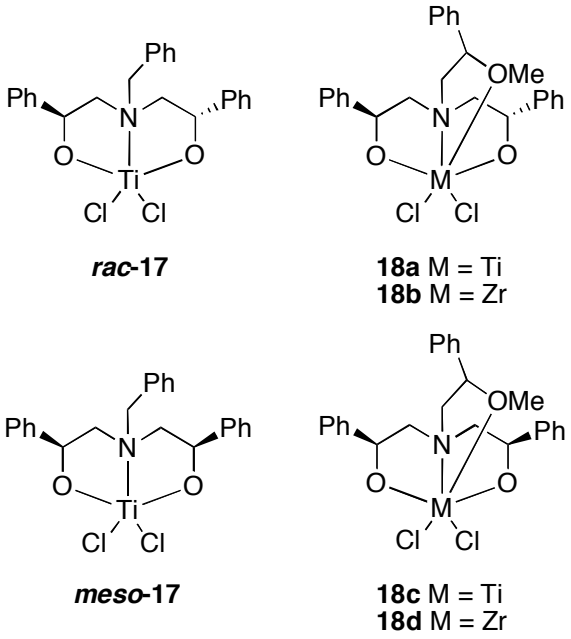

Figure 1.6. Titanium and zirconium complexes bearing aminodiol ligands.

1.2.5 Monocyclopentadienylzirconium Amidinate Catalysts

In 2000 Sita and Jayaratne reported monocyclopentadienyl acetamidinate zirconium dimethyl compounds that exhibited living polymerization behavior at temperatures between -10 and 0 °C.[47] Upon activation with $[PhNMe_2H][B(C_6F_5)_4]$ at 0 °C, **19a** (Figure 1.7) formed atactic poly(1-hexene) with a narrow polydispersity (M_w/M_n = 1.10) and lack of olefinic resonances in ^{13}C and ^{1}H NMR spectra. The C_1-symmetric complex,

19b, when activated in an identical manner at -10 °C furnished highly isotactic poly(1-hexene) ([*mmmm*] > 0.95) with a narrow molecular weight distribution (M_w/M_n = 1.03 – 1.13). The molecular weight was shown to increase linearly with conversion. This was the first report of a Ziegler-Natta polymerization catalyst that was both living and highly isospecific for a-olefin polymerization. Covalently attaching **19b** to a crosslinked PS support was also shown to furnish a living and isoselective 1-hexene polymerization catalyst (**20**, Figure 1.7).[48] The hafnium congener of **19b** (**21a**, Figure 1.7) and its diisobutyl analogue (**21b**) were also shown to be living and isospecific 1-hexene polymerization catalysts albeit with a rate ca. 60 times slower than **19b**.[49]

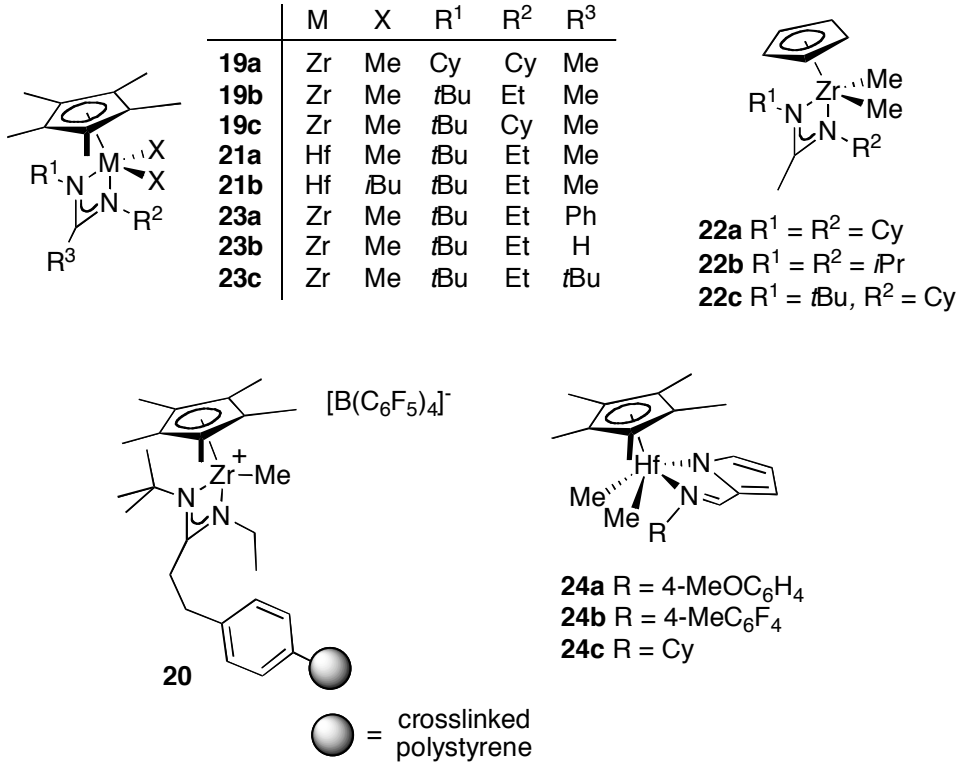

Figure 1.7. Cp-Amidinate and Cp*-Iminopyrrolyl complexes.

By replacing the Cp* moiety with the less sterically demanding Cp ligand, Sita and co-workers were able to greatly increase the 1-hexene polymerization activity for this class of catalysts.[50] When activated with $[PhNMe_2H][B(C_6F_5)_4]$ at -10 °C, compounds **22a-c** (Figure 1.7) furnished atactic poly(1-hexene)s with narrow molecular weight distributions (M_w/M_n = 1.03 – 1.10), however, a decrease in enantiofacial selectivity was also observed. The more open environment of the active site did impart the ability to polymerize the more challenging vinylcyclohexane. Upon activation with $[PhNMe_2H][B(C_6F_5)_4]$ at -10 °C, **22a,b** furnished highly isotactic poly(vinylcyclohexane)s ([*mmmm*] = 0.95) with narrow polydispersities (M_w/M_n = 1.04 – 1.10). The authors postulate that the high degree of isoselectivity displayed is likely the result of chain-end control.

The effect of further structural elaboration of the amidinate ligand framework on polymerization behavior was reported in 2004.[51] Specifically, altering the identity of the distal R^3 substituent (Figure 1.7) led to dramatic effects on both the living character and stereospecificty of 1-hexene polymerization. Polymerization of 1-hexene by **23a** or **23b** (R^3 = Ph or H)/$[PhNMe_2H][B(C_6F_5)_4]$ at -10 °C furnished polymer with a significantly lower degree of isotacticity than the poly(1-hexene) produced by **19b**/$[PhNMe_2H][B(C_6F_5)_4]$, and in the case of **23b**, the polymerization is no longer living. Furthermore, **23c** (R^3 = *t*Bu)/$[PhNMe_2H][B(C_6F_5)_4]$ was found to be completely inactive for polymerization. The loss in stereocontrol of **23a** was attributed to a "buttressing effect" by which the *t*Bu and Et groups were "pushed" forward toward the active site leading to a lack of steric discrimination at the metal center for olefin coordination. The decrease in

stereoselectivity of **23b** was attributed to a low barrier to metal-centered epimerization relative to **19b.**

Mashima and co-workers recently reported on the synthesis and 1-hexene polymerization behavior of Cp* hafnium dimethyl complexes bearing an iminopyrrolyl ligand.[52] When activated with $[Ph_3C][B(C_6F_5)_4]$ at 0 °C or below, compounds **24a-c** (Figure 1.7) polymerized 1-hexene to furnish polymers with narrow molecular weight distributions (M_w/M_n = 1.07 – 1.12) and M_n = 9,000 – 36,100 g/mol. The poly(1-hexene)s were all significantly isoenriched with the highest level of isotacticity ([*mmmm*] = 0.90) being obtained from **24b** at -20 °C. The polymerization of 1-hexene with **24a** exhibited a linear dependence of M_n versus time at -20 and 0 °C.

1.2.6 Pyridylamidohafnium Catalysts

One of the more recent classes of catalysts to emerge are the C_1-symmetric pyridylamidohafnium complexes (**25**, Figure 4.8) developed by Dow and Symyx that furnish high molecular weight and highly isoselective poly(α-olefin)s at high reaction temperatures upon activation.[53-55] Coates and co-workers have shown that the catalyst derived from a C_s-symmetric pyridylamidohafnium complex (**26**, Figure 1.8) furnished isotactic poly(1-hexene) in a living fashion when activated with $B(C_6F_5)_3$.[56] The poly(1-hexene)s exhibited narrow polydispersities ($M_w/M_n \leq 1.20$, M_n up to 152,000 g/mol) and the M_n was shown to increase linearly with monomer conversion. At 50 °C, the molecular weight distribution of the polymer produced by **26**/$B(C_6F_5)_3$ remains narrow suggesting that living behavior is maintained at elevated temperatures.

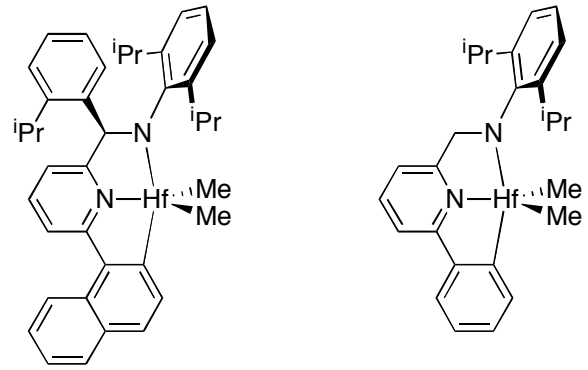

25 **26**

Figure 1.8. Pyridylamidohafnium complexes.

1.2.7 Titanium Catalysts for Styrene Homo- and Copolymerization

As opposed to other homopolymers of higher a-olefins, polystyrene has found extensive use as a commodity material. Recently Okuda and co-workers have demonstrated the first report of living and isospecific polymerization of styrene with a series of titanium complexes bearing tetradentate [OSSO] bis(phenolate) ligands.[57] When activated with $[PhNMe_2H][B(C_6F_5)_4]$ in the presence of $Al(n\text{Oct})_3$ at 25 °C, **27** (Figure 1.9) produced highly isotactic polystyrene (*i*PS) ([*mm*] > 0.95) with narrow molecular weight distributions (M_w/M_n = 1.08 – 1.27) and M_n = 18,300 – 106,100 g/mol. The M_n was shown to increase as a linear function of the conversion.

In 2005, Nomura and Zhang reported on the living copolymerization of ethylene and styrene using a cyclopentadienyl(ketimide)titanium(IV) complex (**28**, Figure 1.9).[58] Upon activation with MAO at 25 °C, **28** furnished poly(ethylene-*co*-styrene) with narrow polydispersities (M_w/M_n = 1.14 – 1.36) and M_n = 53,000 – 173,000 g/mol. The M_n was shown to increase linearly with time. Interestingly, **28**/MAO exhibited non-living behavior for styrene and

ethylene homopolymerizations despite the living behavior observed for the copolymerization of the two monomers.

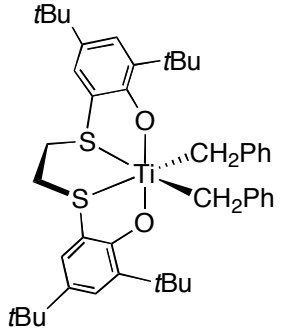

27

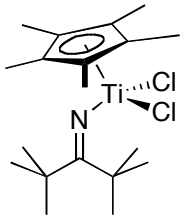

28

Figure 1.9. Titanium-based precatalysts for styrene homo- and copolymerization.

1.2.8 Tripodal Trisoxazoline Scandium Catalysts

While complexes of Group 4 transition metals dominate the field of living olefin polymerization, there are rare examples of group 3 complexes displaying characteristics of living behavior. Recently, Ward *et al.* reported on the synthesis and 1-hexene polymerization behavior of a unique C_3-symmetric scandium complex bearing a tripodal trisoxazoline ligand.[59] When treated with two equivalents of $[Ph_3C][B(C_6F_5)_4]$ at -30 °C in the presence of 1-hexene, **29** (Figure 1.10) produced isotactic poly(1-hexene) ([*mmmm*] = 0.90) lacking olefinic end groups with M_n = 750,000 g/mol and M_w/M_n = 1.18.

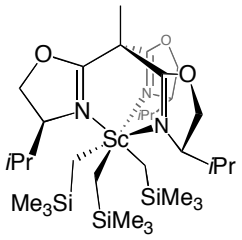

29

Figure 1.10. Tripodal trisoxazoline scandium complex for 1-hexene polymerization.

1.2.9 Late Transition Metal Catalysts

In the mid 1990s, Brookhart and co-workers reported the synthesis and olefin polymerization activity of α-diimine complexes of nickel and palladium.[60] These systems were unique among late metal catalysts in their ability to produce high molar mass materials, rather than oligomers, from both ethylene and higher α-olefins. Furthermore, the metal centers were shown to migrate along polymer chains ("chain walking"),[61] allowing access to polyolefins with a wide variety of microstructures simply by varying ligand substitution patterns, temperature, or pressure. Shortly thereafter, conditions were disclosed which allowed the nickel catalysts **30a** and **31** (Figure 1.11) to polymerize 1-hexene and 1-octadecene in a living fashion.[62] Upon activation with MAO or MMAO at -10 °C and low monomer concentrations, **30a** and **31** resulted in living systems furnishing polymers of M_n = 19,000 to 91,000 g/mol and narrow molecular weight distributions (M_w/M_n as low as 1.09). The systems were further shown to exhibit a linear increase in M_n with time. Branching density was less than that calculated for perfect sequential 1,2-insertions as a result of ω,1-enchainment, or "chain straightening".[63] Poly(1-hexene) with as few as 118 branches/1000 carbons (vs. 167 expected for perfect 1,2-insertions) and poly(1-octadecene) with as few as 39 branches/1000 carbons (vs. 56 expected) were produced at this temperature. Branching density was controlled by reaction conditions and catalyst structure, with **31** producing more linear polymers than **30a**. In a study of several palladium and nickel complexes, Merna *et al*.[64] reported living-like behavior with **30a**/MAO up to 20 °C. These values are considerably more narrow than those reported by Brookhart for similar reactions at 23 °C, although the reason for the improvement is not clear.

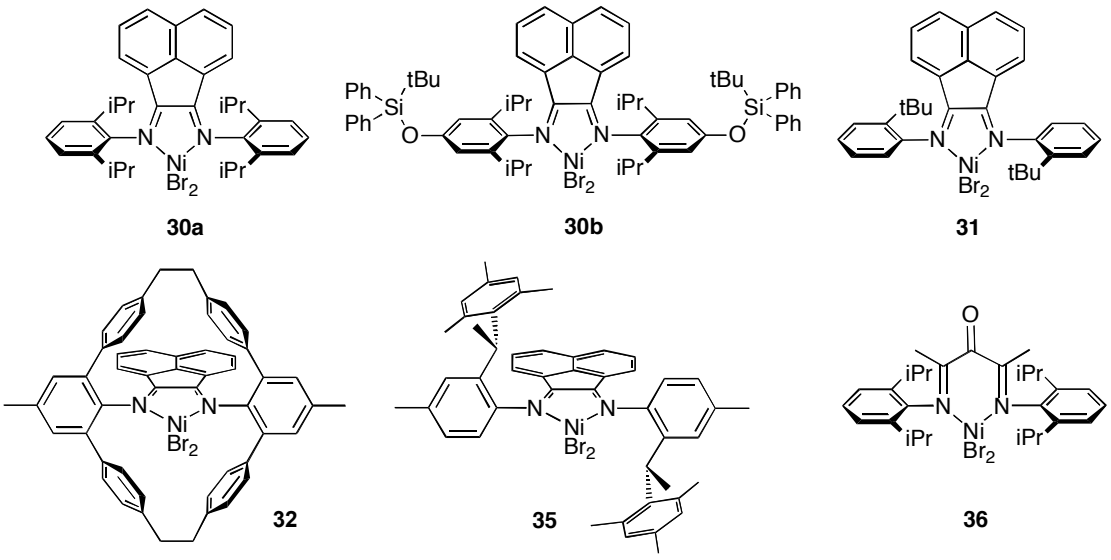

Figure 1.11. Representative nickel diimine complexes for living polymerization of 1-alkenes.

Marques, Gomes and co-workers[65] synthesized a siloxy-substituted analogue of **30a** (**30b**, Figure 1.11) and studied its application for the living polymerization of 1-hexene at -11 °C and up to 16 °C. At the higher temperature, the polydispersity increases somewhat (M_w/M_n = 1.12 – 1.21), and the increase in molecular weight is only linear for the first 40 minutes. In addition, the polymer has a different microstructure, with branching greatly decreased at 16 °C relative to -10 °C (83 vs. 132 branches/1000 carbons, respectively).

Camacho and Guan reported the first living polymerization at elevated temperatures with nickel by using a structural variant of **30a** that utilizing a cyclophane diimine ligand (**32**, Figure 1.11).[66] When activated with MMAO, **32** furnished poly(1-hexene)s with narrow molecular weight distributions (M_w/M_n = 1.13 – 1.22) up to 75 °C and branching densities (52-58 branches/1000 carbons) approximately one-half of those reported for **30a**. The

authors attribute the improved behavior to the cyclophane framework which very effectively blocks the axial sites of the nickel center preventing chain transfer.

Suzuki *et al*. have explored α-diimine complexes of both nickel and palladium (**33a-e**, Figure 1.12) for the polymerization of 1-hexene at very high pressures (up to 750 MPa).[67] While nickel catalysts displayed non-living behavior, the palladium catalysts **33d,e** (Figure 1.12) were living for 1-hexene polymerization and polydispersities decreased at higher pressures (M_w/M_n = 1.27 – 1.29 at 0.1 MPa vs. 1.11 – 1.17 at 500 MPa with **33e**).

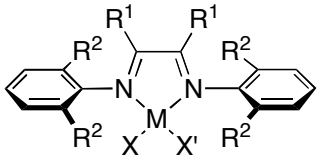

	M	R^1,R^1	R^2	X	X'
33a	Ni	Me,Me	*i*Pr	Br	Br
33b	Ni	Me,Me	Me	Br	Br
33c	Ni	1,8-naphthyl	*i*Pr	Br	Br
33d	Pd	Me,Me	*i*Pr	Cl	Cl
33e	Pd	Me,Me	*i*Pr	Cl	Me

Figure 1.12. Nickel and palladium diimine complexes for 1-hexene polymerization.

Using diimine complexes of palladium, Gottfried and Brookhart have demonstrated conditions which allow for living polymerizations of 1-hexene and 1-octadecene at 0 °C where quenching with Et_3SiH is required to prevent chain coupling.[68] Catalyst **34a** (Figure 1.13) exhibited improved living behavior relative to **34b** for 1-hexene polymerization. This was attributed to the ability of the nitrile donor to compete with 1-hexene for the open coordination site in **34b**. Both **34a** and **34b** showed a linear increase in M_n with time over the course of 3 hours and furnished poly(1-hexene)s with narrow molecular weight distributions (M_w/M_n = 1.10 – 1.15) and branching densities of 75-85 branches/1000 carbons. Catalyst **34b** was likewise applied to the

living polymerization of 1-octadecene. Although M_n was observed to increase linearly over the first 3 h at 0 °C, the molecular weight distribution increased as well (M_w/M_n = 1.34 after 3 h). This was attributed to precipitation of the polymer at this temperature, which also limits the accessible molecular weights to ~40,000 g/mol. Sen and co-workers reported on a structurally similar diimine palladium complex to **34a** bearing a five-membered ester chelate arising from 1,2-insertion of methyl methacrylate into the cationic palladium precusor (**34c**, Figure 1.13).[69] Catalyst **34c** displayed "quasi-living" behavior for 1-hexene polymerization showing an increase in M_n with time over the course of 22 hours.

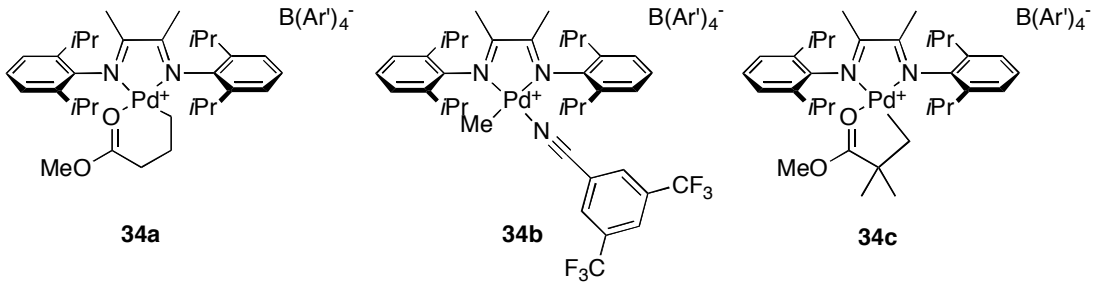

Figure 1.13. Palladium α-diimine catalysts for propylene polymerization.

Coates and co-workers have demonstrated control over polymer microstructure with the chiral, C_2-symmetric nickel diimine complex **35** (Figure 1.11) for living polymerization of α-olefins.[70] A hallmark of the original nickel diimine catalysts is the ability to undergo successive β-hydride eliminations/reinsertions, commonly referred to as "chain walking".[71] This may lead to "chain straightening" with α-olefins, generating regioirregular polymers with less branching than expected. Careful tailoring of reaction conditions (low temperatures and high monomer concentration) with catalyst **35** generates high selectivity for ω,2-enchainment, generating predominantly

methyl branches at regular intervals between methylene units (illustrated for 1-hexene in Scheme 1.2). The technique is applicable to a range of α-olefins, but selectivity for ω,2-enchainment was shown to decrease with increasing chain length (96 mol% ω,2-enchainment for 1-butene vs. 70% for 1-octene).

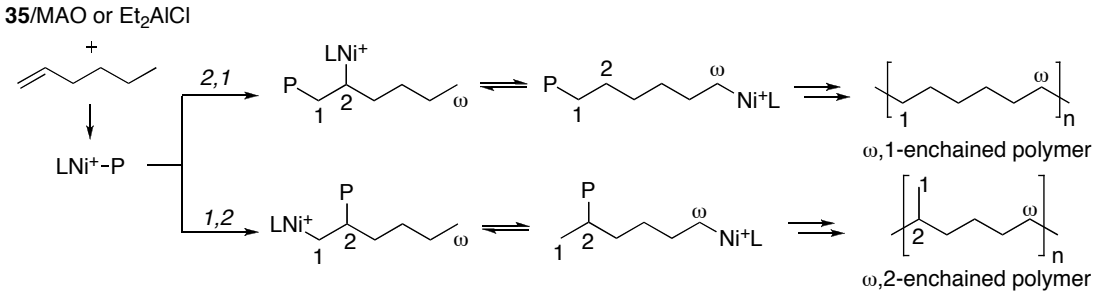

Scheme 1.2. ω,1 vs. ω,2-enchainment of 1-hexene.

Bazan and co-workers recently described the synthesis and olefin polymerization behavior of a nickel α-keto-β-diimine complex.[72] Activation of **36** (Figure 1.11) with MAO in the presence of 1-hexene at 0 °C furnished atactic poly(1-hexene) possessing M_n = 157,000 g/mol and M_w/M_n = 1.2. Microstructural analysis of the polymer by ^{13}C NMR spectroscopy revealed mainly butyl (81.9%) and methyl (12.0%) branches; signatures arising from 2,1-insertions were not detected.

1.3 Living Polypropylene Polymerization

While poly(1-hexene) is an amorphous material regardless of the level of tacticity, polypropylene can range from amorphous to semi-crystalline due to the variability in the level of tacticity. The tacticity of the polymer is intimately related to its bulk properties, with atactic polypropylene (*a*PP; Figure 1.14) being an amorphous material with limited industrial uses (e.g.

adhesives, sealants, and caulks) and syndiotactic polypropylene (*s*PP) and isotactic polypropylene (*i*PP) being semicrystalline materials with relatively high T_m values of ~ 150 °C and ~ 165 °C respectively. The lower crystallinity and the fact that only a very few syndiospecific propylene polymerization catalysts have been discovered to date have limited the commercial impact of *s*PP. On the other hand, numerous catalysts, both heterogeneous and homogeneous, are capable of isospecific propylene polymerization. When combined with *i*PP's highly desirable mechanical properties (durability, chemical resistance, and stiffness), it is obvious why the vast majority of industrially produced polypropylenes are of the isotactic variety.[73]

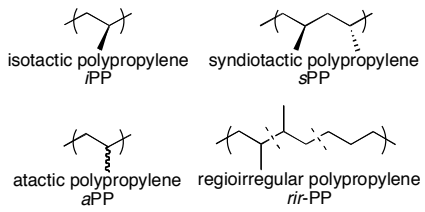

Propylene Microstructure	Precatalysts for Living Polymerization
*i*PP	**13a, 19b, 26, 35, 58a-c, 59a-r, 60a,b, 61a-c, 63a,b, 64a-f**
*s*PP	**2, 37, 38, 42, 43, 45, 47, 49, 50, 51, 52a, 53a-e, 56**
*a*PP	**4a, 39, 40, 41, 44, 52b,c, 54, 55a,b, 58d,e, 62, 80a**
rir-PP	**30a,b, 32, 34b, 35, 64a-f**

Figure 1.14. Microstructures of propylene homopolymers.

1.3.1 Vanadium Acetylacetonoate Catalysts

In the 1960s, Natta and co-workers discovered that activation of VCl_4 with Et_2AlCl at -78 °C in the presence of propylene, furnished syndio-enriched polypropylene with linear growth of molecular weight over time for a period of 25 hours.[74] In a subsequent report the polypropylenes produced by VCl_4/Et_2AlCl were shown to possess monomodal molecular weight distributions ($M_w/M_n = 1.4 – 1.9$).[75]

The first example of a truly living alkene polymerization catalyst was reported by Doi in 1979.[76,77] Upon activation of $V(acac)_3$ (**37**, Figure 1.15) with Et_2AlCl in the presence of propylene at temperatures ≤ -65 °C, syndio-

enriched PP ([*r*] = 0.81) was furnished exhibiting narrow molecular weight distributions (M_w/M_n = 1.07 – 1.18) and M_n as high as 100,000 g/mol. A linear increase in M_n with time over the course of 15 hours was shown. However, only about 4% of vanadium centers were shown to be active which can be partially alleviated by the addition of anisole leading to a 3-fold increase in the number of active vanadium centers.[78]

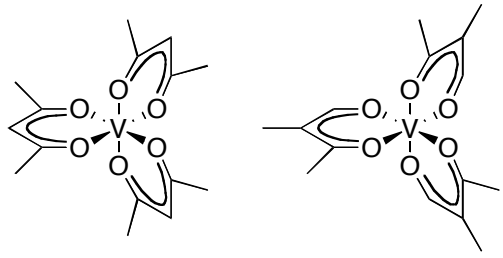

37 **38**

Figure 1.15. Vanadium catalysts for living olefin polymerization.

By replacing the acetylacetonoate ligands of **37** with 2-methyl-1,3-butanedionato ligands (**38**, Figure 1.15) Doi and co-workers found that nearly all of the vanadium centers were active for polymerization with essentially the same degree of syndiotacticity as that formed by **37**/Et_2AlCl.[79] In addition, the living character of propylene polymerization by **38**/Et_2AlCl was maintained up to -40 °C (M_w/M_n as low as 1.4).[80,81] Copolymerization of propylene and ethylene by **38**/Et_2AlCl was also shown to be living.[82]

One of the important applications of living olefin polymerization is in the synthesis of end-functionalized polymers, which is typically achieved by reaction of the living chain end with an electrophile. The vanadium-based living olefin polymerization catalysts discovered by Doi and co-workers proved to be particularly amenable to this application.[83-87] The structures of

end-functionalized *s*PPs prepared in this manner are summarized in Scheme 1.3.

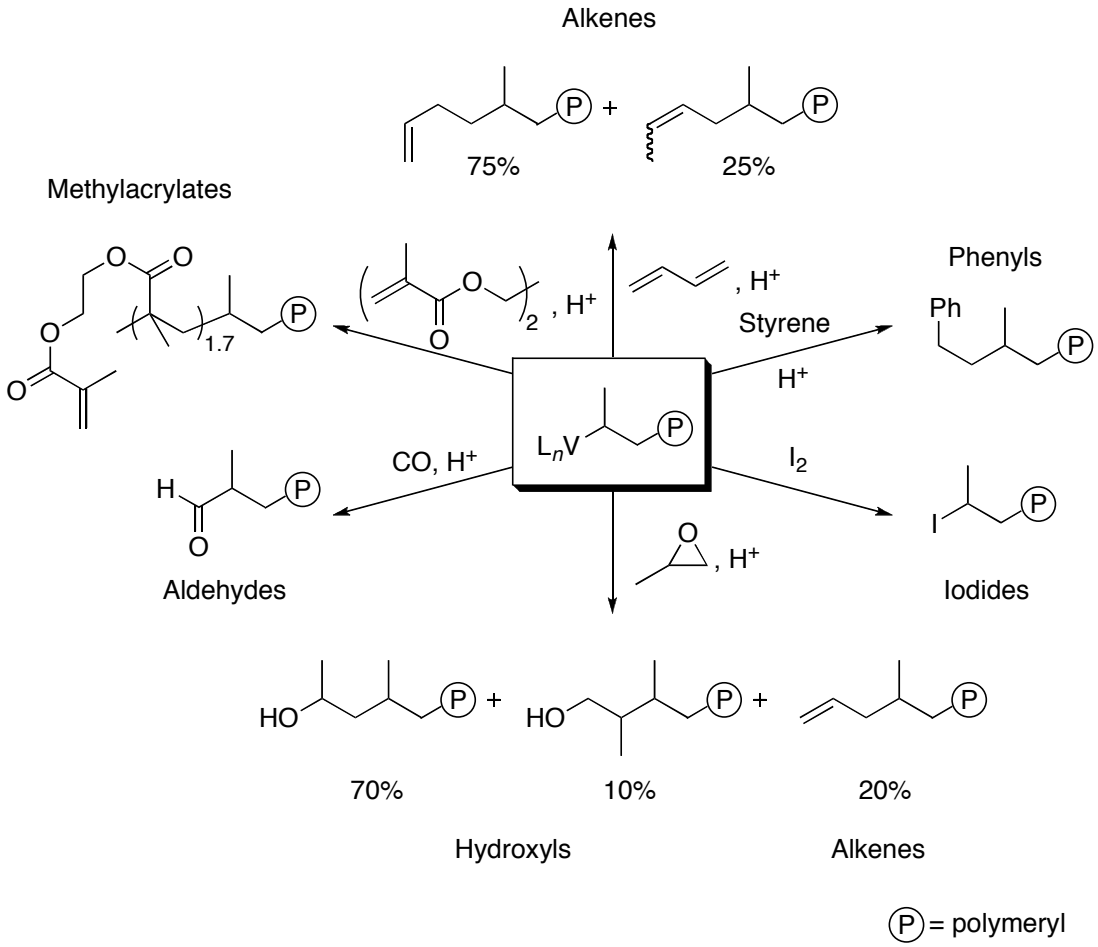

Scheme 1.3. Synthesis of end-functional polypropylenes with a vanadium-based catalyst.

1.3.2 Metallocene-Based Catalysts

Bochmann and co-workers reported that **39** (Figure 1.16) activated with $B(C_6F_5)_3$ at -20 °C produces atactic, high molecular weight PP that exhibits elastomeric properties with M_w = 1,103,000 g/mol and M_w/M_n = 1.4.[88] From analysis of the GPC trace for this sample, it was estimated that 48% of the polymer was composed of PP with a narrow molecular weight distribution

(M_w/M_n = 1.10). The polymerization also showed a linear increase in molecular weight with time.

Fukui and co-workers have reported that [Cp_2ZrMe_2] (**40**, Figure 1.16) activated with $B(C_6F_5)_3$ at -78 °C in the presence of Al(*n*Oct)$_3$ produces PP with $M_w/M_n \leq 1.15$ (M_n = 9,400 – 27,300 g/mol).[18] The polymerization shows a linear increase in M_n with time and it was later reported that quenching the polymerization with CO resulted in aldehyde-functionalized polymer chains.[89,90] The hafnium analogue (**41**) was also shown to be living at -50 °C.

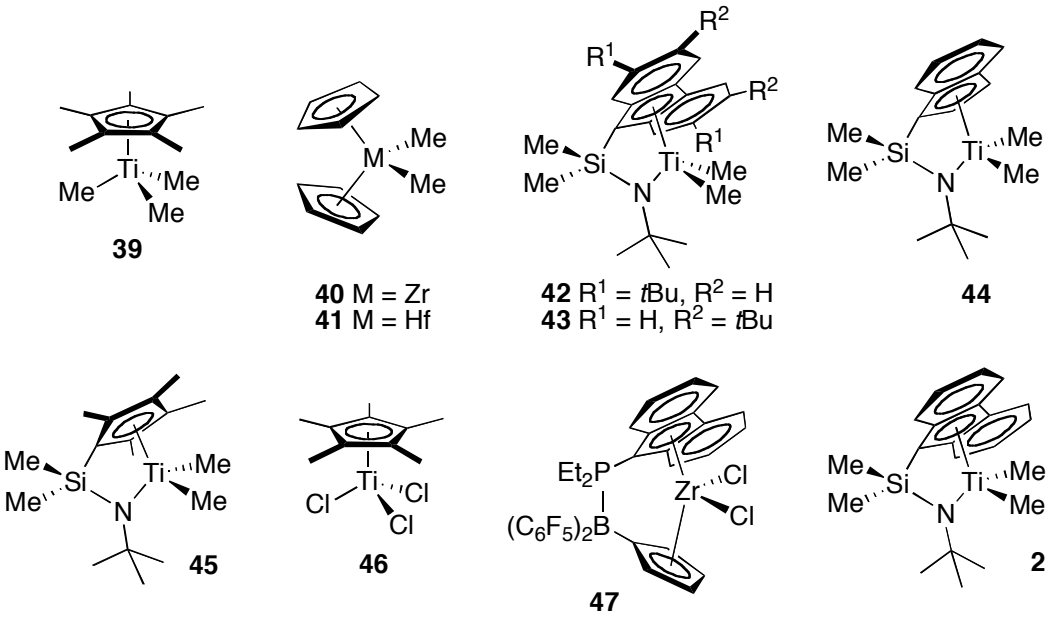

Figure 1.16. Metallocene catalyst precursors for living propylene polymerization.

In addition to living 1-hexene polymerization, **2** (Figure 1.2) upon activation with $B(C_6F_5)_3$ in the presence of Al(*n*Oct)$_3$ can also produce syndio-enriched PP ([*rr*] ~ 0.49) at -50 °C in living fashion.[19] Subsequent studies showed that when activated with "dried" MAO (dMAO) (free of trimethylaluminum), **2** could polymerize propylene at 0 °C producing PP

with a higher degree of syndiotacticity ([*rr*] ~ 0.63) and with a relatively narrow molecular weight distribution (M_w/M_n = 1.22, M_n = 157,000 g/mol).[91] Shiono and co-workers also demonstrated significant solvent effects on the tacticity of the resulting PP.[92] For example, polymerization of propylene in heptane at 0 °C with **2**/dMAO results in polymer with higher tacticity than when the reaction is carried out in toluene ([*rr*] = 0.73 vs. 0.60) or chlorobenzene ([*rr*] = 0.42).

Shiono and co-workers examined structural variants of **2** (**42** and **43**, Figure 1.16) by introducing *tert*-butyl substituents into the fluorenyl ligand framework.[93] When activated with dried MMAO (dMMAO) at 0 °C, **42** produced *s*PP ([*rr*] ~ 0.83). While the molecular weight distribution was somewhat broad (M_w/M_n = 1.68, M_n = 202,000 g/mol), a two-stage sequential polymerization of 0.63 g of propylene revealed a nearly doubling of molecular weight than was obtained from a single-stage polymerization. Catalyst **43**/dMMAO furnished polymer with even higher tacticity ([*rr*] ~ 0.93) and lower molecular weight distribution (M_w/M_n = 1.45). Employing an indenyl-based ligand, **44**/dMAO at 0 °C affords iso-enriched PP ([*mm*] = 0.40) with quasi-living behavior.[94] Later, Dare and co-workers reported that a similar complex **45**/MAO furnished PP at 0 °C that was syndio-enriched ([*rr*] = 0.56) and exhibited a somewhat narrow PDI (M_w/M_n = 1.37, M_n = 108,000 g/mol).[95] Lastly, polymerizations employing catalyst mixtures were reported. Fukui and co-workers showed that iso-enriched PP ([*mm*] = 0.42) could be formed from a mixed catalyst system **40**/$B(C_6F_5)_3$/**46** at -50 °C.[96] The polymerization exhibits a linear increase in M_n with time over 26 hours and M_n up to 17,600 g/mol (M_w/M_n = 1.29 – 1.41).

Starzewski and co-workers have reported a metallocene with the existence of donor and acceptor groups in the sandwich structure (**47**, Figure 1.16) that generates elastomeric PP in a syndioselective fashion ([*rr*] = 0.52) upon activation with MAO at -8 to -6 °C.[97] While the PDIs are somewhat broad (M_w/M_n = 1.5 – 1.6, M_n up to 531,000 g/mol), the M_n was shown to increase linearly with time over 1 hr. The system was also shown to be living for ethylene and propylene copolymerization.

1.3.3 Catalysts Bearing Diamido Ligands

In 2002 Shiono and co-workers reported that upon activation with dMMAO at 0 °C, McConville's dimethyldiamidotitanium complex (**4a**, Figure 1.3) was capable of polymerizing propylene in a living manner.[98] The PPs obtained from **4a**/dMMAO were atactic and displayed narrow molecular weight distributions (M_w/M_n = ca. 1.16 – 1.3). The M_n was shown to increase linearly with polymerization time from 10 – 25 minutes (M_n up to ca. 30,000 g/mol). In subsequent reports, Shiono and co-workers discussed the effects of supported MMAOs on the propylene polymerization behavior of **4a.**[99-102] Three different supports for MMAO were investigated: SiO_2, Al_2O_3, and MgO. Regardless of the support, polymerization of propylene by **4a**/supported MMAO at 0 °C exhibited a linear increase of M_n with time.

1.3.4 Bis(phenoxyimine)titanium Catalysts

In 1999, Fujita and co-workers reported on a class of Group IV complexes bearing chelating phenoxyimine ligands, including **48a** (Figure 1.17). When activated with MAO, these complexes showed extremely high activity for ethylene polymerization.[103-105] Interested in the development of

catalysts that could produce stereoregular polymers, Coates and co-workers used a pooled combinatorial approach to screen Mitsui-type complexes for propylene polymerization behavior and found that **48b**/MAO furnished syndiotactic PP ([*r*] = 0.94) despite the C_2-symmetry of the catalyst precursor, which was the result of a chain-end control mechanism.[106] Later, several studies revealed an unusual 2,1-insertion mechanism.[107-109] In addition, calculations on the system have supported a ligand isomerization event that interconverts the Λ and Δ isomers of the active species between consecutive insertions, causing an alternation between *si* and *re* coordination of propylene which leads to syndiotactic polymer formation.[110-112]

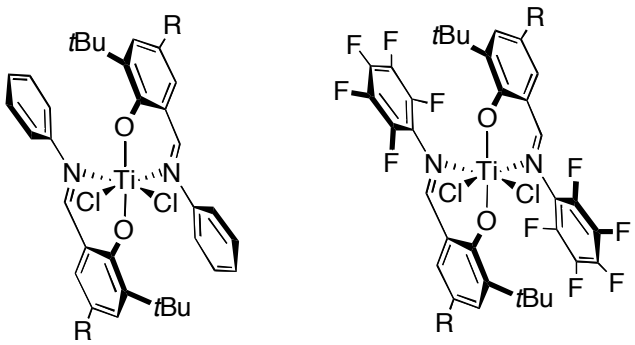

48a R = H
48b R = *t*Bu

49 R = *t*Bu
50 R = H

Figure 1.17. Early bis(phenoxyimine) titanium complexes.

It was later found that the incorporation of fluorinated *N*-aryl moieties into the bis(phenoxyimine) ligand framework could provide catalyst precursors for the syndiotactic and living polymerization of propylene. When activated with MAO at 0 °C, **49** (Figure 1.17) produced highly syndiotactic PP ([*rrrr*] = 0.96) which exhibited a peak melting temperature of 148 °C.[113] The polymerization exhibited a linear increase in M_n with PP yield with narrow

polydispersities ($M_w/M_n \leq 1.11$) for M_n up to 100,000 g/mol. Fujita and co-workers independently reported that **50**/MAO was also living and syndioselective ([*rr*] = 87%) for propylene polymerization at room temperature, producing polymer with M_n = 28,500 – 108,000 g/mol and M_w/M_n = 1.07 – 1.14.[114] Employing a supported cocatalyst with **50** has also shown characteristics of living behavior. Polypropylene formed using **50**/$MgCl_2$/*i*-$Bu_nAl(OCH_2CH(Et)(CH_2)_3CH_3)_{3-n}$ had narrow PDIs (M_w/M_n = 1.09 – 1.17, M_n = 53,000 – 132,000 g/mol) and the polymerization exhibited a linear increase in M_n with reaction time.[115]

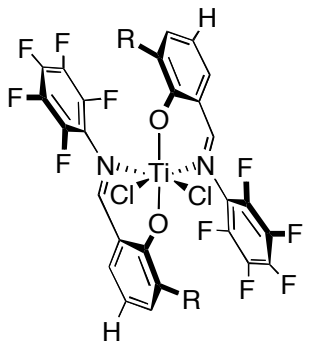

51 R = $SiMe_3$
52a R = $SiEt_3$
52b R = Me
52c R = *i*Pr

Figure 1.18. Bis(phenoxyimine) titanium complexes with various phenoxide substituents.

Changing the *ortho* substituents on the phenolate ring has yielded a number of new complexes. Of note, a complex bearing a *ortho*-phenolate trimethylsilyl group, **51** (Figure 1.18), has been shown to produce *s*PP with very high melting temperatures (T_m up to 156 °C) in a living fashion.[116] Changing the aforementioned *ortho* position to a larger triethylsilyl group (**52a**) gave similar results as **51** with lower activity.[117] However, employment of a methyl (**52b**) or isopropyl (**52c**) group in the *ortho* position resulted in a

substantial loss of stereocontrol producing amorphous PP that exhibited fairly narrow polydispersities (M_w/M_n ~ 1.2).

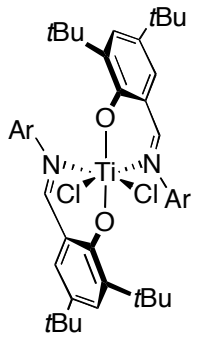

53a Ar = 2-FC_6H_4
53b Ar = 2,6-$F_2C_6H_3$
53c Ar = 2,4,6-$F_3C_6H_2$
53d Ar = 2,3,5,6-F_4C_6H
53e Ar = 2,3,5,6-F_4-4-CF_3-C_6

Figure 1.19. Bis(phenoxyimine) titanium complexes with varying *N*-aryl fluorine substitution patterns.

Studies on the effect of the fluorination pattern of the *N*-aryl ring have been conducted and it has been revealed that complexes bearing the 2,4-di-*tert*-butyl phenoxide moiety require at least one *ortho* fluorine on the *N*-aryl ring to exhibit living propylene polymerization behavior .[118,119] As the amount of fluorination of the *N*-aryl moiety is decreased from the perfluoro complex **49** (Figure 1.17) to the monofluoro complex **53a** (Figure 1.19), activities and tacticities for propylene polymerization decreased while the polydispersities remain consistently low ($M_w/M_n \leq 1.11$, M_n up to 28,900 g/mol) upon MAO activation. Installing a trifluoromethyl group at the *para*-position of the *N*-aryl moiety (**53e**, Figure 1.19) led to an increase in activity of approximately 1.5 times that of **49**/MAO with similar tacticity ([*rrrr*] = 0.91).[120] Interestingly, complexes related to **53a-c** where the *para*-substituent of the phenoxide moiety is H, produced amorphous PP upon MAO activation. These samples gave

bimodal GPC traces each composed of a narrow peak ($M_w/M_n \leq 1.10$) and a broad peak ($M_w/M_n = 4.19 – 14.9$).[121]

Simultaneous changes to both the phenoxide and *N*-aryl moieties, relative to **49** (Figure 1.17) have also been made. For example, **54** (Figure 1.20) exhibits a 2,6-$F_2C_6H_3$ *N*-aryl moiety and iodine substituents on the phenolate ring. When activated with MAO at 25 °C, **54** was reported to produce amorphous PP which exhibited a narrow molecular weight distribution (M_w/M_n = 1.17, M_n = 200,000 g/mol).[122,123] Complexes **55a,b** employ 3,5-difluorophenyl *N*-aryl groups and substituents smaller than *tert*-butyl in the *ortho* position of the phenoxide moiety. Both **55a,b**/MAO were shown to furnish amorphous PP ([*rrrr*] ≤ 0.48) with narrow molecular weight distributions (M_w/M_n = 1.13 – 1.16, M_n up to 240,000 g/mol).[124] This finding was surprising in that both complexes lack *ortho* fluorines on the *N*-aryl moiety.

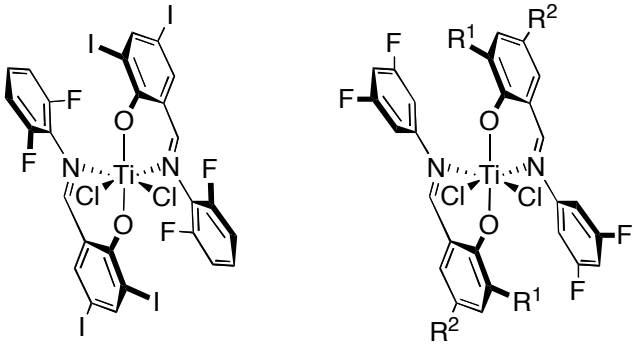

Figure 1.20. Bis(phenoxyimine) titanium complexes.

One final variation to the bis(phenoxyimine) complexes involves the coordination of two different phenoxyimine ligands to one titanium center. Using gel permeation chromatography as a combinatorial screening method,

a number of heteroligated phenoxyimine complexes bearing one non-living (*ortho*-non-fluorinated ligand) and one living ligand (*ortho*-fluorinated ligand) were identified that displayed superior activities over their homoligated counterparts.[119] For example, PP produced with **48b**/MAO (Figure 1.17) exhibited a broad PDI (M_w/M_n = 1.41) and a turn-over frequency (TOF) of 42 h^{-1} while **49**/MAO exhibited a narrow PDI (M_w/M_n = 1.06) and a TOF of 221 h^{-1}. However, the heteroligated catalyst **56**/MAO (Figure 1.21) produced PP with M_n = 70,170 g/mol and M_w/M_n = 1.16 and exhibited a TOF of 760 h^{-1}. Syndiotactic polymer ([*rrrr*] = 0.91]) was formed with this heteroligated catalyst.

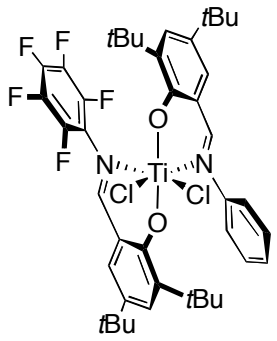

56

Figure 1.21. Heteroligated bis(phenoxyimine) titanium complex.

1.3.5 Bis(phenoxyketimine)titanium Catalysts

While bis(phenoxyimine) titanium complexes furnish sPP, it had been proposed that placing a substituent at the imine carbon of the phenoxyimine ligand could prevent the isomerization responsible for the production of sPP and lead to the formation of *i*PP.[125] Ketimine complexes **57a-c** (Figure 1.22) were sparingly active for propylene polymerization, despite the ability to polymerize ethylene in a living fashion upon activation.[125,126] Complexes

bearing smaller *ortho* substituents on the phenolate ring were reasoned to enable higher propylene activities by providing a sterically less-encumbered active site. With this in mind, complexes **58a-d** were synthesized and screened for propylene polymerization.[125] Upon activation with MAO at 0 °C, each complex produced PP with a narrow molecular weight distribution (M_w/M_n = 1.12 – 1.17, M_n = 2,700 – 35,400 g/mol) and **58c**/MAO was shown to exhibit a linear increase in M_n as a function of yield. The tacticities of the resulting polymers differed with **58c**/MAO furnishing PP with the highest tacticity ([*mmmm*] = 0.53, T_m = 69.5 °C). The aldimine analogue of **58c** (**58e**) in which R^3 = H, furnishes atactic PP with M_n = 123,100 g/mol and M_w/M_n = 1.13.

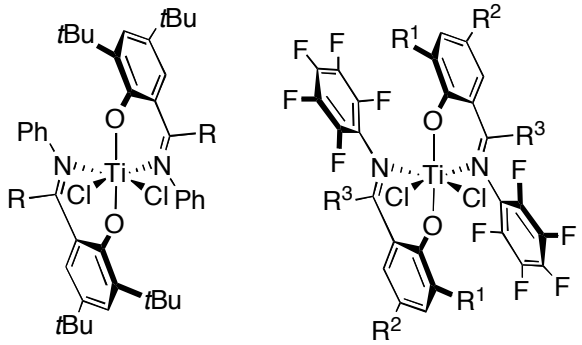

57a R = Me
57b R = Et
57c R = Ph

	R^1	R^2	R^3
58a	*i*Pr	*i*Pr	Ph
58b	Et	Me	Ph
58c	Me	Me	Ph
58d	H	Me	Ph
58e	Me	Me	H

Figure 1.22. Bis(phenoxyketimine) titanium complexes.

In a subsequent report, Coates and co-workers systematically varied *ortho*-, *meta*-, and *para*-substituents on the phenoxide moiety in addition to the ketimine substituent in complexes **59a**-**r** (Figure 1.23) to obtain higher isoselectivity.[127] All the complexes produced PP with a narrow molecular

weight distribution (M_w/M_n = 1.07 – 1.33, M_n = 3,000 – 364,000 g/mol) upon activation with MAO except those bearing ancillary methoxy groups in the ligand framework (**59h** and **59p**). The tacticities of the resulting polymers differed with **59k**/MAO furnishing PP with the highest tacticity ([*mmmm*] = 0.73, T_m = 116.8 °C) in addition to exhibiting a linear increase in M_n as a function of polymer yield.

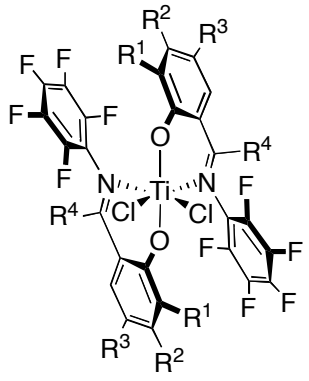

	R1	R2	R3	R4
59a	Cl	H	Me	Ph
59b	Br	H	Me	Ph
59c	Ph	H	Me	Ph
59d	Bn	H	Me	Ph
59e	–$(CH_2)_4$–		H	Ph
59f	Me	H	Cl	Ph
59g	Me	H	F	Ph
59h	Me	H	OMe	Ph
59i	Me	H	Me	Me
59j	Me	H	Me	*i*Pr
59k	Me	H	Me	Cy
59l	Me	H	Me	Cycloheptyl
59m	Me	H	Me	CF_3
59n	Me	H	Me	2-Naphthyl
59o	Me	H	Me	1-Naphthyl
59p	Me	H	Me	4-Methoxyphenyl
59q	Me	H	Me	Mesityl
59r	Me	H	Me	C_6F_5

Figure 1.23. Bis(phenoxyketimine) titanium complexes with varying phenoxide and ketimine substituents.

1.3.6 Amine Bisphenolate Zirconium Catalysts

Busico and co-workers have investigated the propylene polymerization behavior of Kol's octahedral [ONNO] zirconium complexes **13a**,**b** (Figure 1.5).[128] In contrast to the living 1-hexene polymerization observed for

13a/$B(C_6F_5)_3$, the polypropylenes produced by **13a** and **13b**/$[PhNMe_2H][B(C_6F_5)_4]$/$Al(iBu)_3$ showed evidence of termination via chain transfer to Al and β-H transfer to monomer. However, in a subsequent report, Busico and co-workers reported that through ligand modification, the controlled polymerization of propylene with this class of catalyst could be achieved.[129] Specifically, by installing bulky 1-adamantyl (**60a**) or cumyl (**60b**) substituents at the *ortho*-position of the phenol moiety (Figure 1.24) PPs with narrow molecular weight distributions were obtained (M_w/M_n = 1.2 – 1.6) under the same activation procedure. For **60a**/$[PhNMe_2H][B(C_6F_5)_4]$/$Al(iBu)_3$, a linear increase of M_n with time is observed over the course of three hours, while after three hours resonances consistent with terminal vinylidene groups were apparent in the ^{13}C NMR spectrum. Chain transfer to aluminum was suppressed by the addition of 2,6-di-*tert*-butylphenol. The PP formed by **60a**/$[PhNMe_2H][B(C_6F_5)_4]$/$Al(iBu)_3$ was highly isotactic ([*mmmm*] = 0.985, T_m = 151 °C).

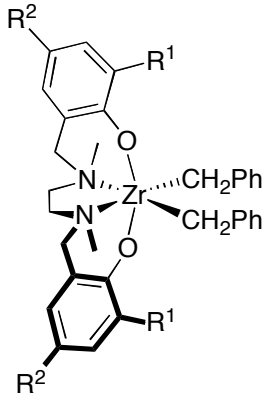

60a R^1 = 1-adamantyl, R^2 = Me
60b R^1 = cumyl, R^2 = Me

Figure 1.24. Zirconium complexes for isospecific propylene polymerization.

1.3.7 Monocyclopentadienylzirconium Amidinate Catalysts

In addition to living 1-hexene polymerization, Sita and co-workers have shown that **19b** activated with $[PhNMe_2H][B(C_6F_5)_4]$ in a stoichiometric ratio furnished highly isotactic PP ([*mmmm*] = 0.71) in a living fashion ($M_w/M_n \leq 1.20$).[130] Interestingly, activation with 0.5 equivalents of $[PhNMe_2H][B(C_6F_5)_4]$ resulted in the production of atactic PP where the M_n was also shown to increase linearly with time ($M_w/M_n \sim 1.05$). A process of degenerative-transfer (DT) polymerization that proceeds through a rapid and reversible methyl group transfer between the cationic (active) and neutral

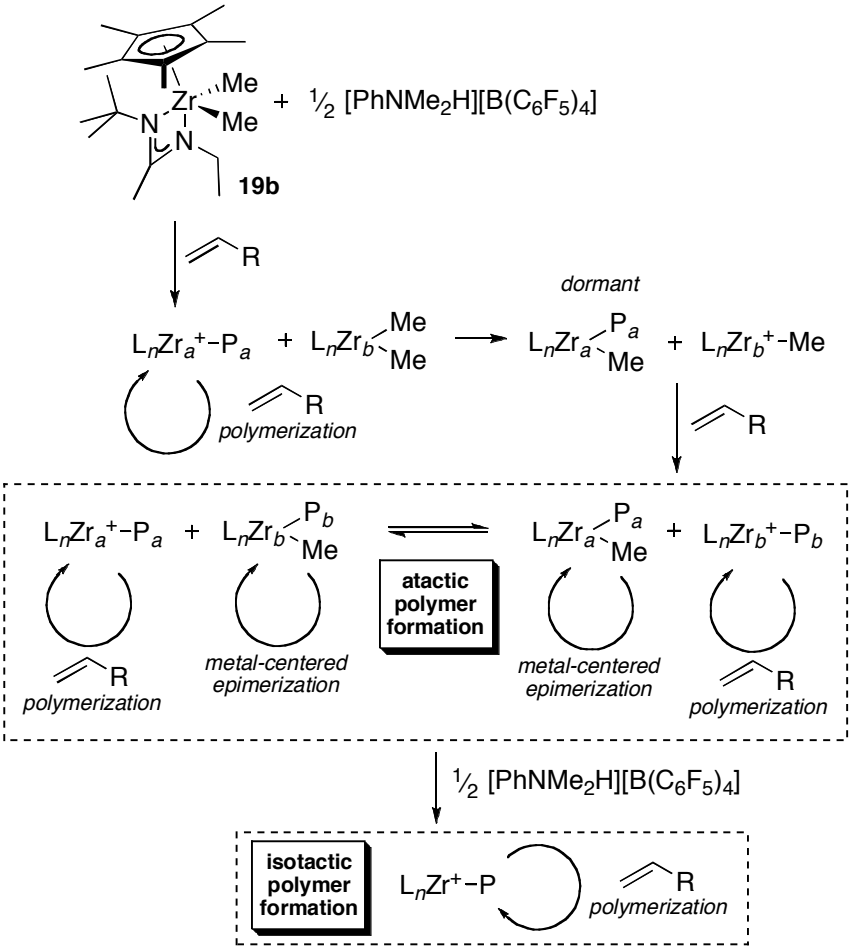

Scheme 1.4. Degenerative group transfer polymerization employing **19b**.

(dormant) zirconium centers was considered as the mechanism for this living system (Scheme 1.4).[131] In addition, the methyl-polymeryl dormant species can undergo epimerization that is faster than propagation. Thus, through a combination of methyl group transfer and epimerization at dormant sites, each occurring faster than propagation, stereocontrol is greatly diminished leading to an atactic microstructure. However, upon addition of a second 0.5 equivalent of $[PhNMe_2H][B(C_6F_5)_4]$, all Zr species become active for polymerization thereby "turning off" DT and initiating isospecific polymerization, which can advantageously be used for the production of block copolymers (to be discussed in later sections). In a subsequent report, Sita and co-workers synthesized stereogradient PP by initial polymerization under DT polymerization conditions followed by slow introduction of $[PhNMe_2H][B(C_6F_5)_4]$ to 100% activation.[132]

Sita and co-workers later prepared bimetallic analogues of **19b** to investigate further the effects of DT polymerization (**61a-c**, Figure 1.25).[133] Compounds **61a-c** were all found to be living and isoselective for propylene polymerization upon activation with 2 equivalents of $[PhNMe_2H][B(C_6F_5)_4]$ at -10 °C (M_n up to 50,000 g/mol, M_w/M_n = 1.1 – 1.2), with the degree of stereoselectivity decreasing as the two metal centers are brought closer together. Activation under sub-stoichiometric conditions led to living DT polymerization. Under these conditions, the frequency of [*mr*] stereoerrors in the PP decrease as the two metal centers are brought closer together resulting from an increased barrier to metal-centered epimerization of the dormant site. A linear increase in M_n with time was observed for **61a** under sub-stoichiometric activation conditions to further illustrate the living behavior.

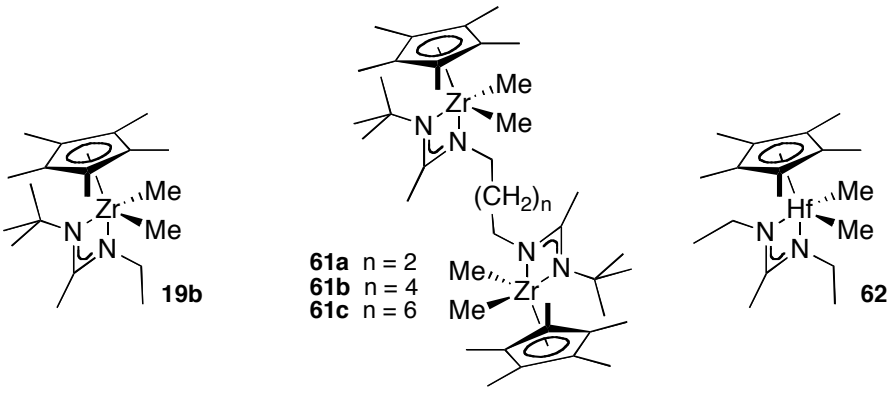

Figure 1.25. Monocyclopentadienyl amidinate complexes.

Sita and co-workers have also recently described a modified amidinate hafnium catalyst (**62**, Figure 1.25) that furnished atactic PP of high molecular weight (M_n = 137,000 g/mol, M_w/M_n = 1.12) upon activation with one equivalent of $[PhNMe_2H][B(C_6F_5)_4]$ at -10 °C.[134] M_n of up to 830,000 g/mol could be obtained with this system, however significant broadening of the PDI was observed (M_w/M_n = 2.43). Furthermore, this system demonstrated the first example of living coordinative chain-transfer polymerization (CCTP)[135] of propylene with diethyl zinc. It was further used for the living CCTP of ethylene, 1-hexene, 1-octene, and 1,5-hexadiene in addition to living CCTP copolymerization of ethylene with the aforementioned higher a-olefins.[136]

1.3.8 Pyridylamidohafnium Catalysts

In addition to living 1-hexene polymerization, Coates and co-workers have shown that the C_s-symmetric pyridylamidohafnium complex (**26**, Figure 1.8) furnished isotactic PP ([*mmmm*] = 0.56) with a narrow molecular weight distribution (M_n = 68,600 g/mol, M_w/M_n = 1.05) upon activation with $B(C_6F_5)_3$ at 20 °C.[56] The mechanism of stereocontrol proceeded by an enantiomorphic

site control mechanism, which is quite unusual for a C_s-symmetric catalyst. Detailed mechanistic studies with **25** (Figure 1.8) by Froese *et al.*[54] have shown the 1,2-insertion of an olefin into the Hf-C_{Aryl} bond generates an sp^3-hybridized carbon donor atom that supports the active metal center; it is likely that the isoselectivity observed with **26**/$B(C_6F_5)_3$ results from a similar activation mechanism. With this in mind, Coates and co-workers prepared a new pyridylamidohafnium complex (*rac*-**63a**,**b**, Figure 1.26) supported by an sp^3-carbon donor that was generated *via* insertion of a ligand-appended alkene into the neutral pyridylamidohafnium trimethyl precursor generating a mixture of diastereomers (61:39 ratio).[137] Upon activation with $B(C_6F_5)_3$, *rac*-**63a**,**b** furnished isotactic PP ([*mmmm*] = 0.80) with a narrow molecular weight distribution ($M_w/M_n \leq 1.05$, M_n up to 124,400 g/mol) and TOF of 2800 h^{-1}. The M_n was shown to increase linearly with polymer yield over the course of 45 min.

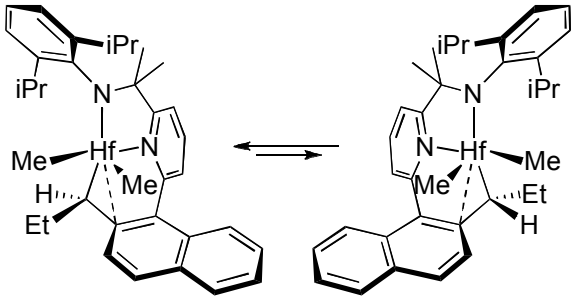

rac-**63a,b**
61:39 mixture of diastereomers

Figure 1.26. Diastereomeric mixture of pyridylamidohafnium complexes.

1.3.9 Late Transition Metal Catalysts

α-Diimine complexes of nickel were the first late transition metal catalysts reported for the living polymerization of propylene.[60] Catalyst **30a**

(Figure 1.11), upon activation with MMAO at –10 °C, afforded PP with a narrow molecular weight distribution (M_w/M_n = 1.13; M_n = 160,000 g/mol) and M_n was shown to increase linearly with conversion. The material obtained had 159 branches/1000 carbons, far less than the theoretical value of 333 for sequential 1,2-insertions, which was attributed to chain straightening. As branching decreased, T_g values decreased as well (as low as -55 °C), illustrating the dramatic effects of enchainment mechanism on physical properties.

Using Pd complexes of related diimine ligands, Gottfried and Brookhart observed a relatively linear increase in M_n with time up to approximately 40,000 g/mol at 0 °C using **34b** (Figure 1.13).[68] However, living systems were not obtained when the palladium ester chelate catalyst **34a** was employed due to slow initiation relative to propagation. Because the weakly bound nitrile group of **34b** is more easily displaced by propylene, this initiation problem could be circumvented. Consistent with previous results, PPs generated by this catalyst are chain-straightened, containing approximately 253 branches per 1000 carbons.

Guan and co-workers reported a dramatic demonstration of chain-straightening of propylene with the cyclophane Ni catalyst **32** (Figure 1.11).[66] When activated with MAO, **32** showed good activity for propylene polymerization at temperatures up to 50 °C, with narrow molecular weight distributions (M_w/M_n = 1.06 – 1.16). In addition, M_n was shown to increase linearly with time at 50 °C. The PPs contain 104 – 113 branches/1000 carbons, indicative of extensive chain-straightening. This implies that the cyclophane ligand geometry favors a 2,1-insertion mechanism.

Coates and co-workers have shown the chiral, C_2-symmetric nickel complex **35** (Figure 1.11) polymerizes propylene in a living fashion at temperatures up to 22 °C in the presence of MAO, with a narrow distribution of molecular weights ($M_w/M_n \leq 1.11$).[138] Both the regio- and stereocontrol of enchainment are temperature dependent, allowing access to a wide variety of polymer microstructures from a single monomer. At low temperatures (-78 °C), no chain straightening is observed furnishing highly isotactic PP, but the percentage of 3,1-enchainment increases up to 56.2% at 22 °C producing an amorphous and regioirregular PP. Thus, this catalyst has the unique ability to maintain living behavior at a variety of temperatures, but with variable tacticity and levels of chain-straightening. In a subsequent report, Coates and co-workers introduced new chiral, C_2-symmetric nickel diimine complexes featuring cumyl-derived ligands in an attempt to obtain higher regio- and isoselectivity at low reaction temperatures.[139] Each of the complexes (**64a-f**, Figure 1.27) exhibited higher regioselectivity than **35** at -60 °C in the presence of MAO. Nickel complex **64f** furnished isotactic PP at -78 °C with the highest melting temperature (T_m = 149 °C) of the complexes studied. Furthermore, a linear increase in M_n with polymer yield is observed at 0 °C.

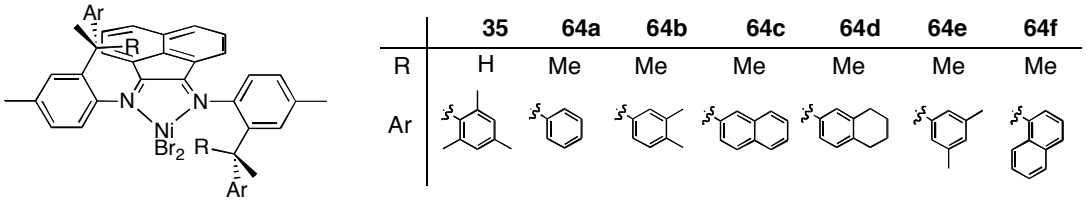

Figure 1.27. Chiral, C_2-symmetric nickel complexes.

Marques and Gomes achieved living polymerization of propylene with **30b** (Figure 1.11).[65] At -11 °C, in the presence of MAO, the catalyst produced

PP with narrow molecular weight distribution (M_w/M_n = 1.17 – 1.19) and a nearly linear increase in molecular weight over 2 hours. Only minimal chain-straightening was observed (316 branches/1000 carbons) and the polymer was somewhat syndioenriched ([*rr*] = 0.54).

In addition to living 1-hexene polymerization, Bazan and co-workers reported that **36**/MAO (Figure 1.11) was also living for propylene polymerization.[72] At 0 °C, the catalyst furnished PP of high molecular weight (M_n = 138,000 g/mol) and narrow polydispersity (M_w/M_n = 1.1). The polymers exhibited no signatures arising from 2,1-insertions.

1.4 Living Polymerization of Ethylene

Considering the simplicity of ethylene, the range of different polymer architectures derived from it is truly intriguing (Figure 1.28). The annual production of PE world wide is in excess of 80 billion pounds.[140] The properties of PEs vary greatly depending on the polymer's microstructure (i.e. branched or linear) from high density plastics with relatively high melting points (linear PE: T_m ~ 135 °C), to low density, branched material with T_m as low as 105 °C. The mechanism by which ethylene is polymerized will ultimately determine the microstructure and therefore the properties of the resultant PE. While most early transition metal olefin polymerization catalysts furnish linear PE, late metal catalysts based on nickel or palladium typically give rise to branched structures.[71]

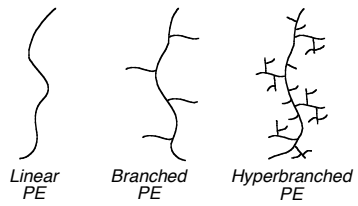

Figure 1.28. Polyethylene (PE) morphologies.

1.4.1 Non-Group 4 Early Metal Polymerization Catalysts

Marks and co-workers showed in 1985 that organolanthanide complexes were promising for living ethylene polymerization.[141] The dimeric bis(Cp*) hydride complexes (**65a-c**, Figure 1.29) furnished high molecular weight PEs (M_n = 96,000 – 648,000 g/mol) and PDIs were for the most part lower than 2.0 (e.g. **65c** exhibited M_w/M_n = 1.37 – 1.68). The living nature of **65a-c** is further supported by observations that catalytic activity is maintained for up to two weeks, M_n increases with time, and the number of polymer chains per metal center is consistently less than one.

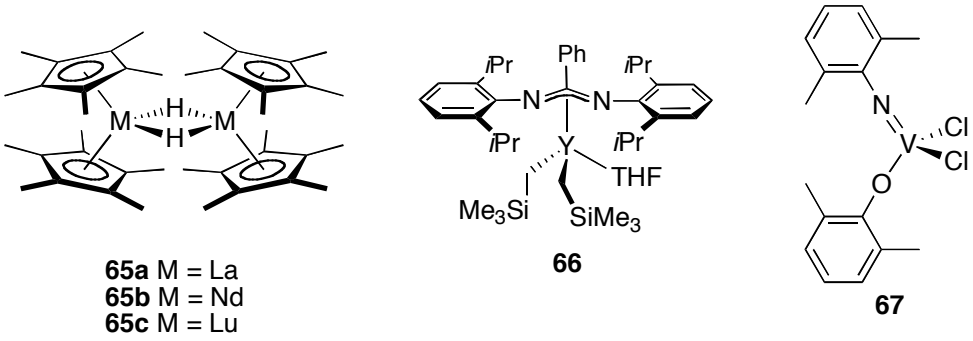

Figure 1.29. Lanthanide, Group 3 metal, and vanadium-based catalysts for living olefin polymerization.

Hessen and co-workers reported on dialkyl(benzamidinate)yttrium complexes which displayed some characteristics of living behavior.[142] When treated with $[PhNMe_2H][B(C_6F_5)_4]$, **66** (Figure 1.29) furnished PE possessing narrow molecular weight distributions (M_w/M_n = 1.1 – 1.2) and high molecular weights (M_w = 430,000 – 1,269,000 g/mol) with about 1.1 polymer chains per metal center being produced.

Nomura and co-workers reported that arylimido(aryloxo)vanadium dichloride complex **67** (Figure 1.29) activated with Et_2AlCl exhibited

characteristics of living ethylene polymerization.[143] The PE furnished had a narrow molecular weight distribution (M_w/M_n = 1.42) and high molecular weight (M_n = 2,570,000 g/mol) at 0 °C. Additionally, the M_n was shown to increase in a linear fashion with increasing TON.

In 1993, Nakamura and co-workers reported on the synthesis and ethylene polymerization behavior of cyclopentadienyl(η^4-diene)tantalum complexes.[144] Upon activation with MAO at temperatures of -20 °C or below, compounds **68a**, **69a** and **70** (Figure 1.30) furnished PEs with narrow molecular weight distributions ($M_w/M_n \leq 1.4$, M_n = 8,600 – 42,900 g/mol). Additionally, below -20 °C, ethylene polymerization by **69a**/MAO displayed a linear increase of M_n with increasing reaction time. The activity for ethylene polymerization was shown to depend on the substitution pattern of the η^4-diene ligand with the highest activity being obtained in the case where 2,3-dimethyl-1,3-butadiene is used (**69b**); the lowest when isoprene is employed (**69c**).[145] The analogous niobium complexes (**71a-d**, Figure 1.30) were also shown to behave as living ethylene polymerization catalysts up to 20 °C when activated with MAO (M_w/M_n = 1.05 – 1.30, M_n = 5,100 – 105,400 g/mol).[146] The dependence of activity on the η^4-diene ligand employed mirrored that observed for the analogous tantalum compounds.

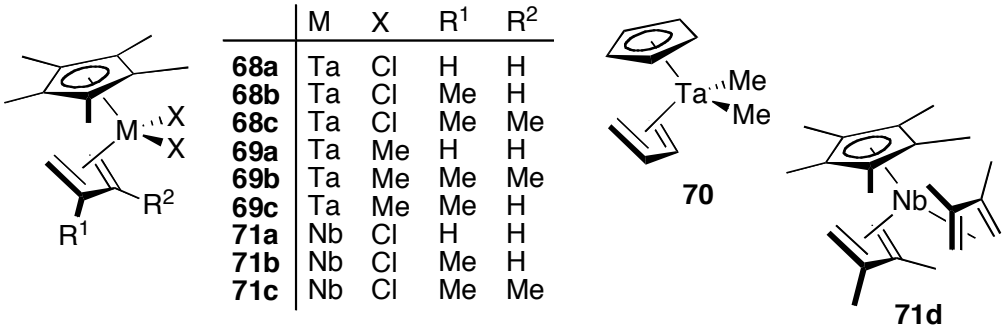

	M	X	R^1	R^2
68a	Ta	Cl	H	H
68b	Ta	Cl	Me	H
68c	Ta	Cl	Me	Me
69a	Ta	Me	H	H
69b	Ta	Me	Me	Me
69c	Ta	Me	Me	H
71a	Nb	Cl	H	H
71b	Nb	Cl	Me	H
71c	Nb	Cl	Me	Me

Figure 1.30. Niobium and tantalum complexes for living ethylene polymerization.

Theopold and co-workers investigated chromium complexes bearing 2,4-pentane-*N,N'*-bis(aryl)ketiminato ($(Ar)_2$nacnac) ligands for ethylene polymerization.[147] When exposed to ethylene at room temperature, **72** (Figure 1.31) formed linear PE with narrow molecular weight distributions (M_w/M_n = 1.17 – 1.4). The M_n was shown to increase linearly with polymer yield. These results represented the first report of living ethylene polymerization with a chromium-based catalyst.

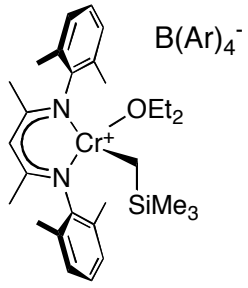

72

Figure 1.31. β-Diiminate chromium complex for living ethylene polymerization.

1.4.2 Bis(phenoxyimine)titanium Catalysts

Many of the same titanium bis(phenoxyimine) catalysts used for living propylene polymerization have also been reported for the living polymerization of ethylene. In 2001, Fujita and co-workers reported that at 25 °C, **50**/MAO (Figure 1.17) furnished linear PE with a high molecular weight and narrow molecular weight distribution (M_n = 412,000 g/mol, M_w/M_n = 1.13).[148] Furthermore, polymerizations at 25 and 50 °C exhibited a linear increase in M_n with reaction time. Coates and co-workers showed that **49**/MAO could copolymerize ethylene and propylene in a living fashion by

cleanly synthesizing a monodisperse PP-*block*-poly(E-*co*-P) sample (M_w/M_n = 1.12, M_n = 145,100 g/mol).[113]

Some of the early titanium bis(phenoxyimine) catalysts have also been used for living ethylene polymerization. In 2003, Coates and co-workers reported that **48b**/MAO polymerized ethylene at 50 °C to produce polyethylene with M_w/M_n = 1.10 and M_n = 44,500 g/mol.[126] In 2004, Ivanchev *et al*. reported a near-linear increase in M_v with time for the polymerization of ethylene with **48a**/MAO at 30 °C.[149] Later, Fujita and co-workers reported on the same system and found that while molecular weight distributions were low at a reaction time of one minute (M_w/M_n = 1.12, M_n = 52,000 g/mol), the PDI broadened significantly at reaction times of just five minutes (M_w/M_n = 1.61, M_n = 170,000 g/mol).[150] Other, related complexes were synthesized and screened for ethylene polymerization. Complexes **73a,b**/MAO (Figure 1.32) showed a near-linear increase in M_v with times up to about 20 minutes.[151]

To investigate the effect of the substituent at the *ortho* position of the phenoxide moiety, complexes **74a,b** and **52b,c** (Figures 1.32 and 1.18) were screened for ethylene polymerization.[152] When activated with MAO at 25 °C, each complex produced PE with a narrow molecular weight distribution (M_w/M_n = 1.05 – 1.16, M_n up to 75,000 g/mol), however reaction times were kept to one minute. While all the catalysts were living, activities were about an order of magnitude less than with **50**/MAO. The role of *N*-aryl fluorination on ethylene polymerization behavior has also been explored. Each of the catalysts **75a-c**/MAO (Figure 1.32) has been shown to be well-behaved for ethylene polymerization at 50 °C and **75a**/MAO and **75b**/MAO produced polymer with narrow molecular weight distributions at reaction times between 1-5 minutes (M_w/M_n ~ 1.05, M_n = 13,000 – 64,000 g/mol).[153,154] Lastly,

Fujita and co-workers reported that $ZnEt_2$ could be used as a chain-transfer agent in the living ethylene polymerization employing **76a**/MAO (Figure 1.32) leading to zinc end-functionalized chains and a titanium species that reinitiates living ethylene polymerization upon the addition of monomer.[155] Despite being living for ethylene polymerization, **76b** was no longer living in the presence of $ZnEt_2$.

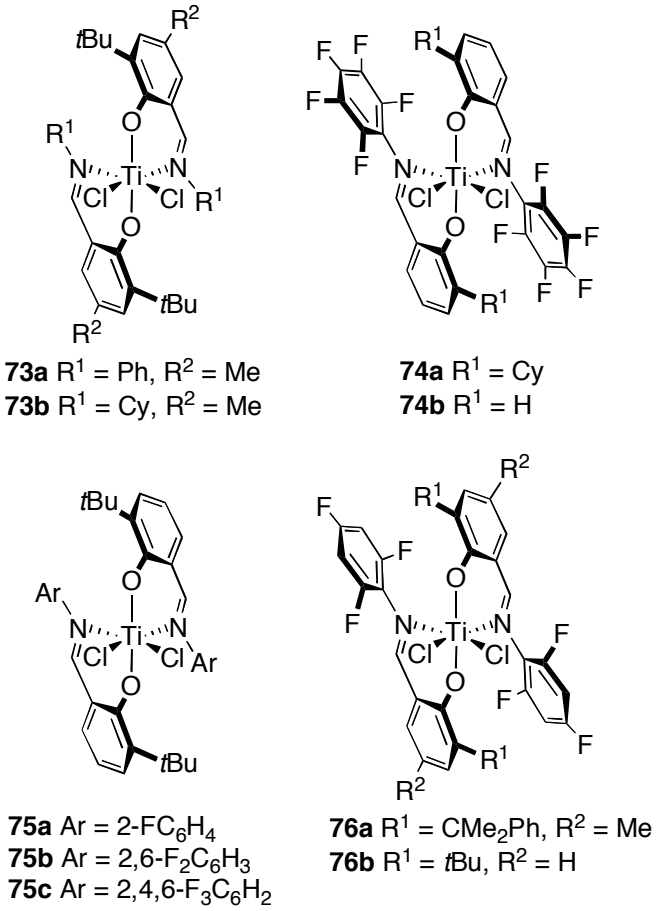

Figure 1.32. Bis(phenoxyimine) titanium catalyst precursors for living ethylene polymerization.

Fujita and co-workers later reported that addition of an equimolar amount of functionalized α-olefin, $H_2C{=}CH(CH_2)_n$-Y (Y = $OAlMe_2$, n = 4 and Y = $OSiMe_3$, n = 9), to **50**/MAO and subsequent living ethylene

polymerization furnished hydroxyl terminated PEs upon acidic workup.[156] This strategy was also successful for the production of hydroxyl terminated syndiotactic PP from **50**/MAO. It was also shown that addition of the aforementioned functionalized α-olefins as a chain end capping agent furnished telechelic syndiotactic PPs bearing hydroxyl groups at both chain ends upon acidic workup.

1.4.3 Bis(phenoxyketimine)titanium Catalysts

Coates and co-workers reported that at 0 and 20 °C, **57a-c**/MAO (Figure 1.33) all produced PE that exhibited a narrow molecular weight distribution ($M_w/M_n \leq 1.08$) and had number average molecular weights (M_n = 15,000 – 47,000 g/mol) that coincided with M_n^{theo}.[126] A linear increase in M_n with polymer yield for the polymerization catalyzed by **57c**/MAO at 0 °C and for **57b**/MAO at 50 °C was demonstrated. A related complex (**77**, Figure 1.33), when activated with MAO at 50 °C, produced PE with M_w/M_n = 1.08 (M_n = 9,000 g/mol).[150]

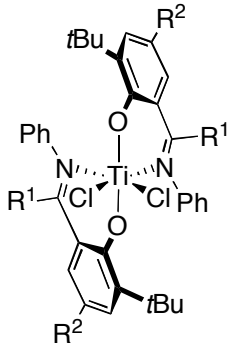

	R^1	R^2
57a	Me	*t*Bu
57b	Et	*t*Bu
57c	Ph	*t*Bu
77	Et	H

Figure 1.33. Bis(phenoxyketimine) titanium catalyst precursors for living ethylene polymerization.

1.4.4 Titanium Indolide-Imine Catalysts

Fujita and co-workers synthesized structurally similar bis(indolide-imine)titanium complexes and evaluated their potential as ethylene polymerization catalysts.[157-161] When activated with MAO at room temperature, compounds **78a-c** (Figure 1.34) furnished PE with narrow molecular weight distributions (M_w/M_n = 1.11 – 1.23) with M_n = 11,000 – ca. 90,000 g/mol. A linear increase of M_n with increasing polymer yield was observed for **78a-c**/MAO at 25 °C. Exhaustive fluorination of the *N*-aryl moiety (**78d**) resulting in living behavior only at -10 °C (M_w/M_n = 1.12 – 1.15), while polymerization at 25 °C led to a broadened molecular weight distribution (M_w/M_n = 1.93).[158,159]

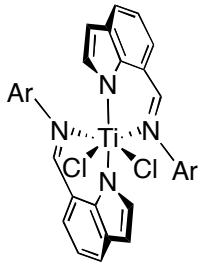

78a Ar = Ph
78b Ar = 2,6-F_2-C_6H_3
78c Ar = 2,4,6-F_3-C_6H_2
78d Ar = C_6F_5

Figure 1.34. Bis(indolide-imine) titanium catalysts.

1.4.5 Bis(enaminoketonato)titanium Catalysts

Li and co-workers reported on the synthesis and ethylene polymerization activity of bis(enaminoketonato)titanium complexes.[162] Upon activation with MMAO at 25 °C, **79a,b** (Figure 1.35) furnish linear PEs with narrow molecular weight distributions (M_w/M_n = 1.25 – 1.45) and M_n = 51,000 g/mol – 129,000 g/mol. A linear increase in M_n with reaction time is observed with **79a**/MMAO at 25 °C. Mecking and co-workers reported *ortho*-

fluorination on the *N*-aryl moiety (**80a**, Figure 1.35) furnished living and thermally robust ethylene polymerization catalysts upon MAO activation.[163] A linear increase in M_n over time was observed at 25, 50, and up to 75 °C. Non-living behavior observed for **80b**/MAO supports the fact that the living behavior of **80a**/MAO is not steric in nature illustrating another example in which *ortho*-fluorination appears beneficial for living polymerization.

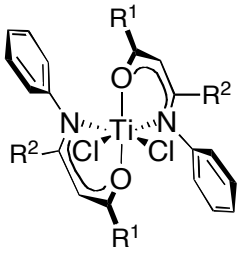

	R^1	R^2
79a	Ph	CF_3
79b	2-thiophenyl	CF_3
79c	2-furanyl	CF_3
79d	CF_3	CH_3
79e	Ph	CH_3

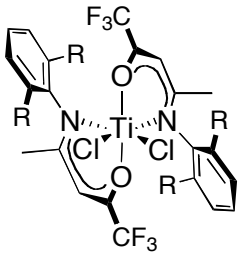

80a R = F
80b R = Me

Figure 1.35. Bis(enaminoketonato) titanium complexes for living olefin polymerization.

1.4.6 Aminopyridinatozirconium Catalysts

Kempe and co-workers have recently described a zirconium catalyst supported by bis(aminopyridinato) ligands (**81**, Figure 1.36) that was living for ethylene polymerization at elevated temperature.[164] Upon activation with $[R_2NMeH][B(C_6F_5)_4]$ ($R = C_{16}H_{33} - C_{18}H_{37}$) in the presence of tetra-(2-phenyl-1-propyl)aluminoxane at 50 °C, **81** furnished linear PE of high molecular weight (M_n = 1,745,000 – 2,301,000 g/mol) and narrow molecular weight distributions (M_w/M_n = 1.26 – 1.30). No evidence for β-H elimination or chain transfer was evident and continued chain growth was observed even after polymer precipitation.

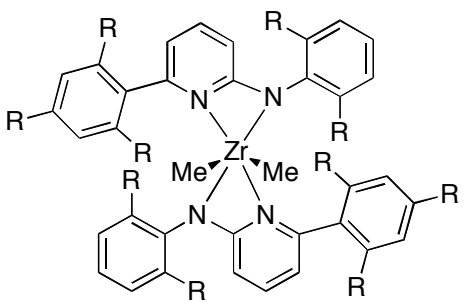

81 R = *i*Pr

Figure 1.36. Bis(aminopyridinato) zirconium complex for living ethylene polymerization.

1.4.7 Tris(pyrazolyl)borate Catalysts

In 2008, Jordan and co-workers described tris(pyrazolyl)borate complexes (**82, 83** Figure 1.37) that displayed characteristics of living ethylene polymerization at low temperatures.[165,166] Upon activation with $[Ph_3C][B(C_6F_5)_4]$ in the presence of 40 equivalents of ethylene at -78 °C, **82** furnished linear PE with M_n = 2,000 g/mol that was in good agreement with M_n^{theo}. No olefinic resonances were observed. Additionally, quenching with Br_2 furnished double-end-capped PE featuring a benzyl group on one polymer chain end and bromine substituent on the opposite polymer chain end. Similar results were obtained with **83**/$[Ph_3C][B(C_6F_5)_4]$ in the presence of 38 equivalents of ethylene at -78 °C, however, observed molecular weights (M_n = 2,800 – 3,800 g/mol) were approximately three times higher than M_n^{theo}. The authors attribute this apparent disparity to incomplete activation of the hafnium complex. In a similar experiment as conducted with **82**/$[Ph_3C][B(C_6F_5)_4]$, double-end-capped polyethylene bearing benzyl and bromine substituents could be synthesized upon bromine quench of **83**/$[Ph_3C][B(C_6F_5)_4]$.

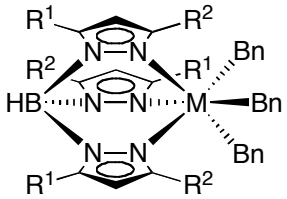

	M	R^1	R^2
82	Zr	Me	Me
83	Hf	H	Ms

Figure 1.37 Tris(pyrazolyl)borate complexes.

1.4.8 Late Transition Metal Catalysts

In 1991, Brookhart and co-workers identified Cp* cobalt complex **84** (Figure 1.38) as a competent catalyst for polymerization of ethylene in a controlled fashion to low molecular weights (M_n = 13,600 g/mol; M_w/M_n = 1.17).[167] Soon thereafter, aryl or silyl groups were introduced in the catalyst framework that prevent chain migration and allow for the production of a variety of end-functionalized PEs under living conditions.[168] Reaction of **85a-e** with ethylene led to the formation of aryl-substituted PEs with quite narrow molecular weight distributions (M_n up to 21,200 g/mol; M_w/M_n = 1.11 – 1.16). Triethylsilane-capped PEs were furnished with catalyst **86** (M_n = 16,100 g/mol; M_w/M_n = 1.15).

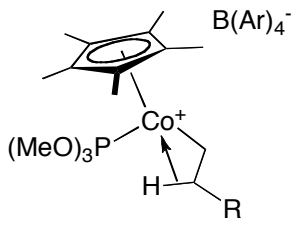

84 R = Me
85a R = C_6H_5
85b R = 4-Cl-C_6H_4
85c R = 4-OAc-C_6H_4
85d R = 4-CF_3-C_6H_4
85e R = C_6F_5
86a R = $(CH_2)_4SiEt_3$
86b R = $(CH_2)_4SiMe_2Cl$

Figure 1.38. Cobalt catalysts for ethylene polymerization.

Brookhart and co-workers demonstrated that specific reaction conditions, particularly quenching reactions with Et_3SiH to prevent chain coupling, were crucial for achieving living polymerizations of ethylene with

palladium catalysts **34a** and **34b** (Figure 1.13).[169] At 5 °C, highly branched (~100 branches / 1000 carbons), amorphous PEs with very narrow molecular weight distributions (M_w/M_n < 1.1) were produced, and M_n was shown to increase linearly over at least 6 hours. At 27 °C, M_n of 237,000 g/mol could be obtained in 2 hours, but the molecular weight distributions broadened (M_w/M_n = 1.19). For **34a**, high pressures of ethylene (400 psig) were required to ensure rapid initiation by displacing the chelated carbonyl group, which is retained in the highly branched PE product. Compound **34b** exhibited similar activity at high pressures, while also yielding polymers with relatively narrow polydispersities (M_w/M_n = 1.15 at 5 °C) at 1 atm ethylene. A telechelic polymer could be produced with **34a** by addition of alkyl acrylates before the silane quench.[68] Acrylates undergo one insertion into the growing chain, forming stable chelates, but do not insert further, allowing for clean end-functionalization to generate polymers with two distinct ester end groups. Additionally, aldehyde end groups could be generated by quenching with 4-penten-1-ol. The vinyl group inserts, followed by Pd migration down the chain, and finally β-hydride elimination to generate the difunctional polymers shown in Scheme 1.5.

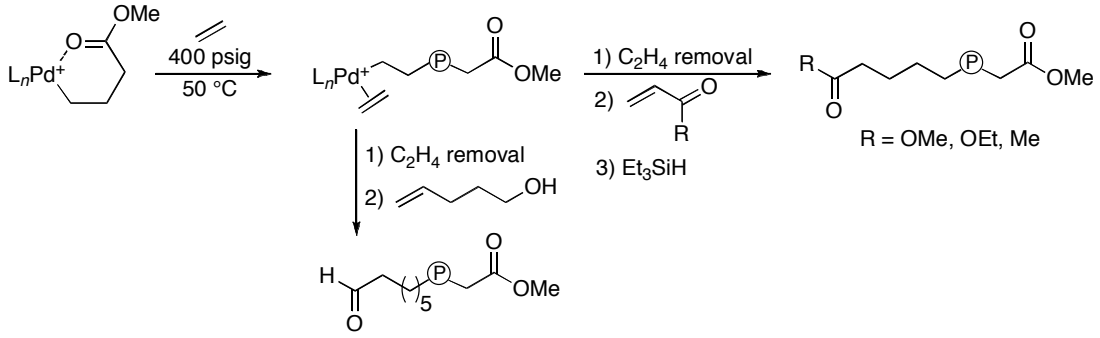

Scheme 1.5. Formation of telechelic polyethylene.

Modification of the palladium ester chelate, **34a**, by immobilization on a polyhedral oligomeric silsesquioxane (POSS) support (**87**, Figure 1.39) by Ye and co-workers furnished POSS end-functionalized PEs.[170] The M_n was shown to increase linearly with time. In a subsequent report, the authors immobilized the palladium ester chelate on silica nanoparticles as a versatile surface-initiated living ethylene polymerization technique for grafting from silica nanoparticles.[171] After cleavage of the PE brushes from the silica nanoparticles, the polymers were found to possess narrow PDIs (M_w/M_n ~ 1.18).

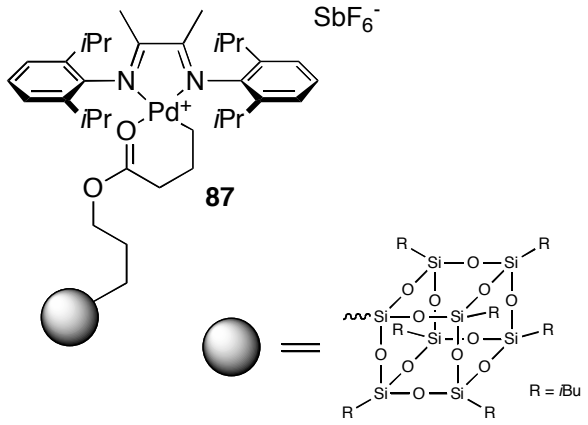

Figure 1.39. Polyhedral oligomeric silsesquioxane supported palladium complex.

First-generation nickel α-diimine catalysts such as **30a** (Figure 1.11) do not polymerize ethylene in a living fashion due to relatively facile chain transfer. Rieger and co-workers have investigated modifications of this framework to prevent chain transfer by enhancing the steric bulk about the metal center.[172] Indeed, when **88** (Figure 1.40) was activated with MAO at

ambient temperature, molecular weight distributions were decreased markedly (M_w/M_n as low as 1.3) for short reaction times and ultra-high molecular weight (> 4,500,000 g/mol), highly linear PE was produced.

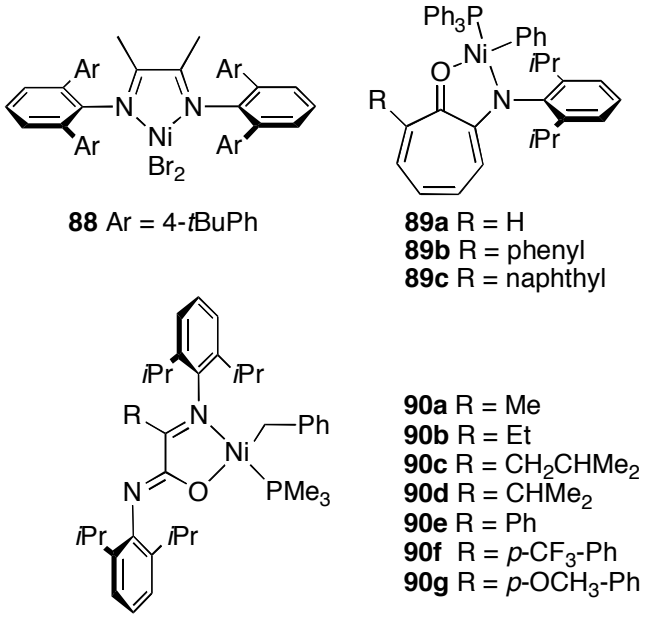

Figure 1.40. Ni complexes for living alkene polymerization.

Guan and co-workers have extended the study of hindered diimine catalysts even further with cyclophane complex **32** (Figure 1.11).[173] When activated with MMAO, **32** is highly active for production of branched PEs (66-97 branches/1000 carbons) with relatively narrow polydispersities (M_w/M_n as low as 1.23 at 50 °C). Most significantly, these catalysts exhibit impressive thermal stability, with good activities even up to 90 °C. However, the polydispersity increases, and the activities decrease somewhat at higher temperatures. Interestingly, a related alkyl cyclophane Ni complex demonstrated almost no activity for ethylene polymerization.[174]

In addition to living 1-hexene and propylene polymerization, Bazan and co-workers have shown that **36**/MAO (Figure 1.11) is also living for ethylene polymerization.[72] At 10 °C, this catalyst produces branched PE (19 branches/1000 carbons) with M_n = 260,000 g/mol and M_w/M_n = 1.1. At 32 °C, high molecular weight (M_n = 1,112,000 g/mol) branched PE (47 branches/1000 carbons) is obtained with a slightly broadened polydispersity (M_w/M_n = 1.3). Importantly, introduction of the carbonyl functionality in **36** leads to an increase in activity of approximately two orders of magnitude for ethylene polymerization over the analogous β-diimine catalyst with no carbonyl functionality. The increase in reactivity was attributed as a result of attachment of a Lewis acid (from the aluminum cocatalyst) to the exocyclic oxygen site on the propagating cationic species.

Brookhart and co-workers have investigated a series of anilinotropone based nickel catalysts **89a-c.**[175] With activation by $Ni(COD)_2$, high activities, and long lifetimes were observed, particularly in the aryl-substituted cases, **89b** and **89c** (Figure 1.40). The M_n was shown to increase in nearly linear fashion with time. PDIs were relatively narrow (as low as 1.2 at room temperature), but increased at higher temperatures and with longer reaction times.

Finally, Bazan and co-workers have investigated nickel diimine variants **90a-g** (Figure 1.40).[176,177] With $Ni(COD)_2$ as the activator, M_n increased linearly with time up to 30 minutes at 20 °C with **90a**, producing PE with low branching (12 – 19 methyl branches/1000 carbons). As the bulk of the ligand framework increases, an increase in activity is observed. The molecular weight distributions remained narrow for all the catalysts studied (M_w/M_n = 1.1 – 1.4).

1.5 Living Non-Conjugated Diene Polymerization

Non-conjugated dienes are versatile monomers in that they can furnish polymers with a variety of microstructures depending on the mechanism by which they are polymerized. For example, 1,5-hexadiene can be cyclopolymerized to furnish a polymer with methylene-1,3-cyclopentane (MCP) units (Figure 1.41). Depending on the selectivity of the ring closing reaction, *cis*- or *trans*-rings may be formed. Polymers containing mostly *cis*-rings exhibit higher T_m values than those with mostly *trans*-rings (e.g. for poly(methylene-1,3-cyclopentane) (PMCP) having > 90% *cis*-ring content the T_m is 189 °C whereas those containing mostly *trans*-rings are waxy materials with $T_m \leq 70$ °C).[178] Polymerization of 1,5-hexadiene can also lead to vinyl-tetramethylene (VTM) units, which may serve as a synthetic handle by which polymer functionalization can be achieved.[179]

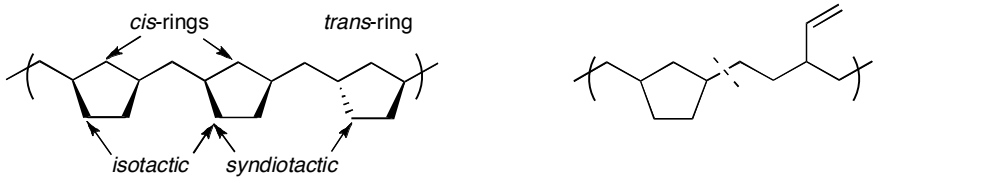

Poly(methylene-1,3-cyclopentane)
PMCP

Poly(methylene-1,3-cyclopentane-*co*-3-vinyltetramethylene)
Poly(MCP-*co*-3-VTM)

Figure 1.41. Polymer structures derived from polymerization of 1,5-hexadiene.

1.5.1 Vanadium Acetylacetonoate Catalysts

In addition to living propylene polymerization, vanadium acetylacetonate complexes (Figure 1.15) have also been shown to be living for 1,5-hexadiene polymerization as well as for 1,5-hexadiene/propylene copolymerization.[180] At -78 °C, **37**/Et_2AlCl polymerized 1,5-hexadiene to produce a low molecular weight polymer (M_n = 6,600 g/mol, M_w/M_n = 1.4)

that contained a mixture of MCP and VTM units in a 54:46 ratio. The distribution of these two units varied in 1,5-hexadiene-propylene random copolymers as a function of 1,5-hexadiene incorporation.

1.5.2 Bis(phenoxyimine)titanium Catalysts

Coates and co-workers later reported that bis(phenoxyimine) titanium complex **49** (Figure 1.17) was also capable of living 1,5-hexadiene polymerization and 1,5-hexadiene/propylene copolymerization.[181] Homopolymerization of 1,5-hexadiene with **49**/MAO at 0 °C produced a high molecular weight polymer with a narrow PDI (M_n = 268,000 g/mol, M_w/M_n = 1.27). The polymer showed the presence of two distinct units – the expected MCP units as well as 3-vinyl tetramethylene (3-VTM) units. As shown in Scheme 1.6, the MCP units are proposed to arise from 1,2-insertion of 1,5-hexadiene followed by a 1,2-cyclization. However, an initial 2,1-insertion of 1,5-hexadiene followed by a 1,2-cyclization forms a strained cyclobutane

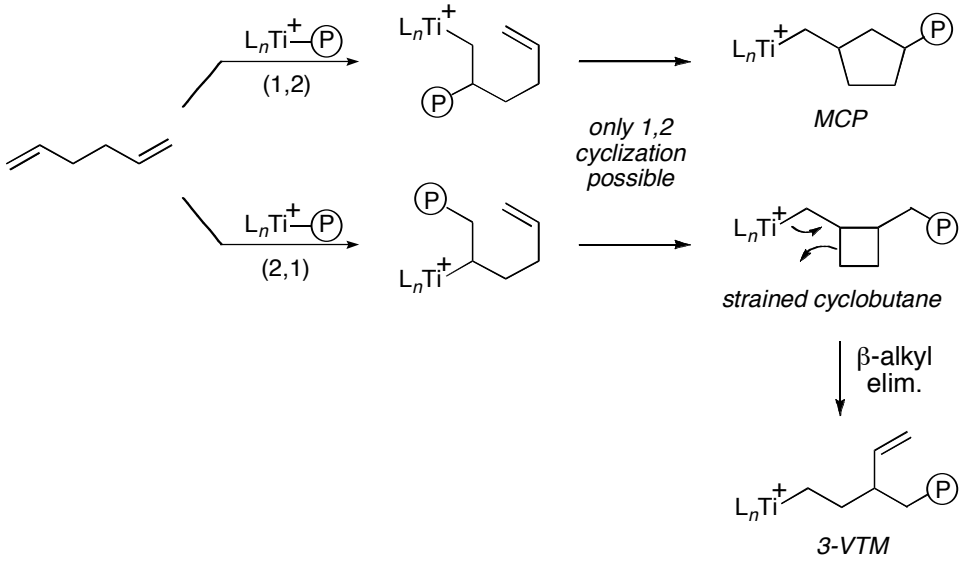

Scheme 1.6. Polymerization of 1,5-hexadiene with **49**/MAO.

species. After a β-alkyl elimination, the 3-VTM unit is generated. Propylene/1,5-hexadiene copolymers with high molecular weights were also produced (M_n = 119,000 – 145,000 g/mol, M_w/M_n = 1.09 – 1.16).

1.5.3 Cyclopentadienyl Acetamidinate Zirconium Catalysts

In 2000, Sita and co-workers showed that **19a-c**/[$PhNMe_2H$][$B(C_6F_5)_4$] (Figure 1.7) were active for the cyclopolymerization of 1,5-hexadiene at -10 °C.[182] The polymers produced possessed ≥ 98 % MCP units, and exhibited narrow polydispersities (M_w/M_n = 1.03 – 1.09). The selectivity of ring-closure was ubiquitously *trans*; the stereoselectivity increasing with increasing steric bulk of the amidinate ligand (**21a**: % *trans* = 64; **21c**: % *trans* = 82).

1.5.4 Late Transition Metal Catalysts

In 2006, Osakada and co-workers reported the polymerization of a number of 1,6-dienes catalyzed by palladium complexes to afford polymers with *trans*-1,2-disubstituted five-membered rings.[183] In a subsequent report, living polymerization of 5-allyl-5-crotyl-2,2-dimethyl-1,3-dioxane with

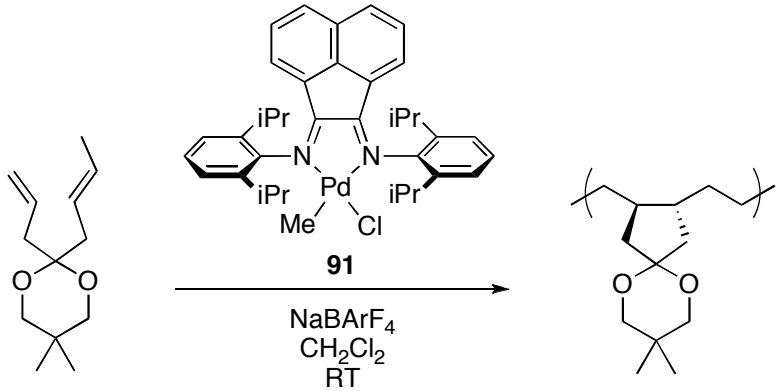

Scheme 1.7. Polymerization of 5-allyl-5-crotyl-2,2-dimethyl-1,3-dioxane with **91**/$NaBArF_4$.

91/$NaBArF_4$ was shown (Scheme 1.7).[184] A linear increase in M_n with monomer conversion was demonstrated with molecular weight distributions remaining relatively narrow (M_w/M_n = 1.20 – 1.24).

1.6 Living Homo- and Copolymerizations of Cyclic Olefins

Homopolymers of cyclic olefins (e.g. polycyclopentene, polynorbornene (PNB), Figure 1.42) are characterized by extremely high melting points and low solubility in most organic solvents. Taken together, these properties of cyclic olefin homopolymers make them difficult to process and therefore commercially insignificant. However, upon incorporation into copolymers with α-olefins, materials with desirable properties can be obtained. The copolymers typically exhibit high chemical resistance, good optical properties, and facile processability.[185]

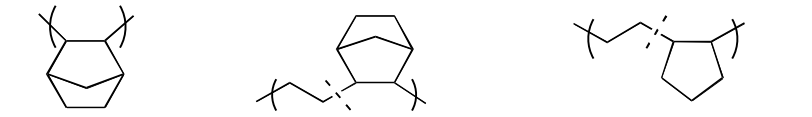

Figure 1.42. Homopolymers and copolymers of cyclic olefins.

1.6.1 Norbornene Homopolymerization

Risse has reported on the polymerization of norbornene (NB) in a controlled fashion with catalyst **92**, $[Pd(MeCN)][BF_4]_2$, obtaining saturated polymers.[186] Renewed chain growth was observed with sequential addition of monomer, but only for low conversion. At 0 °C, narrow molecular weight distributions were obtained for short reaction times (t_{rxn}= 20 minutes; 54% conversion; M_n = 21,400 g/mol; M_w/M_n = 1.07), but broadened as conversion

increased (M_w/M_n = 1.34 at 100% conversion). Ester-functionalized norbornenes were also shown to polymerize with living fashion.[187]

Shiono and co-workers reported that activation of **43** (Figure 1.16) with dMMAO containing 0.4 mol % of triisobutylaluminum (TIBA) in the presence of norbornene catalyzed living polymerization at 20 °C.[188] The molecular weight distributions obtained were narrow (M_w/M_n = 1.07 – 1.08). A two stage reaction was shown to increase the molecular weight of the second-step by double that of the first step when each was carried to quantitative conversion.

1.6.2 Copolymers of Norbornene/Ethylene and Cyclopentene/Ethylene

1.6.2.1 Non-Group 4 Early Transition Metal Catalysts

In addition to living ethylene polymerization, the ability of **67**/Et_2AlCl to catalyze the quasi-living copolymerization of ethylene and norbornene was also reported.[143] Poly(E-*co*-NB) with 5.1 – 39.9 mol% norbornene content was obtained from **67**/Et_2AlCl at 0 °C. The polymers exhibited narrow molecular weight distributions (M_w/M_n = 1.29 – 1.73) and high molecular weights (M_n = 327,000 – 2,570,000 g/mol).

Tritto and co-workers have recently described the copolymerization of ethylene with norbornene catalyzed by rare-earth metal half sandwich complexes **93a-d** (Figure 1.43).[189] Upon activation with $[Ph_3C][B(C_6F_5)_4]$, **93a,b** showed excellent activities, whereas **93d** was inactive. Furthermore, **93b**/$[Ph_3C][B(C_6F_5)_4]$ furnished poly(E-*co*-NB) with 29 – 42 mol% norbornene content and a linear increase in M_n with time while maintaining a narrow PDI (M_w/M_n = 1.22 – 1.35).

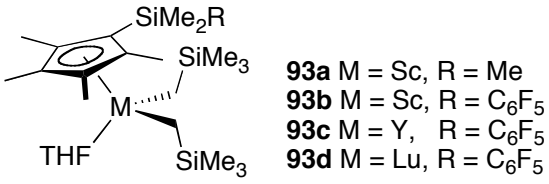

Figure 1.43. Rare-earth metal half-sandwich compounds.

1.6.2.2 Group 4 Metallocene Based Catalysts

Catalyst **2**/MAO (Figure 1.2) can also be used for the living copolymerization of ethylene and norbornene. For example, at 0 °C **2**/MAO can furnish poly(E-*co*-NB) with 53 mol% norbornene and M_n = 78,000 g/mol with M_w/M_n = 1.16.[190] In addition, a linear increase in M_n with reaction time was observed for this system. When activated with MAO at 40 °C, a similar compound, **45** (Figure 1.16), also provided ethylene-norbornene copolymers with fairly narrow PDIs (M_w/M_n = 1.21 – 1.27).[191]

Shiono and co-workers also reported the living copolymerization of propylene and norbornene with **2**/dMAO (Figure 1.2) to produce copolymers with very high T_g values (249 °C) and narrow molecular weight distributions (M_w/M_n = 1.16).[192] In a subsequent report, the copolymerization of higher α-olefins (1-hexene, 1-octene, and 1-decene) with norbornene by **2**/MAO was reported, however, molecular weight distributions were somewhat broadened (M_w/M_n = 1.36 – 1.72).[193]

Lastly, Tritto and co-workers have shown that *rac*-Et(Ind$_2$)ZrCl$_2$/MAO (**94**), 90 % *rac*/10 % *meso*-Et(4,7-Me$_2$Ind)$_2$ZrCl$_2$ (**95**), and *rac*-H$_2$C(3-*t*BuInd)$_2$ZrCl$_2$/MAO (**96**) exhibit quasi-living behavior for ethylene-norbornene copolymerization (Figure 1.44).[194,195]

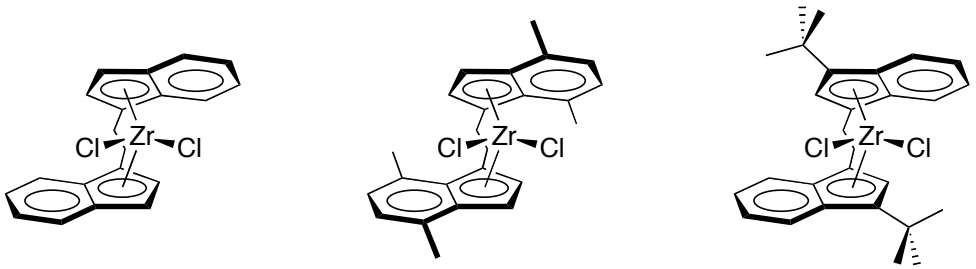

94 ***rac*-95** **96**

Figure 1.44. Zirconocene precatalysts for living ethylene/norbornene copolymerization.

1.6.2.3 Titanium Catalysts for Living Ethylene-Cyclic Olefin Copolymerization

Bis(pyrrolide-imine)titanium complexes were initially reported by Fujita and co-workers in 2000 for ethylene polymerization, however living behavior was not observed.[196] Fujita and co-workers turned their attention to the copolymerization of ethylene and norbornene.[197-199] When activated with MAO at 25 °C, **97a-d** (Figure 1.45) furnished poly(E-*alt*-NB) with narrow molecular weight distributions and high molecular weights (M_w/M_n = 1.10 – 1.24, M_n = 127,000 – 600,000 g/mol). A linear increase of M_n with time over the course of 20 minutes was observed. The copolymers were found to contain 95.4% perfectly alternating units. The polymer chain-end structures were

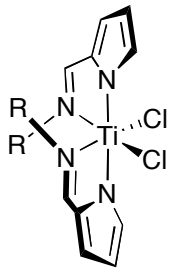

97a R = Ph
97b R = Cy
97c R = Cyclooctyl
97d R = 4-*t*Bu-Cy

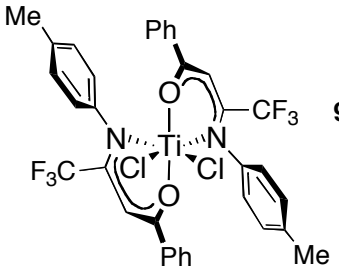

98

Figure 1.45. Bis(pyrrolide-imine) and bis(enaminoketonato) titanium catalysts.

consistent with chain initiation by insertion of norbornene into the Ti-Me bond, and a last inserted norbornene unit after termination by protonolysis. This suggests norbornene plays a stabilizing role for the active species against termination processes.

The copolymerization of ethylene and norbornene by **79a-d**/MMAO (Figure 1.35) was also shown to possess some characteristics of a living polymerization.[162] The polymers obtained from polymerizations conducted at 25 °C exhibited narrow molecular weight distributions (M_w/M_n = 1.07 – 1.54) with M_n = ca. 150,000 – 580,000 g/mol. The norbornene content ranged from 35.3 – 55.4 mol%. A linear increase in M_n with reaction time was demonstrated for **79a**/MMAO at 25 °C over the course of 20 minutes. In a subsequent report Li and co-workers discussed the effects of further ligand modifications on the copolymerization behavior of bis(enaminoketonato)titanium catalysts.[200] At 25 °C, **98**/MMAO (Figure 1.45) produced poly(E-*co*-NB) with narrow polydispersities (M_w/M_n = 1.18 – 1.31, M_n = ca. 200,000 – 570,000 g/mol) and norbornene content ranging from 44.6 – 47.8 mol%. The polymerization displayed a linear increase of M_n with time from t = 5 – 20 minutes. The copolymerization of ethylene and cyclopentene (CP) by **79a**/MMAO and **79d**/MMAO was also shown to possess some characteristics of living behavior.[201] Poly(E-*co*-CP)s with narrow molecular weight distributions (M_w/M_n = 1.23 – 1.82) were produced at temperatures from -10 – 30 °C.

1.6.2.4 Palladium a-Diimine Catalysts

Kaminsky and Kiesewetter applied a combinatorial screening approach to identify catalysts for the copolymerization of norbornene with ethylene.[202] Catalysts **99a** and **99b** (Figure 1.46) were identified and furnished poly(E-*co*-

NB) with 9-62 mol% norbornene incorporation and relatively narrow molecular weight distributions (M_w/M_n as low as 1.4) indicating "quasi-living" behavior.

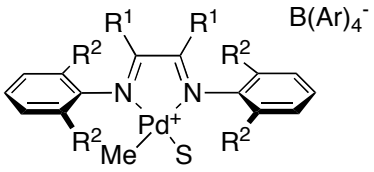

99a R^1 = H, R^2 = Me, S = CH_3CN
99b R^1 = Me, R^2 = *i*Pr, S = CH_3CN

Figure 1.46. Palladium catalysts for ethylene/norbornene copolymerization.

1.7 Random Copolymers

1.7.1 Random Copolymers Incorporating Polar Monomers

Copolymers of polar monomers with olefins are attractive due to enhanced physical properties such as biocompatibility and ease of processing.[203] Coates and co-workers synthesized polyolefin elastomers by addition of small amounts of ureidopyrimidone (UP) functionalized hexene to polymerizations of 1-hexene.[204] Nickel catalyst **30a**/Et_2AlCl (Figure 1.11) was used, exploiting the dual ability of Et_2AlCl to activate the nickel center and to protect the Lewis basic nitrogen functional groups. Polymers incorporating ~2% UP-functionalized monomer were obtained with narrow molecular weight distributions (M_w/M_n = 1.2 – 1.4). The polymers obtained exhibited reversible, non-covalent crosslinking through hydrogen bonding interactions, and thus have elastomeric properties at room temperature.

Bazan has achieved the first quasi-living copolymerization of ethylene with a polar monomer, 5-norbornen-2-yl acetate.[176,177] Upon activation with

$Ni(COD)_2$, **90a-g** (Figure 1.40) incorporated 1-17 mol% 5-norbornen-2-yl acetate into a polyethylene backbone. Molecular weight distributions were relatively narrow (M_w/M_n = 1.2 – 1.6), and the M_n exhibited a nearly linear increase with conversion.

1.8 Block Copolymers

By far, the most important application of living olefin polymerization is the production of block copolymers, which is typically achieved via sequential monomer addition furnishing a near limitless number of materials. Physical blends, or random copolymers often give rise to materials whose properties are intermediate between those of the respective homopolymers. Block copolymers, on the other hand, often furnish materials whose mechanical properties are superior to the sum of their parts. This unique behavior is due to microphase separation of the different segments of the block copolymer into discrete domains which give rise to otherwise unattainable morphologies.[205,206] One of the most highly sought goals in the field of olefin polymerization is the synthesis of block copolymers containing *i*PP domains that are envisioned to possess material properties of great industrial importance. For example diblock copolymers containing *i*PP segments may serve as compatibilizers in blends containing *i*PP homopolymers.[71] One of the most actively pursued block copolymer structures are those with "hard" or semicrystalline end blocks (e.g. PE, *i*PP, *s*PP) and amorphous midblocks (e.g. *a*PP, poly(E-*co*-P)); triblock copolymers of this type have been shown to behave as thermoplastic elastomers.[127,130,139,207-211]

1.8.1 Block Copolymers Containing Poly(α-olefin) Blocks

There are numerous catalysts which have been employed to prepare block copolymers containing poly(α-olefin) blocks; they are listed in Table 1.1. In a previous section, living 1-hexene polymerization with **5**/$B(C_6F_5)_3$ (Figure 1.3) was discussed. Kim and co-workers further prepared a block copolymer of 1-hexene and 1-octene via sequential monomer addition.[25] The polymer produced at 0 °C possessed a narrow polydispersity (M_w/M_n = 1.21) and a M_n = 108,730 g/mol.

Table 1.1. Block alkene copolymers.

Entry	Block Copolymer	Catalyst Precursor(s) Used
1	PH-*block*-PO	**5, 14, 15a, 19b**
2	poly(VCH)-*block*-PH-*block*-poly(VCH)	**22c**
3	PE-*block*-poly(E-*co*-H)	**52b**
4	PE-*block*-POD	**34b**
5	PP-*block*-PH, PP-*block*-PH (chain straightened)	**30a,b**
6	PH-*block*-poly(P-*co*-H)-*block*-PH	**30b**
7	POD-*block*-poly(P-*co*-OD)-*block*-POD	**31**
8	PH/PE *multiblock* copolymer	**30a**

PH = poly(1-hexene), PO = poly(1-octene), VCH = vinylcyclohexane, PE = polyethylene, E = ethylene, H = 1-hexene, POD = poly(1-octadecene), PP = polypropylene, P = propylene

Living homopolymerizations of 1-hexene catalyzed by amine bis(phenolate)titanium complexes were discussed in a previous section of this

review. Kol and co-workers were also able to apply this class of catalyst to the synthesis of block copolymers of 1-hexene and 1-octene.[39,42] Using **14**/$B(C_6F_5)_3$ (Figure 1.5) a block copolymer of 1-hexene and 1-octene was prepared via sequential monomer addition where each domain had an atactic microstructure. The polymer possessed a narrow molecular weight distribution (M_w/M_n = 1.2) and a M_n = 11,600 g/mol. The extremely long-lived catalyst generated from **15a** (Figure 1.5) was also used to prepare a block copolymer of 1-hexene and 1-octene through sequential monomer addition to furnish poly(1-hexene)-*block*-poly(1-octene). The block copolymer had M_n = 34,000 g/mol while maintaining the low M_w/M_n = 1.16.

The 1-hexene and vinylcyclohexane (VCH) homopolymerization behavior of **22c**/$[Ph_3C][B(C_6F_5)_4]$ (Figure 1.7) was discussed in a previous section of this review. Sita and co-workers were able to exploit the living nature of this catalyst to prepare a triblock copolymer of isotactic poly(vinylcyclohexane)-*block*-atactic poly(1-hexene)-*block*-isotactic poly(vinylcyclohexane) via sequential monomer addition.[50] The triblock copolymer exhibited a narrow polydispersity (M_w/M_n = 1.08) and M_n = 24,400 g/mol with a vinylcyclohexane content of 33 mol%.

Having shown that **50, 52b, 74a,b** /MAO (Figures 1.17, 1.18, and 1.32) were living for ethylene polymerization, Fujita and co-workers investigated the ability of these catalysts to produce ethylene/α-olefin copolymers in a living fashion.[152] Copolymerizations with ethylene and either 1-hexene, 1-octene, or 1-decene were carried out with each catalyst at 25 °C. In all cases, polymers exhibiting narrow molecular weight distributions were obtained ($M_w/M_n \leq 1.22$). Increased α-olefin incorporation correlated with decreased *ortho* substituent bulk. A series of PE-*block*-poly(E-*co*-1-hexene) samples was

produced using **52b**/MAO via sequential monomer addition. Molecular weight distributions for the block copolymers were generally low (M_w/M_n = 1.11 – 1.31 for M_n up to 121,000 g/mol) and 1-hexene contents of up to 28.9 mol% were estimated.

As previously discussed, **19b**/[$PhNMe_2H$][$B(C_6F_5)_4$] polymerizes 1-hexene in a living manner to produce highly isotactic poly(1-hexene) with [*mmmm*] > 0.95. However, when a sub-stoichiometric amount of the borate is used (e.g. [$PhNMe_2H$][$B(C_6F_5)_4$] : [**19b**] = 0.5), the resulting polymer is considerably less isotactic with a [*mm*] content of approximately 45 – 50% resulting from degenerative-transfer polymerization (Scheme 1.4). This system has been employed to make a diblock poly(α-olefin) sample.[131] Initially, **19b** was activated with 0.5 equivalent of [$PhNMe_2H$][$B(C_6F_5)_4$] and used to polymerize 1-hexene resulting in the formation of an atactic poly(1-hexene) block. After 2 hours, 1-octene was added along with an additional 0.5 equivalent of the borate leading to the growth of an isotactic poly(1-octene) block. GPC analysis revealed clean formation of the *a*PH-*block*-*i*-poly(1-octene) diblock copolymer with M_n = 12,400 g/mol and M_w/M_n = 1.04.

Brookhart and co-workers demonstrated the living nature of nickel catalysts **30a** and **31** (Figure 1.11) with the synthesis of well-defined di- and tri-block copolymers of α-olefins.[62] Activation of **30a** with MAO at -15 °C, followed by sequential addition of monomers afforded PP-*block*-poly(1-hexene) with monomodal, narrow molecular weight distributions (M_w/M_n = 1.11 – 1.13), which exhibited less branching than predicted, due to partial chain-straightening. Further, triblocks were prepared by activation of **30a** or **31** with MMAO at -10 °C, followed by reaction with 1-octadecene to afford a semicrystalline, chain-straightened block as observed in

homopolymerizations with that monomer. Sequential addition of propylene led to the formation of an amorphous block of poly(1-octadecene)-*co*-PP, which was followed by formation of a third block of poly(1-octadecene) as propylene was removed (Scheme 1.8). The resultant materials exhibited elastomeric properties as expected based on the "hard-soft-hard" triblock structure of the polymers.

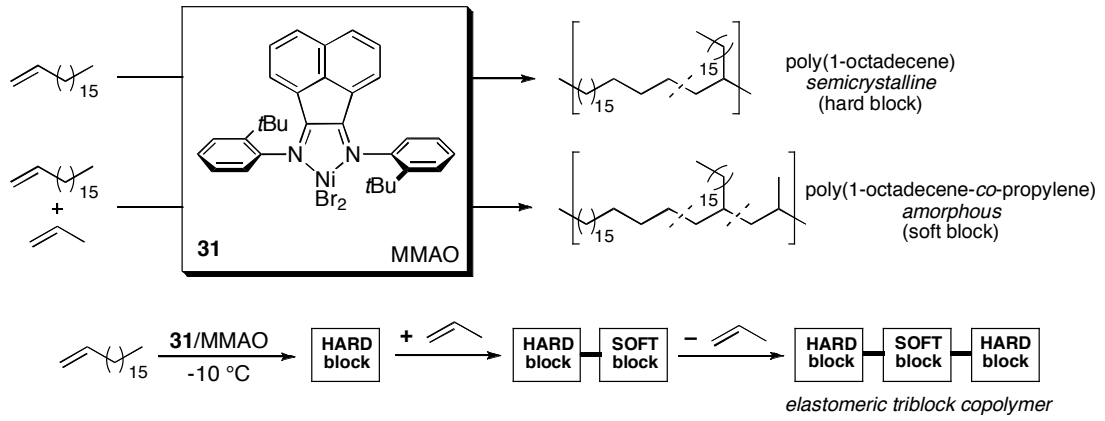

Scheme 1.8. Synthesis of elastomeric triblock copolymers from 1-octadecene and propylene using **31**/MMAO.

Given that palladium diimine catalysts produce highly branched, amorphous materials with ethylene, and produce semicrystalline polymers from long chain α-olefins via a "chain straightening" mechanism, copolymers containing these two segments are an attractive goal. Gottfried and Brookhart investigated this block copolymer synthesis in detail.[68] Block copolymers of ethylene and 1-octadecene were prepared with **34b** (Figure 1.13) by opposite orders of addition to furnish PE-*block*-poly(1-octadecene) and poly(1-octadecene)-*block*-PE. In all cases, materials with narrow molecular weight distributions were obtained (M_w/M_n = 1.06 – 1.22). The copolymer

microstructures differed depending on the order of introduction of the blocks. The most obvious difference between the two structures is that, when ethylene is introduced first, the number of ethyl and propyl branches decreases substantially relative to the case where 1-octadecene is added first.

Marques and Gomes exploited the living nature of **30b** (Figure 1.11) for the production of di- and triblock copolymers.[65] When activated with MAO, **30b** polymerized propylene at -15 °C, generating a syndio-rich polypropylene block, followed by removal of excess monomer under vacuum. Addition of 1-hexene at the same temperature generated a diblock copolymer with M_w/M_n = 1.18 and M_n = 46,400 g/mol. Triblocks were also produced with this catalyst. Polymerization of 1-hexene first, followed by introduction of propylene (with 1-hexene still present), followed by venting and then allowing the residual 1-hexene to react allowed for formation of a shorter (M_n = 31,100 g/mol) ABA triblock copolymer, with the middle block composed of poly(propylene-*ran*-(1-hexene)).

1.8.2 Block Copolymers Containing Polypropylene Blocks

1.8.2.1 Isotactic Polypropylene-Containing Block Copolymers

The catalysts that have been used to prepare PP-based block copolymers are listed in Table 4.2. Until recently, methods of preparing *i*PP in a living manner have been elusive.[125,127,130,137-139] Busico and co-workers reported in 2003 the preparation of a diblock copolymer of *i*PP and PE using Kol's diamino bis(phenolate)zirconium catalyst (**13a**, Figure 1.5) under "quasi-living" conditions.[212] Using **13a**/[$PhNMe_2H$][$B(C_6F_5)_4$] with 2,6-di-*tert*-butylphenol modified Al(*i*Bu)$_3$ as scavenger, a diblock copolymer of ethylene and propylene was prepared by sequential monomer addition of ethylene (1.5

minutes) and propylene (20 minutes). The resultant copolymer possessed a narrow polydispersity (M_w/M_n as low as 1.2 when M_n = 6,500 g/mol).

Table 1.2. Block copolymers based on propylene.

Entry	Block Copolymer	Catalyst Precursor(s) Used
1	*i*PP-*block*-PE	**13a, 60a**
2	*a*PP-*block*-*i*PP-*block*-*a*PP-*block*-*i*PP	**19b/100**
3	*i*PP-*block*-poly(E-*co*-P)	**58c, 59k**
4	*i*PP-*block*-poly(E-*co*-P)-*block*-*i*PP-*block*-poly(E-*co*-P)-*block*-*i*PP-*block*-poly(E-*co*-P)-*block*-*i*PP	**59k**
5	*s*PP-*block*-poly(E-*co*-P)	**49, 50**
6	*s*PP-*block*-poly(E-*co*-P)-*block*-*s*PP	**37, 49**
7	*s*PP-*block*-*a*PP-*block*-*s*PP	**2**
8	PE-*block*-poly(E-*co*-P)-*block*-*s*PP	**50**
9	*a*PP-*block*-PE	**41, 80a**
10	*a*PP-*block*-poly(E-*co*-P)	**40, 41, 101**
11	*i*PP-*block*-*rir*PP-*block*-*i*PP-*rir*PP-*block*-*i*PP	**35, 64f**

*i*PP = isotactic polypropylene, PE = polyethylene, *a*PP = atactic polypropylene, E = ethylene, P = propylene, *s*PP = syndiotactic polypropylene, *rir*PP = regioirregular polypropylene

Characterization of the copolymer by ^{13}C NMR spectroscopy and DSC was consistent with a block structure. These results represented the first synthesis

of an *i*PP-*block*-PE copolymer via sequential monomer addition at polymerization durations greater than one minute. In a subsequent report, **60a** (Figure 1.24) was employed under the same conditions to furnish *i*PP-*block*-PE with a higher molecular weight (M_n = 22,000 g/mol, M_w/M_n = 1.3) and T_m of the *i*PP block (152 °C).[129]

The living degenerative transfer system that was employed by Sita and co-workers to make block copolymers from 1-hexene and 1-octene was later applied to propylene polymerization.[130] Formation of a PP diblock copolymer with **19b**/[PhNMe$_2$H][B(C$_6$F$_5$)$_4$] was accomplished by first activation with 0.5 equivalents of [PhNMe$_2$H][B(C$_6$F$_5$)$_4$] furnishing an atactic PP segment followed by complete activation with another 0.5 equivalents of [PhNMe$_2$H][B(C$_6$F$_5$)$_4$] to furnish the *a*PP-*block*-*i*PP. It was found that related complex **100** could effectively reinvoke degenerative-transfer by *irreversibly* transferring a methyl group to the active polymerization species. In addition to synthesizing an *a*PP-*block*-*i*PP diblock copolymer, an *a*PP-*block*-*i*PP-*block*-*a*PP triblock and an *a*PP-*block*-*i*PP-*block*-*a*PP-*block*-*i*PP tetrablock sample were formed (Scheme 1.9). The polymers had very similar molecular weights (M_n =

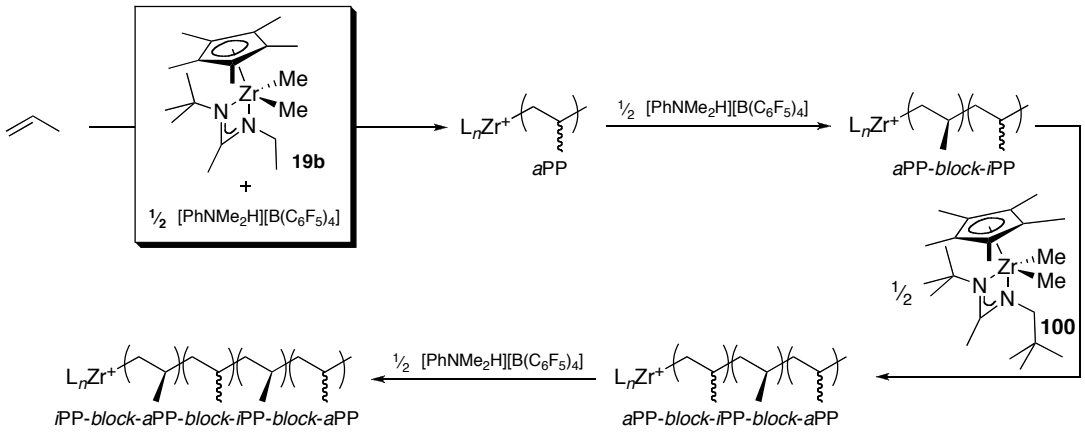

Scheme 1.9. Synthesis of elastomeric propylene-based stereoblock copolymers using **19b** and **100**.

164,200 – 172,400 g/mol, M_w/M_n = 1.19). Testing of the tensile properties of the block copolymers showed good elastomeric behavior. For example, the triblock copolymer displayed an elongation to break of 1530%, the highest of the three samples.

Further exemplifying the living nature of **58c**/MAO (Figure 1.22) for partially isospecific propylene polymerization, an *i*PP-*block*-poly(E-*co*-P) sample was produced with this catalyst.[125] After polymerization of propylene to form an *i*PP block of M_n = 28,100 g/mol (M_w/M_n = 1.10) ethylene was added to the reaction yielding a diblock copolymer with M_n = 62,000 g/mol and M_w/M_n = 1.10. In a subsequent report, Coates and co-workers synthesized block copolymers containing *i*PP blocks of higher tacticity with **59k**/MAO (Figure 1.22) via sequential monomer addition.[127] Specifically, an iPP-*block*-poly(E-*co*-P)-*block*-iPP, iPP-*block*-poly(E-*co*-P)-*block*-iPP-*block*-poly(E-*co*-P)-*block*-iPP, and iPP-*block*-poly(E-*co*-P)-*block*-iPP-*block*-poly(E-*co*-P)-*block*-iPP-*block*-poly(E-*co*-P)-*block*-iPP copolymer were prepared. The polymers had narrow molecular weight distributions (M_w/M_n = 1.13 – 1.30) and high molecular weights (M_n = 102,000 – 235,000 g/mol). Testing of the tensile properties of the block copolymers showed good elastomeric behavior with the triblock copolymer displaying an elongation to break of 1000%.

A strategy for the living formation of block copolymers with one monomer, simply by varying reaction temperature, was recently described by Coates and co-workers.[138] As previously described, catalyst **35** (Figure 1.11) polymerizes propylene with high isoselectivity and regioregularity at low temperatures. At higher temperatures regioirregular, amorphous polypropylene is generated. It was reported that **35**/MAO was used to synthesize regioblock PPs having good elastomeric properties.[211] Both a

triblock and pentablock copolymer were synthesized by simply varying the reaction temperature during the course of the polymerization (Scheme 1.10). For example, an *i*PP-*block*-*rir*PP-*block*-*i*PP (M_n = 109,000 g/mol, M_w/M_n = 1.14) and *i*PP-*block*-*rir*PP-*block*-*i*PP-*block*-*rir*PP-*block*-*i*PP (M_n = 159,000 g/mol, M_w/M_n = 1.39) pentablock copolymer were prepared by toggling the reaction temperature between -60 and 0 °C. Transmission Electron Microscopy (TEM) revealed no microphase separation. However, the pentablock copolymer exhibited an exceptional strain to break of 2400% and good elastomeric recovery out to strains of 1000%. In a subsequent report, similar regioblock polypropylenes were produced with **64f**/MAO (Figure 1.27) that exhibited improved elastomeric performance at elevated temperatures (e.g., 65 °C) over block copolymers synthesized with **35**/MAO.[139]

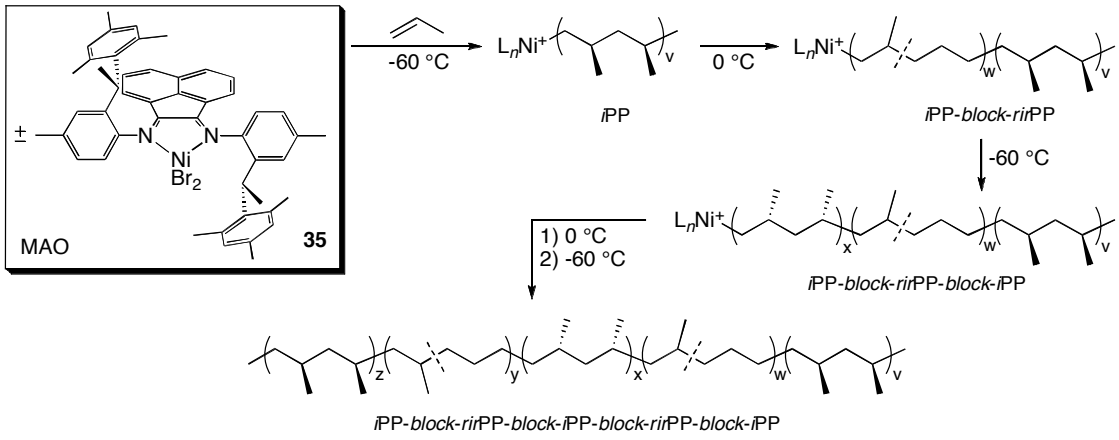

Scheme 1.10. Synthesis of elastomeric propylene-based regioblock copolymers using **35**/MAO.

1.8.2.2 Syndiotactic Polypropylene Containing Block Copolymers

After the seminal report of living propylene polymerization catalyzed by **37**/Et_2AlCl (Figure 1.15)[76,77] and discovering the activating effect of

anisole,[78] Doi and co-workers applied this catalyst system to the synthesis of block copolymers of propylene and ethylene.[213] Specifically, a *s*PP-*block*-poly(E-*co*-P)-*block*-*s*PP triblock copolymer was synthesized *via* sequential monomer addition and exhibited a narrow molecular weight distribution ($M_w/M_n = 1.24$) with $M_n = 94{,}000$ g/mol and a propylene content of 70 mol%.

As previously described, the solvent polarity plays a critical role in determining the tacticity of PP generated from **2**/dMMAO (Figure 1.2).[92] In a subsequent report, Shiono and co-workers cleverly applied this knowledge to prepare stereoblock copolymers of propylene containing *s*PP and *a*PP segments (Scheme 1.11) by initial polymerization in heptane followed by addition of more propylene and chlorobenzene.[214] The resultant *s*PP-*block*-*a*PP had $M_n = 94{,}700$ g/mol with a narrow PDI ($M_w/M_n = 1.27$). Shiono and co-workers have also recently described similar effects of the tacticity of PP generated from **2**/dMMAO under varying propylene pressures.[215] At low pressure (0.2 atm) atactic PP is furnished, but at higher pressure (1 atm) syndiotactic PP is generated. A *s*PP-*block*-*a*PP copolymer and *s*PP-*block*-*a*PP-*block*-*s*PP copolymer were synthesized by varying propylene pressure over the course of the polymerization.

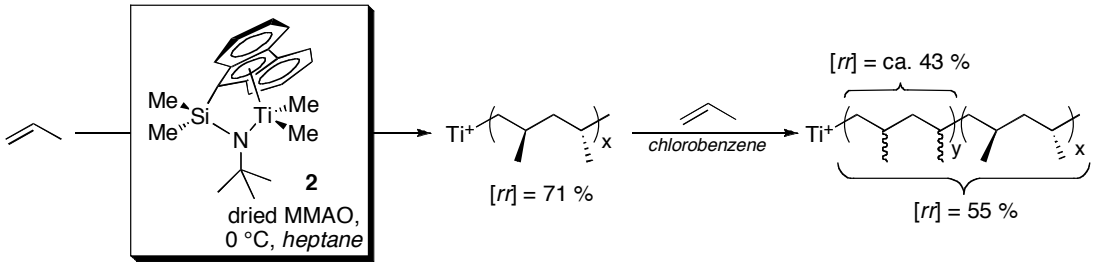

Scheme 1.11. Synthesis of *s*PP-*block*-*a*PP using solvent polarity to control tacticity.

With the ability to produce both PE and *s*PP in a living manner, bis(phenoxyimine) titanium complexes have been employed in the synthesis of ethylene and propylene-containing block copolymers. For example, **49**/MAO (Figure 1.17) has been shown to produce *s*PP-*block*-poly(E-*co*-P) diblock copolymers of high molecular weight (M_n = 145,100 g/mol, M_w/M_n = 1.12) through sequential monomer addition.[113] Several studies on the physical properties of sPP-*block*-poly(E-co-P) diblock copolymers made using **49**/MAO have been conducted including those involving the morphology,[216] thermodynamic behavior, and self-assembly[217] of the materials. The addition of a third block was later employed in the formation of a *s*PP-*block*-poly(E-*co*-P)-*block*-*s*PP triblock copolymer.[211] TEM revealed that the polymer exhibited a microphase-separated morphology with *s*PP cylinders in a poly(E-*co*-P) matrix. Tensile testing revealed a strain to break of about 550%.

Living ethylene/propylene copolymerization and block copolymer formation has also been demonstrated with related complex **50**/MAO.[218] Specifically, a *s*PP-*block*-poly(E-*co*-P), PE-*block*-*s*PP, and PE-*block*-poly(E-*co*-P)-*block*-*s*PP have been prepared through sequential monomer addition.[154,219]

1.8.2.3 Atactic Polypropylene Containing Block Copolymers

In 1991 Hlatky and Turner reported on the synthesis of diblock copolymers of ethylene and propylene using a hafnocene catalyst.[220] Activation of Cp_2HfMe_2 (**41**, Figure 1.16) with $[PhNMe_2H][B(C_6F_5)_4]$ in the presence of propylene furnishes atactic PP. At 0 °C, the rate of termination via β-H transfer was slow enough to allow for the synthesis of *a*PP-*block*-PE via sequential monomer addition. Both orders of monomer addition (ethylene followed by propylene and propylene followed by ethylene) were successful

in furnishing a polymeric product that contained a majority (50 –60 %) of diblock material isolated by hexanes extraction.

In a previous section of this review the low-temperature living polymerization of propylene by Cp_2ZrMe_2 (**40**)/$B(C_6F_5)_3$ and Cp_2HfMe_2 (**41**)/$B(C_6F_5)_3$ (Figure 1.16) as reported by Fukui and co-workers was discussed.[18] In a subsequent report, the synthesis of *a*PP-*block*-poly(E-*co*-P) diblock copolymers using **40**, **41**, and $Cp^*_2HfMe_2$ activated with $B(C_6F_3)_3$ and employing Al(*n*Oct)$_3$ as a scavenger was described through sequential monomer addition at low temperatures (T_{rxn} = -78 °C for **40** and $Cp^*_2HfMe_2$; T_{rxn} = -50 °C for **41**).[90] The resultant polymers exhibited narrow molecular weight distributions (M_w/M_n = 1.07 – 1.30) and M_n = 71,000 – 155,000 g/mol with propylene contents between 65 – 75 mol%.

Mecking and co-workers have used **80a**/MAO (Figure 1.35) for the synthesis of PE-*block*-*a*PP through sequential monomer addition.[163] Polymerization of ethylene in a living fashion followed by removal of excess monomer *in vacuo* and subsequent propylene polymerization furnished the diblock copolymer with M_n = 190,000 g/mol and M_w/M_n = 1.12.

1.8.3 Polyethylene Containing Block Copolymers

The catalysts that have been used to prepare PE-based block copolymers are listed in Table 1.3. While bis(phenoxyimine) titanium complexes can provide highly syndiotactic PP, copolymers that incorporate propylene as part of a poly(E-*co*-P) block have also been synthesized with these catalysts. Using **50**/MAO (Figure 1.17) a PE-*block*-poly(E-*co*-P) diblock and a PE-*block*-poly(E-*co*-P)-*block*-PE triblock copolymer have been synthesized through sequential monomer addition.[154] A PE-*block*-poly(E-*co*-P)

diblock copolymer was also synthesized using **54**/MAO (Figure 1.20).[122,221] While the molecular weight of the polymer was quite high with M_n = 2,000,000 g/mol, the molecular weight distribution was fairly broad (M_w/M_n = 1.60).

The ethylene homopolymerization behavior of bis(indolide-imine)titanium complexes was discussed in a previous section of this review. Using **78c**/MAO (Figure 1.34), Fujita and co-workers were also able to prepare PE-*block*-poly(E-*co*-P) copolymers via sequential monomer addition with M_w/M_n = 1.17 and M_n = 31,400 g/mol and overall propylene content of 8.0 mol%.[159,160] TEM visualization of the block copolymer revealed microphase separation of the poly(E-*co*-P) and PE domains, which were evenly dispersed throughout the sample.

Table 1.3. Block copolymers based on ethylene.

Entry	Block Copolymer	Catalyst Precursor(s) Used
1	PE-*block*-poly(E-*co*-P)	**50, 54, 78c**
2	PE-*block*-poly(E-*co*-P)-*block*-PE	**50**
3	PE-*block*-PS	**109**

PE = polyethylene, E = ethylene, P = propylene, PS = polystyrene

Coates and co-workers have combined two sequential polymerizations to generate a series of poly(E-*co*-P) comb polymers from the corresponding poly(E-*co*-P) macromonomers.[222] First, poly(E-*co*-P) macromonomers featuring one unsaturated chain end were synthesized using a non-living titanium bis(phenoxyimine) catalyst, **101** (Scheme 1.12), generating allyl

(polymerizable) and propenyl (unpolymerizable) end groups. The macromonomers were then homopolymerized using a living nickel diimine catalyst, **30a**/MAO (Figure 1.11, Scheme 1.12), to generate poly(E-*co*-P) comb polymers featuring approximately 7 to 14 arms/molecule after fractionation from the unpolymerizable residual macromonomer; these values correspond well to the theoretical values based on reaction stoichiometry. The molecular weight distributions remained relatively low (M_w/M_n = 1.51 – 1.90, M_n = 74,000 – 209,000 g/mol).

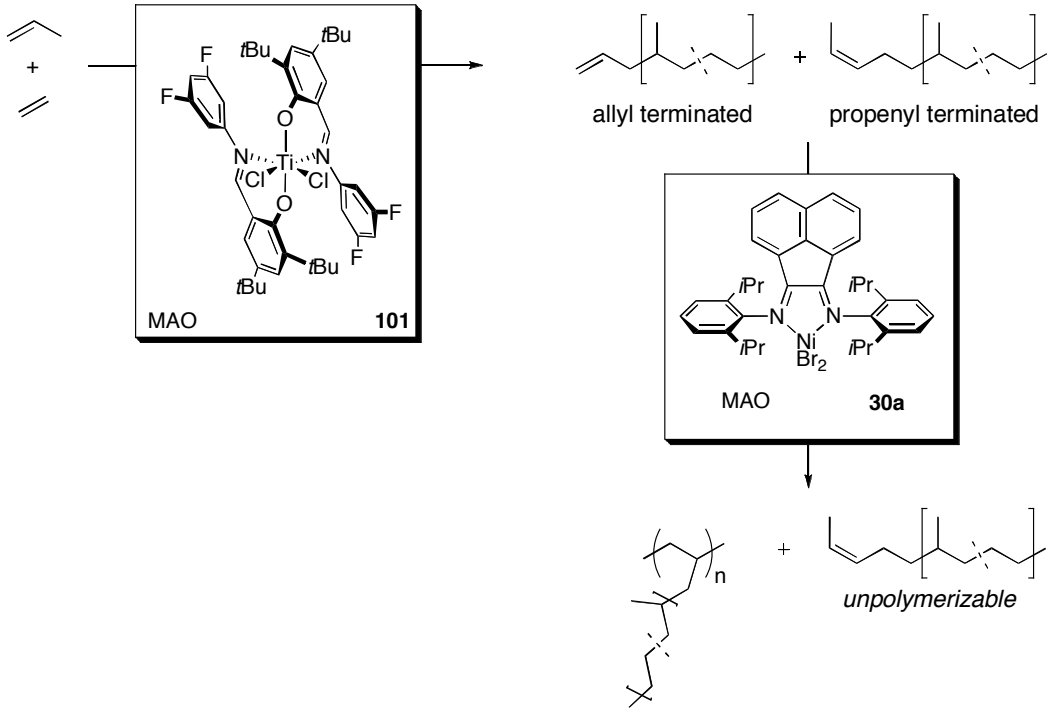

Scheme 1.12. Poly(E-*co*-P) comb synthesis.

1.8.4 Norbornene and Cyclopentene-Containing Block Copolymers

The catalysts that have been used to prepare block copolymers based on cyclic olefins are listed in Table 1.4. The alternating copolymerization of ethylene and norbornene using bis(pyrrolide-imine)titanium catalysts was

discussed in a previous section of this review. Fujita and co-workers were able to utilize **97b**/MAO (Figure 1.45) to prepare block copolymers containing poly(E-*co*-NB) and PE segments as well as block copolymers containing poly(E-*co*-NB) segments with varying degrees of norbornene incorporation.[199] Block copolymers of the type poly(E-*co*-NB)$_x$-*block*-poly(E-*co*-NB)$_y$ with 7.6 mol% norbornene incorporation in the first block and 27.4 mol% norbornene overall were prepared by initiating the polymerization with ethylene containing the desired amount of norbornene. After the first block had been formed, additional norbornene was added while maintaining the ethylene feed (Scheme 1.13). PE-*block*-poly(E-*co*-NB) was prepared through sequential monomer addition. The diblock copolymer exhibited a narrow polydispersity (M_w/M_n = 1.56) and M_n = 414,000 g/mol with a norbornene content of 31.5 mol %.

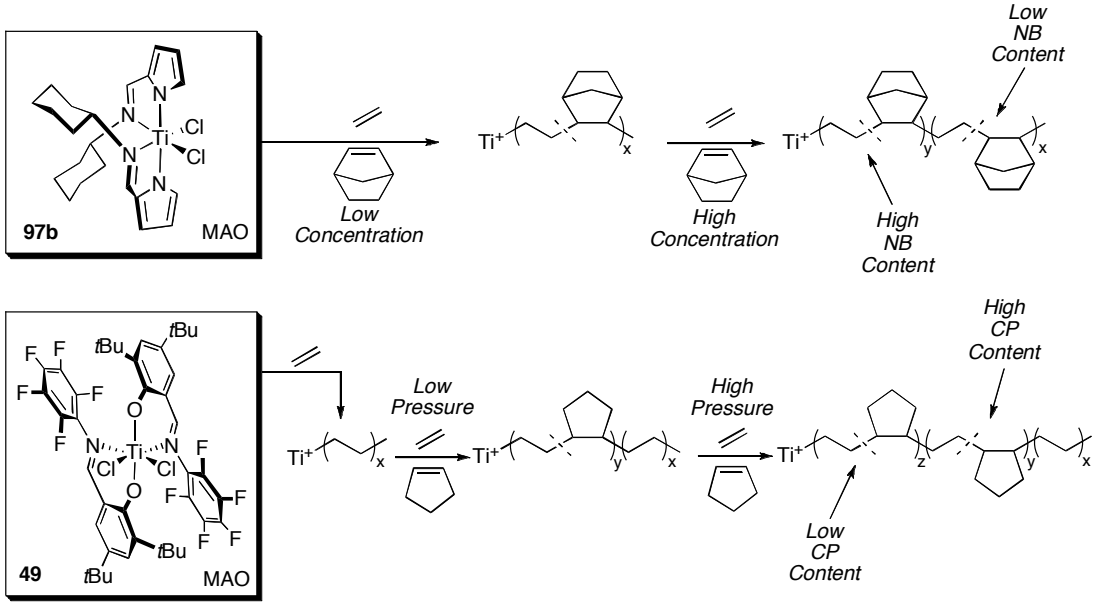

Scheme 1.13. Synthesis of ethylene/norbornene (NB) and ethylene/cyclopentene (CP) block copolymers.

Bis(phenoxyimine) titanium complexes have been employed in the living copolymerization of ethylene and cyclopentene. By varying ethylene pressure, a series of poly(E-*co*-CP)s with different cyclopentene contents were prepared using **49**/MAO (Figure 1.17, Scheme 1.13).[223] When ethylene pressure was low (< 1 psi), an almost perfectly alternating copolymer was formed (M_n = 21,000 g/mol, M_w/M_n = 1.34, T_g = 10.1 °C). However, the use of higher ethylene pressures (3 psi) resulted in the formation of a random copolymer containing 36 mol% cyclopentene (M_n = 133,000 g/mol, M_w/M_n = 1.24, T_g = -4.5 °C). Microstructural analysis using ^{13}C NMR spectroscopy revealed that in both cases, all cyclopentene units were isolated and enchained in a 1,2 fashion. Tri- and multiblock copolymers were synthesized in which the constituent blocks differed in their cyclopentene content.

Copolymers from ethylene and norbornene have also been made using **49**/MAO.[224] With this catalyst, a high molecular weight, low PDI poly(E-*co*-NB) sample was prepared (M_n = 238,000 g/mol, M_w/M_n = 1.05) containing 62 mol% ethylene and a T_g of 86.5 °C. In addition, **49**/MAO was also used to synthesize a high molecular weight poly(E-*co*-P)-*block*-poly(E-*co*-NB) sample (M_n = 576,000 g/mol, M_w/M_n = 1.13).

Bis(enaminoketonato)titanium catalysts have been employed in the living copolymerization of ethylene and cyclic olefins. Li and co-workers have prepared a PE-*block*-poly(E-*co*-NB) block copolymer through sequential monomer addition with **79a**/MAO (Figure 1.35).[162] The diblock copolymer had a narrow polydispersity (M_w/M_n = 1.38, M_n = 143,000 g/mol) and a norbornene content of 11.1 mol%. In a subsequent report PE-*block*-poly(E-*co*-CP) was prepared in a nearly identical manner.[201]

Table 1.4. Block copolymers based on cycloolefins.

Entry	Block Copolymer	Catalyst Precursor(s) Used
1	poly(E-*co*-NB)$_x$-*block*-poly(E-*co*-NB)$_y$	**97b**
2	PE-*block*-poly(E-*co*-NB)	**97b, 79a**
3	PE-*block*-(E-*co*-CP)$_x$-*block*-(E-*co*-CP)$_y$	**49**
4	PE-*block*-poly(E-*co*-CP)	**79a**
5	*s*PP-*block*-poly(P-*co*-NB)	**43**
6	PNB-*block*-poly(P-*co*-NB)-*block*-PP	**43**
7	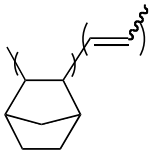 PNB-*block*-poly(acetylene)	**111**

E = ethylene, NB = norbornene, PE = polyethylene, *s*PP = syndiotactic polypropylene, CP = cyclopentene, PNB = polynorbornene

As previously discussed, **43**/MAO (Figure 1.16) is living for the polymerization of propylene as well as for the copolymerization of ethylene and norbornene. In 2006, Shiono and co-workers were able to show that **43**/MAO could also copolymerize propylene and norbornene in a living fashion to form random and block copolymers.[225] For example, three *s*PP-*block*-poly(P-*co*-NB) diblock copolymers were synthesized through sequential monomer addition that had similar molecular weights (M_n ~ 20,000 g/mol, M_w/M_n = 1.21 – 1.32). It was also previously discussed that **43**/dMMAO containing 0.4 mol% TIBA is living for norbornene polymerization to furnish PNB. Shiono and co-workers were also able to show that **43**/dMMAO containing 1.8 mol% TIBA could furnish PNB-*block*-poly(P-*co*-NB)-*block*-PP

triblock copolymers in a catalytic fashion.[188] The successive addition of norbornene and propylene before complete consumption of norbornene gives PNB-*block*-poly(P-*co*-NB)-*block*-PP terminated with a Ti-PP bond, which can be exchanged with TIBA. Repeated addition of norbornene and propylene gives a catalytic synthesis of the triblock copolymers in this system (Scheme 1.14).

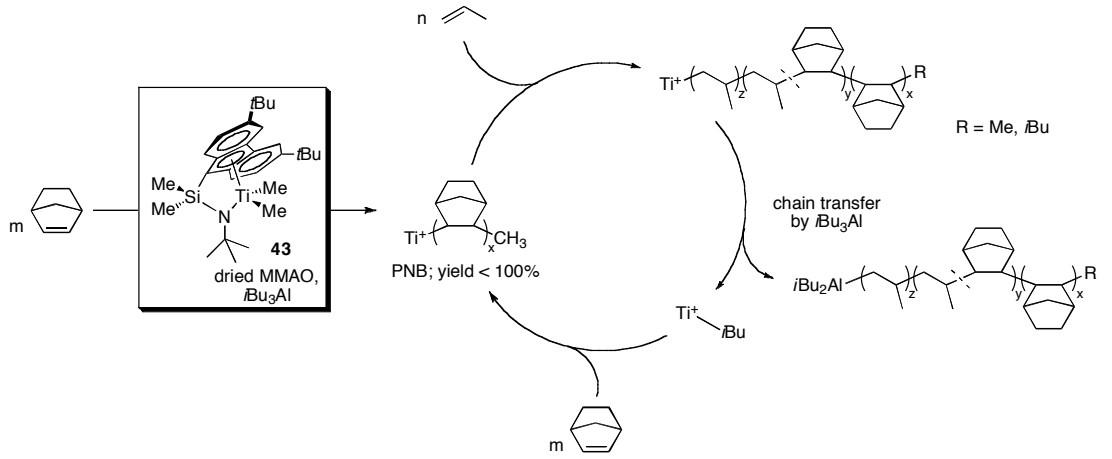

Scheme 1.14. Catalytic synthesis of block copolymers from norbornene and propylene using **43**/dMMAO-TIBA.

1.8.5 Block Copolymers Containing Blocks Derived from 1,5-Hexadiene Polymerization

Several classes of catalyst have been used to prepare block copolymers derived from 1,5-hexadiene; these are listed in Table 1.5. The 1-hexene and 1,5-hexadiene homopolymerization behavior of **19b**/[$PhNMe_2H$][$B(C_6F_5)_4$] (Figure 1.7) were discussed in a previous section of this review. Sita and co-workers were able to prepare diblock and triblock copolymers of 1-hexene and 1,5-hexadiene.[182] Isotactic poly(1-hexene)-*block*-PMCP and isotactic-poly(1-hexene)-*block*-PMCP-*block*-poly(1-hexene) were obtained from **19b**/[$PhNMe_2H$][$B(C_6F_5)_4$] at -10 °C through sequential monomer addition. The diblock copolymer possessed M_w/M_n = 1.05 and M_n = 22,800 g/mol with

T_m = 91 °C. The triblock copolymer had M_w/M_n = 1.10, M_n = 30,900 g/mol, and T_m = 79 °C. Atomic force microscopy (AFM) revealed that microphase separation of the crystalline PMCP and amorphous poly(1-hexene) had occurred.

Table 1.5. Block copolymers based on 1,5-hexadiene.

Entry	Block Copolymer	Catalyst Precursor(s) Used
1	*i*PH-*block*-PMCP-*block*-*i*PH	**19b**
2	*s*PP-*block*-poly(P-*co*-MCP-*co*-VTM)	**49**
3	poly(E-*co*-P)-*block*-poly(MCP-*co*-VTM)	**49**
4	poly(MCP-*block*-VTM)-*block*-poly(E-*co*-NB)	**49**

PH = poly(1-hexene), PMCP = poly(methylene-1,3-cyclopentane), *s*PP = syndiotactic polypropylene, VTM = vinyltetramethylene, E = ethylene, P = propylene, NB = norbornene

Using **49**/MAO (Figure 1.17), Coates and Hustad reported the living copolymerization of propylene and 1,5-hexadiene to produce random copolymers comprised of units of propylene, MCP, and 3-VTM.[181] A *s*PP-*block*-poly(P-*co*-MCP-*co*-3-VTM) diblock copolymer was also synthesized with **49**/MAO through sequential monomer addition (Scheme 1.15). The molecular weight distribution of the block copolymer was low (M_w/M_n = 1.11, M_n = 93,300 g/mol) and contained 4.3 mol% MCP units and 2.7 mol% 3-VTM units. A poly(E-*co*-P)-*block*-poly(MCP-*co*-3-VTM) was also synthesized (M_n = 524,700 g/mol, M_w/M_n = 1.13). Lastly, **49**/MAO has been used to produce a high molecular weight poly(MCP-*co*-3-VTM)-*block*-poly(E-*co*-NB) sample with M_n = 451,000 g/mol and M_w/M_n = 1.41.[224]

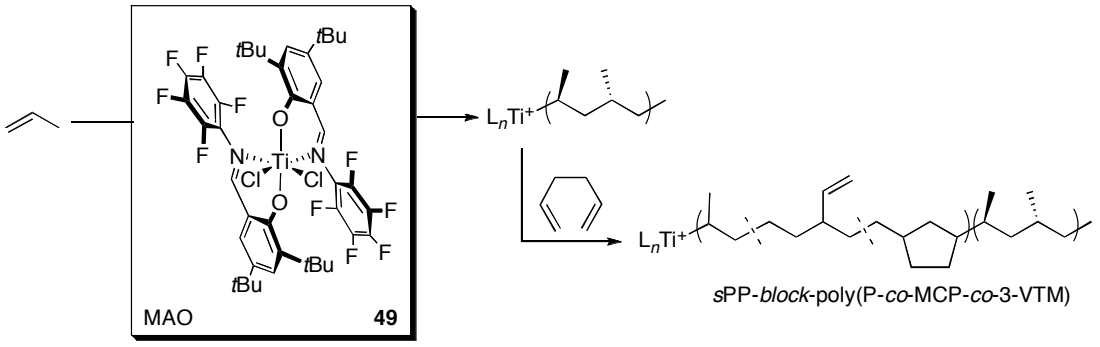

Scheme 1.15. Synthesis of a block copolymer from propylene and 1,5-hexadiene using **49**/MAO.

1.8.6 Block Copolymers Containing Blocks Derived from Polar Monomers

One of the most challenging goals in block copolymer synthesis is the incorporation of polar monomers due to the limited ability of catalysts that can tolerate polar functionalities. Catalysts that have been employed in the synthesis of block copolymers incorporating polar monomers are listed in Table 1.6. In 1983, Doi reported the use of **37**/Et_2AlCl (Figure 1.15) for the synthesis of a series of PP-*block*-poly(tetrahydrofuran) AB-type diblock copolymers by quenching a living propylene polymerization with iodine and using the iodide-terminated PP to initiate cationic polymerization of THF.[83]

Catalyst **37**/Et_2AlCl has also been used to synthesize PP-*block*-PMMA (PMMA = poly(methylmethacrylate).[226] At -78 °C, **37**/Et_2AlCl was used to polymerize propylene to which methyl methacrylate (MMA) was then added. The MMA polymerization, which was proposed to proceed via a radical mechanism, was conducted at 25 °C to form the diblock copolymer.

Yasuda and co-workers described the synthesis of block copolymers containing polyethylene (insertion mechanism) with several polar monomers (non-insertion mechanism) such as MMA, methyl acrylate (MA), ethyl

Table 1.6. Block copolymers based on polar monomers.

Entry	Block Copolymer	Catalyst Precursor(s) Used
1	*s*PP-*block*-poly(THF)	**37**
2	*s*PP-*block*-PMMA	**37**
3	PE-*block*-PMMA	**102, 103**
4	PE-*block*-PCL	**102, 103**
5	PE-*block*-PVL	**102**
6	PMMA-*block*-PE-*block*-PMMA	**107,108**
7	PCL-*block*-PE-*block*-PCL	**107,108**
8	PBA-*block*-PE	**110**

*s*PP = syndiotactic polypropylene, THF = tetrahydrofuran, PMMA = poly(methyl methacrylate), PCL = poly(ε-caprolactone), PVL = poly(δ-valerolactone), PBA = poly(n-butylacrylate)

acrylate (EA), δ-valerolactone (VL), and ε-caprolactone (CL) via sequential addition using [Cp^*_2SmMe(THF)] and [Cp^*_2SmH]$_2$ (**102** and **103**, Figure 1.47).[227] Ethylene was first polymerized (M_w/M_n = 1.39 – 2.01, M_n = 6,600 – 27,000 g/mol) followed by addition of the respective polar monomer to form a diblock copolymer. Reversal of monomer addition led to no block copolymer formation. Thus a PE-*block*-PMMA, PE-*block*-PMA, PE-*block*-PEA, PE-*block*-PVL, and PE-*block*-PCL were synthesized and showed good material properties such as deep coloration with dyes. In a subsequent report, the structurally related **104** (Figure 1.47) was also shown to be a viable block copolymerization catalyst for ethylene, MMA, and CL.[228] Furthermore, in 2000 Yasuda and co-workers reported on the synthesis of diblock copolymers

poly(1-pentene)/poly(1-hexene) and PMMA/PCL using the structurally similar bridged Cp–bearing yttrium and scandium catalysts **105** and **106** (Figure 1.47) via sequential monomer addition.[229]

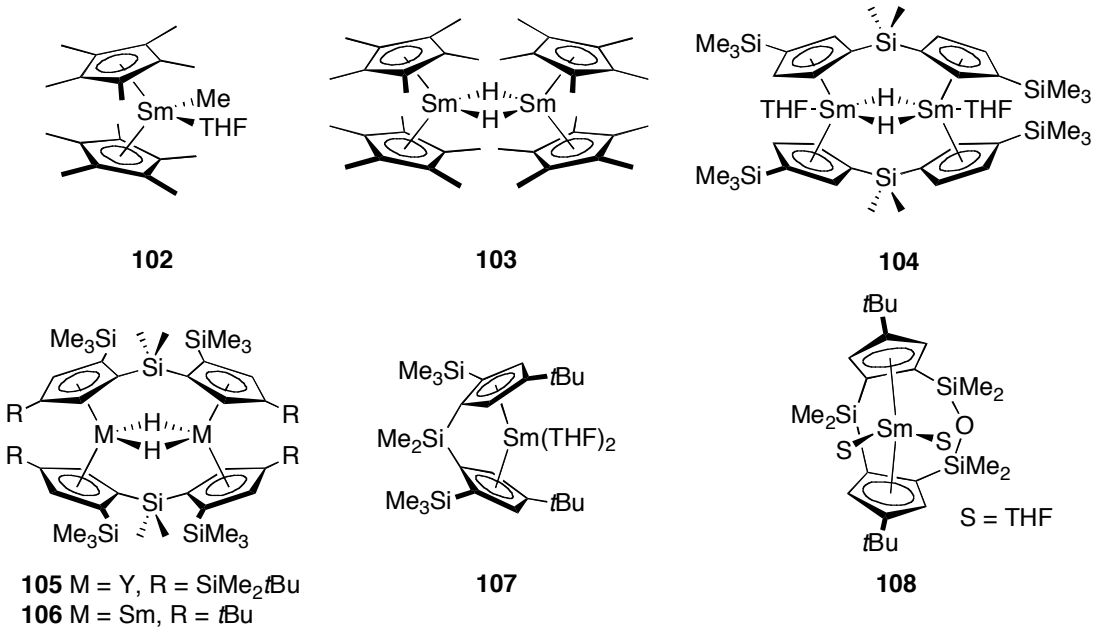

Figure 1.47. Rare-earth metal catalysts for block copolymerization.

It had been previously shown that Cp^*_2Sm is active for ethylene homopolymerization involving coordination of ethylene by two Sm^{II} centers followed by electron transfer to form a telechelic initiator (Scheme 1.16).[230] Yasuda and co-workers cleverly applied this observation to the synthesis of triblock copolymers of ethylene and polar monomers.[231] Thus, triblock copolymers of PMMA-*block*-PE-*block*-PMMA, PCL-*block*-PE-*block*-PCL, and PDTC-*block*-PE-*block*-PDTC (PDTC = poly(2,2-dimethyltrimethylene carbonate)) were prepared through sequential monomer addition with **107** and **108** (Figure 1.47).

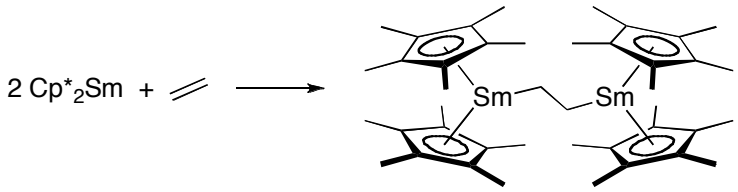

Scheme 1.16. Formation of telechelic initiator for ethylene polymerization from Cp^*_2Sm.

As previously discussed, **34c** (Figure 1.13) is quasi-living for 1-hexene polymerization.[69] It was also discovered that addition of carbon monoxide (CO) in the presence of 1-hexene afforded an alternating copolymer. Taking advantage of this, a poly(1-hexene)-*block*-poly(1-hexene-*alt*-CO) diblock copolymer was made through sequential monomer addition. Similarly, a PE-*block*-poly(ethylene-*alt*-CO) diblock copolymer was also synthesized through sequential monomer addition.

Brookhart and Matyjaszewski combined living insertion polymerization with living ATRP (Atom Transfer Radical Polymerization) techniques to synthesize graft copolymers. Palladium diimine chelate complexes have been previously used for living polymerization of ethylene, affording end-functionalized, branched polyethylenes.[232] Catalyst **109** (Scheme 1.17) builds on this strategy by appending an acrylate ester forming a PE macromonomer that was incorporated into a living ATRP polymerization of *n*-butyl acrylate to generate poly(*n*-butyl acrylate)-*graft*-PE. Graft copolymers of moderate molecular weight (M_n = up to 115,000 g/mol) were obtained with approximately 4-5 grafts per chain and relatively narrow molecular weight distribution (M_w/M_n as low as 1.4).

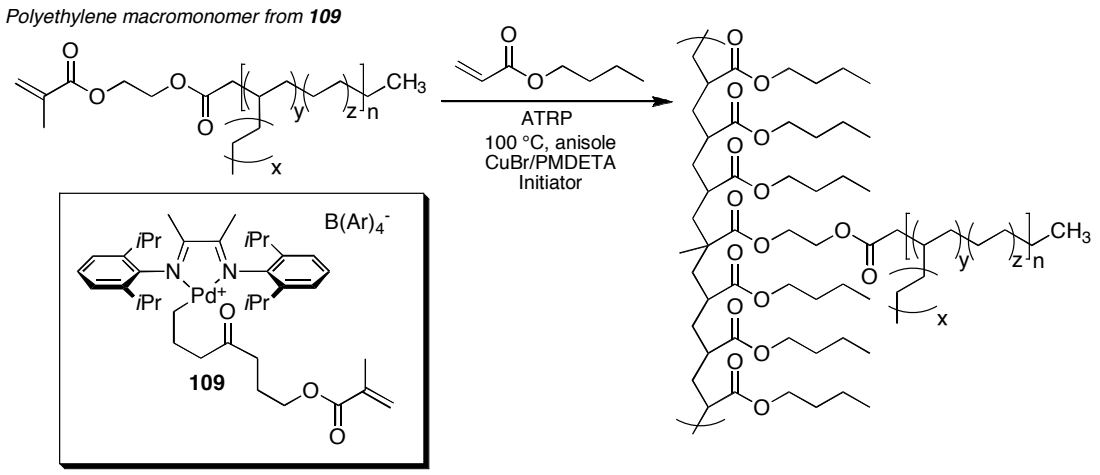

Scheme 1.17. Living insertion/ATRP graft copolymer synthesis.

Ye and co-workers combined living insertion polymerization with living ATRP techniques to generate block copolymers with a functionalized palladium diimine catalyst.[233] Catalyst **110** (Scheme 1.18) appended with bromo-functionality forms a PE macroinitiator that was incorporated into a living ATRP polymerization of *n*-butyl acrylate or styrene to generate poly(*n*-butyl acrylate)-*block*-PE and PS-*block*-PE diblock copolymers (Scheme 1.18).

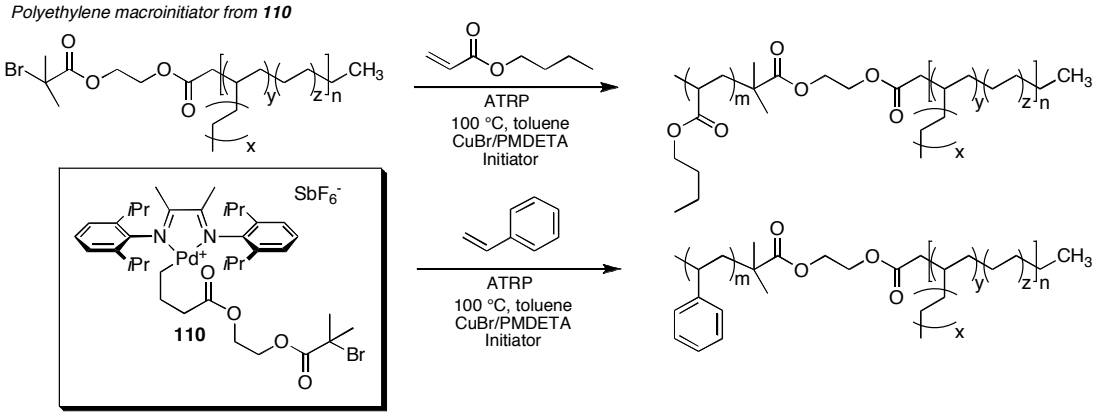

Scheme 1.18. Synthesis of PE-*block*-poly(*n*-butyl acrylate) and PE-*block*-polystyrene diblock copolymers.

Bazan and co-workers adopted a strategy based on a pressure-jump technique to synthesize block copolymers with different ratios of ethylene.[234] Catalyst **90a** (Figure 1.40) was previously shown to copolymerize ethylene with 5-norbornen-2-yl acetate with quasi-living behavior.[176] Polymerization of 5-norbornen-2-yl acetate and 50 psi ethylene generates an amorphous copolymer with approximately 25% polar monomer incorporation. After a given reaction time (8 – 45 minutes), the ethylene pressure was increased to 1100 psi leading to formation of an essentially PE block (Scheme 1.19) with relatively narrow polydispersities (M_w/M_n = 1.3 – 1.6). GPC analysis is consistent with diblock formation, as are the DSC data. TEM analysis demonstrated that the materials are microphase separated, consistent with blocks of distinct compositions. Tapered copolymers (TCP) have also been prepared with this system that allows depletion of 5-norbornen-2-yl acetate under a constant ethylene pressure.[235] It was observed that as 5-norbornen-2-yl acetate concentration depletes semicrystalline properties are obtained after specific reaction times, consistent with the fact that ethylene-rich segments are formed indicating pseudo-diblock copolymer formation. This strategy was used to make pseudo-tetrablock copolymers by addition of a second batch of

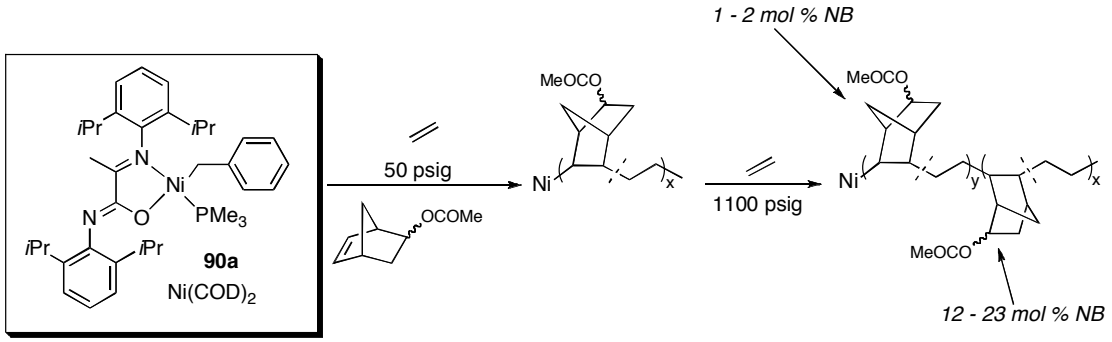

Scheme 1.19. Synthesis of block copolymers from ethylene and 5-norbornen-2-yl acetate using a neutral nickel catalyst.

5-norbornen-2-yl acetate after a prescribed time[236] Tensile testing revealed a strain to break of about 1000% at 65 °C with 80% elastic recovery.

In a subsequent report, Bazan and co-workers combined living insertion polymerization with living ATRP techniques to synthesize graft copolymers.[237] Polymerization of ethylene followed by copolymerization with 5-norbornen-2-yl-2′-bromo-2′-methyl propanoate using **90c** (Figure 1.40) activated with $Ni(COD)_2$ furnished a PE macroinitiator. Subsequent polymerization with MMA by living ATRP methods furnished PE-*graft*-PMMA copolymers (Scheme 1.20).

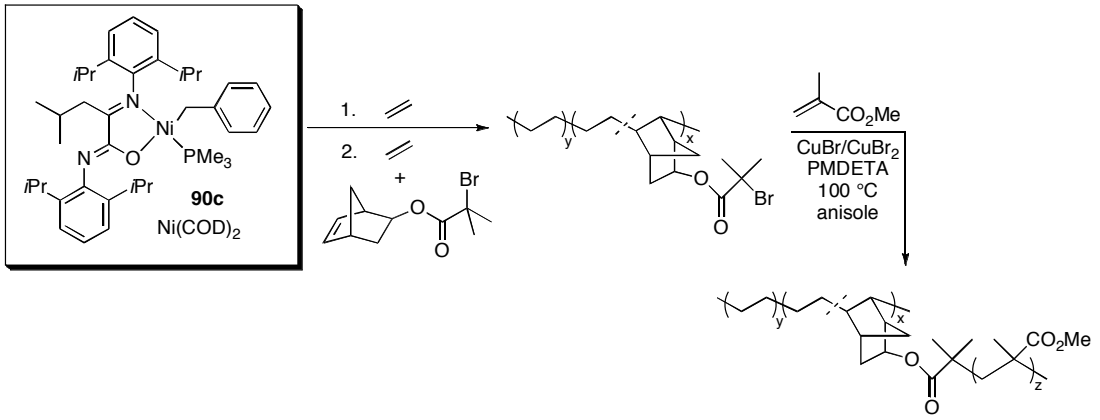

Scheme 1.20. Synthesis of PE-*graft*-PMMA copolymers using a neutral nickel catalyst and ATRP.

Risse showed that $[Pd(MeCN)_4][BF_4]$ polymerized a wide variety of ester-functionalized norbornenes, in some cases with narrow molecular weight distributions, and with linear increase in M_n over time.[187] Sequential addition of a norbornene monomer with different substitution pattern afforded diblock copolymers of moderate molecular weight.

Novak significantly advanced the field of palladium-mediated living olefin polymerization with the design of σ,π-bicyclic Pd catalyst **111** (Figure 1.48), which is both highly air- and moisture-stable, due to chelation by the appended olefin, but exhibits good activity for living polymerization.[238] This unique, robust living behavior was demonstrated by the synthesis of well-defined block copolymers of norbornene and diethyl 7-oxabicyclo[2.2.1]hepta-2,5-diene-2,3-dicarboxylate. A subsequent retro-Diels-Alder reaction on this polymer afforded a discrete PNB-*block*-poly(acetylene) copolymer.

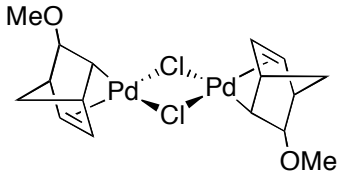

111

Figure 1.48. Palladium catalyst used for the synthesis of norbornene/acetylene block copolymers.

1.9 Outlook and Summary

The last decade has seen significant new advances achieved in the field of living olefin polymerization. Many efficient and selective catalysts are now available for the living polymerization of ethylene in addition to living and stereoselective polymerization of α-olefins. This allows the creation of unlimited new polymer architectures, such as block copolymers and end-functionalized macromolecules. The ability to synthesize such polymers will allow the detailed study of the effect of polymer microstructure on the mechanical and physical properties of this new class of materials.

As we wrote in our previous reviews,[2,3] the main challenge facing this new field is that these expensive metal complexes only form one polymer

chain during the polymerization reaction, resulting in economically non-viable materials for commodity applications. Significant research in developing catalytic systems that can produce multiple chains per metal center must be conducted. One strategy to accomplish this goal is to add excess amounts of an inexpensive metal complex that will rapidly transmetallate the active living catalyst, producing many chains per metal center.[134-136,239-243] This strategy can then be used to create multiple block copolymers per metal center by varying polymerization conditions.[188,244] A second strategy is to add an external agent at specific intervals during the living polymerization to terminate a chain and begin a new one.[155] Third, metal complexes that transmetallate at rates slower than monomer enchainment but faster than chain formation have the potential to produce block copolymers when two different polymerization catalysts are used.[209,210,245-247] Finally, non-living catalysts that can be induced to introduce blocks on a time-scale faster than that of chain formation can be used to make block copolymers.[208]

Future research will continue to uncover new living systems capable of making unique polyolefin structures, and these advances will greatly expand the range of polyolefin materials. New strategies for developing catalyst systems capable of furnishing multiple chains per metal center will allow commodity polyolefin production from living catalysts. Undoubtedly, the future for specialty materials is a bright one in light of continued new developments in the field of living olefin polymerization.

REFERENCES

(1) Resconi, L.; Cavallo, L.; Fait, A.; Piemontesi, F. *Chem. Rev.* **2000**, *100*, 1253-1345.

(2) Coates, G. W.; Hustad, P. D.; Reinartz, S. *Angew. Chem. Int. Ed.* **2002**, *41*, 2236-2257.

(3) Domski, G. J.; Rose, J. M.; Coates, G. W.; Bolig, A. D.; Brookhart, M. *Prog. Polym. Sci.* **2007**, *32*, 30-92.

(4) Szwarc, M. *J. Polym. Sci. Part A: Polym. Chem.* **1998**, *36*, IX-XV.

(5) Webster, O. W. *Science* **1991**, *251*, 887-893.

(6) Vasile, C. *Handbook of Polyolefins*; Second ed.; Marcel Dekker Inc.: New York, 2000.

(7) Ziegler, K.; Holzkamp, E.; Breil, H.; Martin, H. *Angew. Chem.* **1955**, *67*, 426.

(8) Natta, G.; Pino, P.; Corradini, P.; Danusso, F.; Mantica, E.; Mazzanti, G.; Moraglio, G. *J. Am. Chem. Soc.* **1955**, *77*, 1708-1710.

(9) Coates, G. W. *Chem. Rev.* **2000**, *100*, 1223-1252.

(10) Hsieh, H. L.; Quirk, R. P. *Anionic Polymerization: Principles and Practical Applications*; Marcel Dekker Inc.: New York, 1996.

(11) Matyjaszewski, K. *Cationic Polymerizations: Mechanisms, Synthesis, and Applications*; Marcel Dekker Inc.: New York, 1996.

(12) Hawker, C. J.; Bosman, A. W.; Harth, E. *Chem. Rev.* **2001**, *101*, 3661-3688.

(13) Kamigaito, M.; Ando, T.; Sawamoto, M. *Chem. Rev.* **2001**, *101*, 3689-3746.

(14) Matyjaszewski, K.; Xia, J. H. *Chem. Rev.* **2001**, *101*, 2921-2990.

(15) Braunecker, W. A.; Matyjaszewski, K. *Prog. Polym. Sci.* **2007**, *32*, 93-146.

(16) Quirk, R. P.; Lee, B. *Polym. Int.* **1992**, *27*, 359-367.

(17) Chen, E. Y. X.; Marks, T. J. *Chem. Rev.* **2000**, *100*, 1391-1434.

(18) Fukui, Y.; Murata, M.; Soga, K. *Macromol. Rapid Commun.* **1999**, *20*, 637-640.

(19) Hagihara, H.; Shiono, T.; Ikeda, T. *Macromolecules* **1998**, *31*, 3184-3188.

(20) Nishii, K.; Shiono, T.; Ikeda, T. *Kobunshi Ronbunshu* **2002**, *59*, 371-376.

(21) Nomura, K.; Fudo, A. *J. Mol. Catal. A: Chem.* **2004**, *209*, 9-17.

(22) Britovsek, G. J. P.; Gibson, V. C.; Wass, D. F. *Angew. Chem. Int. Ed.* **1999**, *38*, 428-447.

(23) Gibson, V. C.; Spitzmesser, S. K. *Chem. Rev.* **2003**, *103*, 283-315.

(24) Scollard, J. D.; McConville, D. H. *J. Am. Chem. Soc.* **1996**, *118*, 10008-10009.

(25) Jeon, Y. M.; Park, S. J.; Heo, J.; Kim, K. *Organometallics* **1998**, *17*, 3161-3163.

(26) Baumann, R.; Davis, W. M.; Schrock, R. R. *J. Am. Chem. Soc.* **1997**, *119*, 3830-3831.

(27) Schrock, R. R.; Baumann, R.; Reid, S. M.; Goodman, J. T.; Stumpf, R.; Davis, W. M. *Organometallics* **1999**, *18*, 3649-3670.

(28) Mehrkhodavandi, P.; Bonitatebus, P. J.; Schrock, R. R. *J. Am. Chem. Soc.* **2000**, *122*, 7841-7842.

(29) Mehrkhodavandi, P.; Schrock, R. R. *J. Am. Chem. Soc.* **2001**, *123*, 10746-10747.

(30) Mehrkhodavandi, P.; Schrock, R. R.; Pryor, L. L. *Organometallics* **2003**, *22*, 4569-4583.

(31) Schrock, R. R.; Adamchuk, J.; Ruhland, K.; Lopez, L. P. H. *Organometallics* **2003**, *22*, 5079-5091.

(32) Liang, L. C.; Schrock, R. R.; Davis, W. M.; McConville, D. H. *J. Am. Chem. Soc.* **1999**, *121*, 5797-5798.

(33) Schrock, R. R.; Bonitatebus, P. J.; Schrodi, Y. *Organometallics* **2001**, *20*, 1056-1058.

(34) Schrock, R. R.; Adamchuk, J.; Ruhland, K.; Lopez, L. P. H. *Organometallics* **2005**, *24*, 857-866.

(35) Tshuva, E. Y.; Goldberg, I.; Kol, M.; Goldschmidt, Z. *Inorg. Chem. Commun.* **2000**, *3*, 611-614.

(36) Gendler, S.; Groysman, S.; Goldschmidt, Z.; Shuster, M.; Kol, M. *J. Polym. Sci. Part A: Polym. Chem.* **2006**, *44*, 1136-1146.

(37) Tshuva, E. Y.; Goldberg, I.; Kol, M. *J. Am. Chem. Soc.* **2000**, *122*, 10706-10707.

(38) Segal, S.; Goldberg, I.; Kol, M. *Organometallics* **2005**, *24*, 200-202.

(39) Tshuva, E. Y.; Goldberg, I.; Kol, M.; Goldschmidt, Z. *Chem. Commun.* **2001**, 2120-2121.

(40) Groysman, S.; Tshuva, E. Y.; Goldberg, I.; Kol, M.; Goldschmidt, Z.; Shuster, M. *Organometallics* **2004**, *23*, 5291-5299.

(41) Tshuva, E. Y.; Groysman, S.; Goldberg, I.; Kol, M.; Goldschmidt, Z. *Organometallics* **2002**, *21*, 662-670.

(42) Groysman, S.; Goldberg, I.; Kol, M.; Genizi, E.; Goldschmidt, Z. *Inorg. Chim. Acta* **2003**, *345*, 137-144.

(43) Groysman, S.; Goldberg, I.; Kol, M.; Genizi, E.; Goldschmidt, Z. *Organometallics* **2003**, *22*, 3013-3015.

(44) Manivannan, R.; Sundararajan, G. *Macromolecules* **2002**, *35*, 7883-7890.

(45) Sudhakar, P.; Sundararajan, G. *Macromol. Rapid Commun.* **2005**, *26*, 1854-1859.

(46) Suidhakar, P. *J. Polym. Sci. Part A: Polym. Chem.* **2007**, *45*, 5470-5479.

(47) Jayaratne, K. C.; Sita, L. R. *J. Am. Chem. Soc.* **2000**, *122*, 958-959.

(48) Zhang, Y. H.; Sita, L. R. *Chem. Commun.* **2003**, 2358-2359.

(49) Kissounko, D. A.; Zhang, Y. H.; Harney, M. B.; Sita, L. R. *Adv. Synth. Cat.* **2005**, *347*, 426-432.

(50) Keaton, R. J.; Jayaratne, K. C.; Henningsen, D. A.; Koterwas, L. A.; Sita, L. R. *J. Am. Chem. Soc.* **2001**, *123*, 6197-6198.

(51) Zhang, Y. H.; Reeder, E. K.; Keaton, R. J.; Sita, L. R. *Organometallics* **2004**, *23*, 3512-3520.

(52) Yasumoto, T.; Yamagata, T.; Mashima, K. *Organometallics* **2005**, *24*, 3375-3377.

(53) Boussie, T. R.; Diamond, G. M.; Goh, C.; Hall, K. A.; LaPointe, A. M.; Leclerc, M. K.; Murphy, V.; Shoemaker, J. A. W.; Turner, H.; Rosen, R. K.; Stevens, J. C.; Alfano, F.; Busico, V.; Cipullo, R.; Talarico, G. *Angew. Chem. Int. Ed.* **2006**, *45*, 3278-3283.

(54) Froese, R. D. J.; Hustad, P. D.; Kuhlman, R. L.; Wenzel, T. T. *J. Am. Chem. Soc.* **2007**, *129*, 7831-7840.

(55) Zuccaccia, C.; Macchioni, A.; Busico, V.; Cipullo, R.; Talarico, G.; Alfano, F.; Boone, H. W.; Frazier, K. A.; Hustad, P. D.; Stevens, J. C.; Vosejpka, P. C.; Abboud, K. A. *J. Am. Chem. Soc.* **2008**, *130*, 10354-10368.

(56) Domski, G. J.; Lobkovsky, E. B.; Coates, G. W. *Macromolecules* **2007**, *40*, 3510-3513.

(57) Beckerle, K.; Manivannan, R.; Spaniol, T. P.; Okuda, J. *Organometallics* **2006**, *25*, 3019-3026.

(58) Zhang, H.; Nomura, K. *J. Am. Chem. Soc.* **2005**, *127*, 9364-9365.

(59) Ward, B. D.; Bellemin-Laponnaz, S.; Gade, L. H. *Angew. Chem. Int. Ed.* **2005**, *44*, 1668-1671.

(60) Johnson, L. K.; Killian, C. K.; Brookhart, M. *J. Am. Chem. Soc.* **1995**, *117*, 6414-6415.

(61) Guan, Z.; Cotts, P. M.; McCord, E. F.; McLain, S. J. *Science* **1999**, *283*, 2059-2062.

(62) Killian, C. M.; Tempel, D. J.; Johnson, L. K.; Brookhart, M. *J. Am. Chem. Soc.* **1996**, *118*, 11664-11665.

(63) Mohring, V. M.; Fink, G. *Angew. Chem. Int. Ed.* **1985**, *24*, 1001-1003.

(64) Merna, J.; Cihlar, J.; Kucera, M.; Deffieux, A.; Cramail, H. *Eur. Polym. J.* **2005**, *41*, 303-312.

(65) Yuan, J. C.; Silva, L. C.; Gomes, P. T.; Valerga, B.; Campos, J. M.; Ribeiro, M. R.; Chien, J. C. W.; Marques, M. M. *Polymer* **2005**, *46*, 2122-2132.

(66) Camacho, D. H.; Guan, Z. B. *Macromolecules* **2005**, *38*, 2544-2546.

(67) Suzuki, N.; Yu, J.; Masubuchi, Y.; Horiuchi, A.; Wakatsuki, Y. *J. Polym. Sci. Part A: Polym. Chem.* **2003**, *41*, 293-302.

(68) Gottfried, A. C.; Brookhart, M. *Macromolecules* **2003**, *36*, 3085-3100.

(69) Borkar, S.; Yennawar, H.; Sen, A. *Organometallics* **2007**, *26*, 4711-4714.

(70) Rose, J. M.; Cherian, A. E.; Coates, G. W. *J. Am. Chem. Soc.* **2006**, *128*, 4186-4187.

(71) Ittel, S. D.; Johnson, L. K.; Brookhart, M. *Chem. Rev.* **2000**, *100*, 1169-1203.

(72) Azoulay, J. D.; Rojas, R. S.; Serrano, A. V.; Ohtaki, H.; Galland, G. B.; Wu, G.; Bazan, G. C. *Angew. Chem. Int. Ed.* **2008**, *47*, early view.

(73) Karian, H. G. *Handbook of Polypropylene and Polypropylene Composites*; Marcel Dekker Inc.: New York, 2003.

(74) Zambelli, A.; Natta, G.; Pasquon, I.; Signorin, R. *J. Polym. Sci., Part C: Polym. Symp.* **1967**, 2485.

(75) Doi, Y.; Takada, M.; Keii, T. *Bull. Chem. Soc. Jpn.* **1979**, *52*, 1802.

(76) Doi, Y.; Ueki, S.; Keii, T. *Macromolecules* **1979**, *12*, 814-819.

(77) Doi, Y.; Ueki, S.; Keii, T. *Makromol. Chem., Macromol. Chem. Phys.* **1979**, *180*, 1359-1361.

(78) Ueki, S.; Doi, Y.; Keii, T. *Makromol. Chem., Rapid Commun.* **1981**, *2*, 403-406.

(79) Doi, Y.; Suzuki, S.; Soga, K. *Makromol. Chem., Rapid Commun.* **1985**, *6*, 639-642.

(80) Doi, Y.; Suzuki, S.; Soga, K. *Macromolecules* **1986**, *19*, 2896-2900.

(81) Doi, Y.; Suzuki, S.; Hizal, G.; Soga, K. *Trans. Met. Catal. Polym.* **1988**, 182-194.

(82) Doi, Y.; Tokuhiro, N.; Suzuki, S.; Soga, K. *Makromol. Chem., Rapid Commun.* **1987**, *8*, 285-290.

(83) Doi, Y.; Watanabe, Y.; Ueki, S.; Soga, K. *Makromol. Chem., Rapid Commun.* **1983**, *4*, 533-537.

(84) Doi, Y.; Murata, M.; Soga, K. *Makromol. Chem., Rapid Commun.* **1984**, *5*, 811-814.

(85) Doi, Y.; Keii, T. *Adv. Polym. Sci.* **1986**, *73/74*, 201.

(86) Doi, Y.; Hizal, G.; Soga, K. *Makromol. Chem.* **1987**, *188*, 1273-1279.

(87) Ueki, S.; Furuhashi, H.; Murakami, N.; Murata, M.; Doi, Y. *Science And Technology In Catalysis, 1994* **1995**, *92*, 359-362.

(88) Sassmannshausen, J.; Bochmann, M. E.; Rosch, J.; Lilge, D. *J. Organomet. Chem.* **1997**, *548*, 23-28.

(89) Fukui, Y.; Murata, M. *Macromol. Chem. Phys.* **2001**, *202*, 1430-1434.

(90) Fukui, Y.; Murata, M. *Appl. Catal., A* **2002**, *237*, 1-10.

(91) Hasan, T.; Ioku, A.; Nishii, K.; Shiono, T.; Ikeda, T. *Macromolecules* **2001**, *34*, 3142-3145.

(92) Nishii, K.; Matsumae, T.; Dare, E. O.; Shiono, T.; Ikeda, T. *Macromol. Chem. Phys.* **2004**, *205*, 363-369.

(93) Cai, Z. G.; Ikeda, T.; Akita, M.; Shiono, T. *Macromolecules* **2005**, *38*, 8135-8139.

(94) Nishii, K.; Ikeda, T.; Akita, M.; Shiono, T. *J. Mol. Catal. A: Chem.* **2005**, *231*, 241-246.

(95) Dare, E. O.; Ogunniyi, D. S.; Olatunji, G. A.; Chattopadhyay, P. *Bull. Chem. Soc. Ethiopia* **2004**, *18*, 131-141.

(96) Fukui, Y.; Murata, M. *Macromol. Chem. Phys.* **2001**, *202*, 1473-1477.

(97) Starzewski, A. O.; Steinhauser, N.; Xin, B. S. *Macromolecules* **2008**, *41*, 4095-4101.

(98) Hagimoto, H.; Shiono, T.; Ikeda, T. *Macromol. Rapid Commun.* **2002**, *23*, 73-76.

(99) Hagimoto, H.; Shiono, T.; Ikeda, T. *Macromolecules* **2002**, *35*, 5744-5745.

(100) Hagimoto, H.; Shiono, T.; Ikeda, T. *Science and Technology in Catalysis, 2002* **2003**, *145*, 129-132.

(101) Shiono, T. *Catalysis Surveys from Asia* **2003**, *7*, 47-62.

(102) Hagimoto, H.; Shiono, T.; Ikeda, T. *Macromol. Chem. Phys.* **2004**, *205*, 19-26.

(103) Matsui, S.; Mitani, M.; Saito, J.; Tohi, Y.; Makio, H.; Tanaka, H.; Fujita, T. *Chem. Lett.* **1999**, 1263-1264.

(104) Matsui, S.; Tohi, Y.; Mitani, M.; Saito, J.; Makio, H.; Tanaka, H.; Nitabaru, M.; Nakano, T.; Fujita, T. *Chem. Lett.* **1999**, 1065-1066.

(105) Matsui, S.; Mitani, M.; Saito, J.; Matsukawa, N.; Tanaka, H.; Nakano, T.; Fujita, T. *Chem. Lett.* **2000**, 554-555.

(106) Tian, J.; Coates, G. W. *Angew. Chem. Int. Ed.* **2000**, *39*, 3626-3629.

(107) Saito, J.; Mitani, M.; Onda, M.; Mohri, J. I.; Ishi, J. I.; Yoshida, Y.; Nakano, T.; Tanaka, H.; Matsugi, T.; Kojoh, S. I.; Kashiwa, N.; Fujita, T. *Macromol. Rapid Commun.* **2001**, *22*, 1072-1075.

(108) Hustad, P. D.; Tian, J.; Coates, G. W. *J. Am. Chem. Soc.* **2002**, *124*, 3614-3621.

(109) Lamberti, M.; Pappalardo, D.; Zambelli, A.; Pellecchia, C. *Macromolecules* **2002**, *35*, 658-663.

(110) Milano, G.; Cavallo, L.; Guerra, G. *J. Am. Chem. Soc.* **2002**, *124*, 13368-13369.

(111) Talarico, G.; Busico, V.; Cavallo, L. *J. Am. Chem. Soc.* **2003**, *125*, 7172-7173.

(112) Corradini, P.; Guerra, G.; Cavallo, L. *Acc. Chem. Res.* **2004**, *37*, 231-241.

(113) Tian, J.; Hustad, P. D.; Coates, G. W. *J. Am. Chem. Soc.* **2001**, *123*, 5134-5135.

(114) Saito, J.; Mitani, M.; Mohri, J.; Ishii, S.; Yoshida, Y.; Matsugi, T.; Kojoh, S.; Kashiwa, N.; Fujita, T. *Chem. Lett.* **2001**, 576-577.

(115) Nakayama, Y.; Saito, J.; Bando, H.; Fujita, T. *Macromol. Chem. Phys.* **2005**, *206*, 1847-1852.

(116) Mitani, M.; Furuyama, R.; Mohri, J.; Saito, J.; Ishii, S.; Terao, H.; Kashiwa, N.; Fujita, T. *J. Am. Chem. Soc.* **2002**, *124*, 7888-7889.

(117) Mitani, M.; Furuyama, R.; Mohri, J.; Saito, J.; Ishii, S.; Terao, H.; Nakano, T.; Tanaka, H.; Fujita, T. *J. Am. Chem. Soc.* **2003**, *125*, 4293-4305.

(118) Mason, A. F.; Tian, J.; Hustad, P. D.; Lobkovsky, E. B.; Coates, G. W. *Isr. J. Chem.* **2002**, *42*, 301-306.

(119) Mason, A. F.; Coates, G. W. *J. Am. Chem. Soc.* **2004**, *126*, 10798-10799.

(120) Mason, A. F.; Ph. D. Thesis, Cornell University, Ithaca, NY, **2005**.

(121) Saito, J.; Mitani, M.; Onda, M.; Mohri, J.; Ishii, S.; Yoshida, Y.; Furuyama, R.; Nakano, T.; Kashiwa, N.; Fujita, T. *Science and Technology in Catalysis, 2002* **2003**, *145*, 515-516.

(122) Weiser, M. S.; Mulhaupt, R. *Macromol. Symp.* **2006**, *236*, 111-116.

(123) Weiser, M. S.; Wesolek, M.; Mulhaupt, R. *J. Organomet. Chem.* **2006**, *691*, 2945-2952.

(124) Cherian, A. E.; Lobkovsky, E. B.; Coates, G. W. *Macromolecules* **2005**, *38*, 6259-6268.

(125) Mason, A. F.; Coates, G. W. *J. Am. Chem. Soc.* **2004**, *126*, 16326-16327.

(126) Reinartz, S.; Mason, A. F.; Lobkovsky, E. B.; Coates, G. W. *Organometallics* **2003**, *22*, 2542-2544.

(127) Edson, J. B.; Wang, Z. G.; Kramer, E. J.; Coates, G. W. *J. Am. Chem. Soc.* **2008**, *130*, 4968-4977.

(128) Busico, V.; Cipullo, R.; Ronca, S.; Budzelaar, P. H. M. *Macromol. Rapid Commun.* **2001**, *22*, 1405-1410.

(129) Busico, V.; Cipullo, R.; Friederichs, N.; Ronca, S.; Talarico, G.; Togrou, M.; Wang, B. *Macromolecules* **2004**, *37*, 8201-8203.

(130) Harney, M. B.; Zhang, Y. H.; Sita, L. R. *Angew. Chem. Int. Ed.* **2006**, *45*, 2400-2404.

(131) Zhang, Y. H.; Keaton, R. J.; Sita, L. R. *J. Am. Chem. Soc.* **2003**, *125*, 9062-9069.

(132) Harney, M. B.; Zhang, Y. H.; Sita, L. R. *Angew. Chem. Int. Ed.* **2006**, *45*, 6140-6144.

(133) Zhang, W.; Sita, L. R. *Adv. Synth. Cat.* **2008**, *350*, 439-447.

(134) Zhang, W.; Sita, L. R. *J. Am. Chem. Soc.* **2008**, *130*, 442-443.

(135) Kempe, R. *Chem. Eur. J.* **2007**, *13*, 2764-2773.

(136) Zhang, W.; Wei, J.; Sita, L. R. *Macromolecules* **2008**, *41*, 7829-7833.

(137) Domski, G. J.; Edson, J. B.; Keresztes, I.; Lobkovsky, E. B.; Coates, G. W. *Chem. Commun.* **2008**, *46*, 6137-6139.

(138) Cherian, A. E.; Rose, J. M.; Lobkovsky, E. B.; Coates, G. W. *J. Am. Chem. Soc.* **2005**, *127*, 13770-13771.

(139) Rose, J. M.; Deplace, F.; Lynd, N. A.; Wang, Z.; Hotta, A.; Lobkovsky, E. B.; Kramer, E. J.; Coates, G. W. *Macromolecules* **2008**, *41*, 9548-9555.

(140) Peacock, A. J. *Handbook of Polyethylene*; Marcel Dekker Inc.: New York, 2000.

(141) Jeske, G.; Lauke, H.; Mauermann, H.; Swepston, P. N.; Schumann, H.; Marks, T. J. *J. Am. Chem. Soc.* **1985**, *107*, 8091-8103.

(142) Bambirra, S.; van Leusen, D.; Meetsma, A.; Hessen, B.; Teuben, J. H. *Chem. Commun.* **2003**, 522-523.

(143) Wang, W.; Nomura, K. *Macromolecules* **2005**, *38*, 5905-5913.

(144) Mashima, K.; Fujikawa, S.; Urata, H.; Tanaka, E.; Nakamura, A. *J. Am. Chem. Soc.* **1993**, *115*, 10990-10991.

(145) Mashima, K.; Fujikawa, S.; Tanaka, Y.; Urata, H.; Oshiki, T.; Tanaka, E.; Nakamura, A. *Organometallics* **1995**, *14*, 2633-2640.

(146) Mashima, K.; Fujikawa, S.; Urata, H.; Tanaka, E.; Nakamura, A. *J. Chem. Soc.-Chem. Commun.* **1994**, 1623-1624.

(147) MacAdams, L. A.; Buffone, G. P.; Incarvito, C. D.; Rheingold, A. L.; Theopold, K. H. *J. Am. Chem. Soc.* **2005**, *127*, 1082-1083.

(148) Saito, J.; Mitani, M.; Mohri, J.; Yoshida, Y.; Matsui, S.; Ishii, S.; Kojoh, S.; Kashiwa, N.; Fujita, T. *Angew. Chem. Int. Ed.* **2001**, *40*, 2918-2920.

(149) Ivanchev, S. S.; Badaev, V. K.; Ivancheva, N. I.; Khaikin, S. Y. *Dokl. Phys. Chem.* **2004**, *394*, 46-49.

(150) Furuyama, R.; Saito, J.; Ishii, S.; Makio, H.; Mitani, M.; Tanaka, H.; Fujita, T. *J. Organomet. Chem.* **2005**, *690*, 4398-4413.

(151) Ivanchev, S. S.; Trunov, V. A.; Rybakov, V. B.; Al'bov, D. V.; Rogozin, D. G. *Dokl. Phys. Chem.* **2005**, *404*, 165-168.

(152) Furuyama, R.; Mitani, M.; Mohri, J.; Mori, R.; Tanaka, H.; Fujita, T. *Macromolecules* **2005**, *38*, 1546-1552.

(153) Makio, H.; Kashiwa, N.; Fujita, T. *Adv. Synth. Cat.* **2002**, *344*, 477-493.

(154) Mitani, M.; Mohri, J.; Yoshida, Y.; Saito, J.; Ishii, S.; Tsuru, K.; Matsui, S.; Furuyama, R.; Nakano, T.; Tanaka, H.; Kojoh, S.; Matsugi, T.; Kashiwa, N.; Fujita, T. *J. Am. Chem. Soc.* **2002**, *124*, 3327-3336.

(155) Mitani, M.; Mohri, J.; Furuyama, R.; Ishii, S.; Fujita, T. *Chem. Lett.* **2003**, *32*, 238-239.

(156) Makio, H.; Fujita, T. *Macromol. Rapid Commun.* **2007**, *28*, 698-703.

(157) Matsugi, T.; Matsui, S.; Kojoh, S.; Takagi, Y.; Inoue, Y.; Fujita, T.; Kashiwa, N. *Chem. Lett.* **2001**, 566-567.

(158) Matsugi, T.; Kojoh, S.; Fujita, T.; Kashiwa, N. *Kobunshi Ronbunshu* **2002**, *59*, 410-414.

(159) Matsugi, T.; Matsui, S.; Kojoh, S.; Takagi, Y.; Inoue, Y.; Nakano, T.; Fujita, T.; Kashiwa, N. *Macromolecules* **2002**, *35*, 4880-4887.

(160) Matsugi, T.; Matsui, S.; Kojoh, S.; Takagi, Y.; Inoue, Y.; Nakano, T.; Fujita, T.; Kashiwa, N. *Science and Technology in Catalysis, 2002* **2003**, *145*, 523-524.

(161) Yoshida, Y.; Matsui, S.; Fujita, T. *J. Organomet. Chem.* **2005**, *690*, 4382-4397.

(162) Li, X. F.; Dai, K.; Ye, W. P.; Pan, L.; Li, Y. S. *Organometallics* **2004**, *23*, 1223-1230.

(163) Yu, S. M.; Mecking, S. *J. Am. Chem. Soc.* **2008**, *130*, 13204-13205.

(164) Kretschmer, W. P.; Hessen, B.; Noor, A.; Scott, N. M.; Kempe, R. *J. Organomet. Chem.* **2007**, *692*, 4569-4579.

(165) Lee, H.; Nienkemper, K.; Jordan, R. F. *Organometallics* **2008**, *27*, 5075-5081.

(166) Nienkemper, K.; Lee, H.; Jordan, R. F.; Ariafard, A.; Dang, L.; Lin, Z. Y. *Organometallics* **2008**, *27*, 5867-5875.

(167) Brookhart, M.; Volpe Jr., A. F.; DeSimone, J. M. *Polym. Prepr. (Am. Chem. Soc., Div. Polym. Chem.)* **1991**, *32*, 461-462.

(168) Brookhart, M.; DeSimone, J. M.; Grant, B. E.; Tanner, M. J. *Macromolecules* **1995**, *28*, 5378-5380.

(169) Gottfried, A. C.; Brookhart, M. *Macromolecules* **2001**, *34*, 1140-1142.

(170) Zhang, Y. W.; Ye, Z. B. *Chem. Commun.* **2008**, 1178-1180.

(171) Zhang, Y. W.; Ye, Z. B. *Macromolecules* **2008**, *41*, 6331-6338.

(172) Schmid, M.; Eberhardt, R.; Klinga, M.; Leskela, M.; Rieger, B. *Organometallics* **2001**, *20*, 2321-2330.

(173) Camacho, D. H.; Salo, E. V.; Ziller, J. W.; Guan, Z. B. *Angew. Chem. Int. Ed.* **2004**, *43*, 1821-1825.

(174) Camacho, D. H.; Salo, E. V.; Guan, Z. B.; Ziller, J. W. *Organometallics* **2005**, *24*, 4933-4939.

(175) Hicks, F. A.; Jenkins, J. C.; Brookhart, M. *Organometallics* **2003**, *22*, 3533-3545.

(176) Diamanti, S. J.; Ghosh, P.; Shimizu, F.; Bazan, G. C. *Macromolecules* **2003**, *36*, 9731-9735.

(177) Azoulay, J. D.; Itigaki, K.; Wu, G.; Bazan, G. C. *Organometallics* **2008**, *27*, 2273-2280.

(178) Coates, G. W.; Waymouth, R. M. *J. Am. Chem. Soc.* **1991**, *113*, 6270-6271.

(179) Mathers, R. T.; Coates, G. W. *Chem. Commun.* **2004**, 422-423.

(180) Doi, Y.; Tokuhiro, N.; Soga, K. *Makromol. Chem., Macromol. Chem. Phys.* **1989**, *190*, 643-651.

(181) Hustad, P. D.; Coates, G. W. *J. Am. Chem. Soc.* **2002**, *124*, 11578-11579.

(182) Jayaratne, K. C.; Keaton, R. J.; Henningsen, D. A.; Sita, L. R. *J. Am. Chem. Soc.* **2000**, *122*, 10490-10491.

(183) Park, S.; Takeuchi, D.; Osakada, K. *J. Am. Chem. Soc.* **2006**, *128*, 3510-3511.

(184) Okada, T.; Park, S.; Takeuchi, D.; Osakada, K. *Angew. Chem. Int. Ed.* **2007**, *46*, 6141-6143.

(185) Tritto, I.; Boggioni, L.; Ferro, D. R. *Coord. Chem. Rev.* **2006**, *250*, 212-241.

(186) Mehler, C.; Risse, W. *Macromolecules* **1992**, *25*, 4226-4228.

(187) Breunig, S.; Risse, W. *Makromol. Chem.* **1992**, *193*, 2915-2927.

(188) Cai, Z.; Nakayama, Y.; Shiono, T. *Macromol. Rapid Commun.* **2008**, *29*, 525-529.

(189) Ravasio, A.; Zampa, C.; Boggioni, L.; Tritto, I.; Hitzbleck, J.; Okuda, J. *Macromolecules* **2008**, *41*, 9565-9569.

(190) Hasan, T.; Shiono, T.; Ikeda, T. *Macromol. Symp.* **2004**, *213*, 123-129.

(191) Hasan, T.; Ikeda, T.; Shiono, T. *Macromolecules* **2004**, *37*, 8503-8509.

(192) Hasan, T.; Ikeda, T.; Shiono, T. *Macromolecules* **2005**, *38*, 1071-1074.

(193) Shiono, T.; Sugimoto, M.; Hasan, T.; Cai, Z.; Ikeda, T. *Macromolecules* **2008**, *41*, 8292-8294.

(194) Jansen, J. C.; Mendichi, R.; Locatelli, P.; Tritto, I. *Macromol. Rapid. Commun.* **2001**, *22*, 1394-1398.

(195) Jansen, J. C.; Mendichi, R.; Sacchi, M. C.; Tritto, I. *Macromol. Chem. Phys.* **2003**, *204*, 522-530.

(196) Yoshida, Y.; Matsui, S.; Takagi, Y.; Mitani, M.; Nitabaru, M.; Nakano, T.; Tanaka, H.; Fujita, T. *Chem. Lett.* **2000**, 1270-1271.

(197) Yoshida, Y.; Saito, J.; Mitani, M.; Takagi, Y.; Matsui, S.; Ishii, S.; Nakano, T.; Kashiwa, N.; Fujita, T. *Chem. Commun.* **2002**, 1298-1299.

(198) Yoshida, Y.; Matsui, S.; Takagi, Y.; Mitani, M.; Saito, J.; Ishii, S. I.; Nakano, T.; Tanaka, H.; Kashiwa, N.; Fujita, T. *Science and Technology in Catalysis, 2002* **2003**, *145*, 521-522.

(199) Yoshida, Y.; Mohri, J.; Ishii, S.; Mitani, M.; Saito, J.; Matsui, S.; Makio, H.; Nakano, T.; Tanaka, H.; Onda, M.; Yamamoto, Y.; Mizuno, A.; Fujita, T. *J. Am. Chem. Soc.* **2004**, *126*, 12023-12032.

(200) Tang, L. M.; Hu, T.; Bo, Y. J.; Li, Y. S.; Hu, N. H. *J. Organomet. Chem.* **2005**, *690*, 3125-3133.

(201) Tang, L. M.; Duan, Y. Q.; Pan, L.; Li, Y. S. *J. Polym. Sci. Part A: Polym. Chem.* **2005**, *43*, 1681-1689.

(202) Kiesewetter, J.; Kaminsky, W. *Chem. Eur. J.* **2003**, *9*, 1750-1758.

(203) Boffa, L. S.; Novak, B. M. *Chem. Rev.* **2000**, *100*, 1479-1493.

(204) Rieth, L. R.; Eaton, R. F.; Coates, G. W. *Angew. Chem. Int. Ed.* **2001**, *40*, 2153-2156.

(205) Bates, F. S. *Science* **1991**, *251*, 898-905.

(206) Ruzette, A. V.; Leibler, L. *Nat. Mater.* **2005**, *4*, 19-31.

(207) Mallin, D. T.; Rausch, M. D.; Lin, Y. G.; Dong, S. Z.; Chien, J. C. W. *J. Am. Chem. Soc.* **1990**, *112*, 2030-2031.

(208) Coates, G. W.; Waymouth, R. M. *Science* **1995**, *267*, 217-219.

(209) Chien, J. C. W.; Iwamoto, Y.; Rausch, M. D.; Wedler, W.; Winter, H. H. *Macromolecules* **1997**, *30*, 3447-3458.

(210) Lieber, S.; Brintzinger, H. H. *Macromolecules* **2000**, *33*, 9192-9199.

(211) Hotta, A.; Cochran, E.; Ruokolainen, J.; Khanna, V.; Fredrickson, G. H.; Kramer, E. J.; Shin, Y.-W.; Shimizu, F.; Cherian, A. E.; Rose, J. M.; Coates, G. W. *Proc. Natl. Acad. Sci. U. S. A.* **2006**, *42*, 15327-15332.

(212) Busico, V.; Cipullo, R.; Friederichs, N.; Ronca, S.; Togrou, M. *Macromolecules* **2003**, *36*, 3806-3808.

(213) Doi, Y.; Ueki, S.; Keii, T. *Makromol. Chem., Rapid Commun.* **1982**, *3*, 225-229.

(214) Nishii, K.; Shiono, T.; Ikeda, T. *Macromol. Rapid Commun.* **2004**, *25*, 1029-1032.

(215) Cai, Z. G.; Nakayama, Y.; Shiono, T. *Macromolecules* **2008**, *41*, 6596-6598.

(216) Ruokolainen, J.; Mezzenga, R.; Fredrickson, G. H.; Kramer, E. J.; Hustad, P. D.; Coates, G. W. *Macromolecules* **2005**, *38*, 851-860.

(217) Radulescu, A.; Mathers, R. T.; Coates, G. W.; Richter, D.; Fetters, L. J. *Macromolecules* **2004**, *37*, 6962-6971.

(218) Kojoh, S.; Matsugi, T.; Saito, J.; Mitani, M.; Fujita, T.; Kashiwa, N. *Chem. Lett.* **2001**, 822-823.

(219) Sakuma, A.; Weiser, M. S.; Fujita, T. *Polym. J.* **2007**, *39*, 193-207.

(220) Turner, H. W.; Hlatky, G. G. In *PCT Int. Appl. 9112285*; Exxon: 1991.

(221) Weiser, M. S.; Thomann, Y.; Heinz, L. C.; Pasch, H.; Mulhaupt, R. *Polymer* **2006**, *47*, 4505-4512.

(222) Rose, J. M.; Mourey, T. H.; Slater, L. A.; Keresztes, I.; Fetters, L. J.; Coates, G. W. *Macromolecules* **2008**, *41*, 559-567.

(223) Fujita, M.; Coates, G. W. *Macromolecules* **2002**, *35*, 9640-9647.

(224) Yoon, J.; Mathers, R. T.; Coates, G. W.; Thomas, E. L. *Macromolecules* **2006**, *39*, 1913-1919.

(225) Cai, Z. G.; Nakayama, Y.; Shiono, T. *Macromolecules* **2006**, *39*, 2031-2033.

(226) Doi, Y.; Koyama, T.; Soga, K. *Makromol. Chem., Macromol. Chem. Phys.* **1985**, *186*, 11-15.

(227) Yasuda, H.; Furo, M.; Yamamoto, H.; Nakamura, A.; Miyake, S.; Kibino, N. *Macromolecules* **1992**, *25*, 5115-5116.

(228) Desurmont, G.; Li, Y.; Yasuda, H.; Maruo, T.; Kanehisa, N.; Kai, Y. *Organometallics* **2000**, *19*, 1811-1813.

(229) Desurmont, G.; Tokimitsu, T.; Yasuda, H. *Macromolecules* **2000**, *33*, 7679-7681.

(230) Evans, W. J.; Decoster, D. M.; Greaves, J. *Macromolecules* **1995**, *28*, 7929-7936.

(231) Desurmont, G.; Tanaka, M.; Li, Y.; Yasuda, H.; Tokimitsu, T.; Tone, S.; Yanagase, A. *J. Polym. Sci. Part A: Polym. Chem.* **2000**, *38*, 4095-4109.

(232) Hong, S. C.; Jia, S.; Teodorescu, M.; Kowalewski, T.; Matyjaszewski, K.; Gottfried, A. C.; Brookhart, M. *J. Polym. Sci. Part A: Polym. Chem.* **2002**, *40*, 2736-2749.

(233) Zhang, K.; Ye, Z.; Subramanian, R. *Macromolecules* **2008**, *41*, 640-649.

(234) Diamanti, S. J.; Khanna, V.; Hotta, A.; Yamakawa, D.; Shimizu, F.; Kramer, E. J.; Fredrickson, G. H.; Bazan, G. C. *J. Am. Chem. Soc.* **2004**, *126*, 10528-10529.

(235) Diamanti, S. J.; Khanna, V.; Hotta, A.; Coffin, R. C.; Yamakawa, D.; Kramer, E. J.; Fredrickson, G. H.; Bazan, G. C. *Macromolecules* **2006**, *39*, 3270-3274.

(236) Coffin, R. C.; Diamanti, S. J.; Hotta, A.; Khanna, V.; Kramer, E. J.; Fredrickson, G. H.; Bazan, G. C. *Chem. Commun.* **2007**, 3550-3552.

(237) Schneider, Y.; Azoulay, J. D.; Coffin, R. C.; Bazan, G. C. *J. Am. Chem. Soc.* **2008**, *130*, 10464-10465.

(238) Safir, A. L.; Novak, B. M. *Macromolecules* **1995**, *28*, 5396-5398.

(239) Kaneyoshi, H.; Inoue, Y.; Matyjaszewski, K. *Macromolecules* **2005**, *38*, 5425-5435.

(240) van Meurs, M.; Britovsek, G. J. P.; Gibson, V. C.; Cohen, S. A. *J. Am. Chem. Soc.* **2005**, *127*, 9913-9923.

(241) Alfano, F.; Boone, H. W.; Busico, V.; Cipullo, R.; Stevens, J. C. *Macromolecules* **2007**, *40*, 7736-7738.

(242) Hustad, P. D.; Kuhlman, R. L.; Carnahan, E. M.; Wenzel, T. T.; Arriola, D. J. *Macromolecules* **2008**, *41*, 4081-4089.

(243) Sita, L. R. *Angew. Chem. Int. Ed.* **2009**, *48*, 2464-2472.

(244) Hustad, P. D.; Kuhlman, R. L.; Arriola, D. J.; Carnahan, E. M.; Wenzel, T. T. *Macromolecules* **2007**, *40*, 7061-7064.

(245) Chien, J. C. W.; Iwamoto, Y.; Rausch, M. D. *J. Polym. Sci. Part A: Polym. Chem.* **1999**, *37*, 2439-2445.

(246) Jayaratne, K. C.; Sita, L. R. *J. Am. Chem. Soc.* **2001**, *123*, 10754-10755.

(247) Arriola, D. J.; Carnahan, E. M.; Hustad, P. D.; Kuhlman, R. L.; Wenzel, T. T. *Science* **2006**, *312*, 714-719.

Chapter 2

Fluorinated Bis(phenoxyketimine)titanium Complexes for the Living, Isoselective Polymerization of Propylene: Multiblock Isotactic Polypropylene Copolymers via Sequential Monomer Addition

Reprinted in part with permission from

Journal of the American Chemical Society **2008**, *130*, 4968-4977.

2.1 Introduction

One of the ultimate challenges in polymer chemistry is the ability to synthesize polymers and copolymers with well-defined stereochemistry while controlling molecular weight and molecular weight distribution. Development of non-metallocene olefin polymerization catalysts has become a rapidly expanding area as new catalyst systems are discovered and improvements upon existing ones are made.[1,2] Homogeneous catalyst systems now exist that enable precise control over polymer stereochemistry through the design of sterically and electronically-tunable ancillary ligand frameworks that exert a defined geometry around an active metal center.[3] Until recently, olefin polymerization catalysts have been inferior to other chain-growth polymerization methods (e.g. cationic, anionic, radical) in their ability to promote consecutive enchainment of monomer units without chain transfer or termination, i.e. living polymerization (see Scheme 1.1 for chain transfer and termination pathways). However, a number of olefin polymerization catalysts that suppress chain termination or transfer events have been developed; these catalysts display living olefin polymerization behavior.[4,5] Living polymerization allows for the synthesis of a wide variety of polymer architectures such as block copolymers, which are most typically prepared via sequential monomer addition. Block copolymers incorporating isotactic polypropylene (iPP) segments are envisioned to provide materials with many potential applications such as compatibilizers and thermoplastic elastomers.[6-8] Therefore, the synthesis of block copolymers containing iPP domains is one of the most highly sought after goals in the field of olefin polymerization.

2.1.1 Block Copolymers as Thermoplastic Elastomers

One hallmark of living polymerization systems is the ability to synthesize well-defined block copolymers. One of the most important applications of block copolymers is in the synthesis of thermoplastic elastomers (TPEs). A TPE is a class of copolymers that exhibit material properties similar to a thermoset elastomer (e.g. vulcanized natural rubber), but have the processibility of a thermoplastic (e.g. polypropylene) enabling them to be melt processed or extruded. The most important class of thermoplastic elastomers from a commercial standpoint are based on block copolymers containing "hard" endblocks (semicrystalline with a high melting temperature (T_m) or glassy with a high glass transition temperature (T_g)) separated by a "soft" amorphous midblock (low T_g, no T_m). Some of the earliest studied are polystyrene-*block*-polybutadiene-*block*-polystyrene (SBS) or polystyrene-*block*-polyisoprene-*block*-polystyrene (SIS) triblock copolymers marketed under the trade name Kraton™. These polymers are prepared via living anionic polymerization methods.

The elastomeric properties exhibited by these polymers rely on phase separation between the "hard" and "soft" blocks.[9] While a blend of two homopolymers typically form an immiscible mixture (macrophase separation), a dramatic change in the phase behavior can arise by covalently linking the two homopolymers (Figure 2.1).[10] Domain sizes less than 1 μm are formed in a process of macrophase separation while microphase separation gives rise to domain sizes in the range of 5 – 100 nm.

For microphase separated diblock copolymers, four specific ordered morphologies have been identified: spheres, cylinders, gyroids, and lamellae (Figure 2.2).[11] These morphologies are dictated by the volume fraction (*f*) of

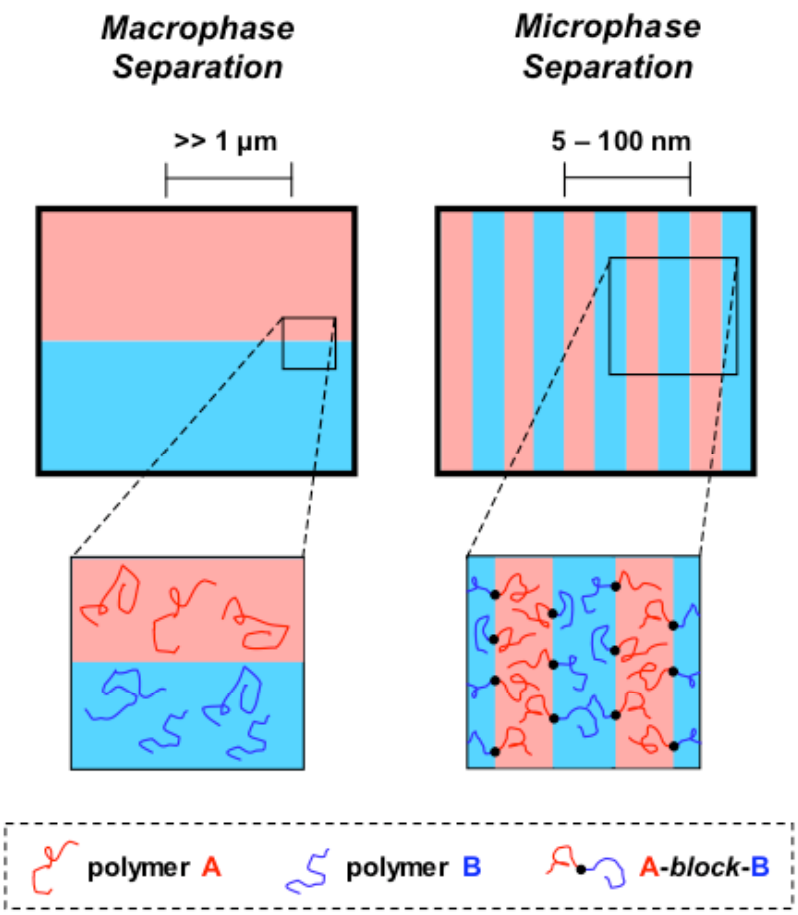

Figure 2.1. Macrophase separation of an immiscible homopolymer blend and microphase separation of a diblock copolymer with immiscible segments.[10]

each block. The ability for a given block copolymer to microphase separate are a function of numerous factors. These are typically dependant on the degree of polymerization (N), volume fraction of each individual component (f_a), and the Flory-Huggins interaction parameter (χ_{AB}). The value of χ_{AB} describes the energy of interaction between the two segments. A positive value indicates a net repulsion between segments A and B while a negative value indicates a free energy drive towards mixing. For most polymers in which there are no strong interactions between the two segments (e.g. hydrogen bonding), χ_{AB} is usually positive.

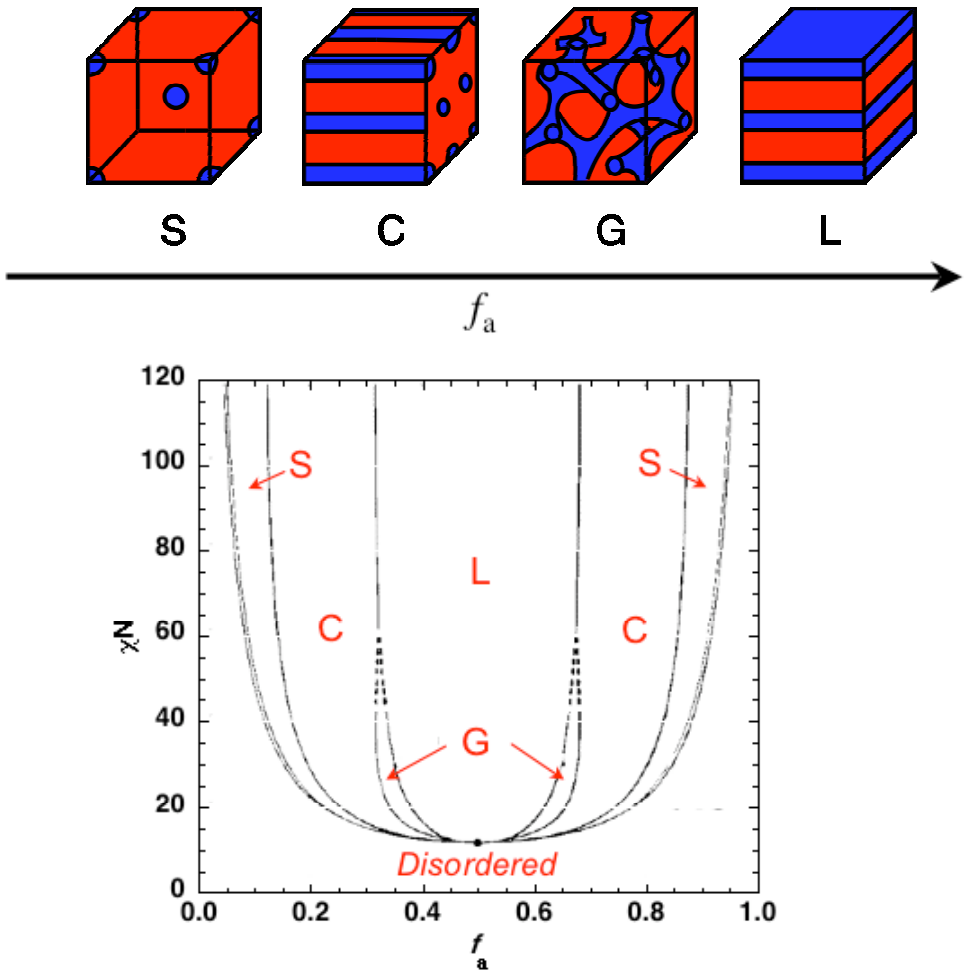

Figure 2.2. Morphologies of linear A-B diblock copolymers and phase diagram as a function of $\chi_{AB}N$, and f_a.[10]

Despite the excellent material properties of SBS and SIS block copolymers, rigorous monomer purification is required that can lead to higher manufacturing costs. Polyolefins are an attractive target to mimic the SBS and SIS thermoplastic elastomers given their excellent properties, low cost, and the growing number of living and stereoselective polymerization catalysts. Since London dispersion forces are the dominant interactive force between polyolefin segments, the χ_{AB} should be positive allowing microphase separation to occur. In order to impart similar elastomeric properties as the

SBS and SIS thermoplastic elastomers, triblock copolymers are required such that the "hard" segments act as physical crosslinks embedded in a "soft" amorphous domain (Figure 2.3). The use of polyolefin-based triblock copolymers featuring semicrystalline end blocks and amorphous midblocks are thus an attractive target for a microphase-separated thermoplastic elastomer.

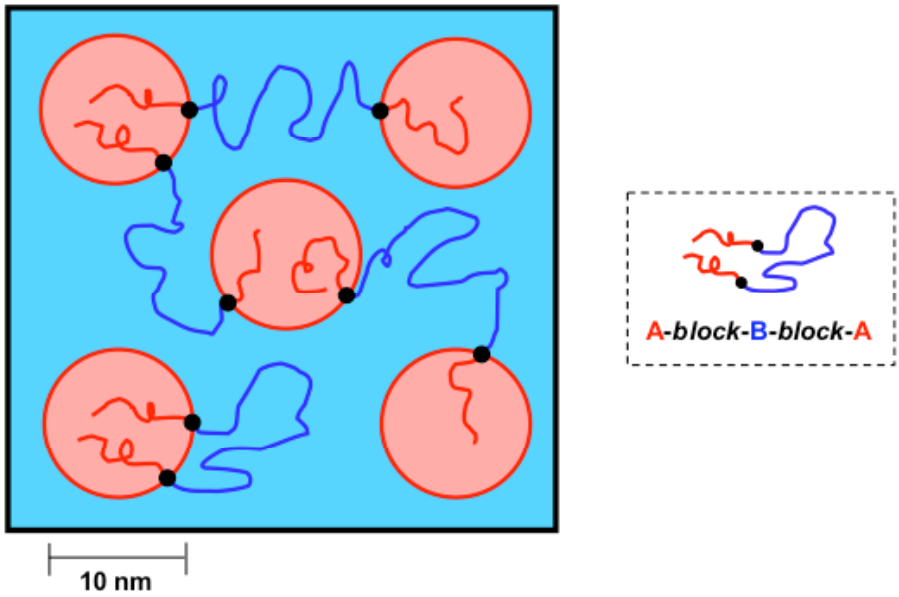

Figure 2.3. Physical crosslinking in a triblock copolymer.[10]

2.1.2 Development of Olefin Polymerization Catalysts for Block Copolymer Synthesis

The living and highly isoselective polymerization of higher α-olefins has been reported. Sita,[12-16] Kol,[17,18] Mashima,[19] Sundararajan,[20] and Coates[21] have independently developed catalyst systems capable of polymerizing 1-hexene in a living manner with moderate to extremely high levels of isoselectivity. However, despite the exquisite stereochemical control manifested in these systems, poly(1-hexene), regardless of its tacticity, is

amorphous and thus not suitable for applications requiring the strength, durability and/or crystallinity of a material such as iPP. While there are numerous catalysts capable of highly isoselective propylene polymerization[3,22] and a growing number of catalysts capable of living olefin polymerization,[4,5] highly active catalysts for both the living and highly isoselective polymerization of propylene remain elusive. This is despite significant research efforts since Natta's first synthesis of iPP more than half a century ago.[23] For example, in 2003 Busico and co-workers reported that various diamine bisphenolate zirconium catalysts exhibit "quasi-living" propylene polymerization behavior producing highly isotactic polypropylene. However, chain lifetimes are relatively short.[24,25] In 2004, Coates and co-workers reported that fluorinated bis(phenoxyketimine)titanium catalysts are living but only moderately isoselective for propylene polymerization producing polypropylene with 53% of five consecutive monomer sequences possessing the same stereoconfiguration ([m^4] = 0.53).[26] The following year, Coates and co-workers reported a C_2-symmetric α-diimine Ni(II) catalyst that is living and highly isoselective for propylene polymerization at low temperatures, however, catalyst activities were extremely low and molecular weight distributions broaden under these conditions.[27] Sita reported in 2006 that monocyclopentadienylzirconium acetamidinate catalysts polymerize propylene in a living manner, albeit with moderate isoselectivity ([m^4] = 0.71).[7] While each of these systems can be considered deficient in some regard (e.g. living behavior, isoselectivity, or activity), each has been utilized to synthesize block copolymers incorporating iPP segments. These catalysts and the block copolymers produced are depicted in Figure 2.4.

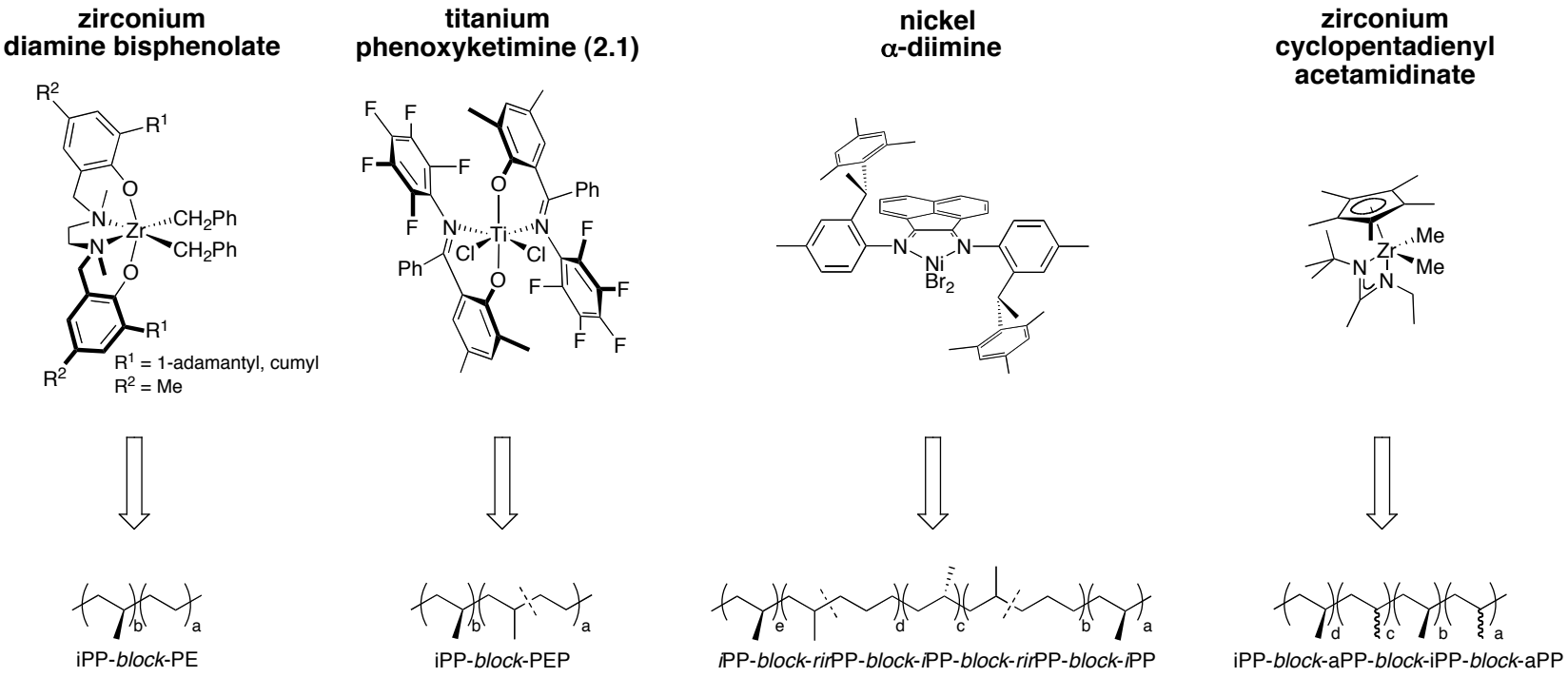

Figure 2.4. Catalysts used for the synthesis of block copolymers incorporating isotactic polypropylene segments.

For example, Busico and co-workers were able to prepare iPP-*block*-PE (PE = polyethylene) copolymers using the aforementioned diamine bisphenolate zirconium catalysts.[24,25] Coates and co-workers reported the synthesis of an iPP-*block*-PEP (PEP = poly(ethylene-*co*-propylene)) diblock copolymer employing 2.**1**/methylaluminoxane (MAO).[26] With their C_2-symmetric α-diimine Ni(II) catalyst, Coates and co-workers were able to prepare an iPP-*block*-rirPP-*block*-iPP (rirPP = regioirregular polypropylene) triblock copolymer and an iPP-*block*-rirPP-*block*-iPP-*block*-rirPP-*block*-iPP pentablock copolymer by adjusting the temperature throughout the course of the polymerization to effect changes in the microstructure of each block.[8] Sita and co-workers utilized a degenerative-transfer living polymerization process with a monocyclopentadienylzirconium acetamidinate catalyst system to generate a number of isotactic-atactic stereoblock polypropylene copolymers.[7] Despite these efforts, the synthesis of block copolymers containing two or more iPP segments via sequential monomer addition has yet been achieved. While the ability to use a single monomer to make block copolymers, as shown by Waymouth,[6] Sita,[7] and Coates[8] is advantageous from both a synthetic and industrial standpoint, a larger variety of architectures are accessible if more than one monomer is used. For example, thermoplastic elastomers employing PEP for amorphous blocks should exhibit utility over a broader temperature range than those employing atactic polypropylene (aPP) amorphous blocks. This is due to the fact that PEP exhibits a much lower glass transitions temperature (T_g) than aPP (-50 °C vs. 0 °C).

Our group[28] and researchers at Mitsui Chemicals[29-31] have independently explored the use of bis(phenoxyimine)titanium dichloride olefin polymerization catalysts for propylene polymerization. Complexes in

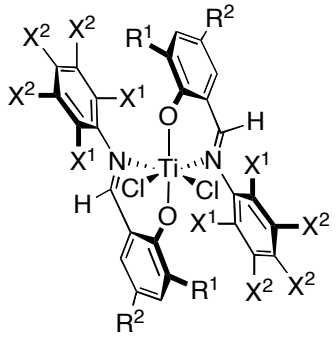

X^1 = F, X^2 = F or H; Living propylene polymerization behavior
X^1 = H, X^2 = F or H; Non-living propylene polymerization behavior

Figure 2.5. Phenoxyimine polymerization catalysts.

which the phenoxyimine ligands (PHI, see Figure 2.5) contain an *ortho*-fluorinated *N*-aryl group and a bulky ortho substituent on the phenolate ring (R^1 = ^{t}Bu), produce highly syndiotactic polypropylene (sPP) in a living manner when activated with MAO.[30,32] The syndioselectivity is a result of chain-end control. These catalysts are C_2-symmetric in the solid state and in solution, and are therefore expected to provide isotactic polymer via a site-control mechanism. However, a proposed catalyst isomerization event that occurs between each successive monomer insertion overrides the expected site control and leads to the unexpected syndioselectivity that is observed.[28,33,34] As the ortho substituent on the phenolate moiety (R^1) decreases in size, the syndioselectivity of propylene polymerization decreases.[35] Using zirconium or hafnium PHI complexes, Fujita and co-workers were able to generate iPP when ^{i}Bu$_3$Al/[Ph$_3$C][B(C$_6$F$_5$)$_4$] was employed as the activator.[36,37] Under these conditions, the PHI ligands react with the aluminum cocatalyst *in situ* to generate a new phenoxyamido complex. Activation with MAO[31] results in the formation of regioirregular, atactic polypropylene. Our group has reported a series of phenoxyketimine (PKI) titanium complexes bearing bulky ^{t}Bu groups at the ortho position of the phenolate ring, which are living for ethylene

polymerization when activated with MAO.[38] These catalysts were sparingly active for propylene polymerization. However, decreasing the steric demand at the ortho position of the phenolate ring and employing the *N*-pentafluorophenyl moiety leads to living and moderately isoselective propylene polymerization.[26]

We have extensively explored the PKI ligand design space in search of a catalyst capable of polymerizing propylene in a living and highly isoselective manner. In the course of our exploration, we found that **2.12**/MAO (Scheme 2.3) was the most isoselective PKI catalyst reported to date. Employing this catalyst, we prepared a number of unique block copolymers including an iPP-*block*-PEP-*block*-iPP triblock copolymer, iPP-*block*-PEP-*block*-iPP-*block*-PEP-*block*-iPP pentablock copolymer, and iPP-*block*-PEP-*block*-iPP-*block*-PEP-*block*-iPP-*block*-PEP-*block*-iPP heptablock copolymer. Mechanical testing revealed that each of these polymers displayed good elastomeric properties.

2.2 Results and Discussion

2.2.1 PHI Polymerization Catalysts

Because of their close structural relationship to PKI catalysts, a brief discussion of the polymerization behavior of PHI catalysts would be beneficial. Bis(phenoxyimine)titanium dichloride complexes were originally explored for the polymerization of ethylene.[39] When activated with MAO, these catalysts displayed high ethylene polymerization activities which prompted a more detailed investigation of this class of catalyst. In our laboratory a pooled, combinatorial approach was used to develop a library of related complexes and from this was identified a catalyst capable of

syndioselective propylene polymerization.[28] Further elaboration of the ligand framework showed that incorporation of *ortho*-fluorine substituents on the *N*-aryl moiety resulted in living and highly syndioselective propylene polymerization.[30,32] Catalysts bearing *meta*- and *para*-fluorine substituents on the *N*-aryl moiety exhibited high activity, but were not living for propylene polymerization.[40] Although isoselective polymerization of propylene would be expected from a C_2-symmetric catalyst precursor,[3] the polypropylene produced by the PHI catalysts is actually syndiotactic. The highly syndioselective polymerization of propylene via chain-end control proceeds with prevailing secondary (2,1) monomer insertion.[28,41-44] It is this highly unusual secondary insertion mode that causes fluxional isomerization of the octahedral sites between successive monomer insertions (Scheme 2.1).[28,33,34] Monomer insertion through the syndiospecific transition state is more favorable than monomer insertion through the isospecific transition state thereby syndiotactic polymer is formed. Calculations indicate that a steric interaction between the ortho phenolate group (R) and the α-methyl group of the growing polymer chain is the most deciding factor in determining which transition state is favored.[33,34] Quantum mechanical/molecular mechanical calculations performed on these catalysts predict high isoselectivity for propylene polymerization if the insertion rate is much faster than catalyst isomerization.[33] Complexes with ligand structures that could possibly prevent catalyst isomerization have been developed. For example, zirconium dichloride complexes bearing binaphthyl-bridged Schiff-base PHI ligands were prepared by Pellecchia and co-workers.[45] When activated with $^{i}Bu_3Al$/MAO or with $^{i}Bu_3Al$//$[Ph_3C][B(C_6F_5)_4]$, these catalysts yielded high molecular weight, atactic polypropylene. In the absence of

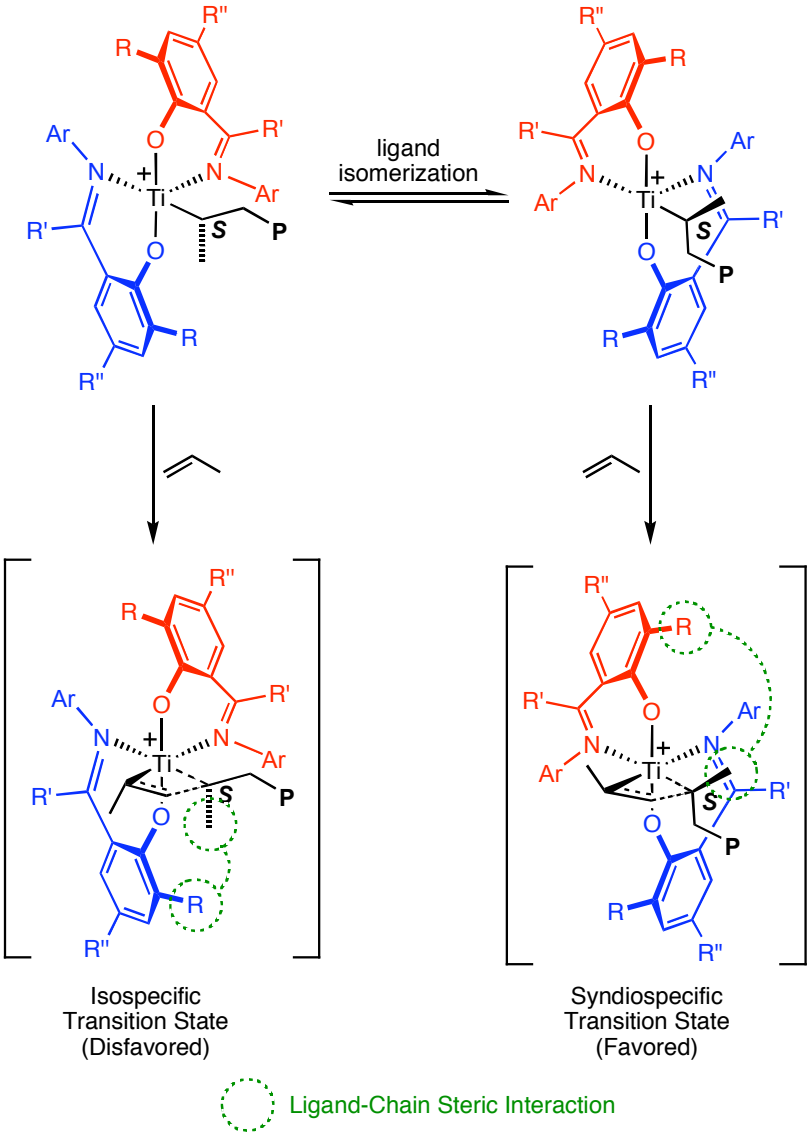

Scheme 2.1. Isoselective and syndioselective transition states for PHI catalysts.

triisobutylaluminum, low olefin polymerization activity was observed. Interestingly, isotactic polymers were obtained under similar conditions from the polymerization of 1-butene, 1-pentene, and 1-hexene. Analogous titanium catalysts yielded mostly aPP with small fractions (ca. 10 wt%) of iPP ([*mm*] = 95%), while complexes bearing a methyl group adjacent to the imine functionality on the phenolate ring resulted in the formation of moderately

isotactic PP ([*mm*] = 75%).[46] In all cases, it appears that reaction between the ligand and the alkylaluminum present in the activation cocktail results in the *in situ* reduction of the imine functionality, leading to multiple active species and broad molecular weight distributions. This *in situ* ligand modification may also be the source of the observed isoselectivity.

We reasoned that placing substituents on the carbon atom of the imine moiety would inhibit the fluxional behavior for this class of catalysts, thereby enforcing the C_2-symmetry of the active species. Titanium complexes bearing these PKI ligands with *N*-pentafluorophenyl groups resulted in the living and moderately isoselective polymerization of propylene.[26] The microstructure of the iPP was consistent with an enantiomorphic site-control mechanism. Zirconium dichloride complexes bearing PKI ligands have been prepared by Hu and co-workers.[47] When activated with MAO, these catalysts yielded high molecular weight polyethylenes with broadened molecular weight distributions ($M_w/M_n \geq 1.7$).

2.2.2 Synthesis of PKI Complexes

The PKI complexes were prepared via the route depicted in Scheme 2.2. The amide precursors were prepared by reaction of the desired acid chloride with perfluoroaniline with pyridine as a sacrificial base to remove hydrogen chloride produced. In our hands, use of triethylamine as a sacrificial base led to side reactions that did not give the desired amide in good yield; reaction with pyridine furnished the amide products in quantitative yield. Formation of the imidoyl chloride was then effected by reaction of the amide with phosphorous pentachloride. Reaction of the appropriately substituted phenol with the crude imidoyl chloride and $AlCl_3$ in 1,2-dichloroethane gave the

corresponding PKI ligands in 4–77% yield, with the major impurity being the *O*-imidoylated product. Deprotonation of the PKI ligand was effected with *n*-BuLi and the resulting ligand salt was transferred to a tetrahydrofuran (THF) solution of 0.5 equivalents $TiCl_4$ to give the bis-ligated complex. Recrystallization of the compounds from CH_2Cl_2/pentane or toluene/pentane provided the complexes as dark brown to red crystals in 27-61% yield. For all complexes, ^1H, ^{13}C, and ^{19}F NMR spectra showed the presence of a single C_2-symmetric isomer in both benzene-d_6 and chloroform-*d* at room temperature.

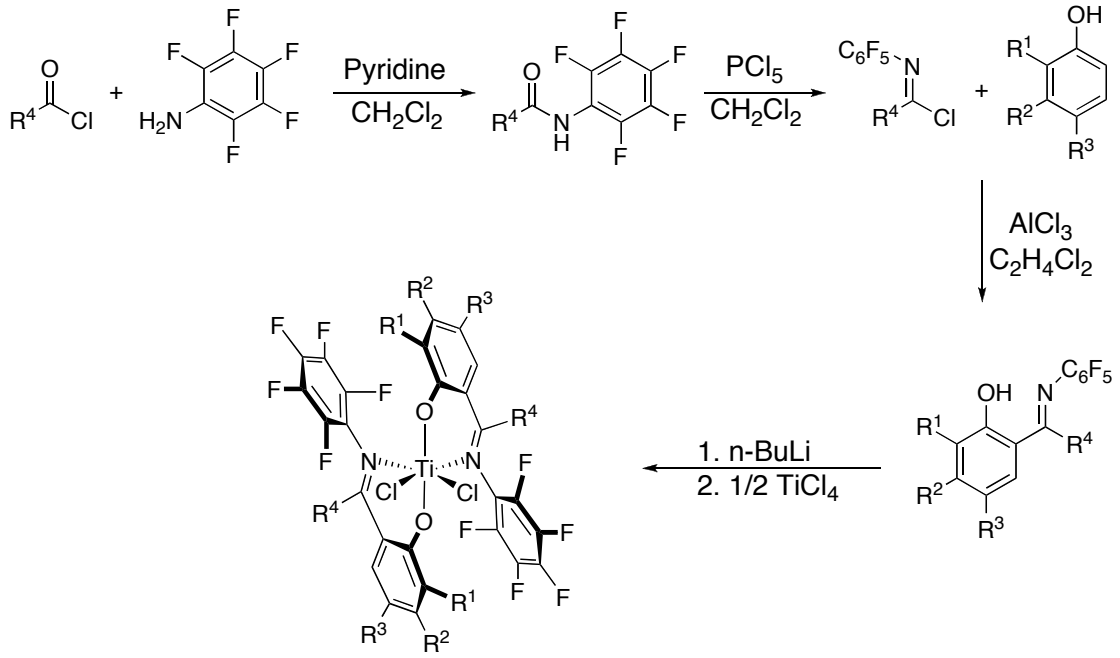

Scheme 2.2. Synthesis of bis(phenoxyketimine)titanium complexes.

2.2.3 Effect of the Ortho Substituent on the Phenolate Ring

Recently, Pellecchia and co-workers have shown that titanium complexes bearing PHI ligands with halide substituents at the ortho position of the phenolate ring and *N*-pentafluorophenyl groups quite unexpectedly promoted moderately isoselective polymerization of propylene ($R^1 = R^3 = I$, R^4

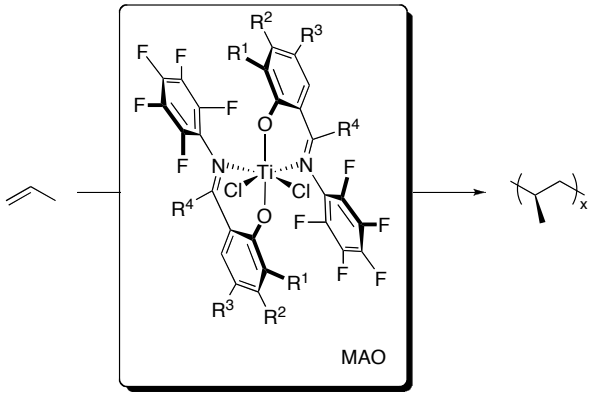

Complex	R^1	R^2	R^3	R^4
2.1	Me	H	Me	Ph
2.2	Cl	H	Me	Ph
2.3	Br	H	Me	Ph
2.4	Ph	H	Me	Ph
2.5	Bn	H	Me	Ph
2.6	$-(CH_2)_4-$		H	Ph
2.7	Me	H	Cl	Ph
2.8	Me	H	F	Ph
2.9	Me	H	OMe	Ph
2.10	Me	H	Me	Me
2.11	Me	H	Me	^{i}Pr
2.12	Me	H	Me	Cy
2.13	Me	H	Me	Cycloheptyl
2.14	Me	H	Me	CF_3
2.15	Me	H	Me	2-Naphthyl
2.16	Me	H	Me	1-Naphthyl
2.17	Me	H	Me	4-Methoxyphenyl
2.18	Me	H	Me	Mesityl
2.19	Me	H	Me	C_6F_5

Scheme 2.3. Titanium phenoxyketimine compounds.

= H; [*mm*] = 0.73, $\alpha = 0.90$; see Scheme 2.3).[48] A related PKI complex ($R^1 = R^3 =$ Br, R^4 = Ph) produced aPP. This lies in stark contrast to the observed isoselectivity of PKI titanium complexes bearing alkyl substituents.[26] In all cases, molecular weight distributions were broad ($M_w/M_n \geq 1.6$) indicative of a non-living polymerization system.

We have previously investigated titanium complexes supported by PKI ligands bearing different alkyl substituents at the ortho position of the phenolate moiety (R^1).[26] As this substituent decreases in size, polymerization activity and the isotacticity of the resultant polypropylene increases. The highest isotacticity was observed with complexes bearing *ortho*-methyl substituents on the phenolate rings of the ligand. Due to the interesting behavior reported by Pellecchia for halogenated PHI catalysts,[48] we reasoned that complexes bearing halogens at the ortho position of the phenolate ring could be worth investigating.

A series of PKI complexes with pentafluorophenyl *N*-aryl groups, a phenyl ketimine (R^4) substituent and various ortho substituents on the phenolate ring (R^1) were investigated to optimize facial selectivity (Scheme 2.3, complexes **2.1-6**). In this series, the ortho substituents on the phenolate moiety were chosen on the basis of having pronounced steric and electronic differences. We expected that the propylene polymerization catalyzed by **1-6**/MAO would follow the trends observed for previously reported PKI catalysts, where decreasing the size of the R substituent leads to higher activities and stereoselectivites.[26] From this initial report, it was shown that a methyl group at the ortho position of the phenolate ring was optimally sized to provide good facial selectivity for propylene polymerization.

Table 2.1 provides the propylene polymerization data for complexes **2.1**-**6**. When activated with MAO, all complexes were active with the exception of **2.4**, and produced isoenriched polypropylene with [m^4]-values ranging from 0.30 - 0.57. All active catalysts formed polymers with very narrow molecular weight distributions ($M_w/M_n \leq 1.12$), which suggests living behavior. Compared to **2.1**, the halogenated complexes (**2.2** and **2.3**) showed much higher activity, which could be attributed to the electron withdrawing character of the halogen substituents. Catalyst activity increased as the halogen decreased in size. This could be attributed to both the increase in electronegativity of the halogen substituent as well as a decrease in steric congestion near the active site. Interestingly, **2.3** (R^1 = Br) was approximately two times more active than **2.1** for propylene polymerization and the resultant polymer had an [m^4]-value of 0.57 and a melting temperature (T_m) of 73.4 °C. However, **2.2** (R^1 = Cl) provided polypropylene with an [m^4]-value of 0.31 and no melting transition, thus illustrating the extreme sensitivity of the

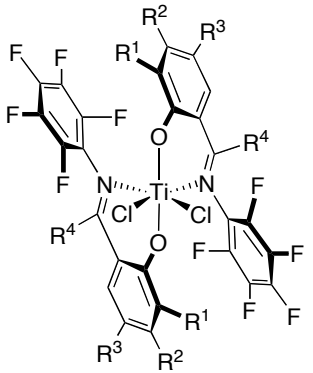

Complex	R^1	R^2	R^3	R^4
2.1	Me	H	Me	Ph
2.2	Cl	H	Me	Ph
2.3	Br	H	Me	Ph
2.4	Ph	H	Me	Ph
2.5	Bn	H	Me	Ph
2.6	$-(CH_2)_4-$		H	Ph

Table 2.1. Propylene polymerization data for compounds **2.1-6**/MAO.[a]

	Cplx	Time (h)	Yield (g)	TOF (h^{-1})[b]	M_n^{theo} (g/mol)	M_n (g/mol)[c]	M_w/M_n[c]	[*mmmm*][d]	α[e]	T_g (°C)[f]	T_m (°C)[f]
1	**2.1**	6.0	0.55	230	55,000	43,000	1.10	0.52	0.88	-12.4	n.d.[g]
2	**2.2**	6.0	2.24	890	224,000	148,000	1.09	0.31	0.79	-9.4	n.d.[g]
3	**2.3**	6.0	1.34	530	134,000	93,300	1.08	0.57	0.89	-14.3	73.4
4	**2.4**	6.0	trace[h]	—	—	—	—	—	—	—	—
5	**2.5**	6.0	0.04	20	4,000	3,000	1.10	0.43	0.84	-23.2	n.d.[g]
6	**2.6**	6.0	0.15	58	15,000	15,000	1.12	0.54	0.89	-13.3	85.1

[a]General conditions: 10 μmol of the complex in toluene (5 mL) was added to a propylene-saturated PMAO-IP solution (100 mL of toluene; [Al]/[Ti] = 150) at 0 °C. [b]Average turnover frequency (TOF): mol propylene/(mol Ti·h). [c]Determined using gel permeation chromatography in 1,2,4-$C_6H_3Cl_3$ at 140 °C versus polyethylene standards. [d]Determined by integration of the methyl region of the ^{13}C NMR spectrum. [e]Enantiofacial selectivity parameter, calculated from the ^{13}C NMR spectrum using the equation $[m^4] = \alpha^5 + (1-\alpha)^5$. [f]Determined using differential scanning calorimetry (2nd heating). [g]None detected. [h]Polymer yield was insufficient for characterization.

relationship between the facial selectivity and the size of the ortho substituent of the phenolate ring. Complex **2.4** (R^1 = Ph) only produced trace amounts of polymer, while complex **2.5,** bearing a bulkier benzyl substituent, showed a marginally higher activity. Complex **2.6**, derived from tetrahydronaphthol, was sparingly active and produced a polymer with an [m^4]-value of 0.54 and T_m of 85.1 °C. The polypropylene produced by **2.6**/MAO, despite having a similar [m^4]-value, showed a higher T_m than the polypropylene produced by **2.3**/MAO. This could be attributed to a decrease in the number of regioinversions of the polypropylene produced by **2.6**/MAO versus **2.3**/MAO.

2.2.4 Effect of the Para Substituent on the Phenolate Ring

Once the role of the ortho substituent on the phenolate ring (R^1) was established, the effect of the para substituent (R^3) was investigated. Scheme 2.3 (entries **2.7**-**9**) summarizes the series of complexes that were synthesized and screened for propylene polymerization behavior. We anticipated that electron-withdrawing R^3 groups with greater electronegativities would increase catalyst activity by increasing the electrophilicity of the metal center. We did not expect these changes to effect the facial selectivity of the catalyst due to the remote location of the para substituent relative to the active site.

Table 2.2 provides the propylene polymerization data for complexes **2.7**-**9**. When activated with MAO, all catalysts were active and produced polypropylene with [m^4]-values ranging from 0.51 - 0.53. Catalyst activities did not follow the expected trend where more electron-withdrawing substituents give higher activities. For example, **2.7** (R^3 = Cl) had an activity approximately half that of **2.1**, whereas **2.8** (R^3 = F) had an activity approximately twice that

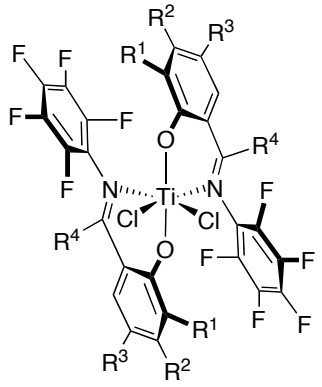

Complex	R^1	R^2	R^3	R^4
2.7	Me	H	Cl	Ph
2.8	Me	H	F	Ph
2.9	Me	H	OMe	Ph

Table 2.2. Propylene polymerization data for compounds **2.7-9**/MAO.[a]

Entry	Cplx	Time (h)	Yield (g)	TOF (h^{-1})[b]	M_n^{theo} (g/mol)	M_n (g/mol)[c]	M_w/M_n[c]	[*mmmm*][d]	α[e]	T_g (°C)[f]	T_m (°C)[f]
1	**2.7**	6.0	0.32	130	32,000	70,000	1.13	0.53	0.88	-14.2	n.d.[g]
2	**2.8**	6.0	1.05	420	105,000	77,500	1.07	0.51	0.87	-12.8	n.d.[g]
3	**2.9**	3.0	1.45	1170	146,000	78,200	1.98	0.51	0.87	-8.5	145.8

[a]General conditions: 10 μmol of the complex in toluene (5 mL) was added to a propylene-saturated PMAO-IP solution (100 mL of toluene; [Al]/[Ti] = 150) at 0 °C. [b]Average turnover frequency (TOF): mol propylene/(mol Ti·h). [c]Determined using gel permeation chromatography in 1,2,4-$C_6H_3Cl_3$ at 140 °C versus polyethylene standards. [d]Determined by integration of the methyl region of the ^{13}C NMR spectrum. [e]Enantiofacial selectivity parameter, calculated from the ^{13}C NMR spectrum using the equation $[m^4] = \alpha^5 + (1-\alpha)^5$. [f]Determined using differential scanning calorimetry (2nd heating). [g]None detected.

of **2.1**. Both **2.7** and **2.8** formed polypropylene with very narrow molecular weight distributions ($M_w/M_n \leq 1.13$). Surprisingly, **2.9** (R^3 = OMe) had an activity five times higher than **2.1**. The GPC trace for the polypropylene produced by **2.9** was broad and multimodal, indicative of multiple active species. The resultant polypropylene showed a T_m of 145.8 °C and could be separated into ether soluble (ca. 24 wt%) and ether insoluble (ca. 76 wt%) fractions both giving GPC traces that were again broad and multimodal. One possible explanation for this observation is that the methoxy group on the ancillary ligand reacts with the co-catalyst *in situ* to generate one or more new active species. We are currently investigating the source of this unusual polymerization behavior.

2.2.5 Effect of Alkyl Substituents on the Ketimine Carbon

PKI catalysts previously studied for propylene polymerization contained a phenyl ketimine substituent (R^4). Although remote from the active center, we reasoned that by investigating other substituents off of the ketimine carbon that improved isoselectivity for propylene polymerization could be achieved. To probe the difference between a phenyl and alkyl groups at this position, complexes bearing various alkyl ketimine substituents (R^4) incorporating the 2,4-dimethylphenol moiety were synthesized and screened for propylene polymerization behavior (Scheme 2.3, entries **2.10**-**14**).

Table 2.3 provides the propylene polymerization data for complexes **2.10**-**14**. When activated with MAO, all catalysts were active and produced polypropylene with [m^4]-values ranging from 0.61 - 0.73. In all cases, catalysts bearing alkyl substituents on the ketimine carbon were more isoselective for propylene polymerization than **2.1** (R^4 = Ph). Catalyst **2.10** (R^4 = Me) furnished

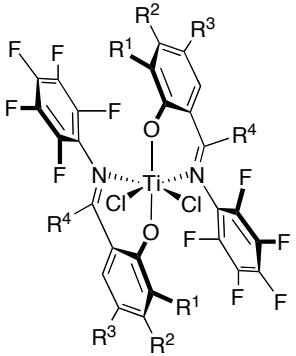

Complex	R^1	R^2	R^3	R^4
2.10	Me	H	Me	Me
2.11	Me	H	Me	^{i}Pr
2.12	Me	H	Me	Cy
2.13	Me	H	Me	Cycloheptyl
2.14	Me	H	Me	CF_3

Table 2.3. Propylene polymerization data for compounds **2.10-14**/MAO.[a]

Entry	Cplx	Time (h)	Yield (g)	TOF (h^{-1})[b]	M_n^{theo} (g/mol)	M_n (g/mol)[c]	M_w/M_n[c]	[*mmmm*][d]	α[e]	T_g (°C)[f]	T_m (°C)[f]
1	**2.10**	6.0	0.08	30	8,000	8,000	1.14	0.61	0.91	-14.4	90.3
2	**2.11**	6.0	0.10	41	10,000	8,500	1.25	0.67	0.92	-11.4	114.5
3	**2.12**	6.0	0.07	30	7,000	8,000	1.22	0.73	0.94	-12.9	116.8
4	**2.13**	6.0	0.09	30	9,000	8,000	1.23	0.69	0.93	-11.5	111.9
5	**2.14**	6.0	1.53	604	153,000	364,000	1.33	0.68	0.93	-11.3	93.8
6[g]	**2.14**	4.0	0.29	340	58,000	76,000	1.09	0.67	0.92	-13.0	93.3

[a]General conditions: 10 μmol of the complex in toluene (5 mL) was added to a propylene-saturated PMAO-IP solution (100 mL of toluene; [Al]/[Ti] = 150) at 0 °C. [b]Average turnover frequency (TOF): mol propylene/(mol Ti·h). [c]Determined using gel permeation chromatography in 1,2,4-$C_6H_3Cl_3$ at 140 °C versus polyethylene standards. [d]Determined by integration of the methyl region of the ^{13}C NMR spectrum. [e]Enantiofacial selectivity parameter, calculated from the ^{13}C NMR spectrum using the equation $[m^4] = \alpha^5 + (1-\alpha)^5$. [f]Determined using differential scanning calorimetry (2nd heating). [g]5 μmol of the complex in toluene (5 mL) was added to a propylene-saturated PMAO-IP solution (100 mL of toluene; [Al]/[Ti] = 150) at -40 °C.

a polymer with [m^4] = 0.61 and T_m = 90.3 °C, but the activity was approximately an order of magnitude lower than **2.1**. Increasing the steric demand of the R^4 substituent lead to improved tacticity. For example, catalyst **2.11** (R^4 = ^{i}Pr) polymerized propylene with an activity comparable to **2.10** and furnished a polymer with [m^4] = 0.67 and T_m = 114.5 °C. A further gain in tacticity was achieved upon replacing the ^{i}Pr ketimine substituent with cyclohexyl as catalyst **2.12** exhibited similar activity to **2.10** and **2.11** but provided polymer with [m^4] = 0.73 and T_m = 116.8 °C. Despite incorporating the bulkier cycloheptyl ketimine substituent, catalyst **2.13** resulted in a polymer with [m^4] = 0.69 and T_m = 111.9 °C, although the activity was comparable to that observed with **2.12**. Catalysts **2.10-13** formed polypropylene with narrow molecular weight distributions ($M_w/M_n \leq 1.25$) and with good agreement between the number average molecular weight (M_n) and that expected based on the assumption of one chain per metal center (M_n^{theo}). To investigate the difference between alkyl and fluorinated alkyl substituents, catalyst **2.14**, which bears a trifluoromethyl ketimine substituent (R^4 = CF_3) was synthesized. Polymerization of propylene with **2.14**/MAO proceeded with an activity approximately 20 times that of **2.10** and provided a polymer with [m^4] = 0.68 and T_m = 93.8 °C. The resultant molecular weight distribution (M_w/M_n = 1.33) was slightly broadened upon replacing the methyl ketimine substitution for CF_3, and there was a discrepancy between M_n and M_n^{theo}. Cooling the reaction to -40 °C lead to a more controlled polymerization where the disparity between M_n and M_n^{theo} was smaller and the resultant polypropylene showed a much narrower molecular weight distribution (M_w/M_n = 1.09). However, lower reaction temperature did not

have a pronounced effect on the activity of the polymerization and furnished polypropylene with similar tacticity; [m^4] = 0.67 and T_m = 93.3 °C.

2.2.6 Effect of Aryl Substituents on the Ketimine Carbon

To investigate the effect of the aryl ketimine substituents (R^4), catalysts incorporating the 2,4-dimethylphenol moiety were synthesized and screened for propylene polymerization (Scheme 2.3, entries **2.15-19**). In light of the trends observed with PKI catalysts bearing different alkyl substituents, we reasoned that bulkier aryl substituents would give increased isoselectivity for propylene polymerization.

Table 2.4 provides the propylene polymerization data for complexes **2.15-19**. When activated with MAO, all catalysts were active and produced polypropylene with [m^4]-values ranging from 0.32 - 0.66. Catalyst **2.15**/MAO bearing a 2-naphthyl ketimine substituent behaved almost identically to catalyst **1**, giving approximately the same molecular weight, activity and level of isoselectivity. Upon changing the connectivity (**2.16**, R^4 = 1-naphthyl), the activity decreases five-fold from **2.15** and furnishes PP with an [m^4] = 0.66 and T_m = 105.2 °C. Catalyst **2.17** (R^4 = 4-methoxyphenyl) provided polypropylene with a high T_m (144.1 °C) but behaved similarly to **2.9** in that a multimodal GPC trace was obtained. Because this behavior is only observed with ligands featuring methoxy groups, we believe an interaction between the aluminum co-catalyst and the methoxy group could be causing this unusual behavior. Catalyst **2.18**, which contains a mesityl ketimine (R^4) substituent, exhibits an activity that is slightly higher than **2.1** and produces PP with [m^4] = 0.32. Employing a perfluorophenyl ketimine substituent, **2.19**/MAO exhibited an activity twice that of **2.1** and produced PP with [m^4] = 0.58 and T_m = 68.8 °C.

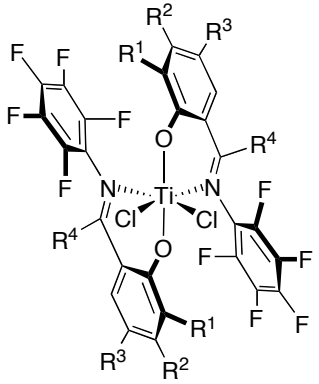

Complex	R^1	R^2	R^3	R^4
2.15	Me	H	Me	2-Naphthyl
2.16	Me	H	Me	1-Naphthyl
2.17	Me	H	Me	4-Methoxyphenyl
2.18	Me	H	Me	Mesityl
2.19	Me	H	Me	C_6F_5

Table 2.4. Propylene polymerization data for compounds **2.15-19**/MAO.[a]

Entry	Cplx	Time (h)	Yield (g)	TOF (h^{-1})[b]	M_n^{theo} (g/mol)	M_n (g/mol)[c]	M_w/M_n[c]	[*mmmm*][d]	α[e]	T_g (°C)[f]	T_m (°C)[f]
1	**2.15**	6.0	0.65	250	65,000	45,000	1.08	0.52	0.88	-12.0	n.d.[g]
2	**2.16**	6.0	0.12	49	12,000	12,000	1.19	0.66	0.92	-12.4	105.2
3	**2.17**	2.0	0.41	490	41,000	87,000	3.19	0.53	0.88	-7.1	144.1
4	**2.18**	6.0	0.76	310	76,000	83,000	1.28	0.32	0.80	-6.5	n.d.[g]
5	**2.19**	6.0	1.33	538	133,000	170,000	1.11	0.58	0.89	-15.1	68.8

[a]General conditions: 10 μmol of the complex in toluene (5 mL) was added to a propylene-saturated PMAO-IP solution (100 mL of toluene; [Al]/[Ti] = 150) at 0 °C. [b]Average turnover frequency (TOF): mol propylene/(mol Ti·h). [c]Determined using gel permeation chromatography in 1,2,4-$C_6H_3Cl_3$ at 140 °C versus polyethylene standards. [d]Determined by integration of the methyl region of the ^{13}C NMR spectrum. [e]Enantiofacial selectivity parameter, calculated from the ^{13}C NMR spectrum using the equation $[m^4] = \alpha^5 + (1-\alpha)^5$. [f]Determined using differential scanning calorimetry (2nd heating). [g]None detected.

In all cases the PP produced from **2.15-19**/MAO displayed narrow molecular weight distributions ($M_w/M_n \leq 1.28$).

2.2.7 Microstructural Analysis of Polypropylenes by ^{13}C NMR Spectroscopy

Figure 2.6 provides the ^{13}C NMR spectrum of iPP obtained from **2.12/**MAO at 0 °C. The major stereoerrors present correspond to *mmmr*, *mmrr*, and *mrrm* pentads. These three pentads are present in a 2:2:1 ratio, which is indicative of an enantiomorphic site-control enchainment mechanism. The ^{13}C NMR spectra of iPPs obtained from **2.1-11** and **2.13-19**/MAO were similar in appearance to that obtained from **2.12**/MAO (see Appendix) and show varying degrees of stereocontrol with the major stereoerrors present corresponding to *mmmr*, *mmrr*, and *mrrm* pentads in a 2:2:1 ratio. This is consistent with previously reported PKI catalysts,[26] but is quite different from the previously reported syndioselective PHI catalysts which have stereoerrors resulting from a chain-end control mechanism.[28]

While the polymer obtained from **2.12**/MAO is very regioregular, resonances corresponding to head-to-head and tail-to-tail misinsertions can be detected in the δ 14 - 16 and δ 31 - 46 ppm regions of the ^{13}C NMR spectrum.[22] The occurrence of regioerrors varied in polypropylenes produced using **2.1-19**/MAO. The PP produced by **2.18**/MAO displayed the lowest occurrence of regioerrors. Despite being more isoselective than **2.1**, the PP produced by **2.19**/MAO displayed the highest occurrence of regioerrors of the catalysts studied.

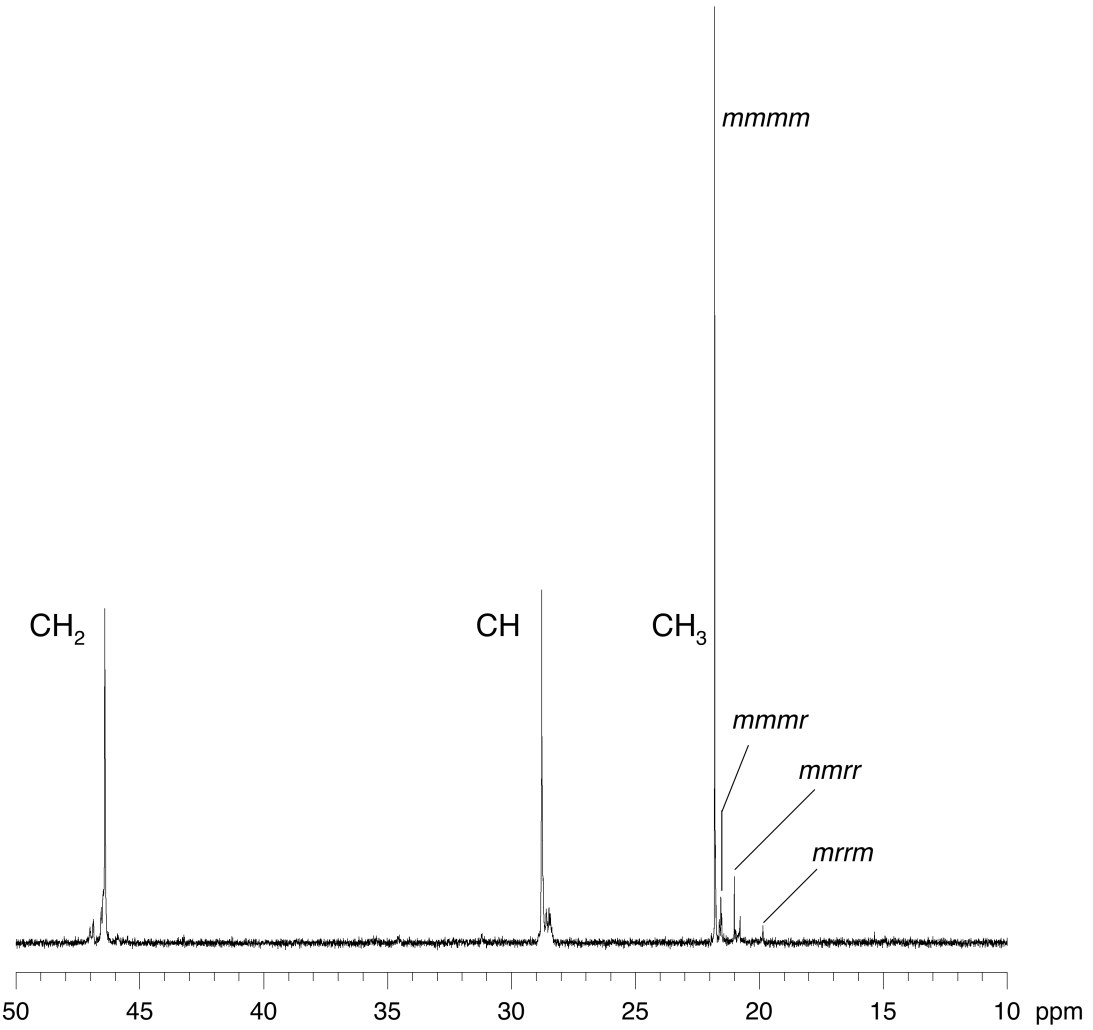

Figure 2.6. ^{13}C NMR (1,1,2,2-$C_2D_2Cl_4$, 125 MHz, 135 °C) of isotactic polypropylene formed by **2.12**/MAO at 0 °C. The presence of the unmarked peak in the methyl region is due to regioinversions.

2.2.8 Living Behavior of Bis(phenoxyketimine)titanium Complexes

The narrow molecular weight distribution of the iPP produced by **2.12**/MAO, coupled with the observed good agreement between M_n and M_n^{theo}, indicate that propylene polymerization catalyzed by **2.12**/MAO is living. The living behavior of **2.12**/MAO is further exemplified by the observation that M_n increases linearly with polypropylene yield (Figure 2.7).

The molecular weight distribution for shorter reaction times is somewhat broadened (t = 6 hrs; M_w/M_n = 1.30), but narrows for longer reaction times (t = 48 hrs; M_w/M_n = 1.15). This is presumably due to slow initiation.

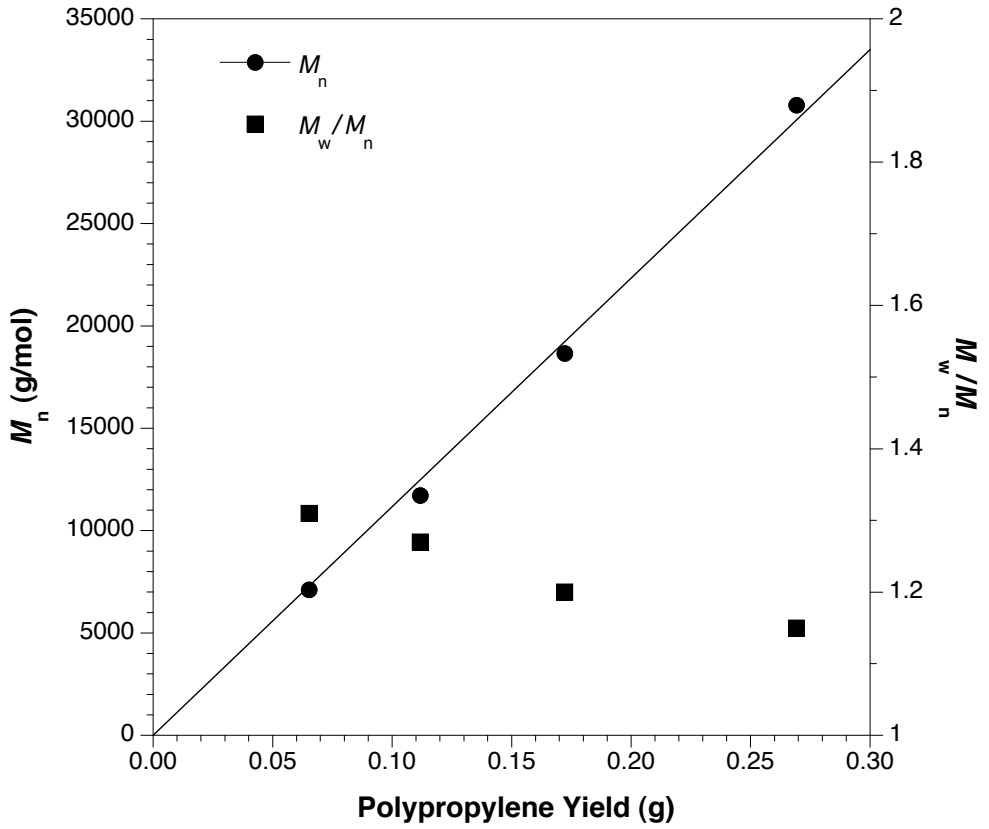

Figure 2.7. Plot of polypropylene M_n (○) and M_w/M_n (■) vs polypropylene yield using **2.12**/MAO at 0 °C.

2.2.9 Block Copolymers from Propylene and Ethylene

While one drawback of a living polymerization system is that only one polymer chain per metal center is produced, the real utility of these systems lies in the ability to synthesize well-defined block copolymers and identify new polymer architectures with promising physical, mechanical, and chemical properties. There are few examples of block copolymers incorporating iPP

segments in the literature,[5-8,24-26] which is due in large part to the fact that few catalyst systems have been reported that are capable of polymerizing propylene in a living manner with high isoselectivity and activity. Block copolymers incorporating sPP, however, have been synthesized with much greater ease.

In 1988, Doi and co-workers synthesized an *s*PP-*block*-PEP-*block*-*s*PP triblock copolymer with a narrow molecular weight distribution (M_w/M_n = 1.24) and a high molecular weight (M_n = 94 kg/mol) utilizing a catalyst system comprised of $V(acac)_3/Et_2AlCl/anisole$.[49] Bis(phenoxyimine)titanium complexes employing the *N*-pentafluoroaniline moiety and bulky *tert*-butyl R groups have been used to synthesize an *s*PP-*block*-PEP diblock[32,50] and an *s*PP-*block*-PEP-*block*-*s*PP triblock copolymer.[8] This class of catalysts has also been used to produce a PE-*block*-*s*PP diblock copolymer and a PE-*block*-PEP-*block*-*s*PP triblock copolymer.[51] A sPP-*block*-poly(propylene-*co*-MCP-*co*-3-VTM) (MCP = methylene-1,3-cyclopentane; 3-VTM = 3-vinyl tetramethylene) diblock copolymer has also been produced via sequential monomer addition using propylene and 1,5-hexadiene with this class of catalysts.[52]

Owing to the living behavior and the relatively high isoselectivity of **2.12**/MAO for propylene polymerization, we reasoned that it would make an ideal catalyst for the synthesis of block copolymers incorporating iPP segments (Scheme 2.4). Living polymerization of propylene at 0 °C resulted in the formation of iPP ([m^4] = 0.73). Once a block of the desired length was formed (typically after 15 h), a slight overpressure of ethylene was added and copolymerized with the unreacted propylene to produce a PEP block. The molecular weight of the PEP block was adjusted by varying the duration of polymerization (Table 2.5, entries 1-3). Triblock iPP-*block*-PEP-*block*-iPP

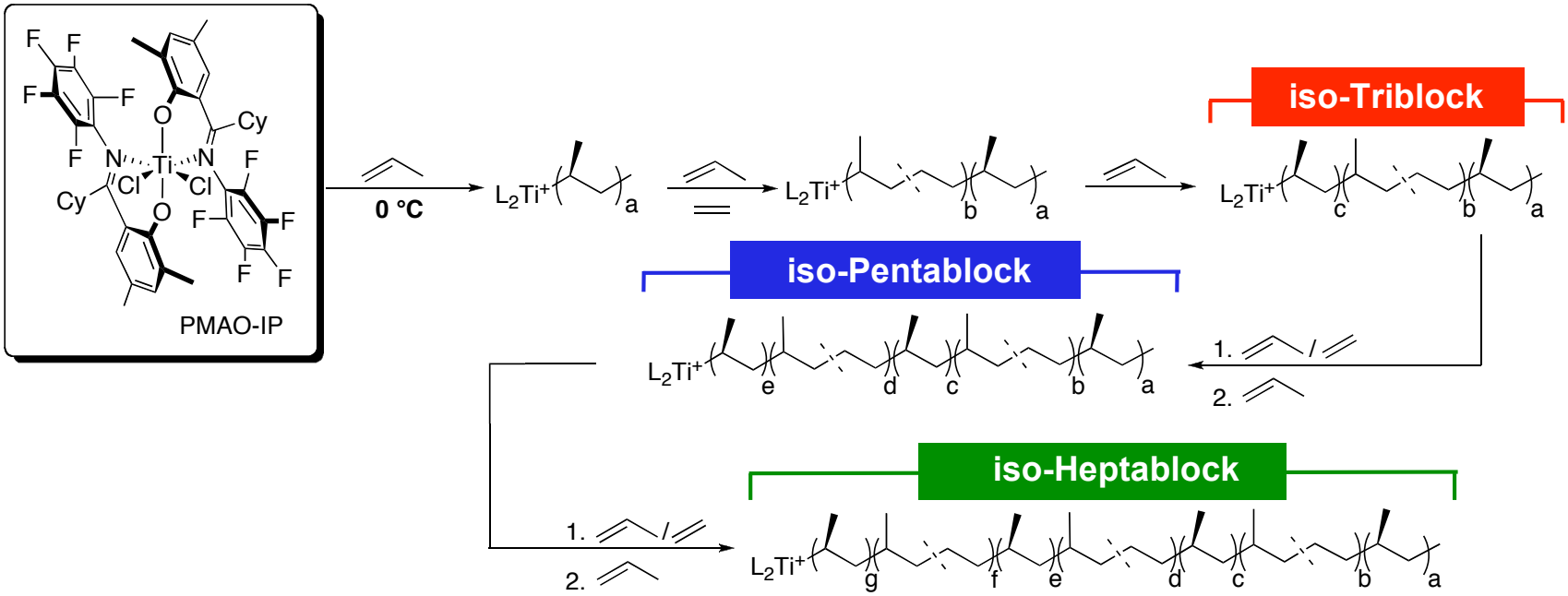

Scheme 2.4. Synthesis of block copolymers from ethylene and propylene.

Table 2.5. Block copolymer characterization.[a]

Sample	$M_{n,tot}$ (kg/mol)[b]	M_w/M_n [b]	Block Lengths (kg/mol)[b]	Wt. % of Hard Blocks[c]	F_e total (mol%)[d]	T_g (°C)[e]	T_m (°C)[e]
*i*PP-*b*-PEP-*b*-*i*PP (*iso***TB**-**1**)	102	1.13	12-75-15	26	16	-35	115
*i*PP-*b*-PEP-*b*-*i*PP (*iso***TB**-**2**)	144	1.18	14-117-13	17	17	-33	107
*i*PP-*b*-PEP-*b*-*i*PP (*iso***TB**-**3**)	235	1.30	14-206-15	12	15	-39	95
*i*PP-*b*-PEP-*b*-*i*PP-*b*-PEP-*b*-*i*PP (*iso***PB**)	195	1.15	14-74-15-78-14	22	20	-40	94
*i*PP-*b*-PEP-*b*-*i*PP-*b*-PEP-*b*-*i*PP-*b*-PEP-*b*-*i*PP (*iso***HB**)	227	1.13	13-74-7-51-32-44-6	26	18	-33	88

[a]General conditions: 10 μmol of **2.12** in toluene (5 mL) was added to a propylene-saturated PMAO-IP solution (100 mL of toluene; [Al]/[Ti] = 150) at 0 °C. After the desired time, a C_2H_4 feed was established. The C_2H_4 feed was discontinued and the reactor was vented to 0 psig, 30 psig of propylene reconnected and polymerization allowed to proceed for the desired time. [b]Determined by the difference in M_n of aliquots pulled after the formation of each block using gel permeation chromatography in 1,2,4-$C_6H_3Cl_3$ at 140 °C versus polyethylene standards. [c]Wt. % of Hard Blocks = (Σ $M_{n,hard}$) / ($M_{n,tot}$). [d]Mole fraction of ethylene (F_e) determined by integration of the ^{13}C NMR spectrum. [e]Determined using differential scanning calorimetry (2nd heating).

copolymers were synthesized by the removal of ethylene and by reestablishing the propylene feed for the specified time. To our knowledge, this is the first synthesis of an iPP-*block*-PEP-*block*-iPP triblock copolymer via sequential monomer addition. A pentablock copolymer (*iso***PB**) and heptablock copolymer (*iso***HB**) were made in an analogous manner (Table 2.5, entries 4 and 5). Due presumably to decreased diffusion efficiency resulting from the high viscosity of the polymerization mixture, a higher overpressure of ethylene was required to install the second and third PEP block of the pentablock and heptablock copolymer, respectively.

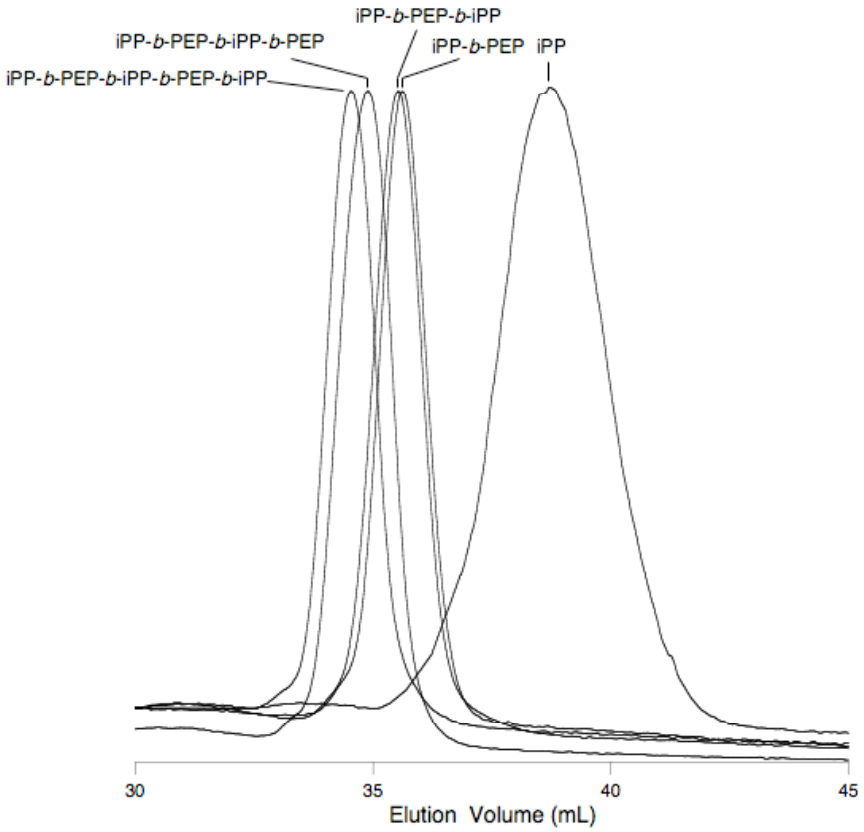

Figure 2.8. GPC profiles after the formation of each block of the *iso***PB** synthesized using complex **2.12**/MAO at 0 °C.

The iPP segments had a melting temperature between 99 and 115 °C, decreasing with increasing overall molecular weight for the triblock copolymer samples (Table 2.5, entries 1-3). Ethylene fractions (F_e) in the triblock copolymers ranged from 15-17 mol%. The melting temperature of the pentablock copolymer was 94 °C and had an F_e of 20 mol% while the heptablock copolymer had a T_m of 88 °C and an F_e of 18 mol%. All block copolymers showed a T_g between -40 and -33 °C. The high melting temperatures and low glass transition temperatures are indicative of block copolymers incorporating iPP and PEP segments. A representative GPC profile of the pentablock copolymer is shown in Figure 2.8 where aliquots were removed from the polymerization mixture after the formation of each block and the resultant polymers were analyzed via gel permeation chromatography.

Table 2.6. Block copolymer mechanical testing data

Sample	Young's modulus (MPa)[a]	Strain at break (%)	True stress at break (MPa)	Melting enthalpy (J/g)	Elastic recovery (%)[b]
*iso***TB-1**	10.9	~1000	120	14.3	80
*iso***TB-2**	6.9	~800	64	11.8	81
*iso***TB-3**	12.0	~950	112	16.1	68
*iso***PB**	11.7	~790	84	16.8	79
*iso***HB**	9.0	~830	100	13.1	85

[a] Measured in tension at strain of 15%. [b] After 750% prestrain

2.2.10 Mechanical Properties of Block Copolymers

The initial Young's modulus is partly determined by the connectivity between crystalline lamellae, which is why it correlates roughly with the melting enthalpy and thus crystallinity. After about a 500% prestrain, the Young's modulus after unloading decreases dramatically to values between 1.2 and 2.5 MPa that are more typical of an elastomer. The prestrain presumably breaks up the network of crystalline lamellae into individual iPP fibrils separated by the rubbery PEP blocks.

Table 2.6 lists the block copolymers elastomeric behavior that was surprisingly similar. Plots of true stress (σ_{true}) versus percent strain are provided in Figure 2.9. The elastic recovery of the samples was also evaluated (Figure 2.10). The triblock copolymer (*iso***TB-1**) displayed an elongation at break of ~ 1000% with a tensile true stress of 120 MPa and an 80% recovery up to elongation of 750%. Increasing the midblock PEP segment length of the triblock copolymers lead to diminished values for elongations at break and tensile true stress. For example, *iso***TB-2**, exhibited an elongation at break of ~ 800% and a tensile true stress of 64 MPa with an 81% recovery up to elongation of 750% while *iso***TB-3** exhibited an elongation at break of ~ 950% and a tensile true stress of 112 MPa with a 68% recovery up to elongation of 750%. The pentablock copolymer (*iso***PB**) displayed an elongation at break of ~ 790% with a tensile true stress of 84 MPa and a 79% recovery up to elongation of 750% while the heptablock copolymer showed an elongation at break of ~ 830% with a tensile true stress of 100 MPa and an 85% recovery up to elongation of 750%. While the mechanical properties of the block copolymers are similar, it is apparent that incorporation of large PEP segments leads to a decrease in the percent recovery of the materials.

The triblock copolymer (*iso***TB-1**) displayed the highest ultimate elongation at break (~ 1000%) relative to the other copolymers studied herein. This value is lower than the triblock copolymer comprised of iPP-*b*-rirPP-*b*-iPP (~ 1700%)[8] and tetrablock copolymer comprised of iPP-*b*-aPP-*b*-iPP-*b*-aPP (~ 1200%).[7] The lower elongation at break displayed for *iso***TB-1** could be due to a number of factors such as overall crystallinity, molecular weight, or amorphous segment identity.

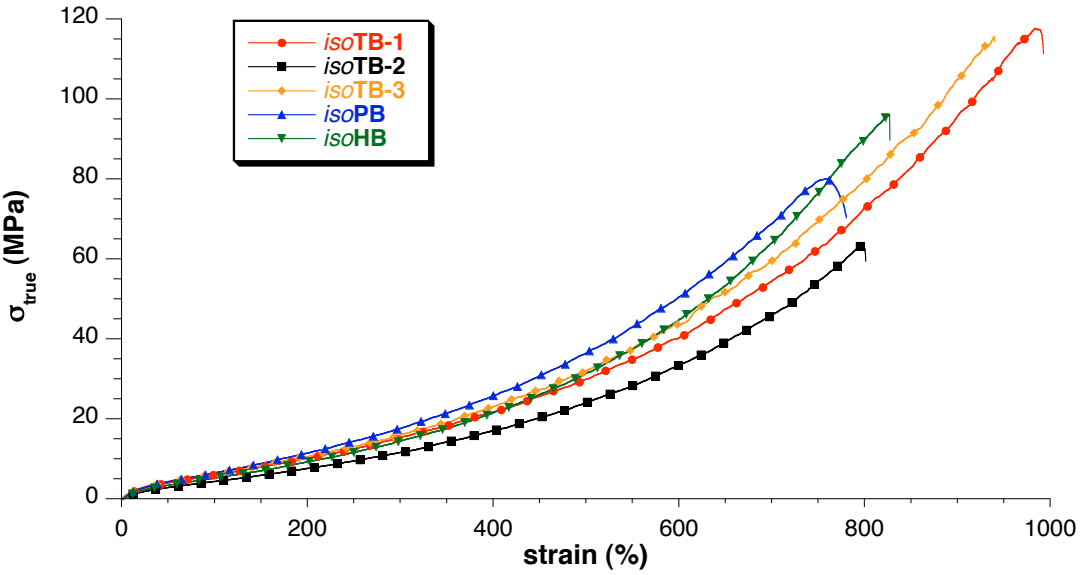

Figure 2.9. Tensile true stress-strain curves for *iso***TB-1**, *iso***TB-2**, *iso***TB-3**, *iso***PB**, and *iso***HB**.

2.3 Conclusions

Bis(phenoxyketimine)titanium catalyst systems bearing different substituents at the ortho and para positions of the phenolate rings, and ketimine carbon susbstituents featuring an *N*-pentafluorophenyl moiety all displayed activity for propylene polymerization. All catalysts were isoselective with [m^4]-values between 0.31 and 0.73 for the resultant

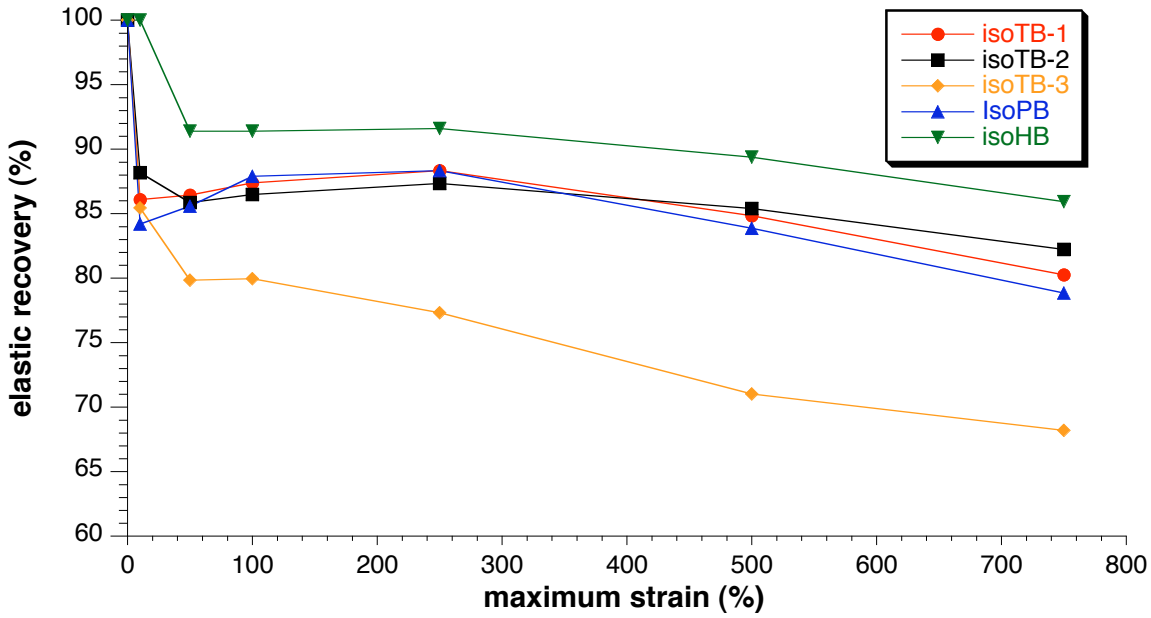

Figure 2.10. Elastic recovery of *iso***TB-1**, *iso***TB-2**, *iso***TB-3**, *iso***PB**, and *iso***HB** as a function of maximum tensile strain.

polypropylenes. The prevailing mode of stereocontrol was an enatiomorphic site-control mechanism as evidenced by the 2:2:1 ratio of the resonances corresponding to the *mmmr*:*mmrr*:*mrrm* pentads in the ^{13}C NMR spectra of the polypropylenes formed. Complexes bearing *ortho*-halide substituents on the phenolate ring displayed much higher activity than those bearing alkyl substituents with the size of the substituent determining the level of facial selectivity. The identity of the para substituent had a dramatic influence on the activity of the polymerization but had no effect on the selectivity. Varying the substituents at the ketimine carbon of the ancillary ligand had the most pronounced effect on both the activity and the isoselectivity of propylene polymerization. All catalyst systems screened showed living behavior except those with methoxy groups on the ancillary ligand. Using **2.12**/MAO, a number of new block copolymers from propylene and ethylene were

synthesized via sequential monomer addition. Specifically an iPP-*block*-PEP-*block*-iPP triblock copolymer, iPP-*block*-PEP-*block*-iPP-*block*-PEP-*block*-iPP pentablock copolymer, and iPP-*block*-PEP-*block*-iPP-*block*-PEP-*block*-iPP-*block*-PEP-*block*-iPP heptablock copolymer were prepared. The block copolymers displayed elastomeric behavior and exhibited excellent mechanical properties.

2.4 Experimental

2.4.1 Complex Syntheses

General Methods. All manipulations of air- and/or water-sensitive compounds were carried out under dry nitrogen using an MBraun Unilab drybox or standard Schlenk line techniques. ^{1}H and ^{19}F NMR spectra of ligands and complexes were recorded using a Varian Inova (500 MHz) spectrometer and were referenced versus residual non-deuterated solvent shifts (^{1}H) or versus a hexafluorobenzene external standard (^{19}F). ^{13}C NMR spectra of ligands, complexes, and polymers were recorded on a Varian Inova (500 MHz) spectrometer equipped with a ^{1}H/BB switchable with Z-pulse field gradient probe referenced versus residual non-deuterated solvent signals. The polymer samples were dissolved in 1,1,2,2-tetrachloroethane-d_2 in a 5 mm O.D. tube, and spectra were recorded at 135 °C. For quantitative analysis, an inverse decoupling sequence was used with a 30° pulse width, 2.0 s acquisition time, and 10 s delay time. Molecular weights (M_n and M_w) and molecular weight distributions (M_w/M_n) were determined by high temperature gel permeation chromatography (GPC). Analyses were performed using a Waters Alliance GPCV 2000 GPC equipped with a Waters DRI detector and viscometer. The column set (four Waters HT 6E and one Waters HT2) was eluted with 1,2,4-trichlorobenzene containing 0.01 wt. % di-

tert-butylhydroxytoluene (BHT) at 1.0 mL/min at 140 °C. Data were measured relative to a polyethylene calibration curve (Polymer Standards Service). Polymers were usually placed in a 140 °C oven for 24 h prior to molecular weight measurements. Polymer melting points (T_ms) and glass transition temperatures (T_gs) were measured by differential scanning calorimetry (DSC) using a TA Instruments Q1000 calorimeter equipped with an automated sampler. Analyses were performed in crimped aluminum pans under nitrogen and data were collected from the second heating run at a heating rate of 10 °C/min from –100 to 200 °C, and processed with the TA Q series software. Mass spectra were acquired using a JEOL GCMate II mass spectrometer operating at 3000 resolving power for high resolution measurements in positive ion mode and an electron ionization potential of 70 eV. Samples were introduced via a GC inlet using an Agilent HP 6890N GC equipped with a 30 m (0.25 μm i.d.) HP-5ms capillary GC column. The carrier gas was helium with a flow rate of 1 mL/min. Samples were introduced into the GC using a split/splitless injector at 230 °C with a split ratio of 10:1.

Materials. Toluene and pentane were purified over columns of alumina and copper (Q5) prior to use. Tetrahydrofuran (THF) and methylene chloride were purified over a column of alumina and degassed by three freeze-pump thaw cycles and stored under nitrogen. Benzene-d_6 was distilled from sodium benzophenone ketyl under nitrogen, degassed, and stored over 4Å molecular sieves under nitrogen. Chloroform-*d* was stirred over CaH_2 for several days, degassed by three freeze-pump thaw cycles, vacuum distilled, and stored under nitrogen. Propylene (Matheson, ultra high purity) was purified over columns of alumina COS and copper Q5. Ethylene (Matheson, Matheson purity) was purified over columns of copper Q5 and 4Å molecular sieves.

Methylaluminoxane (Akzo Nobel PMAO-IP, 13 wt. % Al in toluene) was dried in vacuo to remove residual trimethylaluminum and used as a solid white powder. Anhydrous 1,2-dichloroethane, $TiCl_4$ (1.0 M solution in toluene), 2,3,4,5,6-pentafluoroaniline, 2,4-dimethylphenol, 2-benzyl-4-methylphenol, 2-bromo-4-methylphenol, 2-chloro-4-methylphenol, 4-chloro-2-methylphenol, 4-fluoro-2-methylphenol, 2-hydroxy-5-methoxybenzaldehyde, and 5,6,7,8-tetrahydro-1-naphthol were purchased from commercial sources and used as received. The synthesis of PKI ligand **L2.1** and the corresponding complex **2.1** has been reported.[26]

General procedure for phenoxyketimine ligand synthesis. Phenoxyketimine ligands were synthesized as previously described.[38] Phosphorus pentachloride (5.0 mmol) was added to a methylene chloride solution (20 mL) of the desired amide (5.0 mmol) under a stream of nitrogen. The resultant suspension was stirred at room temperature under nitrogen for 4-6 hours. The solvent was removed in vacuo and the resulting white imidoyl chloride was dried to remove residual $POCl_3$. The crude imidoyl chloride was dissolved in anhydrous 1,2-dichloroethane (5 mL) and transferred via cannula to a Schlenk tube containing aluminum chloride (6.0 mmol) and 1,2-dichloroethane (5 mL). A solution of the desired phenol (5.0 mmol in 5 mL 1,2-dichloroethane) was then added resulting in a color change from light brown to deep orange-red. The reaction was heated at 75 °C under nitrogen overnight. After cooling, the reaction was poured into water (40 mL) and the organic layer was collected and washed with aqueous sodium carbonate solution followed by brine. The organic layer was then dried over sodium sulfate and filtered. The solvent was removed in vacuo to give the crude

ligand as a yellow to orange-red oil. When possible ligands were purified by column chromatography or recystallization.

2-Chloro-4-methyl-6-[phenyl (pentafluorophenylimino) methyl] phenol (L2.2). *N*-Pentafluorophenylbenzamide (0.77 g, 2.7 mmol) and 2-chloro-4-methylphenol (0.32 mL, 2.7 mmol) were reacted as described above to give the crude product as an orange oil. Recrystallization from methanol at -20 °C produced an orange crystalline solid (0.13 g, 12%). ^{1}H NMR ($CDCl_3$, 500 MHz): 13.51 (s, 1H, O*H*), 7.36-7.44 (m, 4H, Ph*H*), 7.16, 7.15 (s, 1H each, Ar*H*), 6.73 (m, 1H, Ph*H*), 2.14 (s, 3H, ArCH_3). ^{13}C NMR ($CDCl_3$, 125MHz): 181.3 (N=*C*-Ph), 156.1 (Ar*C*-OH), 136.1, 134.2, 131.9, 130.4, 128.8, 128.3, 127.0, 122.6, 120.0 (Ar*C* or Ph*C*), 20.6 (ArCH_3). The three Ar_FC-F and Ar_FC_{ipso} signals are hidden. ^{19}F NMR ($CDCl_3$, 470 MHz): -151.6, -162.5, -165.1 (m, Ar_FF). HRMS EI (*m*/*z*): calc. for $C_{20}H_{11}ClF_5NO$, 411.0449; found, 411.0440.

2-Bromo-4-methyl-6-[phenyl(pentafluorophenylimino)methyl]phenol (L2.3). *N*-Pentafluorophenylbenzamide (2.37 g, 8.24 mmol) and 2-bromo-4-methylphenol (1.0 mL, 8.3 mmol) were reacted as described above to give the crude product as an orange oil. Recrystallization from methanol at -20 °C produced an orange crystalline solid (0.42 g, 11%). ^{1}H NMR ($CDCl_3$, 500 MHz): 13.64 (s, 1H, O*H*), 7.54 (m, 1H, Ar*H*), 7.36-7.42 (m, 3H, Ph*H*), 7.15 (m, 2H, Ph*H*), 6.78 (m, 1H, Ar*H*), 2.14 (s, 3H, ArCH_3). ^{13}C NMR ($CDCl_3$, 125MHz): 181.2 (N=*C*-Ph), 157.0 (Ar*C*-OH), 139.1 (Ar*C*), 138.6 (Ar_FC-F, m, J_{CF} = 250 Hz), 138.3 (Ar_FC-F, m, J_{CF} = 250 Hz), 137.8 (Ar_FC-F, m, J_{CF} = 250 Hz), 134.1, 132.7, 130.4, 128.9, 128.8, 127.0 (Ar*C* or Ph*C*), 123.1 (Ar_FC_{ipso}, m), 119.8, 111.9 (Ar*C*), 20.4 (ArCH_3). ^{19}F NMR ($CDCl_3$, 470 MHz): -151.6, -162.5, -165.1 (m, Ar_FF). HRMS EI (*m*/*z*): calc. for $C_{20}H_{11}BrF_5NO$, 454.9944; found, 454.9943.

2-(2-Bromo-4-methylphenoxy)tetrahydro-2*H*-pyran. An oven-dried,

Schenk-adapted tube was charged with 2-bromo-4-methylphenol (2.0 mL, 16.5 mmol), 3,4-dihydro-2*H*-pyran (2.2 mL, 24.1 mmol), pyridinium toluene-*p*-sulfonate (0.43 g, 1.65 mmol) and methylene chloride (20 mL) under N_2. The reaction was stirred overnight at room temperature. Brine (20 mL) was added and the organic phase was separated, dried over Na_2SO_4, filtered and solvent removed in vacuo to yield a colorless oil (4.48 g, 100%). The crude product was used without further purification. ^{1}H NMR (C_6D_6, 500 MHz): 7.27 (d, 1H, J = 1.5 Hz, Ar*H*), 7.06 (d, 1H, J = 8.5 Hz, Ar*H*), 6.77 (dd, 1H, J = 1.5, 8.5 Hz, Ar*H*), 5.27 (t, 1H, J = 2.5 Hz, ArOC*H*), 3.77, 3.35, 2.01 (m, 1H each, ArOTHP-*H*), 1.92 (s, 1H, ArCH_3), 1.78, 1.53 (m, 1H each, ArOTHP-*H*), 1.35 (m, 2H, ArOTHP-*H*), 1.20 (m, 1H, ArOTHP-*H*). ^{13}C NMR (C_6D_6, 125MHz): 152.3 (Ar*C*-OTHP), 134.3, 132.8, 129.4, 117.2, 113.6 (Ar*C*), 97.2 (ArO*C*H), 61.7, 30.8, 25.9 (ArOTHP-*C*), 20.5 (Ar*C*H$_3$), 18.9 (ArOTHP-*C*). HRMS EI (*m*/*z*): calc. for $C_{12}H_{15}BrO_2$, 270.0255; found, 270.0244.

5-Methylbiphenyl-2-ol. An oven-dried, Schenk-adapted tube was charged with 2-(2-bromo-4-methylphenoxy)tetrahydro-2*H*-pyran (3.90 g, 14.4 mmol) and $Pd(PPH_3)_4$ (0.83 g, 0.72 mmol) in anhydrous dimethoxyethane (15 mL) under N_2. The solution was degassed for 20 minutes by sparging with N_2: this solution was transferred via cannula to a flask containing a degassed solution of phenylboronic acid (2.11 g, 17.3 mmol) and 2.0 M aqueous Na_2CO_3 (14.4 mL, 28.8 mmol) in dimethoxyethane (15 mL). Under an active N_2 purge, a reflux condenser was attached and reaction was heated to reflux and stirred under N_2 for 16 hours. After cooling, 30 mL of ethyl acetate was added and the solution was dried over Na_2SO_4, filtered and solvent removed in vacuo to yield a black oil. To the crude oil was added HCl (0.3 mL) in methanol (1 mL) and ethyl acetate (1 mL). The solution was heated at 40 °C for 4 hours. After

cooling the solvent was removed in vacuo and the crude product was purified by flash chromatography (hexanes/ethyl acetate 20:1) to yield a colorless oil that solidified as a white solid upon drying in vacuo (2.12 g, 80%). ^{1}H NMR (C_6D_6, 300 MHz): 7.31-7.34 (m, 2H, Ar*H*), 7.12-7-17 (m, 2H, Ar*H*), 7.05-7.09 (m, 1H,, Ar*H*), 6.97 (m, 1H, Ar*H*), 6.85-6.88 (m, 1H, Ar*H*), 6.79 (d, 1H, J = 6 Hz, Ar*H*), 4.62 (s, 1H, ArO*H*), 2.11 (s, 3H, ArCH_3). ^{13}C NMR (C_6D_6, 125MHz): 151.4 (Ar*C*-OH), 138.5, 131.5, 130.2, 130.1, 129.8, 129.5, 128.8, 127.9, 116.6 (Ar*C* or Ph*C*), 20.8 (ArCH_3). HRMS EI (*m*/*z*): calc. for $C_{13}H_{12}O$, 184.0888; found, 184.0893.

5-Methyl-3-[phenyl(pentafluorophenylimino)methyl) biphenyl-2-ol (L2.4). *N*-Pentafluorophenylbenzamide (2.25 g, 7.83 mmol) and 5-methylbiphenyl-2-ol (1.37 g, 7.44 mmol) were reacted as described above to give the crude product as a yellow solid. Repeated recrystallizations from methanol at -20 °C was necessary to obtain the product as small yellow needles (0.12 g, 4%). ^{1}H NMR ($CDCl_3$, 500 MHz): 13.41 (s, 1H, O*H*), 7.63 (m, 2H, Ph*H*), 7.34-7.46 (m, 7H, Ar*H* or Ph*H*), 7.20 (m, 2H, Ph*H*), 6.82 (m, 1H, Ar*H*), 2.19 (s, 3H, ArCH_3). ^{13}C NMR ($CDCl_3$, 125MHz): 181.7 (N=*C*-Ph), 157.9 (Ar*C*-OH), 138.6 (Ar_FC-F, m, J_{CF} = 250 Hz), 138.1 (Ar_FC-F, m, J_{CF} = 250 Hz), 137.8 (Ar_FC-F, m, J_{CF} = 250 Hz), 137.7, 137.3, 134.8, 132.6, 131.0, 130.1, 129.7, 128.7, 128.4, 127.7, 127.5, 127.0 (Ar*C* or Ph*C*), 123.6 (Ar_FC_{ipso}, m), 119.2 (Ar*C*), 20.7 (ArCH_3). ^{19}F NMR ($CDCl_3$, 470 MHz): -152.4, -163.8, -166.0 (m, Ar_FF). HRMS EI (*m*/*z*): calc. for $C_{26}H_{16}F_5NO$, 453.1152; found, 453.1131.

2-Benzyl-4-methyl-6-[phenyl (pentafluorophenylimino) methyl) phenol (L2.5). *N*-Pentafluorophenylbenzamide (1.49 g, 5.17 mmol) and 2-benzyl-4-methylphenol (0.98 g, 4.9 mmol) were reacted as described above to give the crude product as a brown oil. Recrystallization from

methanol/toluene 9:1 at -20 °C produced a yellow crystalline solid (0.64 g, 28%). ^{1}H NMR ($CDCl_3$, 500 MHz): 13.22 (s, 1H, O*H*), 7.32-7.42 (m, 7H, Ph*H*), 7.20-7.26 (m, 3H, Ph*H*), 7.12, 6.72 (s, 1H each, Ar*H*), 4.10 (s, 2H, ArCH_2Ph), 2.12 (s, 3H, ArCH_3). ^{13}C NMR ($CDCl_3$, 125MHz): 181.6 (N=*C*-Ph), 158.6 (Ar*C*-OH), 140.8 (Ph*C*), 138.6 (Ar_FC-F, m, J_{CF} = 250 Hz), 138.0 (Ar_FC-F, m, J_{CF} = 250 Hz), 137.7 (Ar_FC-F, m, J_{CF} = 250 Hz), 137.0, 134.9, 131.4, 130.3, 130.0, 129.3, 128.63, 128.59, 127.4, 127.0, 126.3 (Ar*C* or Ph*C*), 123.8 (Ar_FC_{ipso}, m), 118.7 (Ar*C*), 35.7 (ArCH_2Ph), 20.7 (ArCH_3). ^{19}F NMR ($CDCl_3$, 470 MHz): -152.3, -164.0, -166.2 (m, Ar_FF). HRMS EI (*m*/*z*): calc. for $C_{27}H_{18}F_5NO$, 467.1309; found, 467.1324.

2-[Phenyl (pentafluorophenylimino)methyl]-5,6,7,8-tetrahydro-1-naphthol (L2.6). *N*-Pentafluorophenylbenzamide (1.01 g, 3.52 mmol) and 5,6,7,8-tetrahydro-1-naphthol (0.50 g, 3.3 mmol) were reacted as described above to give the crude product as a yellow solid. Recrystallization from methanol produced a light yellow crystalline solid (0.34 g, 25%). ^{1}H NMR ($CDCl_3$, 500 MHz): 13.41 (s, 1H, O*H*), 7.34-7.49 (m, 3H, Ph*H*), 7.18 (m, 2H, Ph*H*), 6.65 (dd, 2H, J = 8.0 Hz, 132 Hz, Ar*H*), 2.77 (m, 4H, ArCH_2-), 1.83 (m, 4H, ArCH_2CH_2-). ^{13}C NMR ($CDCl_3$, 125MHz): 181.3 (N=*C*-Ph), 160.9 (Ar*C*-OH), 145.6 (Ar*C*), 138.8 (Ar_FC-F, m, J_{CF} = 244 Hz), 137.9 (Ar_FC-F, m, J_{CF} = 250 Hz), 137.8 (Ar_FC-F, m, J_{CF} = 250 Hz), 135.0, 129.9, 129.8, 128.5, 127.1, 126.5 (Ar*C* or Ph*C*), 123.9 (Ar_FC_{ipso}, m), 119.6, 116.1 (Ar*C*), 30.5, 23.0, 22.7 (Ar-(CH_2)$_4$-Ar). ^{19}F NMR ($CDCl_3$, 470 MHz): -152.6, -164.3, -166.4 (m, Ar_FF). HRMS EI (*m*/*z*): calc. for $C_{23}H_{16}F_5NO$, 417.1152; found, 417.1151.

4-Chloro-2-methyl-6-[phenyl (pentafluorophenylimino)methyl] phenol (L2.7). *N*-Pentafluorophenylbenzamide (3.69 g, 12.9 mmol) and 4-chloro-2-methylphenol (1.83 g, 12.9 mmol) were reacted as described above to give the crude product as a yellow oil. Recrystallization from methanol at -20

°C produced a yellow crystalline solid (0.46 g, 9%). ^{1}H NMR ($CDCl_3$, 500 MHz): 13.26 (s, 1H, O*H*), 7.35-7.44 (m, 3H, Ph*H*), 7.27 (m, 1H, Ar*H*), 7.16 (m, 2H, Ph*H*), 6.84 (m, 1H, Ar*H*), 2.31 (s, 3H, ArCH_3). ^{13}C NMR ($CDCl_3$, 125MHz): 181.0 (N=*C*-Ph), 159.7 (Ar*C*-OH), 138.6 (Ar_FC-F, m, J_{CF} = 250 Hz), 138.3 (Ar_FC-F, m, J_{CF} = 250 Hz), 137.8 (Ar_FC-F, m, J_{CF} = 250 Hz), 135.7, 134.1, 130.5, 129.8, 129.7, 128.9, 127.0 (Ar*C* or Ph*C*), 123.4 (Ar_FC_{ipso}, m), 122.8, 119.3 (Ar*C*), 16.0 (ArCH_3). ^{19}F NMR ($CDCl_3$, 470 MHz): -151.7, -162.7, -165.2 (m, Ar_FF). HRMS EI (*m*/*z*): calc. for $C_{20}H_{11}ClF_5NO$, 411.0449; found, 411.0447.

4-Fluoro-2-methyl-6-[phenyl(pentafluorophenylimino)methyl]phenol (L2.8). *N*-Pentafluorophenylbenzamide (1.52 g, 5.29 mmol) and 4-fluoro-2-methylphenol (0.63 g, 5.1 mmol) were reacted as described above to give the crude product as an orange oil. The crude product was flash chromatographed (silica gel, hexanes/ethyl acetate 20:1) to yield a yellow oil. Recrystallization from methanol at -20 °C produced a yellow crystalline solid (0.10 g, 5%). ^{1}H NMR ($CDCl_3$, 500 MHz): 13.05 (s, 1H, O*H*), 7.35-7.43 (m, 3H, Ph*H*), 7.17 (m, 2H, Ph*H*), 7.07 (dd, 1H, J = 3.0 Hz, 8.0 Hz, Ar*H*), 6.56 (dd, 1H, J = 3.0 Hz, 9.5 Hz, Ar*H*), 2.33 (s, 3H, ArCH_3). ^{13}C NMR ($CDCl_3$, 125MHz): 181.0 (N=*C*-Ph), 159.7 (Ar*C*-OH), 154.4 (ArC-F, d, J_{CF} = 234 Hz), 138.6 (Ar_FC-F, m, J_{CF} = 250 Hz), 138.2 (Ar_FC-F, m, J_{CF} = 250 Hz), 137.8 (Ar_FC-F, m, J_{CF} = 250 Hz), 134.3, 130.4 (Ph*C*), 129.5 (Ar*C*, d, J_{CF} = 6.8 Hz), 128.8, 127.0 (Ph*C*), 123.5 (Ar_FC_{ipso}, m), 123.4 (Ar*C*, d, J_{CF} = 22.8 Hz), 118.2 (Ar*C*, d, J_{CF} = 7.6 Hz), 115.6 (Ar*C*, d, J_{CF} = 24.3 Hz), 16.2 (ArCH_3). ^{19}F NMR ($CDCl_3$, 470 MHz): -128.5 (m, ArF), -152.4, -163.5, -165.9 (m, Ar_FF). HRMS EI (*m*/*z*): calc. for $C_{20}H_{11}F_6NO$, 395.0745; found, 395.0758.

4-Methoxy-2-methylphenol. An Schenk-adapted tube was charged with 2-hydroxy-5-methoxybenzaldehyde (0.94 g, 6.19 mmol) and potassium

hydroxide (1.75 g, 31.2 mmol) in di(ethylene gycol) (40 mL). Hydrazine hydrate (2.1 mL, 43.3 mmol) was added via syringe and a reflux condenser was attached. The reaction was brought to reflux for 15 hours. After cooling, 1.0 M HCl (40 mL) was slowly added followed by methylene chloride (40 mL). The organic phase was separated, washed with copious amounts of water, dried over Na_2SO_4, filtered and solvent removed in vacuo to yield a white crystalline solid (0.56 g, 65%). The crude product was used directly for the synthesis of ligand **L2.9**. ^{1}H NMR (C_6D_6, 500 MHz): 6.69 (d, 1H, J = 3.0 Hz, Ar*H*), 6.56 (dd, 1H, J = 3.0, 8.5 Hz, Ar*H*), 6.47 (d, 1H, J = 8.5 Hz, Ar*H*), 4.83 (s, 1H, ArO*H*), 3.35 (s, 3H, ArOCH_3), 2.11 (s, 3H, ArCH_3). ^{13}C NMR (C_6D_6, 125MHz): 154.3 (Ar*C*-OH), 148.8 (Ar*C*-OMe), 125.9, 117.4, 116.1, 112.5 (Ar*C*), 55.7 (ArOCH_3), 16.7 (ArCH_3). HRMS EI (*m*/*z*): calc. for $C_8H_{10}O_2$, 138.0681; found, 138.0675.

4-Methoxy-2-methyl-6-[phenyl (pentafluorophenylimino)methyl] phenol (L2.9). *N*-Pentafluorophenylbenzamide (1.05 g, 3.66 mmol) and 4-methoxy-2-methylphenol (0.50 g, 3.6 mmol) were reacted as described above to give the crude product as a yellow oil. The crude product was flash chromatographed (silica gel, hexanes/ethyl acetate 20:1) to yield a yellow oil. Recrystallization from methanol at -20 °C produced a yellow crystalline solid (0.13 g, 9%). ^{1}H NMR ($CDCl_3$, 500 MHz): 12.85 (s, 1H, O*H*), 7.32-7.40 (m, 3H, Ph*H*), 7.16 (m, 2H, Ph*H*), 6.96 (d, 1H, J = 3 Hz, Ar*H*), 6.35 (d, 1H, J = 3 Hz, Ar*H*), 3.56 (s, 3H, ArOCH_3), 2.31 (s, 3H, ArCH_3). ^{13}C NMR ($CDCl_3$, 125MHz): 181.4 (N=*C*-Ph), 155.6 (Ar*C*-OH), 151.0 (Ar*C*-OCH$_3$), 138.6 (Ar$_F$*C*-F, m, J_{CF} = 250 Hz), 138.1 (Ar$_F$*C*-F, m, J_{CF} = 250 Hz), 137.8 (Ar$_F$C-F, m, J_{CF} = 250 Hz), 134.8, 130.1, 128.6, 127.0 (Ar*C* or Ph*C*), 123.9 (Ar$_F$C$_{ipso}$, m), 123.7, 118.2, 116.5, 114.2 (Ar*C* or Ph*C*), 55.9 (ArOCH_3), 16.3 (ArCH_3). ^{19}F NMR ($CDCl_3$, 470 MHz): -151.9,

-163.4, -165.5 (m, Ar_FF). HRMS EI (*m*/*z*): calc. for $C_{21}H_{14}F_5NO_2$, 407.0945; found, 407.0943.

2,4-Dimethyl-6-[1-(pentafluorophenylimino)ethyl]phenol (L2.10). *N*-Pentafluorophenylethanamide (2.53 g, 11.2 mmol) and 2,4-dimethylphenol (1.35 mL, 11.2 mmol) were reacted as described above to give the crude product as a green oil. The crude product was flash chromatographed (silica gel, hexanes/ethyl acetate 20:1) to yield a yellow solid. Recrystallization from methanol at -20 °C produced fine yellow needles (0.27 g, 7%). ^{1}H NMR ($CDCl_3$, 500 MHz): 13.30 (s, 1H, O*H*), 7.30, 7.14 (s, 1H each, Ar*H*), 2.36 (s, 3H, N=C-CH_3), 2.29, 2.26 (s, 3H each, ArCH_3). ^{13}C NMR ($CDCl_3$, 125MHz): 178.3 (N=*C*-CH_3), 158.2 (Ar*C*-OH), 139.0 (Ar_FC-F, m, J_{CF} = 250 Hz), 138.4 (Ar_FC-F, m, J_{CF} = 250 Hz), 138.2 (Ar_FC-F, m, J_{CF} = 250 Hz), 136.8, 127.4, 127.2 (Ar*C*), 122.5 (Ar_FC_{ipso}, m), 118.2 (Ar*C*), 20.8 (ArCH_3), 19.3 (N=C-CH_3), 16.0 (ArCH_3). ^{19}F NMR ($CDCl_3$, 470 MHz): -152.6, -163.0, -165.0 (m, Ar_FF). HRMS EI (*m*/*z*): calc. for $C_{16}H_{12}F_5NO$, 329.0839; found, 329.0855.

2,4-Dimethyl-6-[2-methyl-1-(pentafluorophenylimino)propyl]phenol (L2.11). 2-Methyl-*N*-pentafluorophenylpropanamide (3.12 g, 12.3 mmol) and 2,4-dimethylphenol (1.40 mL, 11.7 mmol) were reacted as described above to give the crude product as a yellow oil. The crude product was flash chromatographed (alumina, hexanes/ethyl acetate 98:2) to yield a light yellow solid (0.67 g, 16%). ^{1}H NMR ($CDCl_3$, 500 MHz): 13.45 (s, 1H, O*H*), 7.49, 7.13 (s, 1H each, Ar*H*), 3.15 (septet, 1H, J = 7.5 Hz, N=C-C*H*$(CH_3)_2$), 2.30, 2.26 (s, 3H each, ArCH_3), 1.40 (d, 6H, J = 7.5 Hz, N=C-CH(CH_3)$_2$). ^{13}C NMR ($CDCl_3$, 125MHz): 185.8 (N=*C*-CH$(CH_3)_2$), 159.1 (Ar*C*-OH), 138.5 (Ar_FC-F, m, J_{CF} = 250 Hz), 138.2 (Ar_FC-F, m, J_{CF} = 250 Hz), 138.0 (Ar_FC-F, m, J_{CF} = 250 Hz), 136.6, 127.9, 127.4, 126.3 (Ar*C*), 122.4 (Ar_FC_{ipso}, m), 116.3 (Ar*C*), 35.2 (N=C-*C*H$(CH_3)_2$),

21.0, 20.8, 16.3 (N=C-CH(CH_3)$_2$ or ArCH_3). ^{19}F NMR ($CDCl_3$, 470 MHz): -153.7, -164.6, -165.7 (m, Ar_FF). HRMS EI (*m*/*z*): calc. for $C_{18}H_{16}F_5NO$, 357.1152; found, 357.1151.

2-[Cyclohexyl (pentafluorophenylimino)methyl)-4,6-dimethylphenol (L2.12). *N*-Pentafluorophenylcyclohexanecarboxamide (1.33 g, 4.53 mmol) and 2,4-dimethylphenol (0.55 mL, 4.6 mmol) were reacted as described above to give the crude product as a green oil. Recrystallization from pentane at -20 °C produced a light yellow crystalline solid (0.27 g, 15%). ^{1}H NMR ($CDCl_3$, 500 MHz): 13.43 (s, 1H, O*H*), 7.52, 7.11 (s, 1H each, Ar*H*), 2.85 (m, 1H, N=C-Cy*H*), 2.30, 2.24 (s, 3H each, ArCH_3), 1.68-1.88 (m, 7H, Cy*H*), 1.18-1.23 (m, 3H, Cy*H*). ^{13}C NMR ($CDCl_3$, 125MHz): 184.5 (N=*C*-Cy), 158.9 (Ar*C*-OH), 138.4 (Ar_F*C*-F, m, $^1J_{CF}$ = 250 Hz), 138.0 (Ar_F*C*-F, m, $^1J_{CF}$ = 250 Hz), 136.8 (Ar_F*C*-F, m, $^1J_{CF}$ = 250 Hz), 136.3, 127.9, 127.3, 126.3 (Ar*C*), 122.7 (Ar_FC_{ipso}, m), 117.2 (Ar*C*), 47.0, 30.4, 26.8, 25.9 (N=C-Cy*C*) 21.1, 16.0 (ArCH_3). ^{19}F NMR ($CDCl_3$, 470 MHz): -152.9, -164.1, -165.0 (m, Ar_FF). HRMS EI (*m*/*z*): calc. for $C_{21}H_{20}F_5NO$, 397.1465; found, 397.1466.

2-[Cycloheptyl(pentafluorophenylimino)methyl)-4,6-dimethylphenol (L2.13). *N*-Pentafluorophenylcycloheptanecarboxamide (2.04 g, 6.63 mmol) and 2,4-dimethylphenol (0.79 mL, 6.6 mmol) were reacted as described above to give the crude product as a yellow oil. The crude product was flash chromatographed (silica gel, hexanes/ethyl acetate 20:1) to yield a yellow oil. Recrystallization from methanol/toluene 3:1 at -20 °C produced a bright yellow crystalline solid (0.43 g, 16%). ^{1}H NMR ($CDCl_3$, 500 MHz): 13.48 (s, 1H, O*H*), 7.37, 7.11 (s, 1H each, Ar*H*), 2.82 (m, 1H, N=C-Cycloheptyl*H*), 2.29, 2.25 (s, 3H each, ArCH_3), 1.97-2.05 (m, 2H, Cycloheptyl*H*), 1.78-1.89 (m, 4H, Cycloheptyl*H*), 1.34-1.58 (m, 6H, Cycloheptyl*H*). ^{13}C NMR ($CDCl_3$, 125MHz):

186.3 (N=*C*-Cycloheptyl), 159.2 (Ar*C*-OH), 138.7 (Ar_FC-F, m, J_{CF} = 250 Hz), 138.1 (Ar_FC-F, m, J_{CF} = 250 Hz), 138.0 (Ar_FC-F, m, J_{CF} = 250 Hz), 136.2, 127.9, 126.2 (Ar*C*), 122.5 (Ar_FC_{ipso}, m), 116.0 (Ar*C*), 47.2, 32.2, 29.0, 28.3 (N=C-Cycloheptyl*C*) 21.1, 16.3 ($ArCH_3$). ^{19}F NMR ($CDCl_3$, 470 MHz): -153.3, -163.6, -165.0 (m, Ar_FF). HRMS EI (*m*/*z*): calc. for $C_{22}H_{22}F_5NO$, 411.1622; found, 411.1632.

2,4-Dimethyl – 6 - (2,2,2-trifluoro-1-(pentafluorophenylimino)ethyl) phenol (L2.14). 2,2,2-Trifluoro-*N*-pentafluorophenylethanimidoyl chloride (1.92 g, 6.46 mmol), prepared according to the procedure described by Uneyama and coworkers,[53] and 2,4-dimethylphenol (0.79 mL, 6.6 mmol) were reacted in the Friedel-Crafts reaction as described above to give the crude product as a brown oil. The crude product was flash chromatographed (silica gel, hexanes/ethyl acetate 20:1) to yield an orange oil. Recrystallization from pentane at -20 °C produced large orange crystals (1.77 g, 72%). ^{1}H NMR ($CDCl_3$, 500 MHz): 12.13 (s, 1H, O*H*), 7.33, 7.23 (s, 1H each, Ar*H*), 2.30, 2.26 (s, 3H each, ArCH_3). ^{13}C NMR ($CDCl_3$, 125MHz): 161.9 (N=*C*-CF_3, q, J_{CF} = 30 Hz), 159.4 (Ar*C*-OH), 138.7 (Ar_FC-F, m, J_{CF} = 250 Hz), 138.6 (Ar*C*), 138.1 (Ar_FC-F, m, J_{CF} = 250 Hz), 137.8 (Ar_FC-F, m, J_{CF} = 250 Hz), 128.1, 128.0 (Ar*C*), 127.2 (Ar*C*-C=N, q, J_{CF} = 4.5 Hz), 121.4 (Ar_FC_{ipso}, m), 118.6 (N=C-*C*F_3, q, J_{CF} = 290 Hz), 113.3 (Ar*C*), 20.9, 16.2 ($ArCH_3$). ^{19}F NMR ($CDCl_3$, 470 MHz): -64.0 (s, N=C-CF_3), -153.7, -162.1, -164.9 (m, Ar_FF). HRMS EI (*m*/*z*): calc. for $C_{16}H_9F_8NO$, 383.0556; found, 383.0553.

2,4-Dimethyl - 6 - [naphthalen-2-yl(pentafluorophenylimino)methyl] phenol (L2.15). *N*-Pentafluorophenylnaphthalene-2-carboxamide (1.80 g, 5.34 mmol) and 2,4-dimethylphenol (0.64 mL, 5.3 mmol) were reacted as described above to give the crude product as a red-brown oil. Recrystallization from

methanol at -20 °C produced a yellow crystalline solid (0.61 g, 26%). ^{1}H NMR ($CDCl_3$, 500 MHz): 13.12 (s, 1H, O*H*), 7.81-7.87 (m, 3H, Ar*H*), 7.67 (s, 1H, Ar*H*), 7.52-7.59 (m, 2H, Ar*H*), 7.27 (d, 1H, J = 8 Hz, Ar*H*), 7.15, 6.64 (s, 1H each, Ar*H*), 2.33, 2.07 (s, 3H each, ArCH_3). ^{13}C NMR ($CDCl_3$, 125MHz): 181.6 (N=*C*-Ar), 158.9 (Ar*C*-OH), 138.7 (Ar_FC-F, m, J_{CF} = 250 Hz), 137.9 (Ar_FC-F, m, J_{CF} = 250 Hz), 137.7 (Ar_F*C*-F, m, J_{CF} = 250 Hz), 137.4, 133.6, 132.5, 132.4, 130.8, 128.8, 128.6, 128.1, 127.7, 127.3, 127.24, 127.19, 126.7, 124.2 (Ar*C*), 123.8 (Ar_FC_{ipso}, m), 118.5 (Ar*C*), 20.6, 16.0 (ArCH_3). ^{19}F NMR ($CDCl_3$, 470 MHz): -152.0, -163.4, -165.4 (m, Ar_FF). HRMS EI (*m*/*z*): calc. for $C_{25}H_{16}F_5NO$, 441.1152; found, 441.1150.

2,4-Dimethyl – 6 - [naphthalen-1-yl(pentafluorophenylimino)methyl] phenol (L2.16). *N*-Pentafluorophenylnaphthalene-1-carboxamide (1.79 g, 5.30 mmol) and 2,4-dimethylphenol (0.64 mL, 5.3 mmol) were reacted as described above to give the crude product as a yellow solid. Recrystallization from methanol at -20 °C produced a yellow crystalline solid (1.2 g, 50%). ^{1}H NMR ($CDCl_3$, 500 MHz): 13.33 (s, 1H, O*H*), 7.87 (d, 1H, J = 8.5 Hz, Ar*H*), 7.82 (d, 1H, J = 8.5 Hz, Ar*H*), 7.69 (d, 1H, J = 8.5 Hz, Ar*H*), 7.40-7.49 (m, 4H, Ar*H*), 7.14, 6.50 (s, 1H each, Ar*H*), 2.37, 1.99 (s, 3H each, ArCH_3). ^{13}C NMR ($CDCl_3$, 125MHz): 181.5 (N=*C*-Ar), 158.8 (Ar*C*-OH), 138.7 (Ar_FC-F, m, J_{CF} = 250 Hz), 137.7 (Ar_F*C*-F, m, J_{CF} = 250 Hz), 137.6 (Ar_F*C*-F, m, J_{CF} = 250 Hz), 137.5, 133.2, 132.5, 130.5, 130.2, 129.8, 128.6, 127.4, 127.3, 127.2, 126.9, 125.5, 125.2, 124.8 (Ar*C*), 123.6 (Ar_FC_{ipso}, m), 118.8 (Ar*C*), 20.5, 16.0 (ArCH_3). ^{19}F NMR ($CDCl_3$, 470 MHz): -151.2, -163.5, -165.6 (m, Ar_FF). HRMS EI (*m*/*z*): calc. for $C_{25}H_{16}F_5NO$, 441.1152; found, 441.1167.

2-[4-Methoxyphenyl (pentafluorophenylimino)methyl]-4,6-dimethyl phenol (L2.17). 4-Methoxy-*N*-pentafluorophenylbenzamide (2.31 g, 7.28

mmol) and 2,4-dimethylphenol (0.87 mL, 7.3 mmol) were reacted as described above to give the crude product as a brown oil. Recrystallization from methanol at -20 °C produced an orange crystalline solid (0.41 g, 13%). ^{1}H NMR ($CDCl_3$, 500 MHz): 13.13 (s, 1H, O*H*), 7.13 (s, 1H, Ar*H*), 7.09 (d, 2H, J = 8.5 Hz, Ar*H*), 6.85 (d, 2H, J = 9.0 Hz, Ar*H*), 6.71 (s, 1H, Ar*H*), 3.81 (s, 3H, ArOCH_3), 2.30, 2.13 (s, 3H each, ArCH_3). ^{13}C NMR ($CDCl_3$, 125MHz): 181.5 (N=*C*-Ar), 160.6 (Ar*C*-OCH_3), 158.9 (Ar*C*-OH), 138.8 (Ar_FC-F, m, J_{CF} = 250 Hz), 137.9 (Ar_FC-F, m, J_{CF} = 250 Hz), 137.8 (Ar_FC-F, m, J_{CF} = 250 Hz), 137.2, 130.8, 128.9, 127.2, 127.1, 127.0 (Ar*C*), 124.1 (Ar_FC_{ipso}, m), 118.6, 113.9 (Ar*C*), 20.7, 16.0 (ArCH_3). ^{19}F NMR ($CDCl_3$, 470 MHz): -152.1, -163.8, -165.7 (m, Ar_FF). HRMS EI (*m*/*z*): calc. for $C_{22}H_{16}F_5NO_2$, 421.1101; found, 421.1097.

2-[Mesityl (pentafluorophenylimino)methyl]-4,6-dimethylphenol (L2.18). 2,4,6-Trimethyl-*N*-pentafluorophenylbenzamide (1.93 g, 5.87 mmol) and 2,4-dimethylphenol (0.70 mL, 5.8 mmol) were reacted as described above to give the crude product as a yellow oil. The crude product was flash chromatographed (silica gel, hexanes/ethyl acetate 20:1) to yield a yellow oil. Repeated recrystallization from methanol/toluene 4:1 at -20 °C was necessary to obtain the product as a yellow crystalline solid (0.12 g, 5%). ^{1}H NMR ($CDCl_3$, 500 MHz): 13.44 (s, 1H, O*H*), 7.11 (s, 1H, Ar*H*), 6.79 (s, 2H, Mes*H*), 6.53 (s, 1H, Ar*H*), 2.30 (s, 3H, ArCH_3), 2.26 (s, 3H, Mes-CH_3), 2.10 (s, 3H, ArCH_3), 2.02 (s, 6H, Mes-CH_3). ^{13}C NMR ($CDCl_3$, 125MHz): 182.1 (N=*C*-Mes), 158.7 (Ar*C*-OH), 139.2, 137.3, 135.4, 131.4, 129.5, 128.7, 127.5, 127.2, 118.5 (Ar*C* or Mes*C*), 21.4, 20.7, 19.9, 16.0 (ArCH_3 or MesCH_3). The three Ar_FC-F and Ar_FC_{ipso} signals are hidden. ^{19}F NMR ($CDCl_3$, 470 MHz): -150.2, -163.1, -165.7 (m, Ar_FF). HRMS EI (*m*/*z*): calc. for $C_{24}H_{20}F_5NO$, 433.1465; found, 433.1454.

2,4-Dimethyl-6-[pentafluorophenyl (pentafluorophenylimino) methyl]phenol (L2.19). 2,3,4,5,6-Pentafluoro-*N*-pentafluorophenylbenzamide (1.55 g, 4.10 mmol) and 2,4-dimethylphenol (0.49 mL, 4.1 mmol) were reacted as described above to give the crude product as a yellow solid. The crude solid was washed with pentane and the filtrate was collected and solvent removed in vacuo to give a yellow solid. Recrystallization from methanol at -20 °C afforded the product as a bright yellow crystalline solid (0.12 g, 6%). ^{1}H NMR ($CDCl_3$, 500 MHz): 12.54 (s, 1H, O*H*), 7.21 (s, 1H, Ar*H*), 6.56 (s, 1H, Ar*H*), 2.30, 2.19 (s, 3H each, ArCH_3). ^{13}C NMR ($CDCl_3$, 125MHz): 167.0 (N=*C*-Ar_F), 158.9 (Ar*C*-OH), 143.1 (Ar_F*C*-F, m, J_{CF} = 250 Hz), 142.9 (Ar_F*C*-F, m, J_{CF} = 250 Hz), 139.0 (Ar_F*C*-F, m, J_{CF} = 250 Hz), 138.8 (Ar_F*C*-F, m, J_{CF} = 250 Hz), 138.7 (Ar*C*), 138.0 (Ar_F*C*-F, m, J_{CF} = 250 Hz), 137.9 (Ar_F*C*-F, m, J_{CF} = 250 Hz), 128.3, 128.2, 127.9 (Ar*C*), 122.2 ($Ar_F C_{ipso}$, m), 117.1 (Ar*C*), 109.0 ($Ar_F C_{ipso}$, m), 20.7, 16.0 (Ar*C*H_3). ^{19}F NMR ($CDCl_3$, 470 MHz): -139.6, -150.5, -152.1, -160.5, -160.8, -163.9 (m, Ar_FF). HRMS EI (*m*/*z*): calc. for $C_{21}H_9F_{10}NO$, 481.0524; found, 481.0527.

General procedure for titanium dichloride complex synthesis. Phenoxyketimine complexes were synthesized by a modified previously reported procedure.[26,38] To a stirred solution of the PKI ligand (1.00 mmol) in THF (ca. 10 mL) was added *n*-butyllithium (1.6 M in hexanes, 1.05 mmol) by syringe at -78 °C. The deprotonated ligand solution is warmed to room temperature and stirred for about 20 minutes. This solution was transferred via cannula to a THF solution of $TiCl_4$ (1.0 M in toluene, 0.50 mmol) at -78 °C. After warming to room temperature the dark red solution was stirred overnight. After solvent removal in vacuo, the residues were taken up in CH_2Cl_2 and filtered through a plug of celite. The solution was concentrated in

vacuo and layered with pentane in order to crystallize the desired complex.

Bis(2-chloro-4-methyl-6-[phenyl (pentafluorophenylimino)methyl] phenolato)titanium dichloride (2.2). Ligand **L2.2** (0.10 g, 0.21 mmol) was reacted as described above to give **2.2** as an orange-red crystalline solid (0.06 g, 54%). ^{1}H NMR ($CDCl_3$, 500 MHz): 7.28-7.40 (m, 4H, Ph*H*), 7.23 (m, 1H, Ph*H*), 7.07, 6.55 (m, 1H each, Ar*H*), 2.11 (s, 3H, ArCH_3). ^{13}C NMR ($CDCl_3$, 125MHz): 180.9 (N=*C*-Ar), 157.1 (Ar*C*-OTi), 137.7, 135.6, 134.1, 131.6, 130.6, 128.8, 126.2, 126.1, 125.7, 125.0, 122.3 (Ar*C* or Ph*C*), 20.7 ($ArCH_3$). The Ar_FC-F and Ar_FC_{ipso} signals are hidden. ^{19}F NMR ($CDCl_3$, 470 MHz): -140.7, -148.7, -160.8, -163.4, -167.7 (m, Ar_FF). Anal. calc. for $C_{40}H_{20}Cl_4F_{10}N_2O_2Ti$: C, 51.10; H, 2.14; N, 2.98. Anal. found: C, 50.72; H, 2.13; N, 2.77.

Bis(2-bromo-4-methyl-6-[phenyl (pentafluorophenylimino)methyl] phenolato)titanium dichloride (2.3). Ligand **L2.3** (0.23 g, 0.51 mmol) was reacted as described above to give **2.3** as a dark red crystalline solid (0.13 g, 51%). ^{1}H NMR ($CDCl_3$, 500 MHz): 7.55 (m, 1H, Ar*H*), 7.28-7.40 (m, 3H, Ph*H*), 7.22, 7.07 (m, 1H each, Ph*H*), 6.60 (m, 1H each, Ar*H*), 2.11 (s, 3H, ArCH_3). ^{13}C NMR ($CDCl_3$, 125MHz): 181.0 (N=*C*-Ar), 157.9 (Ar*C*-OH), 140.8 (Ph*C* or Ar*C*), 140.0 (Ar_FC-F, m, J_{CF} = 250 Hz), 139.5 (Ar_FC-F, m, J_{CF} = 250 Hz), 138.0 (Ar_FC-F, m, J_{CF} = 250 Hz), 136.9 (Ar_FC-F, m, J_{CF} = 250 Hz), 135.6, 134.9, 132.1, 130.6, 128.8, 128.7, 126.2, 125.7 (Ar*C* or Ph*C*), 125.1 (Ar_FC_{ipso}, m), 124.8, 111.8 (Ph*C* or Ar*C*), 20.6 ($ArCH_3$). ^{19}F NMR ($CDCl_3$, 470 MHz): -140.5, -148.5, -160.7, -163.0, -167.6 (m, Ar_FF). Anal. calc. for $C_{40}H_{20}Br_2Cl_2F_{10}N_2O_2Ti$: C, 46.68; H, 1.96; N, 2.72. Anal. found: C, 46.91; H, 2.02; N, 2.60.

Bis(5-methyl-3-[phenyl (pentafluorophenylimino)methyl)biphenyl-2-olato)titanium dichloride (2.4). Ligand **L2.4** (0.09 g, 0.20 mmol) was reacted as described above to give **2.4** as a brown-red crystalline solid (0.04 g, 35%). ^{1}H

NMR ($CDCl_3$, 500 MHz): 7.73 (d, 2H, J = 7.5 Hz, Ph*H*), 7.43-7.46 (m, 3H, Ph*H*), 7.22-7.34 (m, 4H, Ph*H* or Ar*H*), 7.18, 7.00 (m, 1H each, Ph*H*), 6.60 (m, 1H, Ar*H*), 2.15 (s, 3H, ArCH_3). ^{13}C NMR ($CDCl_3$, 125MHz): 180.9 (N=*C*-Ar), 159.3 (Ar*C*-OTi), 138.7, 136.2, 135.4, 134.9, 131.3, 130.2, 129.7, 129.3, 128.6, 128.5, 128.48, 127.9, 126.1, 125.6, 124.8 (Ar*C* or Ph*C*), 21.0 ($ArCH_3$). The Ar_FC-F and Ar_FC_{ipso} signals are hidden. ^{19}F NMR ($CDCl_3$, 470 MHz): -142.2, -148.9, -159.7, -163.4, -168.1 (m, Ar_FF). Anal. calc. for $C_{52}H_{30}Cl_2F_{10}N_2O_2Ti$: C, 61.02; H, 2.95; N, 2.74. Anal. found: C, 60.57; H, 3.20; N, 2.59.

Bis(2-benzyl-4-methyl-6-[phenyl (pentafluorophenylimino)methyl] phenolato)titanium dichloride (2.5). Ligand **L2.5** (0.10 g, 0.21 mmol) was reacted as described above to give **2.5** as a dark red crystalline solid (0.06 g, 54%). ^{1}H NMR ($CDCl_3$, 500 MHz): 7.27-7.40 (m, 7H, Ph*H*), 7.18-7.22 (m, 2H, Ph*H*), 7.14 (m, 1H, Ph*H*), 7.07, 6.47 (s, 1H each, Ar*H*), 3.77 (dd, 2H, J = 15, 364 Hz, ArCH_2Ph), 2.04 (s, 3H, ArCH_3). ^{13}C NMR ($CDCl_3$, 125MHz): 181.1 (N=*C*-Ar), 159.8 (Ar*C*-OTi), 140.0 (Ar_FC-F, m, J_{CF} = 250 Hz), 139.8, 138.8 (Ph*C* or Ar*C*), 138.8 (Ar_FC-F, m, J_{CF} = 250 Hz), 137.6 (Ar_FC-F, m, J_{CF} = 250 Hz), 136.7 (Ar_FC-F, m, J_{CF} = 250 Hz), 136.1, 133.5, 131.1, 130.4, 130.2, 129.5, 128.8, 128.56, 128.54, 126.5, 126.0 (Ar*C* or Ph*C*), 125.5 (Ar_FC_{ipso}, m), 124.1 (Ar*C*), 35.3 ($ArCH_2Ph$), 20.9 ($ArCH_3$). ^{19}F NMR ($CDCl_3$, 470 MHz): -141.0, -147.1, -160.5, -164.5, -167.3 (m, Ar_FF). Anal. calc. for $C_{54}H_{34}Cl_2F_{10}N_2O_2Ti$: C, 61.67; H, 3.26; N, 2.66. Anal. found: C, 61.40; H, 2.98; N, 2.67.

Bis(2-[phenyl (pentafluorophenylimino)methyl]-5,6,7,8-tetrahydro-1-naphtholato)titanium dichloride (2.6). Ligand **L2.6** (0.15 g, 0.21 mmol) was reacted as described above to give **2.6** as a light orange powder (0.05 g, 27%). ^{1}H NMR ($CDCl_3$, 500 MHz): 7.25-7.35 (m, 3H, Ph*H*), 7.18, 7.12 (m, 1H each, Ph*H*), 6.59 (dd, 2H, J = 9.0, 21.5 Hz, Ar*H*), 2.66-2.80 (m, 3H, Ar-(CH_2)$_4$-Ar), 2.08

(m, 1H, Ar-(CH_2)$_4$-Ar), 1.65-1.76 (m, 4H, Ar-(CH_2)$_4$-Ar). ^{13}C NMR ($CDCl_3$, 125MHz): 180.5 (N=*C*-Ar), 162.1 (Ar*C*-OTi), 149.1 (Ar*C*), 140.1 (Ar_F*C*-F, m, J_{CF} = 250 Hz), 138.9 (Ar_F*C*-F, m, J_{CF} = 250 Hz), 137.5 (Ar_F*C*-F, m, J_{CF} = 250 Hz), 136.8 (Ar_F*C*-F, m, J_{CF} = 250 Hz), 136.2, 132.1, 130.2, 128.5, 126.5, 126.4, 126.0, 125.9 (Ar*C* or Ph*C*), 125.9 (Ar_FC_{ipso}, m), 122.7, 121.8 (Ar*C* or Ph*C*), 30.4, 23.3, 22.4, 22.2 (Ar-(*C*H_2)$_4$-Ar). ^{19}F NMR ($CDCl_3$, 470 MHz): -140.9, -146.7, -161.4, -164.5, -167.2 (m, Ar_FF). Anal. calc. for $C_{46}H_{30}Cl_2F_{10}N_2O_2Ti$: C, 58.07; H, 3.18; N, 2.94. Anal. found: C, 57.82; H, 2.95; N, 2.85.

Bis(4-chloro-2-methyl-6-[phenyl (pentafluorophenylimino)methyl] phenolato)titanium dichloride (2.7). Ligand **L2.7** (0.28 g, 0.69 mmol) was reacted as described above to give **2.7** as a red crystalline solid (0.20 g, 61%). ^{1}H NMR ($CDCl_3$, 500 MHz): 7.31-7.41 (m, 4H, Ar*H* or Ph*H*), 7.18, 7.10 (m, 1H each, Ph*H*), 6.66 (m, 1H, Ar*H*), 2.08 (s, 3H, ArCH_3). ^{13}C NMR ($CDCl_3$, 125MHz): 180.8 (N=*C*-Ar), 160.8 (Ar*C*-OTi), 139.8 (Ar_F*C*-F, m, J_{CF} = 250 Hz), 139.1 (Ar_F*C*-F, m, J_{CF} = 250 Hz), 137.8 (Ar*C*), 137.7 (Ar_F*C*-F, m, J_{CF} = 250 Hz), 136.7 (Ar_F*C*-F, m, J_{CF} = 250 Hz), 135.2, 132.0, 130.9, 129.0, 128.95, 128.9, 126.3, 126.2, 125.8 (Ar*C* or Ph*C*), 125.1 (Ar_FC_{ipso}, m), 124.7 (Ph*C* or Ar*C*), 15.7 (ArCH_3). ^{19}F NMR ($CDCl_3$, 470 MHz): -141.1, -147.4, -160.0, -164.1, -166.8 (m, Ar_FF). Anal. calc. for $C_{40}H_{20}Cl_4F_{10}N_2O_2Ti$: C, 51.10; H, 2.14; N, 2.98. Anal. found: C, 50.65; H, 1.93; N, 2.85.

Bis(4-fluoro-2-methyl-6-[phenyl (pentafluorophenylimino)methyl] phenolato)titanium dichloride (2.8). Ligand **L2.8** (0.13 g, 0.32 mmol) was reacted as described above to give **2.8** as a dark purple-red crystalline solid (0.05 g, 36%). ^{1}H NMR ($CDCl_3$, 500 MHz): 7.30-7.40 (m, 4H, Ar*H* or Ph*H*), 7.20, 7.12 (m, 1H each, Ph*H*), 6.38 (dd, 1H, J = 3, 9 Hz Ar*H*), 2.09 (s, 3H, ArCH_3). ^{13}C NMR ($CDCl_3$, 125MHz): 180.9 (N=*C*-Ph), 158.7 (Ar*C*-OTi), 155.9 (ArC-F, d, J_{CF} =

240 Hz), 139.8 (Ar_FC-F, m, J_{CF} = 250 Hz), 139.1 (Ar_FC-F, m, J_{CF} = 250 Hz), 137.7 (Ar_FC-F, m, J_{CF} = 250 Hz), 136.8 (Ar_FC-F, m, J_{CF} = 250 Hz), 135.4, 130.8 (Ph*C*), 129.2 (Ar*C*, d, J_{CF} = 7.5 Hz), 128.9 (Ar*C*, d, J_{CF} = 9.1 Hz), 126.2, 125.8, 125.7, 125.5 (Ph*C*), 125.2 (Ar_FC_{ipso}, m), 123.9 (Ar*C*, d, J_{CF} = 8.3 Hz), 117.8 (Ar*C*, d, J_{CF} = 25 Hz), 15.9 (Ar*C*H_3). ^{19}F NMR ($CDCl_3$, 470 MHz): -123.0, -141.1, -147.5, -160.2, -164.2, -167.0 (m, Ar_FF). Anal. calc. for $C_{40}H_{20}Cl_2F_{12}N_2O_2Ti$: C, 52.95; H, 2.22; N, 3.09. Anal. found: C, 52.42; H, 1.98; N, 2.86.

Bis(4-methoxy-2-methyl-6-[phenyl (pentafluorophenylimino)methyl] phenolato)titanium dichloride (2.9). Ligand **L2.9** (0.09 g, 0.21 mmol) was reacted as described above to give **2.9** as a dark purple-red crystalline solid (0.04 g, 37%). ^{1}H NMR ($CDCl_3$, 500 MHz): 7.27-7.36 (m, 3H, Ph*H*), 7.21, 7.12 (m, 1H each, Ph*H*), 6.97, 6.12 (m, 1H each, Ar*H*), 3.50 (s, 3H, ArOCH_3), 2.07 (s, 3H, ArCH_3). ^{13}C NMR ($CDCl_3$, 125MHz): 180.8 (N=*C*-Ar), 157.5 (Ar*C*-OTi), 153.1 (Ar*C*-OCH_3), 139.9 (Ar_FC-F, m, J_{CF} = 250 Hz), 138.9 (Ar_FC-F, m, J_{CF} = 250 Hz), 137.6 (Ar_FC-F, m, J_{CF} = 250 Hz), 136.8 (Ar_FC-F, m, J_{CF} = 250 Hz), 136.0, 130.5, 128.64, 128.59, 128.0, 126.4, 125.9 (Ar*C* or Ph*C*), 125.5 (Ar_FC_{ipso}, m), 125.5, 124.1, 116.0 (Ph*C* or Ar*C*), 55.8 ($ArOCH_3$), 15.9 (Ar*C*H_3). ^{19}F NMR ($CDCl_3$, 470 MHz): -141.1, -147.2, -161.0, -164.7, -167.4 (m, Ar_FF). Anal. calc. for $C_{42}H_{26}Cl_2F_{10}N_2O_4Ti$: C, 54.16; H, 2.81; N, 3.01. Anal. found: C, 53.88; H, 2.84; N, 2.89.

Bis(2,4-dimethyl – 6 - [1-(pentafluorophenylimino)ethyl]phenolato) titanium dichloride (2.10). Ligand **L2.10** (0.23 g, 0.69 mmol) was reacted as described above to give **2.10** as a brown-red crystalline solid (0.16 g, 61%). ^{1}H NMR (C_6D_6, 300 MHz): 6.94, 6.76 (s, 1H each, Ar*H*), 2.05, 2.02, 1.65 (s, 3H each, ArCH_3 or N=C-CH_3). ^{13}C NMR ($CDCl_3$, 125MHz): 178.3 (N=*C*-Ar), 159.3 (Ar*C*-OTi), 140.4 (Ar_FC-F, m, J_{CF} = 250 Hz), 140.0 (Ar_FC-F, m, J_{CF} = 250 Hz), 139.3 (Ar_FC-F, m, J_{CF} = 250 Hz), 138.9 (Ar*C*), 138.1 (Ar_FC-F, m, J_{CF} = 250 Hz), 137.4

(Ar_FC-F, m, J_{CF} = 250 Hz), 131.2, 128.8, 126.9 (Ar*C*), 124.5 (Ar_FC_{ipso}, m), 123.2 (Ar*C*), 21.9, 21.1, 15.7 (N=C-*C*H_3 or Ar*C*H_3). ^{19}F NMR ($CDCl_3$, 470 MHz): -144.9, -149.3, -161.2, -164.0, -166.5 (m, Ar_FF). Anal. calc. for $C_{32}H_{22}Cl_2F_{10}N_2O_2Ti$: C, 49.57; H, 2.86; N, 3.61. Anal. found: C, 49.09; H, 2.87; N, 2.51.

Bis(2,4-dimethyl - 6 - [2-methyl-1-(pentafluorophenylimino)propyl] phenolato)titanium dichloride (2.11). Ligand **L2.11** (0.15 g, 0.42 mmol) was reacted as described above to give **2.11** as a dark red crystalline solid from toluene/pentane (0.07 g, 41%). ^{1}H NMR ($CDCl_3$, 500 MHz): 7.59, 7.19 (s, 1H each, Ar*H*), 3.00 (s, 1H, J = 7.5 Hz, N=C-C*H*$(CH_3)_2$), 2.32, 2.03 (s, 3H each, ArC*H*$_3$), 1.40 (d, 6H, J = 7.5Hz, N=C-CH(C*H*$_3)_2$). ^{13}C NMR ($CDCl_3$, 125MHz): 185.5 (N=*C*-Ar), 160.4 (Ar*C*-OTi), 140.2 (Ar_FC-F, m, J_{CF} = 250 Hz), 139.1 (Ar_FC-F, m, J_{CF} = 250 Hz), 138.2 (Ar_FC-F, m, J_{CF} = 250 Hz), 138.1 (Ar*C*), 137.4 (Ar_FC-F, m, J_{CF} = 250 Hz), 130.0, 129.2, 127.1 (Ar*C*), 123.8 (Ar_FC_{ipso}, m), 120.9 (Ar*C*), 36.9 (N=C-*C*H$(CH_3)_2$), 21.7, 21.4 (N=C-CH(*C*H$_3)_2$), 21.2, 16.0 (Ar*C*H$_3$). ^{19}F NMR ($CDCl_3$, 470 MHz): -143.8, -148.1, -161.6, -164.2, -166.5 (m, Ar_FF). Anal. calc. for $C_{36}H_{30}Cl_2F_{10}N_2O_2Ti$: C, 52.01; H, 3.64; N, 3.37. Anal. found: C, 52.70; H, 3.87; N, 3.19.

Bis(2-[cyclohexyl (pentafluorophenylimino)methyl]-4,6-dimethyl phenolato)titanium dichloride (2.12). Ligand **L2.12** (0.25 g, 0.63 mmol) was reacted as described above to give **2.12** as a red crystalline solid (0.17 g, 59%). ^{1}H NMR ($CDCl_3$, 500 MHz): 7.72, 7.18 (s, 1H each, Ar*H*), 2.61 (m, 1H, Cy*H*), 2.33, 2.03 (s, 3H each, ArC*H*$_3$), 1.66-1.80 (m, 6H, Cy*H*), 1.25, 0.95 (m, 2H each, Cy*H*). ^{13}C NMR ($CDCl_3$, 125MHz): 184.1 (N=*C*-Ar), 160.4 (Ar*C*-OTi), 140.2 (Ar_FC-F, m, J_{CF} = 250 Hz), 139.1 (Ar_FC-F, m, J_{CF} = 250 Hz), 138.0 (Ar*C*), 138.0 (Ar_FC-F, m, J_{CF} = 250 Hz), 137.2 (Ar_FC-F, m, J_{CF} = 250 Hz), 129.8, 129.4, 126.9 (Ar*C*), 123.8 (Ar_FC_{ipso}, m), 121.7 (Ar*C*), 49.5, 31.1, 30.9, 30.8, 27.1, 25.7 (Cy*C*),

21.3, 16.1 (Ar*C*H_3). ^{19}F NMR ($CDCl_3$, 470 MHz): -143.8, -147.8, -161.4, -164.2, -166.4 (m, Ar_FF). Anal. calc. for $C_{42}H_{38}Cl_2F_{10}N_2O_2Ti$: C, 55.34; H, 4.20; N, 3.07. Anal. found: C, 55.50; H, 4.48; N, 2.84.

Bis(2-[cycloheptyl (pentafluorophenylimino)methyl)-4,6-dimethyl phenolato)titanium dichloride (2.13). Ligand **L2.13** (0.26 g, 0.64 mmol) was reacted as described above to give **2.13** as a brown-red crystalline solid (0.11 g, 37%). ^{1}H NMR ($CDCl_3$, 500 MHz): 7.41, 7.17 (s, 1H each, Ar*H*), 2.75 (m, 1H, Cycloheptyl*H*), 2.32, 2.02 (s, 3H each, ArCH_3), 1.71-1.80 (m, 5H, Cycloheptyl*H*), 1.10-1.53 (m, 7H, Cycloheptyl*H*). ^{13}C NMR ($CDCl_3$, 125MHz): 185.8 (N=*C*-Ar), 160.4 (Ar*C*-OTi), 140.3 (Ar_F*C*-F, m, J_{CF} = 250 Hz), 139.0 (Ar_F*C*-F, m, J_{CF} = 250 Hz), 138.0 (Ar*C*), 138.0 (Ar_F*C*-F, m, J_{CF} = 250 Hz), 137.2 (Ar_F*C*-F, m, J_{CF} = 250 Hz), 129.9, 129.7, 126.9 (Ar*C*), 124.1 (Ar_FC_{ipso}, m), 121.0 (Ar*C*), 48.6, 32.8, 32.6, 29.6, 29.0, 28.8, 28.1 (Cycloheptyl*C*), 21.3, 15.9 (Ar*C*H_3). ^{19}F NMR ($CDCl_3$, 470 MHz): -143.8, -148.3, -161.4, -164.4, -166.5 (m, Ar_FF). Anal. calc. for $C_{44}H_{42}Cl_2F_{10}N_2O_2Ti$: C, 56.25; H, 4.51; N, 2.98. Anal. found: C, 56.27; H, 4.62; N, 2.69.

Bis(2,4-dimethyl -6- (2,2,2-trifluoro-1-(pentafluorophenylimino)ethyl) phenolato)titanium dichloride (2.14). Ligand **L2.14** (0.32 g, 0.83 mmol) was reacted as described above to give **2.14** as a dark brown-red crystalline solid (0.12 g, 33%). ^{1}H NMR ($CDCl_3$, 500 MHz): 7.44, 7.37 (s, 1H each, Ar*H*), 2.36, 2.05 (s, 3H each, ArCH_3). ^{13}C NMR ($CDCl_3$, 125MHz): 164.7 (N=*C*-CF_3, q, J_{CF} = 29 Hz), 162.9 (Ar*C*-OTi), 140.8, 131.8 (Ar*C*), 129.0 (Ar*C*-C=N, q, J_{CF} = 5.3 Hz), 126.8 (Ar*C*), 119.2 (N=C-*C*F_3, q, J_{CF} = 290 Hz), 118.1 (Ar*C*), 21.3, 15.8 (Ar*C*H_3). The Ar_F*C*-F and Ar_FC_{ipso} signals are hidden. ^{19}F NMR ($CDCl_3$, 470 MHz): -59.6 (s, 3F, N=C-C*F*$_3$), -148.2 (br s, 2F, Ar_FF), -160.3 (m, Ar_FF), -164.3, -166.8 (br s, 1F each, Ar_FF). Despite repeated attempts, this compound proved to be too

sensitive for transport for elemental analysis.

Bis(2,4-dimethyl - 6 - [naphthalen-2-yl(pentafluorophenylimino) methyl]phenolato)titanium dichloride (2.15). Ligand **L2.15** (0.46 g, 1.04 mmol) was reacted as described above to give **2.15** as a red crystalline solid (0.29 g, 55%). ^{1}H NMR (C_6D_6, 500 MHz): 7.74 (dd, 1H, J = 7, 206 Hz, Ar*H*), 7.25-7.49 (m, 4H, Ar*H*), 6.97-7.15 (m, 2H, Ar*H*), 6.67 (s, 1H, Ar*H*), 6.57 (d, 1H, J = 10 Hz, Ar*H*), 2.11, 1.56 (s, 3H each, ArCH_3). ^{13}C NMR (C_6D_6, 125MHz): 181.6 (N=*C*-Ar), 161.7 (Ar*C*-OTi), 141.1 (Ar_FC-F, m, J_{CF} = 250 Hz), 140.0 (Ar*C*), 139.5 (Ar_FC-F, m, J_{CF} = 250 Hz), 138.4 (Ar_FC-F, m, J_{CF} = 250 Hz), 137.5 (Ar_FC-F, m, J_{CF} = 250 Hz), 134.6, 134.1, 133.9, 133.3, 132.7, 131.1, 129.0, 128.7, 128.1, 127.3 (Ar*C*), 126.5 (Ar_FC_{ipso}, m), 126.3, 124.5, 124.1, 123.5 (Ar*C*), 20.5, 15.9 (ArCH_3). ^{19}F NMR ($CDCl_3$, 470 MHz): -141.3, -147.3, -161.0, -164.7, -167.3 (m, Ar_FF). Anal. calc. for $C_{50}H_{30}Cl_2F_{10}N_2O_2Ti$: C, 60.08; H, 3.03; N, 2.80. Anal. found: C, 59.85; H, 3.31; N, 2.74.

Bis(2,4-dimethyl – 6 - [naphthalen-1-yl(pentafluorophenylimino) methyl]phenolato)titanium dichloride (2.16). Ligand **L2.16** (0.53 g, 1.20 mmol) was reacted as described above to give **2.16** as a red crystalline solid (0.36 g, 60%). ^{1}H NMR ($CDCl_3$, 500 MHz): 7.77-7.83 (m, 2H, Ar*H*), 7.67 (m, 1H, Ar*H*), 7.33-7.48 (m, 4H, Ar*H*), 7.11, 6.31 (s, 1H each, Ar*H*), 2.04, 1.90 (s, 3H each, ArCH_3). ^{13}C NMR ($CDCl_3$, 125MHz): 181.6 (N=*C*-Ar), 160.1 (Ar*C*-OTi), 140.5 (Ar_FC-F, m, J_{CF} = 250 Hz), 140.1 (Ar_FC-F, m, J_{CF} = 250 Hz), 139.5 (Ar*C*), 137.5 (Ar_FC-F, m, J_{CF} = 250 Hz), 136.6 (Ar_FC-F, m, J_{CF} = 250 Hz), 133.5, 133.0, 132.8, 131.1, 130.8, 129.9, 128.3, 127.5, 127.3, 126.5, 126.4 (Ar*C*), 125.3 (Ar_FC_{ipso}, m), 124.5, 124.3, 124.2 (Ar*C*), 20.6, 15.4 (ArCH_3). ^{19}F NMR ($CDCl_3$, 470 MHz): -139.7, -145.8, -161.6, -164.6, -168.0 (m, Ar_FF). Anal. calc. for $C_{50}H_{30}Cl_2F_{10}N_2O_2Ti$: C, 60.08; H, 3.03; N, 2.80. Anal. found: C, 60.26; H, 3.31; N, 2.65.

Bis(2-[4-methoxyphenyl (pentafluorophenylimino)methyl]-4,6-dimethylphenolato)titanium dichloride (2.17). Ligand **L2.17** (0.30 g, 0.70 mmol) was reacted as described above to give **2.17** as a red crystalline solid (0.15 g, 43%). ^{1}H NMR ($CDCl_3$, 500 MHz): 7.17 (s, 1H, Ar*H*), 7.08, 7.01 (m, 1H each, Ar*H*), 6.79 (m, 2H, Ar*H*), 6.48 (s, 1H, Ar*H*), 3.78 (s, 3H, ArOCH_3), 2.10, 2.06 (s, 3H each, ArCH_3). ^{13}C NMR ($CDCl_3$, 125MHz): 180.9 (N=*C*-Ar), 160.6 (Ar*C*-OTi), 140.0 (Ar_FC-F, m, J_{CF} = 250 Hz), 139.3 (Ar*C*), 138.8 (Ar_FC-F, m, J_{CF} = 250 Hz), 137.6 (Ar_FC-F, m, J_{CF} = 250 Hz), 136.8 (Ar_FC-F, m, J_{CF} = 250 Hz), 133.0, 130.7, 128.42, 128.4, 128.2, 128.0, 126.3 (Ar*C*), 125.6 (Ar_FC_{ipso}, m), 124.2, 114.2, 113.5 (Ar*C*), 55.5 ($ArOCH_3$), 20.8, 15.6 ($ArCH_3$). ^{19}F NMR ($CDCl_3$, 470 MHz): -141.6, -147.4, -161.5, -164.9, -167.7 (m, Ar_FF). Anal. calc. for $C_{44}H_{30}Cl_2F_{10}N_2O_4Ti$: C, 55.08; H, 3.15; N, 2.92. Anal. found: C, 54.98; H, 3.21; N, 2.81.

Bis(2-[mesityl (pentafluorophenylimino)methyl]-4,6-dimethyl phenolato)titanium dichloride (2.18). Ligand **L2.18** (0.10 g, 0.24 mmol) was reacted as described above to give **2.18** as a light brown-red crystalline solid (0.05 g, 44%). ^{1}H NMR ($CDCl_3$, 500 MHz): 7.12, 6.79, 6.64, 6.52 (s, 1H each, Ar*H*), 2.21, 2.10, 2.07, 1.96, 1.92 (s, 3H each, ArCH_3). ^{13}C NMR ($CDCl_3$, 125MHz): 183.8 (N=*C*-Ar), 159.6 (Ar*C*-OTi), 140.9 (Ar_FC-F, m, J_{CF} = 250 Hz), 140.6 (Ar_FC-F, m, J_{CF} = 250 Hz), 139.5, 138.8 (Ar*C*), 137.6 (Ar_FC-F, m, J_{CF} = 250 Hz), 137.2 (Ar*C*), 136.8 (Ar_FC-F, m, J_{CF} = 250 Hz), 134.3, 132.3, 131.51, 131.49, 129.2, 128.4, 126.1 (Ar*C*), 125.0 (Ar_FC_{ipso}, m), 124.8 (Ar*C*), 21.2, 20.9, 20.8, 19.1, 15.3 ($ArCH_3$). ^{19}F NMR ($CDCl_3$, 470 MHz): -137.3, -145.1, -161.9, -165.3, -168.5 (m, Ar_FF). Anal. calc. for $C_{48}H_{38}Cl_2F_{10}N_2O_2Ti$: C, 58.61; H, 3.89; N, 2.85. Anal. found: C, 58.16; H, 3.90; N, 2.70.

Bis(2,4-dimethyl - 6 - [pentafluorophenyl(pentafluorophenylimino) methyl]phenolato)titanium dichloride (2.19). Ligand **L2.19** (0.12 g, 0.26

mmol) was reacted as described above to give **2.19** as a dark red crystalline solid (0.05 g, 38%). ^{1}H NMR ($CDCl_3$, 500 MHz): 7.30, 6.48 (s, 1H each, Ar*H*), 2.20, 2.07 (s, 3H each, ArCH_3). ^{13}C NMR ($CDCl_3$, 125MHz): 168.7 (N=*C*-Ar), 161.0 (Ar*C*-OTi), 140.9, 132.3, 129.9, 127.3 (Ar*C*), 123.8 (Ar_FC_{ipso}, m), 122.8 (Ar*C*), 110.2 (Ar_FC_{ipso}, m), 20.9, 15.5 (ArCH_3). The Ar_F*C*-F signals are not baseline separated due to C-F coupling. ^{19}F NMR ($CDCl_3$, 470 MHz): -137.7, -139.3, -143.1, -145.5, -149.5, -158.6, -160.8, -161.1, -163.2, -165.7 (m, Ar_FF). Despite repeated attempts, this compound proved to be too sensitive for transport for elemental analysis.

2.4.2 Propylene Polymerization

General Procedure for propylene polymerization. A six-ounce Lab-Crest pressure reaction vessel (Andrews Glass) equipped with a magnetic stir bar was charged with dry PMAO-IP (150 equivalents Al per Ti) and toluene (100 mL). The reactor was then equilibrated at 0 °C and the solution was saturated with propylene (30 psig). A toluene solution (5 mL) of PKI catalyst (0.01 mmol) was injected via syringe to initiate the polymerization. A constant pressure of propylene (30 psig) was maintained throughout the polymerization. After an appropriate time (generally 6 hours) at 0 °C, the reaction was quenched with methanol (5 mL) and the reactor was vented. The polymer was precipitated in copious amounts of methanol/HCl (2% acid, 400 mL), collected, washed with methanol, and dried to constant weight.

Synthesis of iPP-*block*-PEP-*block*-iPP triblock copolymers. A six-ounce Lab-Crest pressure reaction vessel (Andrews Glass) equipped with a magnetic stir bar was charged with dry PMAO-IP (150 equivalents Al per Ti) and toluene (100 mL). The reactor was then equilibrated at 0 °C and the

solution was saturated with propylene (30 psig). A toluene solution (5 mL) of **2.12** (0.04 mmol) was injected via syringe to initiate the polymerization. A constant pressure of propylene (30 psig) was maintained for 15-16 hours. An aliquot of iPP was removed from the reactor via cannula and quenched with acidified methanol. The reactor was placed under ethylene pressure (32 psig), and the polymerization was continued for 14-56 minutes at 0 °C. The reactor was vented free of ethylene and propylene for approximately 10 min. An aliquot of iPP-*block*-PEP was removed from the reactor via cannula and quenched with acidified methanol. Propylene (30 psig) was reconnected and polymerization continued for an additional 15-16 hours. The polymerization was quenched with methanol (5 mL) and the reactor was vented. The polymer was precipitated in copious amounts of methanol/HCl (2% acid, 400 mL), collected, washed with methanol, and dried to constant weight.

Synthesis of iPP-*block*-PEP-*block*-iPP-*block*-PEP-*block*-iPP pentablock copolymer. An iPP-*block*-PEP-*block*-iPP triblock copolymer was made as described above. An aliquot of iPP-*block*-PEP-*block*-iPP was removed from the reactor via cannula and quenched with acidified methanol. The reactor was placed under ethylene pressure (40 psig), and the polymerization was continued for 14 minutes at 0 °C. The reactor was vented free of ethylene and propylene for approximately 10 min. An aliquot of iPP-*block*-PEP-*block*-iPP-*block*-PEP was removed from the reactor via cannula and quenched with acidified methanol. Propylene (30 psig) was reconnected and polymerization continued for an additional 15 hours. The polymerization was quenched with methanol (5 mL) and the reactor was vented. The polymer was precipitated in copious amounts of methanol/HCl (2% acid, 400 mL), collected, washed with methanol, and dried to constant weight.

Synthesis of iPP-*block*-PEP-*block*-iPP-*block*-PEP-*block*-iPP-*block*-PEP-*block*-iPP heptablock copolymer. An iPP-*block*-PEP-*block*-iPP-*block*-PEP-*block*-iPP pentablock copolymer was made as described above. An aliquot of iPP-*block*-PEP-*block*-iPP-*block*-PEP-*block*-iPP was removed from the reactor via cannula and quenched with acidified methanol. The reactor was placed under ethylene pressure (40 psig), and the polymerization was continued for 12 minutes at 0 °C. The reactor was vented free of ethylene and propylene for approximately 10 min. An aliquot of iPP-*block*-PEP-*block*-iPP-*block*-PEP-*block*-iPP-*block*-PEP was removed from the reactor via cannula and quenched with acidified methanol. Propylene (30 psig) was reconnected and polymerization continued for an additional 15 hours. The polymerization was quenched with methanol (5 mL) and the reactor was vented. The polymer was precipitated in copious amounts of methanol/HCl (2% acid, 400 mL), collected, washed with methanol, and dried to constant weight.

APPENDIX

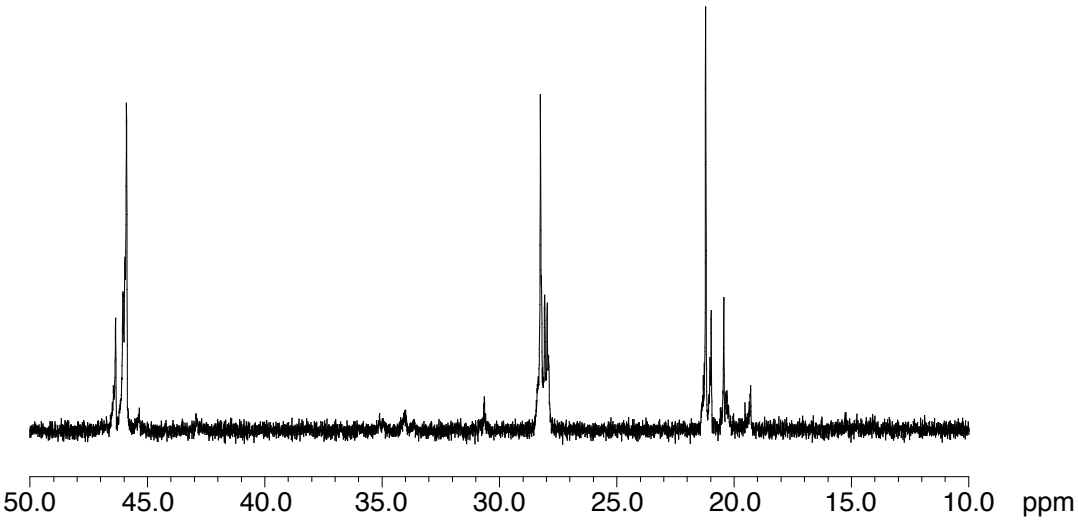

Figure 2.11. ^{13}C NMR (1,1,2,2-$C_2D_2Cl_4$, 125 MHz, 135 °C) of isotactic PP formed by **2.1**/MAO at 0 °C.

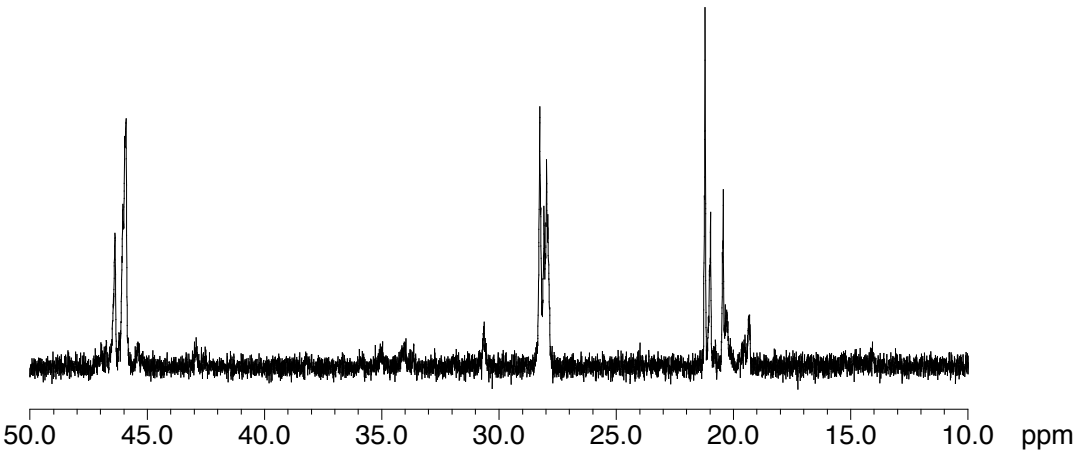

Figure 2.12. ^{13}C NMR (1,1,2,2-$C_2D_2Cl_4$, 125 MHz, 135 °C) of isotactic PP formed by **2.2**/MAO at 0 °C.

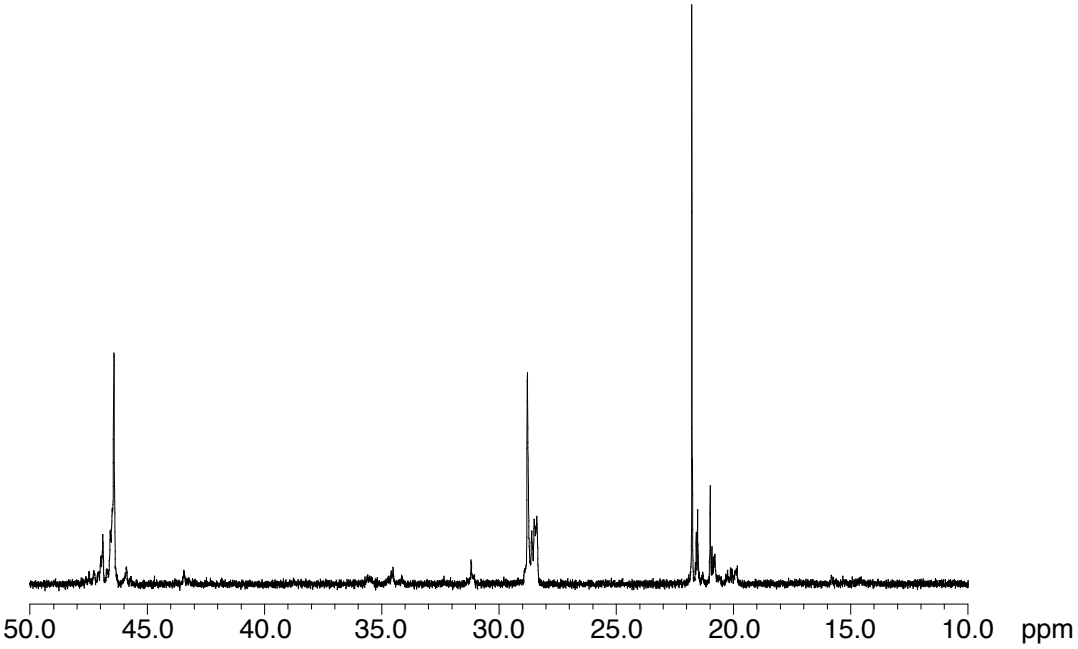

Figure 2.13. ^{13}C NMR (1,1,2,2-$C_2D_2Cl_4$, 125 MHz, 135 °C) of isotactic PP formed by **2.3**/MAO at 0 °C.

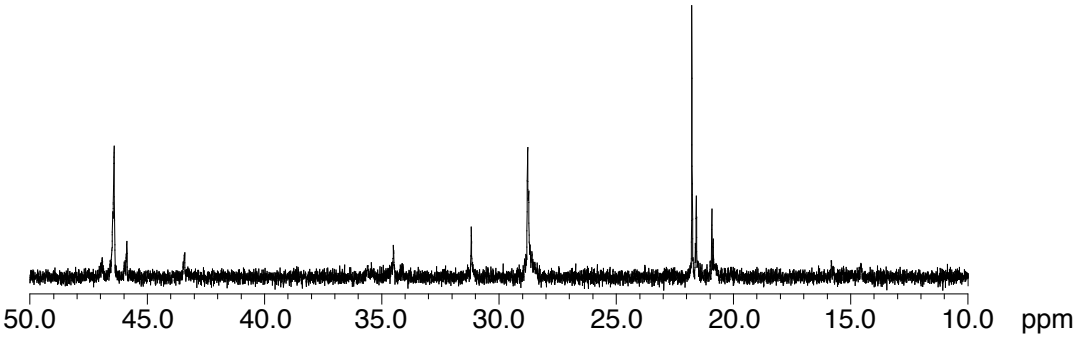

Figure 2.14. ^{13}C NMR (1,1,2,2-$C_2D_2Cl_4$, 125 MHz, 135 °C) of isotactic PP formed by **2.5**/MAO at 0 °C.

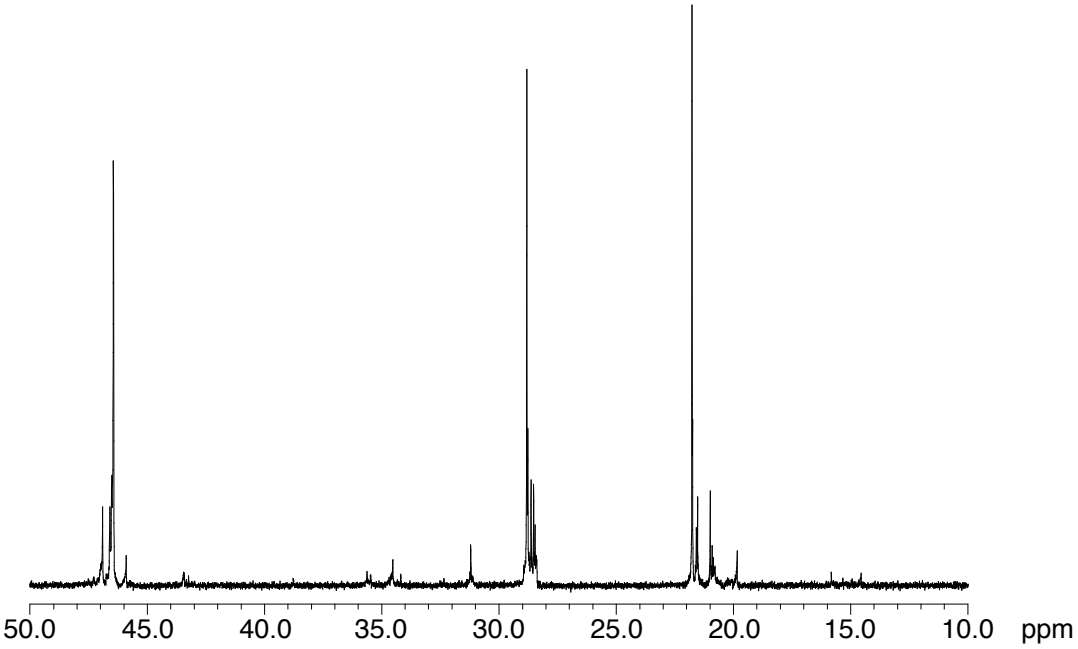

Figure 2.15. ^{13}C NMR (1,1,2,2-$C_2D_2Cl_4$, 125 MHz, 135 °C) of isotactic PP formed by **2.6**/MAO at 0 °C.

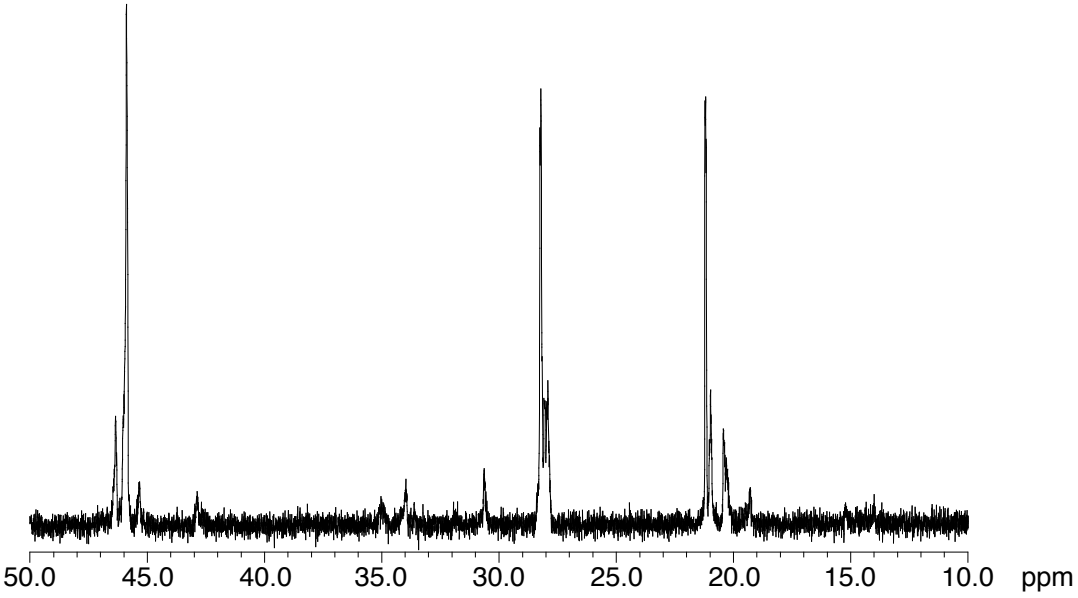

Figure 2.16. ^{13}C NMR (1,1,2,2-$C_2D_2Cl_4$, 125 MHz, 135 °C) of isotactic PP formed by **2.7**/MAO at 0 °C.

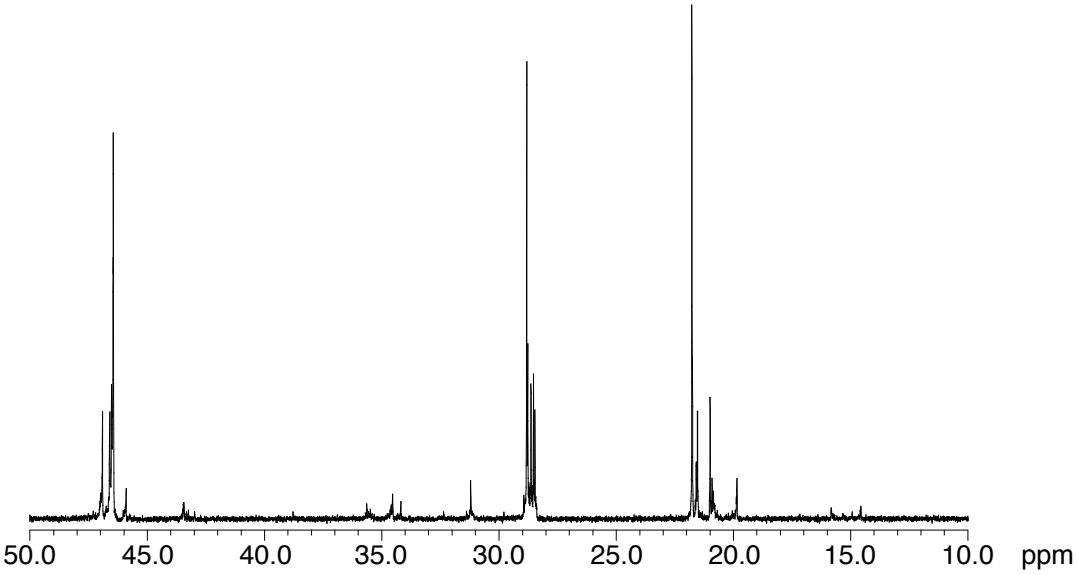

Figure 2.17. ^{13}C NMR (1,1,2,2-$C_2D_2Cl_4$, 125 MHz, 135 °C) of isotactic PP formed by **2.8**/MAO at 0 °C.

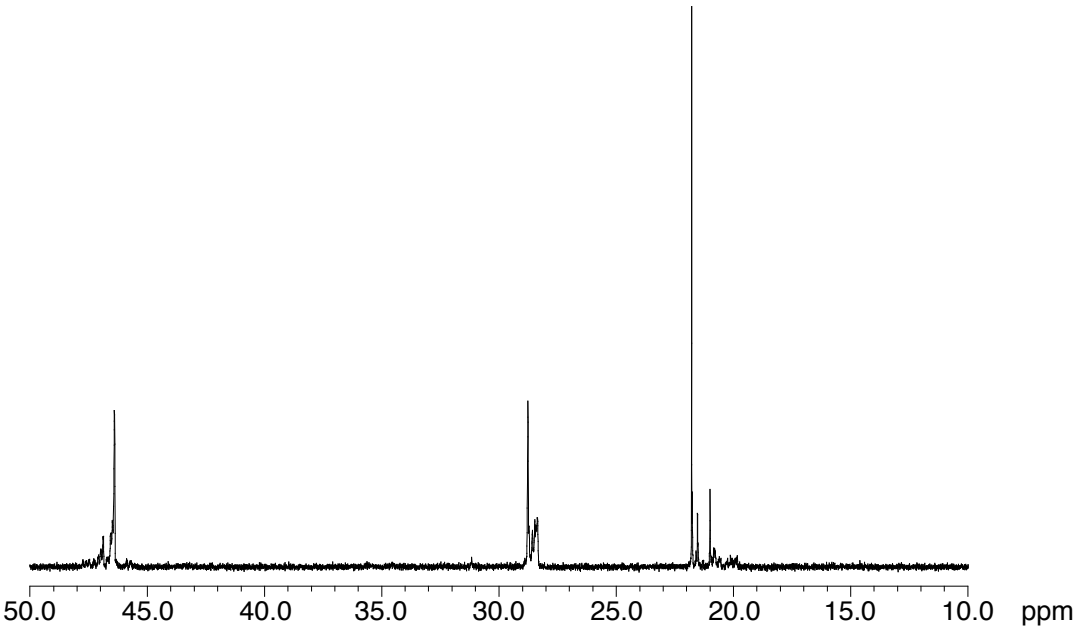

Figure 2.18. ^{13}C NMR (1,1,2,2-$C_2D_2Cl_4$, 125 MHz, 135 °C) of isotactic PP formed by **2.9**/MAO at 0 °C.

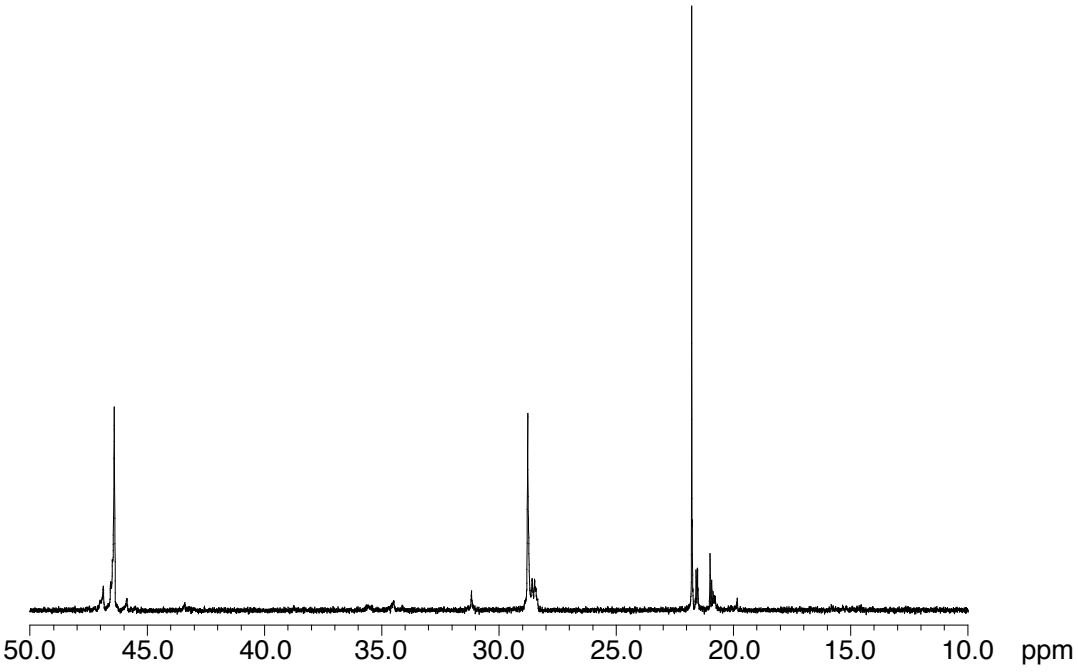

Figure 2.19. ^{13}C NMR (1,1,2,2-$C_2D_2Cl_4$, 125 MHz, 135 °C) of isotactic PP formed by **2.10**/MAO at 0 °C.

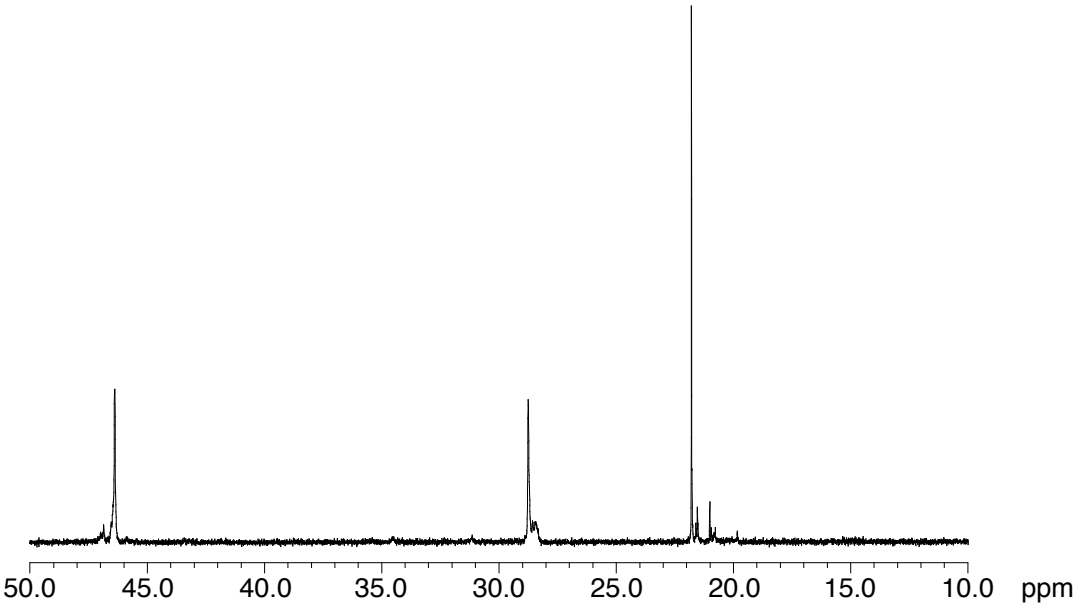

Figure 2.20. ^{13}C NMR (1,1,2,2-$C_2D_2Cl_4$, 125 MHz, 135 °C) of isotactic PP formed by **2.11**/MAO at 0 °C.

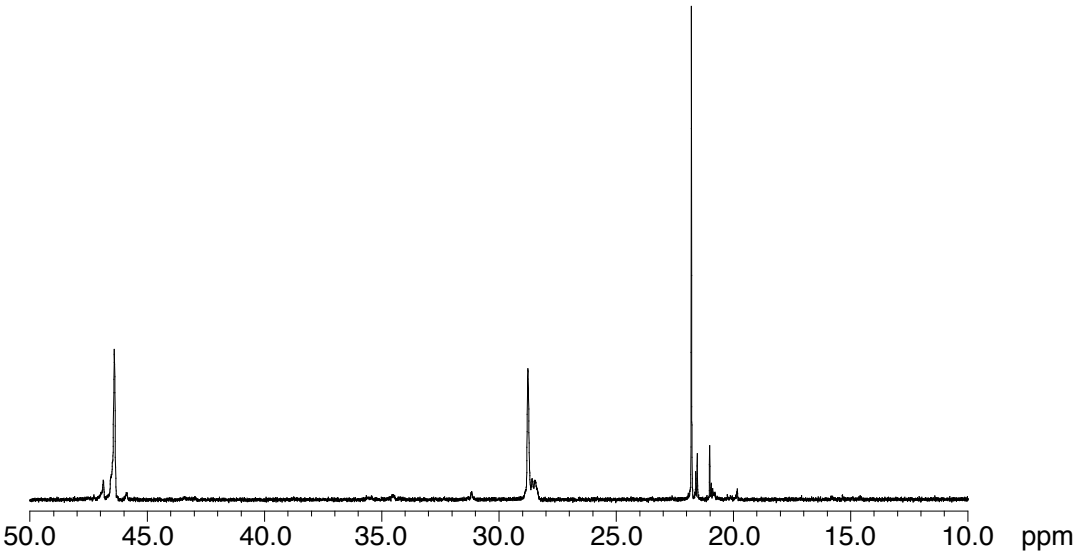

Figure 2.21. ^{13}C NMR (1,1,2,2-$C_2D_2Cl_4$, 125 MHz, 135 °C) of isotactic PP formed by **2.13**/MAO at 0 °C.

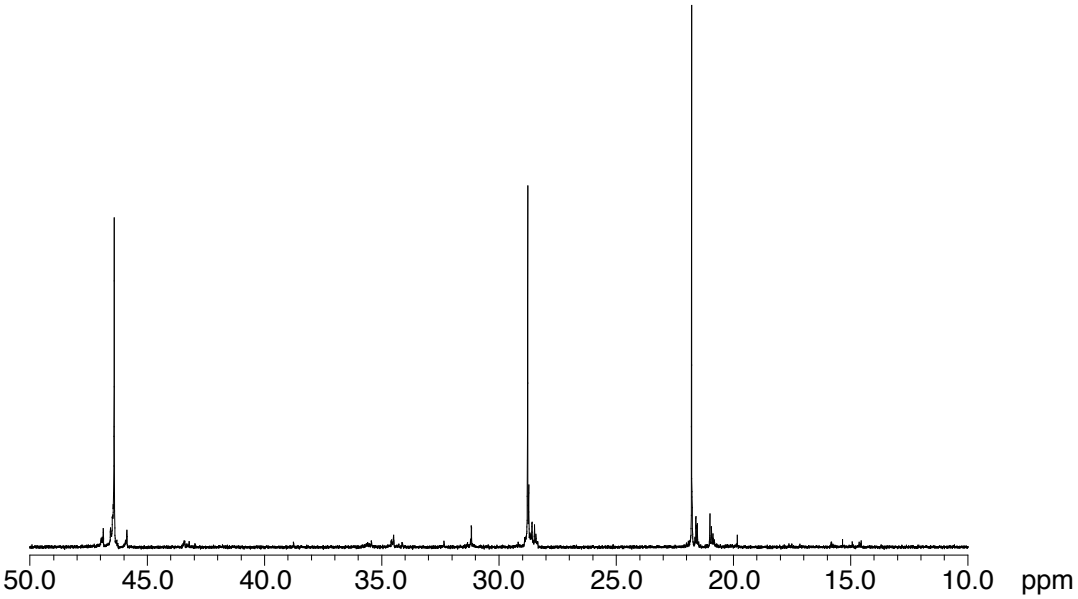

Figure 2.22. ^{13}C NMR (1,1,2,2-$C_2D_2Cl_4$, 125 MHz, 135 °C) of isotactic PP formed by **2.14**/MAO at 0 °C.

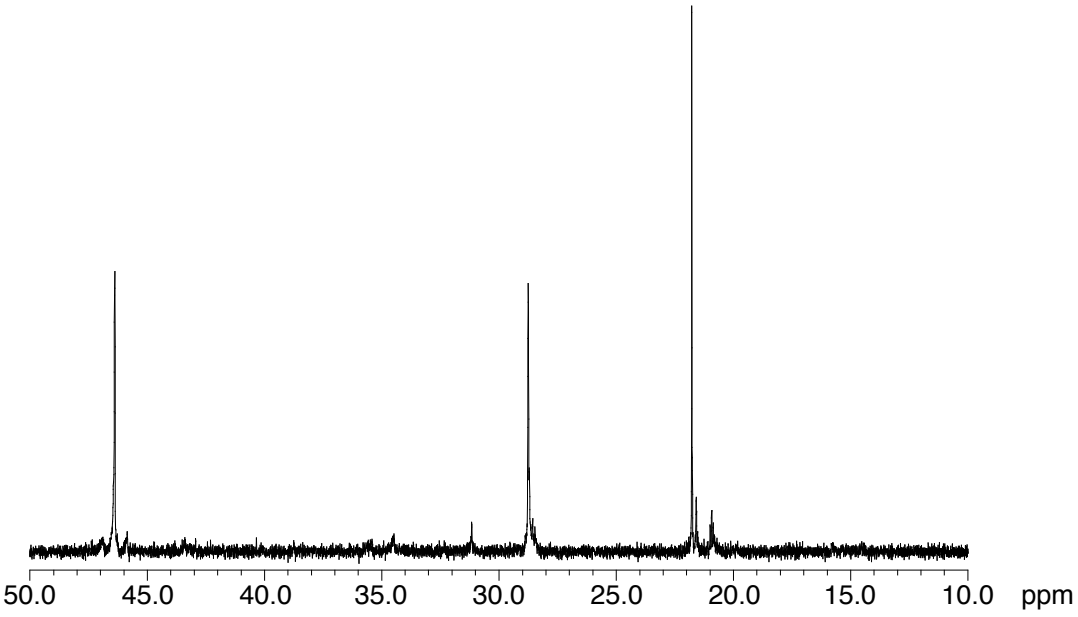

Figure 2.23. ^{13}C NMR (1,1,2,2-$C_2D_2Cl_4$, 125 MHz, 135 °C) of isotactic PP formed by **2.14**/MAO at -40 °C.

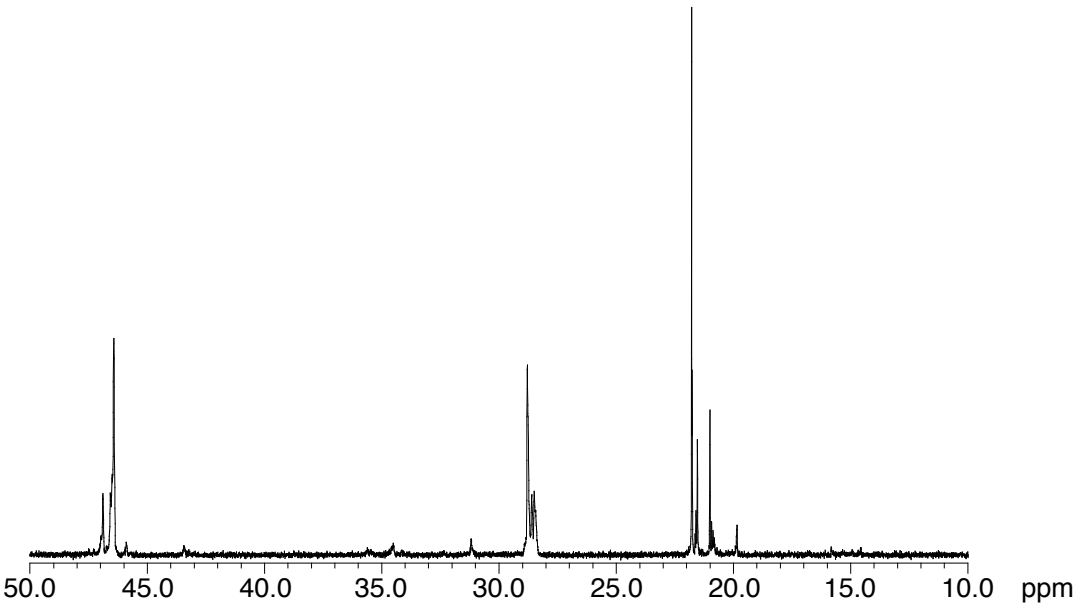

Figure 2.24. ^{13}C NMR (1,1,2,2-$C_2D_2Cl_4$, 125 MHz, 135 °C) of isotactic PP formed by **2.15**/MAO at 0 °C.

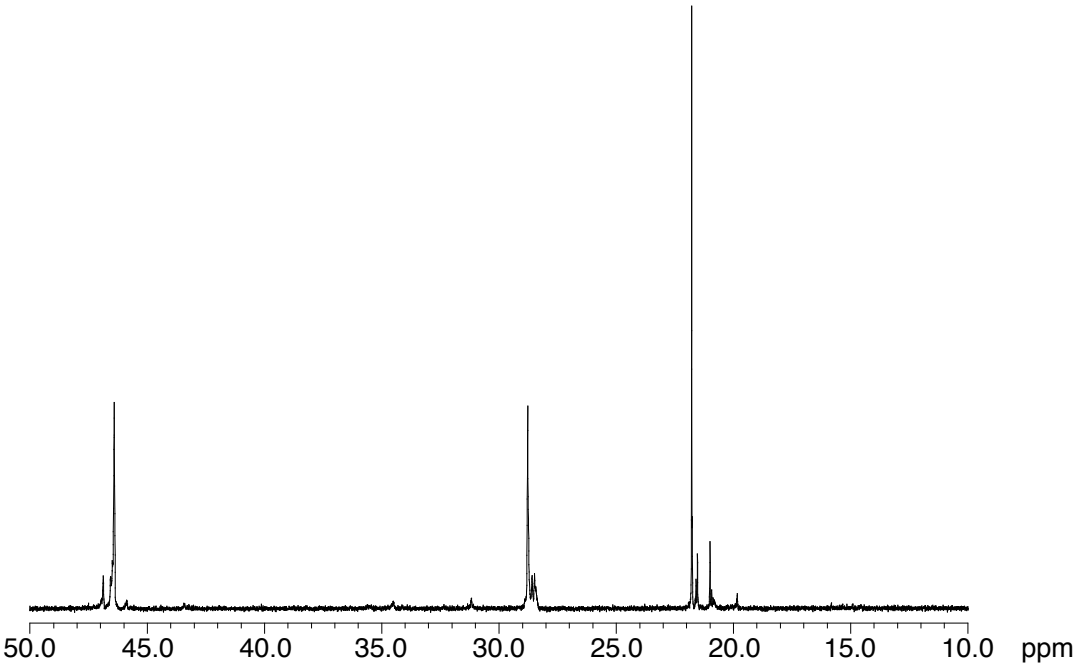

Figure 2.25. ^{13}C NMR (1,1,2,2-$C_2D_2Cl_4$, 125 MHz, 135 °C) of isotactic PP formed by **2.16**/MAO at 0 °C.

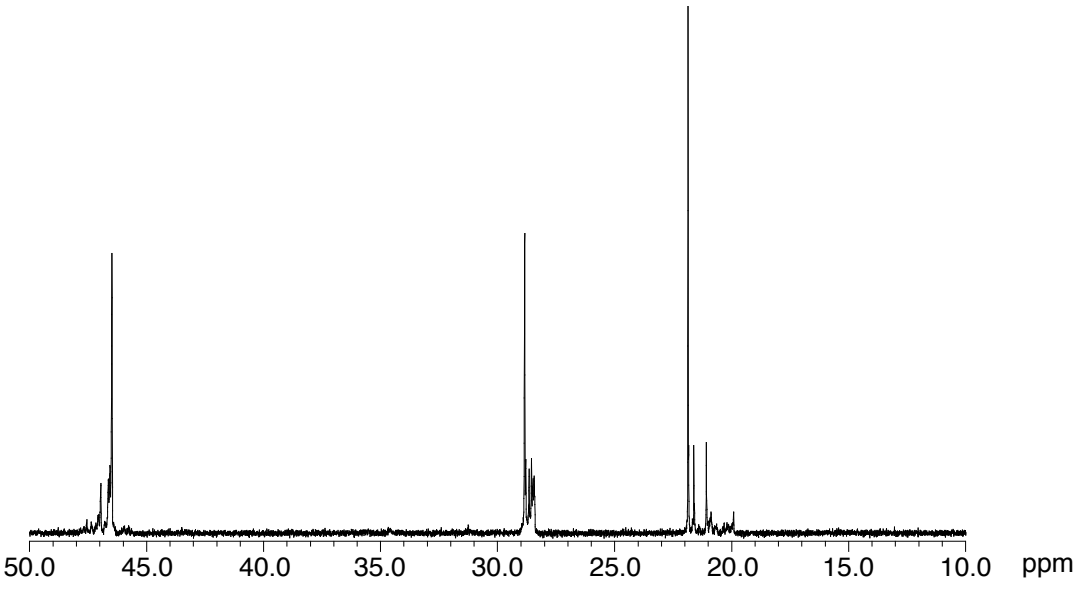

Figure 2.26. ^{13}C NMR (1,1,2,2-$C_2D_2Cl_4$, 125 MHz, 135 °C) of isotactic PP formed by **2.17**/MAO at 0 °C.

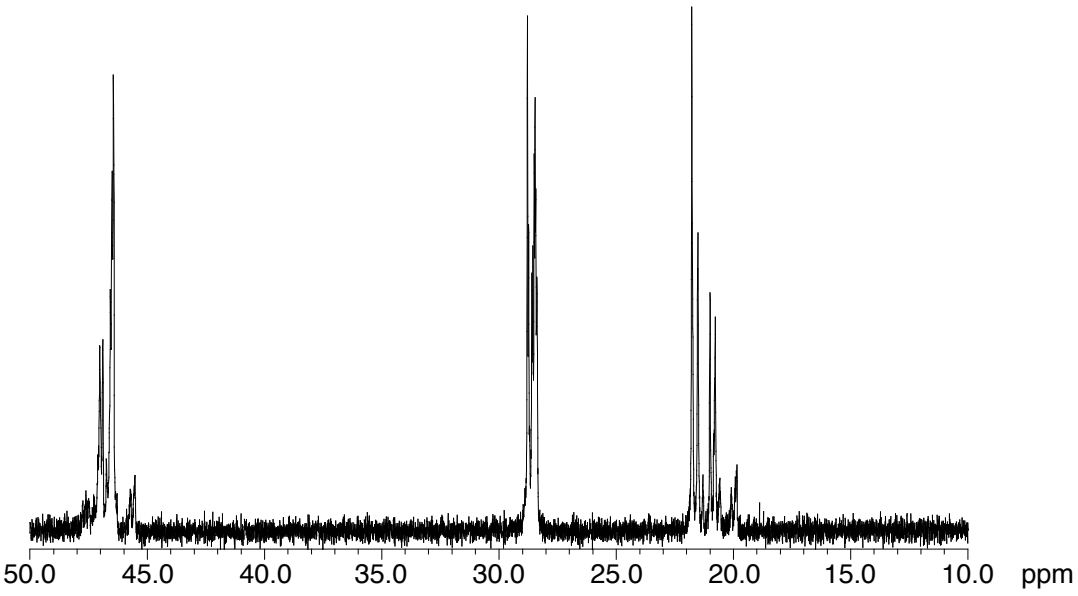

Figure 2.27. ^{13}C NMR (1,1,2,2-$C_2D_2Cl_4$, 125 MHz, 135 °C) of isotactic PP formed by **2.18**/MAO at 0 °C.

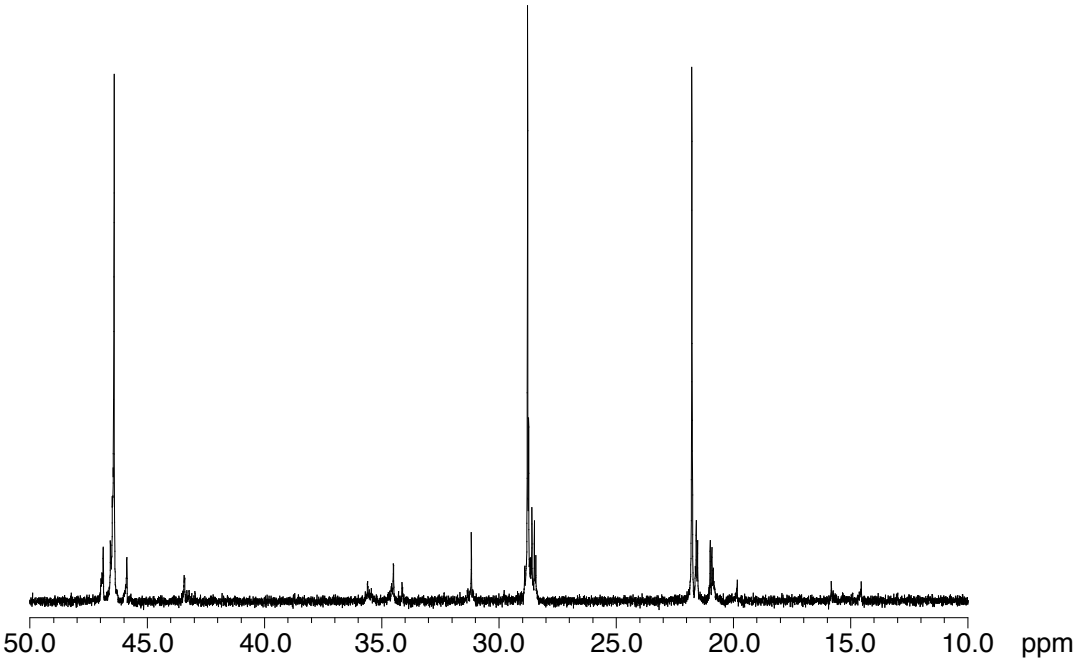

Figure 2.28. ^{13}C NMR (1,1,2,2-$C_2D_2Cl_4$, 125 MHz, 135 °C) of isotactic PP formed by **2.19**/MAO at 0 °C.

REFERENCES

(1) Britovsek, G. J. P.; Gibson, V. C.; Wass, D. F. *Angew. Chem. Int. Ed.* **1999**, *38*, 428-447.

(2) Gibson, V. C.; Spitzmesser, S. K. *Chem. Rev.* **2003**, *103*, 283-315.

(3) Coates, G. W. *Chem. Rev.* **2000**, *100*, 1223-1252.

(4) Coates, G. W.; Hustad, P. D.; Reinartz, S. *Angew. Chem. Int. Ed.* **2002**, *41*, 2236-2257.

(5) Domski, G. J.; Rose, J. M.; Coates, G. W.; Bolig, A. D.; Brookhart, M. *Prog. Polym. Sci.* **2007**, *32*, 30-92.

(6) Coates, G. W.; Waymouth, R. M. *Science* **1995**, *267*, 217-219.

(7) Harney, M. B.; Zhang, Y. H.; Sita, L. R. *Angew. Chem. Int. Ed.* **2006**, *45*, 2400-2404.

(8) Hotta, A.; Cochran, E.; Ruokolainen, J.; Khanna, V.; Fredrickson, G. H.; Kramer, E. J.; Shin, Y. W.; Shimizu, F.; Cherian, A. E.; Hustad, P. D.; Rose, J. M.; Coates, G. W. *Proc. Natl. Acad. Sci. U. S. A.* **2006**, *103*, 15327-15332.

(9) Bates, F. S. *Science* **1991**, *251*, 898-905.

(10) Figures taken from: (a) Domski, G. J.; Ph. D. Thesis, Cornell University, Ithaca, NY, **2008**. (b) Rose, J. M.; Ph. D. Thesis, Cornell University, Ithaca, NY, **2008.**

(11) Matsen, M. W.; Schick, M. *Phys. Rev. Lett.* **1994**, *72*, 2660-2663.

(12) Jayaratne, K. C.; Sita, L. R. *J. Am. Chem. Soc.* **2000**, *122*, 958-959.

(13) Zhang, Y. H.; Keaton, R. J.; Sita, L. R. *J. Am. Chem. Soc.* **2003**, *125*, 9062-9069.

(14) Zhang, Y. H.; Sita, L. R. *Chem. Commun.* **2003**, 2358-2359.

(15) Zhang, Y. H.; Sita, L. R. *J. Am. Chem. Soc.* **2004**, *126*, 7776-7777.

(16) Kissounko, D. A.; Zhang, Y. H.; Harney, M. B.; Sita, L. R. *Adv. Synth. Catal.* **2005**, *347*, 426-432.

(17) Tshuva, E. Y.; Goldberg, I.; Kol, M. *J. Am. Chem. Soc.* **2000**, *122*, 10706-10707.

(18) Segal, S.; Goldberg, I.; Kol, M. *Organometallics* **2005**, *24*, 200-202.

(19) Yasumoto, T.; Yamagata, T.; Mashima, K. *Organometallics* **2005**, *24*, 3375-3377.

(20) Sudhakar, P.; Sundararajan, G. *Macromol. Rapid Commun.* **2005**, *26*, 1854-1859.

(21) Domski, G. J.; Lobkovsky, E. B.; Coates, G. W. *Macromolecules* **2007**, *40*, 3510-3513.

(22) Resconi, L.; Cavallo, L.; Fait, A.; Piemontesi, F. *Chem. Rev.* **2000**, *100*, 1253-1345.

(23) Natta, G.; Pino, P.; Corradini, P.; Danusso, F.; Mantica, E.; Mazzanti, G.; Moraglio, G. *J. Am. Chem. Soc.* **1955**, *77*, 1708-1710.

(24) Busico, V.; Cipullo, R.; Friederichs, N.; Ronca, S.; Togrou, M. *Macromolecules* **2003**, *36*, 3806-3808.

(25) Busico, V.; Cipullo, R.; Friederichs, N.; Ronca, S.; Talarico, G.; Togrou, M.; Wang, B. *Macromolecules* **2004**, *37*, 8201-8203.

(26) Mason, A. F.; Coates, G. W. *J. Am. Chem. Soc.* **2004**, *126*, 16326-16327.

(27) Cherian, A. E.; Rose, J. M.; Lobkovsky, E. B.; Coates, G. W. *J. Am. Chem. Soc.* **2005**, *127*, 13770-13771.

(28) Tian, J.; Coates, G. W. *Angew. Chem. Int. Ed.* **2000**, *39*, 3626-3629.

(29) Mitani, M.; Fujita, T. In *Beyond Metallocenes: Next-Generation Polymerization Catalysts*; Patil, H. O., Hlatky, G. G., Eds.; American Chemical Society: Washington, D.C., 2003; Vol. 857, pp 26-45.

(30) Saito, J.; Mitani, M.; Mohri, J.; Ishii, S.; Yoshida, Y.; Matsugi, T.; Kojoh, S.; Kashiwa, N.; Fujita, T. *Chem. Lett.* **2001**, 576-577.

(31) Makio, H.; Kashiwa, N.; Fujita, T. *Adv. Synth. Catal.* **2002**, *344*, 477-493.

(32) Tian, J.; Hustad, P. D.; Coates, G. W. *J. Am. Chem. Soc.* **2001**, *123*, 5134-5135.

(33) Milano, G.; Cavallo, L.; Guerra, G. *J. Am. Chem. Soc.* **2002**, *124*, 13368-13369.

(34) Corradini, P.; Guerra, G.; Cavallo, L. *Acc. Chem. Res.* **2004**, *37*, 231-241.

(35) Mitani, M.; Furuyama, R.; Mohri, J.; Saito, J.; Ishii, S.; Terao, H.; Nakano, T.; Tanaka, H.; Fujita, T. *J. Am. Chem. Soc.* **2003**, *125*, 4293-4305.

(36) Saito, J.; Onda, M.; Matsui, S.; Mitani, M.; Furuyama, R.; Tanaka, H.; Fujita, T. *Macromol. Rapid Commun.* **2002**, *23*, 1118-1123.

(37) Prasad, A. V.; Makio, H.; Saito, J.; Onda, M.; Fujita, T. *Chem. Lett.* **2004**, *33*, 250-251.

(38) Reinartz, S.; Mason, A. F.; Lobkovsky, E. B.; Coates, G. W. *Organometallics* **2003**, *22*, 2542-2544.

(39) Matsui, S.; Tohi, Y.; Mitani, M.; Saito, J.; Makio, H.; Tanaka, H.; Nitabaru, M.; Nakano, T.; Fujita, T. *Chem. Lett.* **1999**, 1065-1066.

(40) Mason, A. F.; Tian, J.; Hustad, P. D.; Lobkovsky, E. B.; Coates, G. W. *Isr. J. Chem.* **2002**, *42*, 301-306.

(41) Saito, J.; Mitani, M.; Onda, M.; Mohri, J. I.; Ishi, J. I.; Yoshida, Y.; Nakano, T.; Tanaka, H.; Matsugi, T.; Kojoh, S. I.; Kashiwa, N.; Fujita, T. *Macromol. Rapid Commun.* **2001**, *22*, 1072-1075.

(42) Hustad, P. D.; Tian, J.; Coates, G. W. *J. Am. Chem. Soc.* **2002**, *124*, 3614-3621.

(43) Lamberti, M.; Pappalardo, D.; Zambelli, A.; Pellecchia, C. *Macromolecules* **2002**, *35*, 658-663.

(44) Talarico, G.; Busico, V.; Cavallo, L. *J. Am. Chem. Soc.* **2003**, *125*, 7172-7173.

(45) Lamberti, M.; Consolmagno, M.; Mazzeo, M.; Pellecchia, C. *Macromol. Rapid Commun.* **2005**, *26*, 1866-1871.

(46) Strianese, M.; Lamberti, M.; Mazzeo, M.; Tedesco, C.; Pellecchia, C. *Journal Of Molecular Catalysis A-Chemical* **2006**, *258*, 284-291.

(47) Chen, S. T.; Zhang, X. F.; Ma, H. W.; Lu, Y. Y.; Zhang, Z. C.; Li, H. Y.; Lu, Z. X.; Cui, N. N.; Hu, Y. L. *J. Organomet. Chem.* **2005**, *690*, 4184-4191.

(48) Mazzeo, M.; Strianese, M.; Lamberti, M.; Santoriello, I.; Pellecchia, C. *Macromolecules* **2006**, *39*, 7812-7820.

(49) Doi, Y.; Ueki, S.; Keii, T. *Makromol. Chem. Rapid. Commun.* **1982**, *3*, 225-229.

(50) Kojoh, S.; Matsugi, T.; Saito, J.; Mitani, M.; Fujita, T.; Kashiwa, N. *Chem. Lett.* **2001**, 822-823.

(51) Mitani, M.; Mohri, J.; Yoshida, Y.; Saito, J.; Ishii, S.; Tsuru, K.; Matsui, S.; Furuyama, R.; Nakano, T.; Tanaka, H.; Kojoh, S.; Matsugi, T.; Kashiwa, N.; Fujita, T. *J. Am. Chem. Soc.* **2002**, *124*, 3327-3336.

(52) Hustad, P. D.; Coates, G. W. *J. Am. Chem. Soc.* **2002**, *124*, 11578-11579.

(53) Tamura, K.; Mizukami, H.; Maeda, K.; Watanabe, H.; Uneyama, K. *J. Org. Chem.* **1993**, *58*, 32-35.

Chapter 3

Synthesis of New Tridentate Phenoxyamine Catalysts Supported by an sp^3-C Donor via Insertion of a Ligand-appended Alkene into a Neutral Group IV Alkyl Complex: Coordination Chemistry and Olefin Polymerization Behavior

3.1 Introduction

One of the ultimate challenges in the field of polymer synthesis is the ability to control material properties by manipulating molecular weight, molecular weight distribution and stereochemistry. Over the years, a number of homogeneous olefin polymerization catalysts have been developed that offer remarkable control over polymer stereochemistry.[1,2] While metallocene catalysts dominated the olefin polymerization field from the early 1980s to the mid 1990s, a new generation of "non-metallocene" catalysts has since become the major focus.[3,4] In particular, advances in living olefin polymerization[5-7] have allowed access to new polyolefin architectures, specifically block copolymers, that exhibit promising material properties.[8-12] One recent class of catalysts to emerge are the C_1-symmetric pyridylamidohafnium dialkyl complexes (**3.1**, R = 2-^{i}PrC$_6$H$_4$, Figure 3.1) developed by Dow and Symyx, which feature a cyclometalated Hf-C_{aryl} bond.[13-15] In addition to producing high molecular weight polymer, these catalysts can exhibit high levels of isoselectivity, thermal stability, and activity for olefin polymerization. Investigations into the catalyst activation mechanism have shown that a single 1,2-insertion of an olefin into the Hf-C_{Aryl} bond results in a seven-membered metallacycle bearing an sp^3-hybridized carbon donor atom that supports the active metal center rather than participating in further olefin insertion (Scheme 3.1).[14] Efforts in our group have demonstrated that C_s-symmetric **3.2** precatalysts (R = H, Figure 3.1) activated with B(C$_6$F$_5$)$_3$ furnish isotactic polypropylene (iPP) via an enantiomorphic site-control enchainment mechanism. This suggests the observed isoselectivity results from formation of a C_1-symmetric catalyst through 1,2-insertion of an olefin into the Hf-C_{Aryl} bond (Scheme 3.1).[16] We have further shown that precatalysts supported by an

sp^3-C donor could be generated by insertion of a ligand-appended alkene into the Hf-C bond of a neutral pyridylamidohafnium trimethyl complex to produce pyridylamidohafnium dimethyl six-membered metallacycle complexes as a racemic mixture of diastereomers (*rac*-**3.3a**,**b**, Figure 3.1).[17] Activation of these precatalysts with $B(C_6F_5)_3$ promoted the living and isoselective polymerization of propylene.

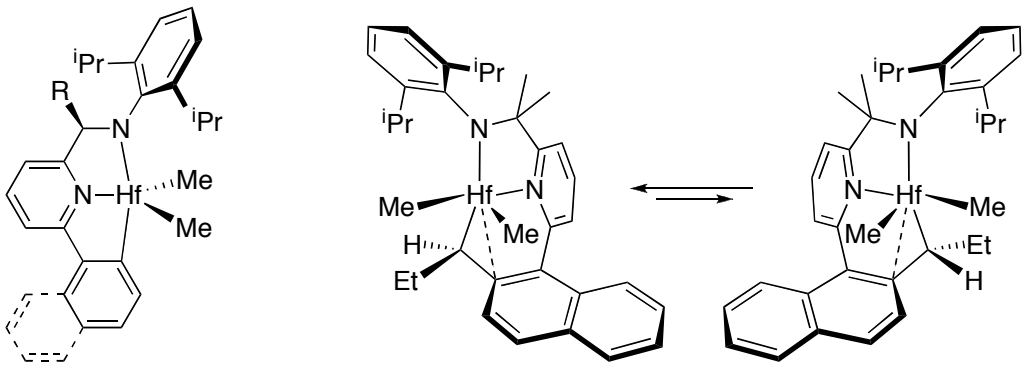

3.1 R = 2-*i*PrC$_6$H$_4$
3.2 R = H

rac-**3.3a,b**

Figure 3.1. Pyridylamidohafnium polymerization precatalysts.

Inspired by these results, and intrigued at the possibly of synthesizing a new class of olefin polymerization catalysts incorporating an ancillary sp^3-C donor into the ligand framework, we set out to prepare ligands bearing pendant vinyl group functionality. We initially targeted vinyl-appended phenoxyamine ligands[18-21] in hopes of preparing similar tridentate group IV complexes arising from insertion of the alkene into the metal trialkyl precursors. The phenoxyamine ligands were prepared through a Mannich reaction[22] between *N*-methyl-1-(2-vinylphenyl)methanamine,

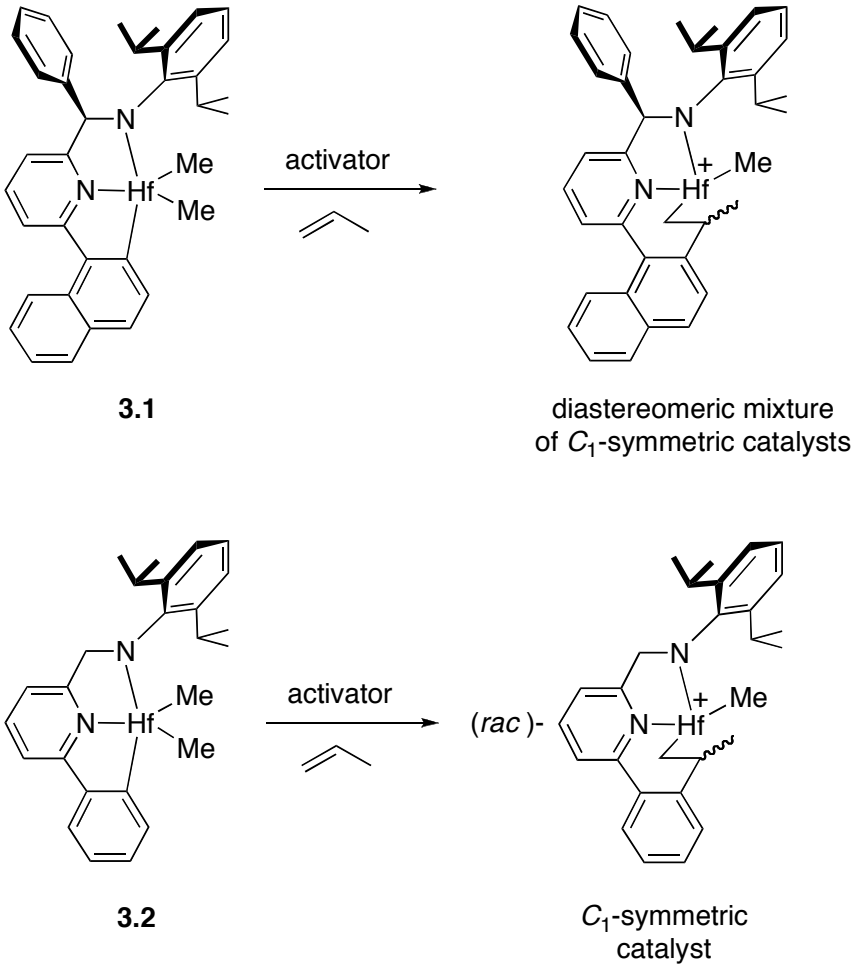

Scheme 3.1. Insertion of propylene into the Hf-C_{Aryl} bond of **3.1** and **3.2**.

paraformaldehyde, and a 2,4-disubstituted phenol (Scheme 3.2). Metalation of the resultant phenoxyamine ligands with tetrabenzyl group IV precursors afforded new sp^3-C bound six-membered metallacycle complexes as a mixture of two diastereomers arising from intramolecular insertion of the ligand-appended alkene into the neutral group IV tribenzyl precursor (Scheme 3.3). In the case of zirconium (*rac*- **Lig^{1}ZrBn$_2$-a,b**) and hafnium (*rac*- **Lig^{1}HfBn$_2$-a,b**), highly active and isoselective 1-hexene and propylene polymerization catalysts were formed upon activation. The six-membered sp^3-C bound

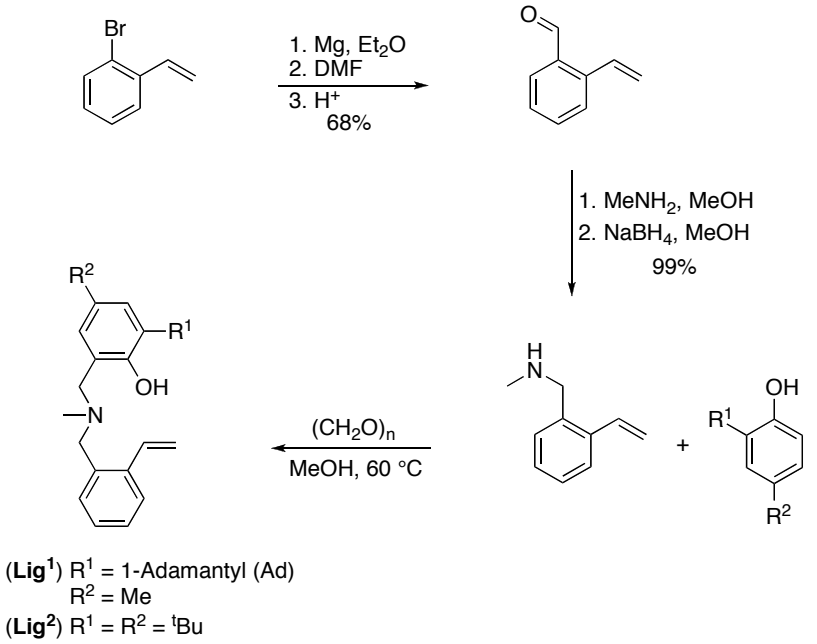

Scheme 3.2. Vinyl group ligand-appended phenoxyamine synthesis.

phenoxyamine titanium complex underwent further reaction through toluene elimination to form an unusual tetrahedral titanium complex (*rac*-**Lig^{2}TiBn**, Scheme 3.4) featuring a bound ligand-appended alkene. This complex was found to be inactive for olefin polymerization upon activation, however, reaction with ethylene leads to the formation of a titanacyclopentane complex.

We have explored the 1-hexene and propylene polymerization behavior of both *rac*-**Lig^{1}ZrBn$_2$-a,b** and *rac*-**Lig^{1}HfBn$_2$-a,b** under a number of activation conditions. In the course of our exploration, we found that *rac*-**Lig^{1}ZrBn$_2$-a,b**/$B(C_6F_5)_3$ furnished isotactic polypropylene ([m^4] = 0.76) in a living manner at 0 °C with high activity, while isotactic poly(1-hexene) was obtained with living behavior from *rac*-**Lig^{1}HfBn$_2$-a,b**/$B(C_6F_5)_3$ at 0 °C. Employing *rac*-**Lig^{1}ZrBn$_2$-a,b**/$B(C_6F_5)_3$, we prepared an iPP-*block*-PEP (PEP = poly(ethylene-*co*-propylene)) diblock copolymer. The results presented herein illustrate a

rare example of intramolecular vinyl group insertion for ligand-appended phenoxyamines upon metalation with tetrabenzyl group IV metal precursors as a unique method to generate sp^3-C bound precatalysts for olefin polymerization.

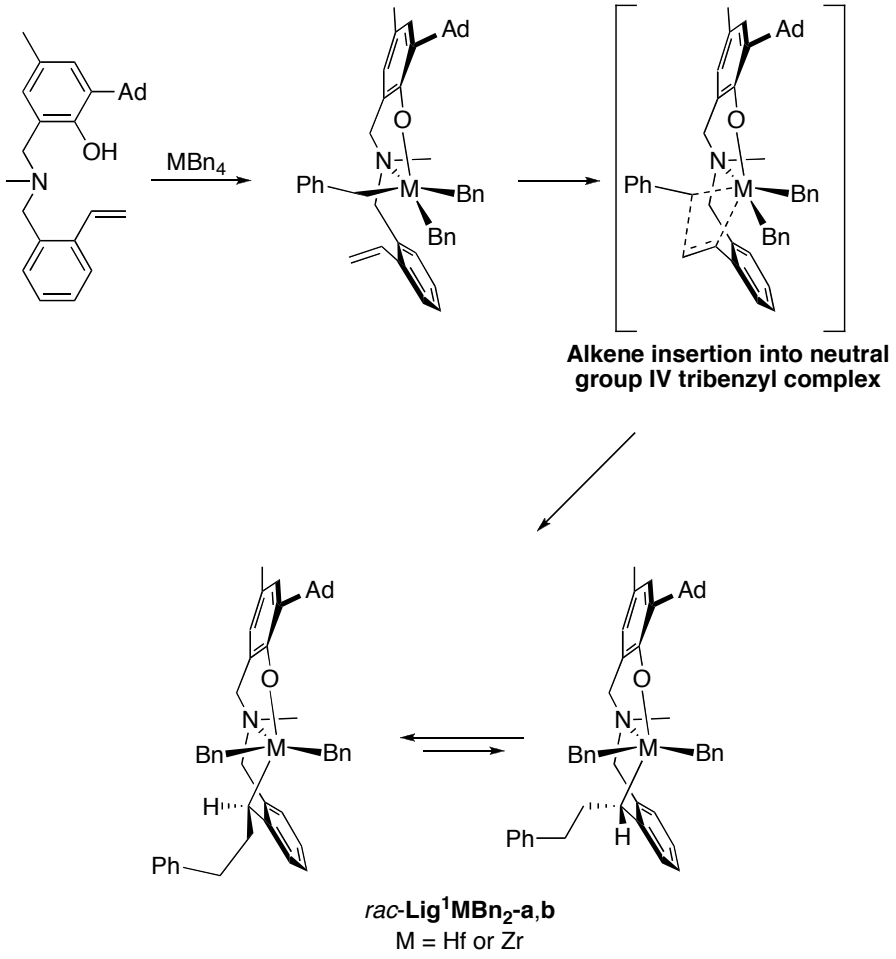

Scheme 3.3. Synthesis of *rac*-**Lig^{1}ZrBn$_2$-a,b** and *rac*-**Lig^{1}HfBn$_2$-a,b**.

3.2 Results and Discussion

3.2.1 Synthesis of *rac*-Lig^{1}HfBn$_2$-a,b and *rac*-Lig^{1}ZrBn$_2$-a,b

Reaction of **Lig^1** with $HfBn_4$ in C_6D_6 at 25 °C immediately provided a phenoxyaminehafnium dibenzyl complex arising from intramolecular

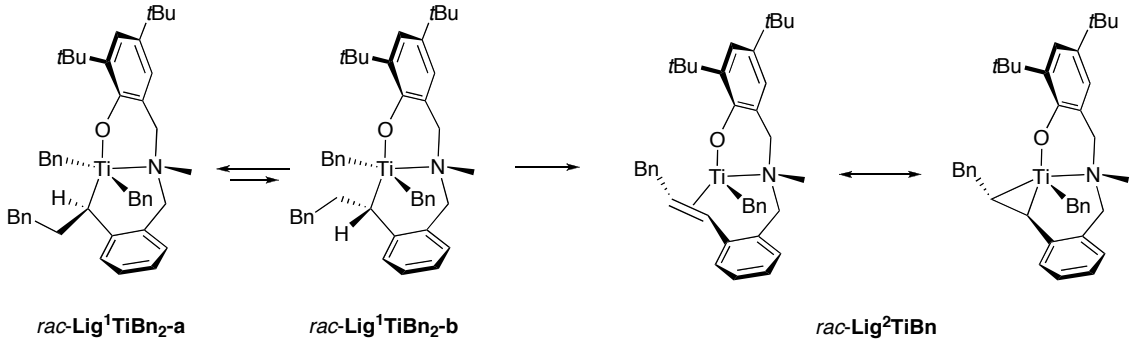

Scheme 3.4. Formation of *rac*-**Lig^{2}TiBn**.

insertion of the pendant vinyl moiety in a 2,1-fashion. The ^{1}H NMR spectrum showed complete disappearance of vinyl resonances and the selective formation of one major diastereomer (*rac*-**Lig^{1}Hf-b**, Figure 3.2). Heating the C_6D_6 solution at 60 °C for one hour led to a 55:45 ratio of a mixture of diastereomers (*rac*-**Lig^{1}HfBn$_2$-a,b**). Prolonged reaction at 25 °C (10-11 days) resulted in the same ratio of diastereomers, which suggests that an equilibrium exists for the mixture of diastereomers in solution with possible interconversion proceeding through β-hydride elimination and reinsertion of the opposite face of the newly formed alkene (Scheme 3.5). The reaction of **Lig^1** with $ZrBn_4$ in toluene-d_8 at 25 °C resulted in the immediate formation of a diastereomeric mixture (58:42 ratio) of *rac*-**Lig^{1}ZrBn$_2$-a,b** as monitored by ^{1}H NMR spectroscopy. It is reasonable to suggest that rapid interconversion of the diastereomers occurs in solution at 25 °C, which is in complete contrast to that observed with the hafnium complex.

Broad peaks for many of the methylene resonances appear in the room-temperature ^{1}H NMR spectrum in toluene-d_8 for both complexes making assignment difficult, but upon cooling to -10 °C, some of the methylene resonances can be resolved as doublets. In the ^{1}H NMR spectrum of *rac*-

Lig^{1}HfBn$_2$-a,b, resonances for the *meta*-H's on the phenolate ring in between the Ar-CH_3 and Ar-CH_2N substituents appear as two isolated singles at 6.37 (major) and 6.22 (minor) ppm. These diagnostic resonances are consistent with the formation of *rac*-**Lig^{1}HfBn$_2$-a,b** as a mixture of diastereomers. In the ^{1}H NMR spectrum of *rac*-**Lig^{1}ZrBn$_2$-a,b**, the distinguishing resonances consistent with the formation of a mixture of diastereomers are the methylene H's on the *N*-CH_2 substituent attached to the lower phenyl ring system, which appear as two isolated doublets at 3.58 (major) and 3.50 (minor) ppm. The ^{13}C{^{1}H} NMR spectrum of both complexes reveal 74 resonances, 37 corresponding to each

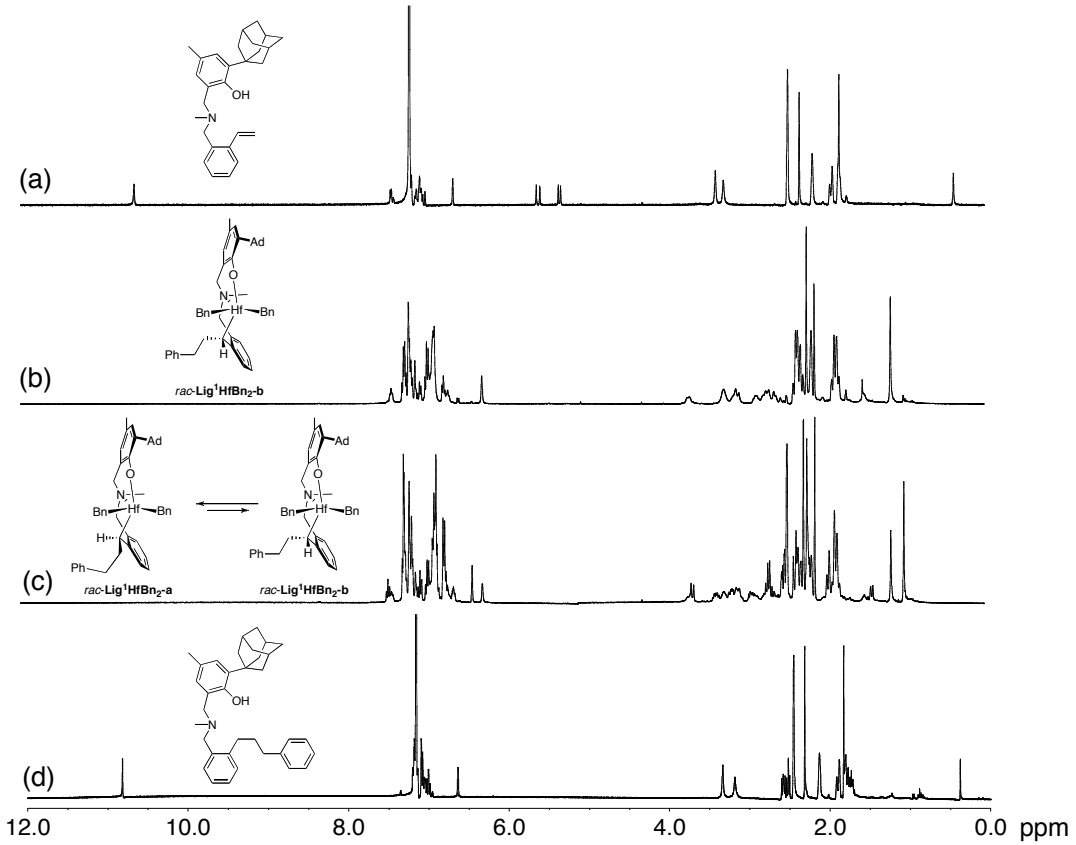

Figure 3.2. ^{1}H NMR Spectra (C_6D_6, 400 MHz) of (a) 2-(1-adamantyl)-4-methyl-6-((methyl(2-vinylbenzyl)amino)methyl)phenol; (b) *rac*-**Lig^{1}HfBn$_2$-b**; (c) *rac*-**Lig^{1}HfBn$_2$-a,b**; (d) ligand residues from methanolysis of *rac*-**Lig^{1}HfBn$_2$-a,b**.

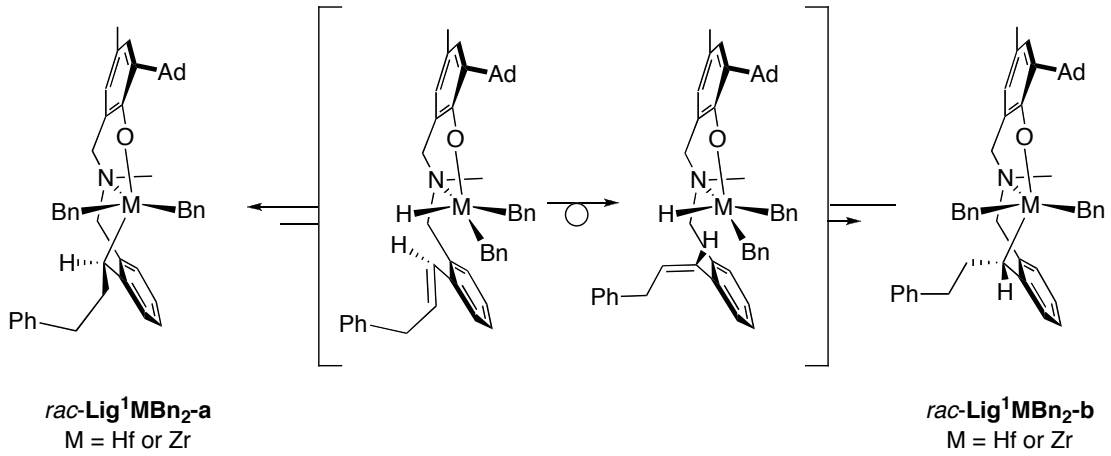

Scheme 3.5. Interconversion of diastereomers *rac*-**Lig^{1}MBn$_2$-a,b**.

diastereomer. The resonances for each carbon of *rac*-**Lig^{1}HfBn$_2$-a,b** and *rac*-**Lig^{1}ZrBn$_2$-a,b** were fully assigned with the aid of COSY, ^{1}H-^{13}C HMBC, ^{1}H-^{13}C HSQC, and ROESY NMR experiments. In the ROESY NMR spectra at -10 °C, both *rac*-**Lig^{1}HfBn$_2$-b** and *rac*-**Lig^{1}ZrBn$_2$-b** exhibit exchange peaks with a third confomer, which could potentially arise from a ring-flip of the six-membered metallacycle giving a possibility of four total conformers (Scheme 3.6).[17,23] No such exchange was observed for *rac*-**Lig^{1}HfBn$_2$-a** and *rac*-**Lig^{1}ZrBn$_2$-a** at this temperature. Furthermore, the third confomer is undetectable in the ^{1}H NMR spectra. Methanolysis of either diastereomeric mixture afforded a phenoxyamine with a 3-phenylpropyl group bound to the carbon atom at the 2-position (Figure 3.2) of the benzyl moiety consistent with intramolecular 2,1-insertion of the ligand-appended alkene into the M-C_{Alkyl} (M = Hf, Zr) bond for the neutral benzyl compound.

Single crystals of *rac*-**Lig^{1}HfBn$_2$-a** suitable for structural determination *via* X-ray crystallography were grown from slow diffusion of pentane into a saturated toluene solution over several weeks at -30 °C to afford a colorless

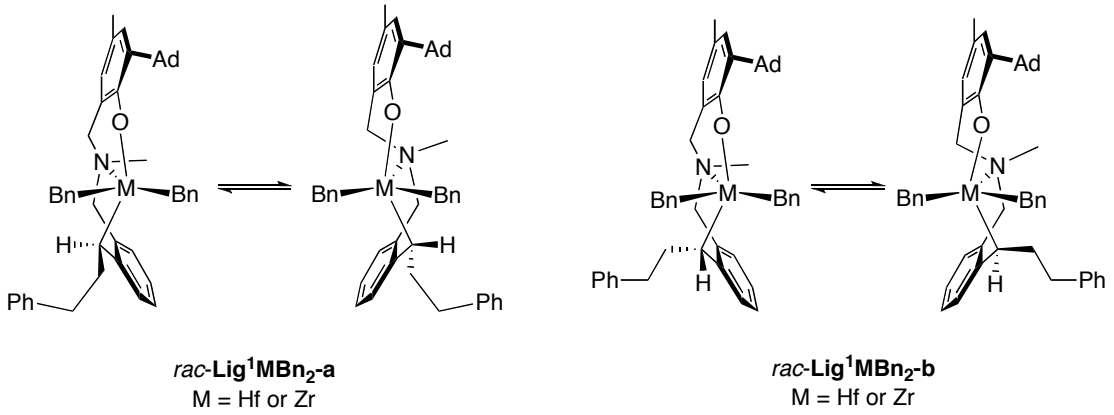

Scheme 3.6. Interconversion of confomers *rac*-**Lig^{1}MBn$_2$-a,b** via ring-flip of six-membered metallacycle.

crystalline solid. The solid state molecular structure of *rac*-**Lig^{1}HfBn$_2$-a** (Figure 3.3) revealed that the coordination geometry about hafnium is best described as distorted trigonal bipyramidal with C(41) and O(1) occupying the axial positions (∠O(1)-Hf(1)-C(41) = 159.54(7)°). Crystals of *rac*-Lig^{1}Zr-**a** suitable for X-ray diffraction were grown from a saturated pentane solution over several weeks at 25 °C to provide a thermally sensitive orange crystalline solid. The solid state molecular structure of *rac*-**Lig^{1}ZrBn$_2$-a** (Figure 3.3) was nearly isostructural to *rac*-**Lig^{1}HfBn$_2$-a** and revealed a coordination geometry around zirconium best described as distorted trigonal bipyramidal with C(8) and O(1) occupying the axial positions (∠O(1)-Zr(1)-C(8) = 158.22(13)°). Inspection of the extended unit cell of both complexes revealed the presence of only one diastereomer.

3.2.2 Synthesis of *rac*-Lig^{2}TiBn

Having shown that **1** reacts with $HfBn_4$ and $ZrBn_4$ to furnish complexes arising from the intramolecular 2,1-insertion of the pendant vinyl moiety in

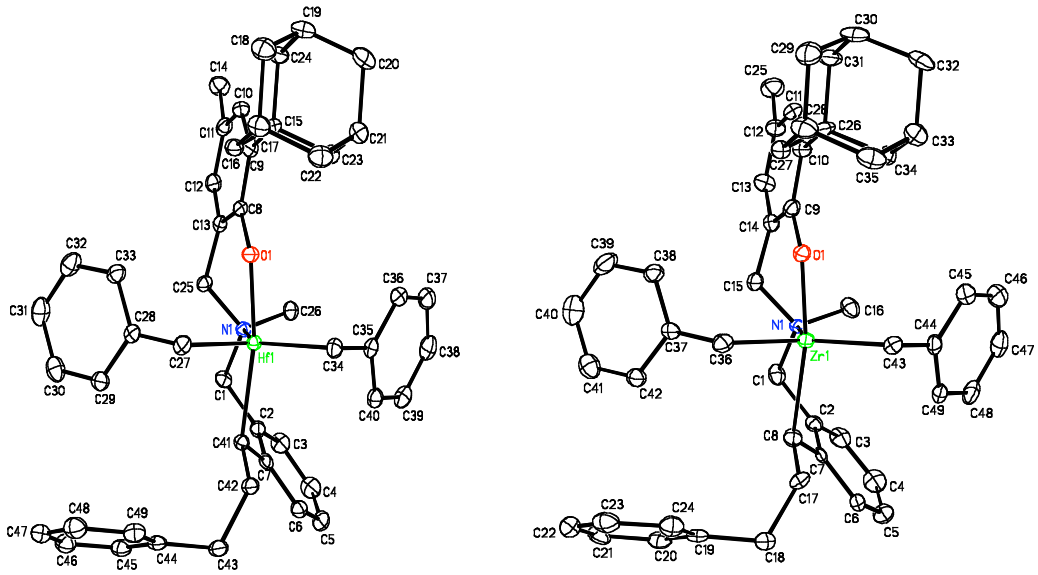

rac-**Lig^{1}HfBn$_2$-a** *rac*-**Lig^{1}ZrBn$_2$-a**

Figure 3.3. ORTEP diagram of *rac*-**Lig^{1}HfBn$_2$-a** and *rac*-**Lig^{1}ZrBn$_2$-a**. Thermal ellipsoids are drawn at the 40% probability level.

the ligand framework, we proceeded to investigate the reaction with $TiBn_4$. However, suitable crystals for X-ray diffraction could not be obtained from the reaction of **1** with $TiBn_4$ so we proceeded to investigate the reaction of a similar phenoxyamine ligand, **2**, with $TiBn_4$. Monitoring the reaction of **2** with $TiBn_4$ in C_6D_6 at 25 °C by ^1H NMR spectroscopy initially showed a tribenzylphenoxyaminetitanium complex and one equivalent of toluene from phenol deprotonation. Over the next 3 hours, slow insertion of the pendant vinyl moiety resulted in a mixture of diastereomers, similar to the hafnium and zirconium complexes. Continued reaction at 25 °C over 2 additional days resulted in liberation of a second equivalent of toluene, which gave rise to a phenoxyaminetitanium alkene complex (*rac*-**Lig^{2}TiBn**) as a racemic mixture of only one diastereomer as evidenced from the presence of only one *N*-methyl

resonance and two *tert*-butyl resonances in the ^{1}H NMR spectrum. The ^{13}C{^{1}H} NMR spectrum revealed 31 resonances, which is also consistent with the formation of *rac*-**Lig^{2}TiBn** as a racemic mixture of a single diastereomer. The resonances for each carbon were fully assigned with the aid of COSY, ^{1}H-^{13}C HMBC, and ^{1}H-^{13}C HSQC NMR experiments. It is possible that toluene elimination can only occur from one of the six-membered metallacycles, which may explain the formation of only one diastereomer. Negishi and co-workers have proposed that $Cp_2Zr(n\text{-Bu})_2$ will undergo β-hydride elimination with loss of butene to give $Cp_2Zr(H)(n\text{-Bu})$, which reductively eliminates butane to generate free Cp_2Zr.[24] A similar mechanism could be involved in the formation of *rac*-**Lig^{2}TiBn** as a titanium(II) alkene complex. Initial β-hydride elimination would generate a ligand-appended alkene that could coordinate to the titanium(IV) metal center followed by reductive elimination of toluene to generate *rac*-**Lig^{2}TiBn**. Interestingly, Buchwald and co-workers have reported that warming $Cp_2Zr(n\text{-Bu})_2$ in the presence of PMe_3 yields Cp_2Zr(1-butene)(PMe_3), which suggests that butane is eliminated from $Cp_2Zr(n\text{-Bu})_2$ before butene is lost.[25] Therefore, direct toluene loss to give *rac*-**Lig^{2}TiBn** as a titanium(II) alkene complex is also plausible. We are currently investigating the mechanism for this reaction.

Single crystals of *rac*-**Lig^{2}TiBn** as a black crystalline solid suitable for X-ray diffraction were grown from a saturated pentane solution over several weeks at -30 °C. The solid state molecular structure (Figure 3.4) revealed a distorted tetrahedral coordination geometry about titanium. From the short Ti(1)-C(25) and Ti(1)-C(26) distances (2.510(5) Å and 2.699(5) Å respectively) and significant bending of the phenyl ring towards the metal center (∠C(25)-C(24)-Ti(1) = 85.3(3)°), it is apparent that the benzyl substituent is bound in an

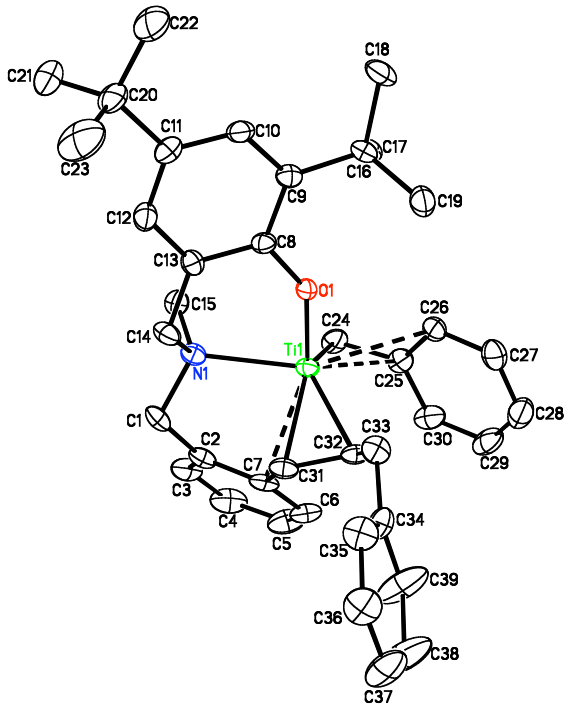

Figure 3.4. ORTEP diagram of *rac*-**Lig^{2}TiBn**. Thermal ellipsoids are drawn at the 40% probability level.

η^3-fashion. This binding mode has been observed for neutral electron-deficient zirconium complexes.[26] Furthermore, the short Ti(1)-C(7) distance (2.560(5) Å) and significant bending of the phenyl ring adjacent the titanium-bound alkene towards the metal center (∠C(7)-C(31)-Ti(1) = 89.3(3)°), suggests that there is η^3-coordination of this substituent as well. The pi-bonding of the benzyl sigma ligand in addition to the pi-bonding of the supported tridentate ligand is a result of the electron-deficient character of the titanium metal center. The short C(31)-C(32), Ti(1)-C(31), and Ti(1)-C(32) distances (1.436(7) Å, 2.118(4) Å, and 2.148(4) Å respectively) are similar to that reported for η^2-olefin complexes of titanium supported by aryloxide ligands[27,28] and bis(pentamethylcyclopentadienyl)(ethylene)titanium(II).[29,30] Notably, the

C(31)-C(32) bond distance shows significant lengthening from free alkene which is indicative of substantial electron back-donation from the titanium metal center.[31,32] Based on comparisons with other structural data, *rac*-**Lig^{2}TiBn** appears to be intermediate along the continuum between the titanium(II) alkene adduct and a titanium(IV) metallacyclopropane.[27-29,31,32]

3.2.3 Reaction of *rac*-Lig^{2}TiBn with Ethylene

While, as expected, *rac*-**Lig^{2}TiBn** proved to be unreactive towards olefin polymerization upon benzyl abstraction, titanacyclopropanes have been shown to be versatile reagents for many fundamental organic and organometallic transformations.[27-30,33-35] Bercaw and co-workers have shown that treatment of bis(pentamethylcyclopentadienyl)(ethylene)titanium(II) with ethylene results in an equilibrium mixture containing the newly formed Cp^*_2Ti metallacyclopentane complex, however, it was not sufficiently stable to allow isolation.[29] Treatment of a black solution of *rac*-**Lig^{2}TiBn** with one atmosphere of ethylene in C_6D_6 at 25 °C resulted in an immediate color change to dark red. The ^{1}H NMR spectrum indicated quantitative conversion of *rac*-**Lig^{2}TiBn** to a titanacyclopentane complex, *rac*-**Lig^2(CH$_2$)$_2$TiBn**. Prolonged exposure to ethylene yields trace amounts of polyethylene, but no change in the resonances of *rac*-**Lig^2(CH$_2$)$_2$TiBn**, which suggests a trace impurity is responsible. A large scale reaction was carried out to isolate *rac*-**Lig^2(CH$_2$)$_2$TiBn** as a stable, dark red solid. Single crystals suitable for structural analysis by X-ray diffraction could not be obtained for *rac*-**Lig^2(CH$_2$)$_2$TiBn** due to its high degree of solubility, even in non-polar solvents. However, characterization of *rac*-**Lig^2(CH$_2$)$_2$TiBn** by ^{1}H, ^{13}C{^{1}H}, COSY, ^{1}H-^{13}C HMBC, ^{1}H-^{13}C HSQC, and ROESY NMR spectroscopy allowed three

dimensional structural determination of the product in solution, which, on the basis of the solid state molecular structure of *rac*-**Lig^{2}TiBn**, is consistent with pericyclic migratory insertion of ethylene and formation of the product as a racemic mixture of only one diastereomer (Scheme 3.7). The resonances for the methine and methylene carbons attached to the titanium in the metallacyclopentane ring appear at 102.48 and 95.56 ppm in the $^{13}C\{^1H\}$ NMR spectrum, which is consistent with Ti-C chemical shifts observed in titanacyclopentane compounds supported by aryloxide ligands.[36] The remaining methine and methylene carbon resonances in the titanacyclopentane ring appear at 46.80 and 39.93 ppm in the $^{13}C\{^1H\}$ NMR spectrum. In the ROESY NMR spectrum, no exchange peaks are observed for the methylene protons resulting from the pericyclic migratory insertion of ethylene at temperatures up to 50 °C. Taken together, this supports the view of *rac*-**Lig^2(CH$_2$)$_2$TiBn** as a titanium(IV) metallacyclopentane complex and not a titanium(II) bis-alkene complex.

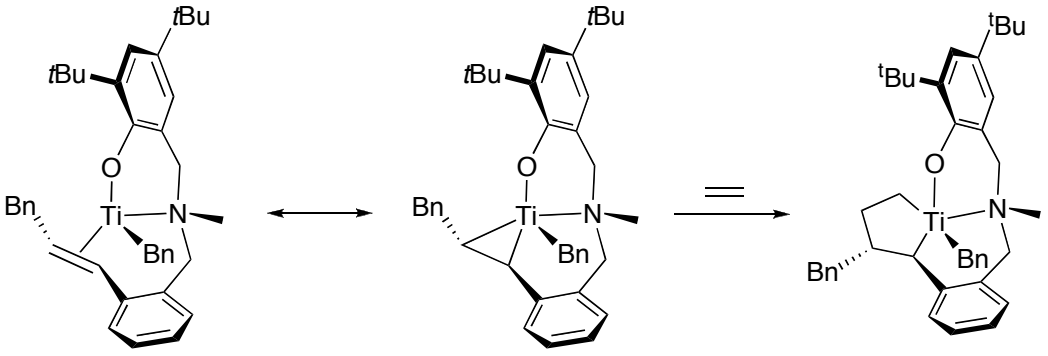

Scheme 3.7. Reaction of *rac*-**Lig^{2}TiBn** with ethylene.

3.2.4 1-Hexene Polymerization Behavior

We proceeded to investigate 1-hexene polymerization behavior of the catalysts derived from *rac*-**Lig^{1}HfBn$_2$-a,b** and *rac*-**Lig^{1}ZrBn$_2$-a,b** (Table 3.1). Addition of *rac*-**Lig^{1}HfBn$_2$-a,b** to a solution of $[Ph_3C][B(C_6F_5)_4]$ and 1-hexene (1:1:1600) in toluene at 25 °C led to the formation of 1.22 g of poly(1-hexene) (91% conversion) in 10 minutes. The polymer possessed a molecular weight (M_n) of 178 kg/mol and a relatively narrow molecular weight distribution (M_w/M_n = 1.48). Similar molecular weights and molecular weight distributions were obtained upon activation with $B(C_6F_5)_3$ and $[PhNMe_2H][B(C_6F_5)_4]$ at 25 °C, albeit with lower activity. Upon noticing the molecular weight distribution of the poly(1-hexene) prepared using *rac*-**Lig^{1}HfBn$_2$-a,b**/$B(C_6F_5)_3$ was quite narrow (M_w/M_n = 1.31), we proceeded to investigate the polymerization behavior of this catalyst at lower reaction temperatures. Activation of *rac*-**Lig^{1}HfBn$_2$-a,b** with $B(C_6F_5)_3$ at 0 °C in toluene resulted in the formation of 0.45 g of poly(1-hexene) (33% conversion) in 30 minutes. The obtained polymer had an M_n of 238 kg/mol and an extremely narrow molecular weight distribution (M_w/M_n = 1.08), which suggests the polymerization is living under these reaction conditions. A linear increase in molecular weight versus poly(1-hexene) yield at 0 °C further illustrated the living behavior of *rac*-**Lig^{1}HfBn$_2$-a,b**/$B(C_6F_5)_3$ (Figure 3.5). In all cases, the obtained molecular weights were five times higher than that predicted based on the assumption of one chain per metal center (M_n^{theo}), which indicates that approximately 20% of the metal centers are active in the polymerization. We are currently investigating the cause of this apparent disparity. Analysis of the poly(1-hexene) microstructure by $^{13}C\{^1H\}$ NMR spectroscopy revealed that the polymer was regioregular and highly isotactic; the spectrum showed no

signals corresponding to stereoerrors (Figure 3.6). The high degree of stereoselectivity observed for this catalyst is likely due to the chiral structure of *rac*-**Lig^{1}HfBn$_2$-a,b**. Therefore, *rac*-**Lig^{1}HfBn$_2$-a,b**/$B(C_6F_5)_3$ represents a new, highly isoselective catalyst for living 1-hexene polymerization.[16,19,37-44] Interestingly, we carried out a polymerization with *rac*-**Lig^{1}HfBn$_2$-b**, which is cleanly synthesized upon initial metalation of **Lig^1** with $HfBn_4$ (see Figure 3.2), and obtained nearly identical polymerization results upon activation with $B(C_6F_5)_3$ at 0 °C as was obtained with *rac*-**Lig^{1}HfBn$_2$-a,b**/$B(C_6F_5)_3$. This suggests that upon activation of the diastereomeric mixture of *rac*-**Lig^{1}HfBn$_2$-a,b** a similar active species is generated for each separate diastereomer. We are currently investigating this unusual behavior.

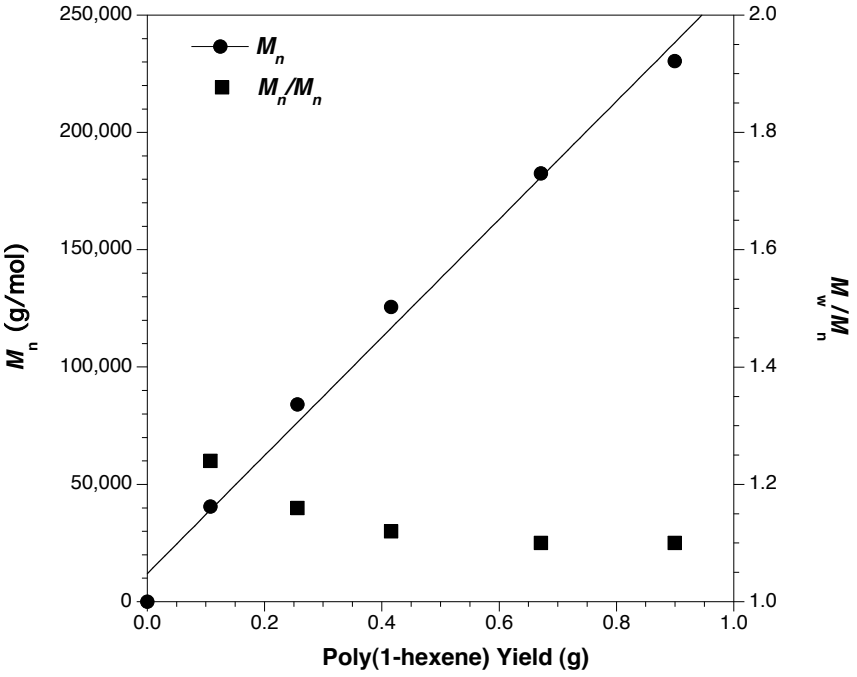

Figure 3.5. Plot of M_n (●) and M_w/M_n (■) versus polymer yield for 1-hexene polymerization at 0 °C catalyzed by *rac*-**Lig^{1}HfBn$_2$-a,b**/$B(C_6F_5)_3$. M_n and M_w/M_n values were determined by gel permeation chromatography in 1,2,4-$C_6H_3Cl_3$ at 140 °C (polystyrene standards).

Table 3.1. 1-Hexene polymerization data for *rac*-**Lig^{1}HfBn$_2$-a,b** and *rac*-**Lig^{1}ZrBn$_2$-a,b**.[a]

Cplx	Activator	Temp (°C)	Time (min)	Yield (g)	Conv (%)	TOF (h^{-1})[b]	M_n (kg/mol)[c]	M_n^{theo} (kg/mol)[c]	M_w/M_n[c]
rac-**Lig^{1}HfBn$_2$-a,b**	$B(C_6F_5)_3$	25	10	0.30	23	2,200	180	30	1.31
rac-**Lig^{1}HfBn$_2$-a,b**	$[Ph_3C][B(C_6F_5)_4]$	25	10	1.22	91	8,700	178	122	1.48
rac-**Lig^{1}HfBn$_2$-a,b**	$[PhNMe_2H][B(C_6F_5)_4]$	25	10	0.89	66	6,300	218	89	1.44
rac-**Lig^{1}HfBn$_2$-a,b**	$B(C_6F_5)_3$	0	30	0.45	34	1,100	238	45	1.08
rac-**Lig^{1}ZrBn$_2$-a,b**	$B(C_6F_5)_3$	25	10	0.13	10	930	79	13	1.75
rac-**Lig^{1}ZrBn$_2$-a,b**	$[Ph_3C][B(C_6F_5)_4]$	25	10	0.47	35	3,300	67	47	1.91
rac-**Lig^{1}ZrBn$_2$-a,b**	$[PhNMe_2H][B(C_6F_5)_4]$	25	10	0.28	21	2,000	66	28	1.88
rac-**Lig^{1}ZrBn$_2$-a,b**[d]	$B(C_6F_5)_3$	0	30	0.93	46	1,100	105	46	1.63

[a] General conditions: Cplx = 10 mmol, [Cplx]/[B] = 1.0, 10 mL toluene, 2.0 mL 1–hexene. [b] Average turnover frequency (TOF): mol 1-hexene/(mol Cplx·h). [c] Determined using gel permeation chromatography in 1,2,4-$C_6H_3Cl_3$ at 140 °C versus polystyrene standards. [d] Cplx = 20 mmol, [Cplx]/[B] = 1.0, 3.0 mL toluene, 3.0 mL 1–hexene.

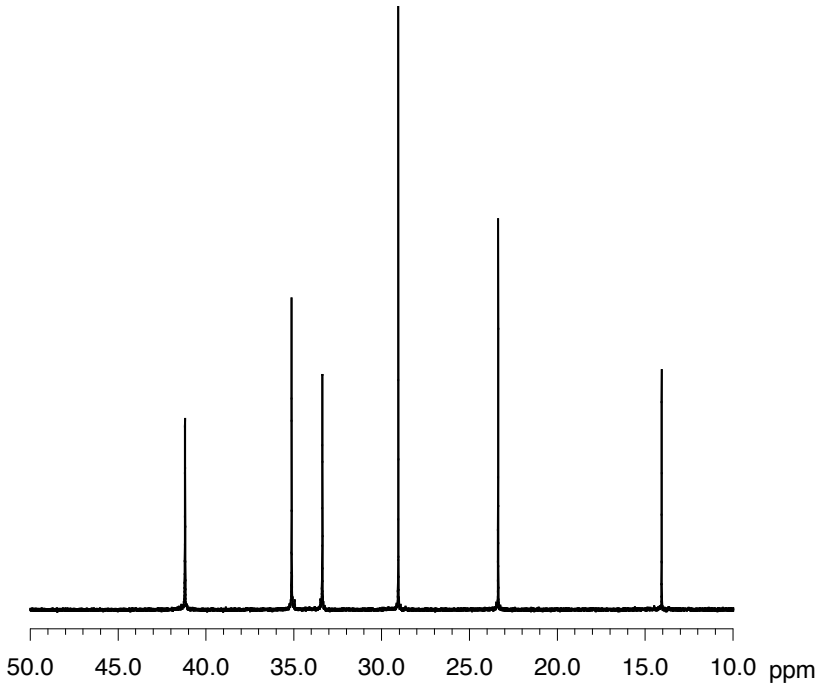

Figure 3.6. $^{13}C\{^{1}H\}$ NMR spectrum of poly(1-hexene) furnished from *rac*-**Lig^{1}HfBn$_2$-a,b**/$B(C_6F_5)_3$ at 0 °C (150 MHz, 1,1,2,2-$C_2D_2Cl_4$, 135 °C).

We moved on to investigate the 1-hexene polymerization behavior of *rac*-**Lig^{1}ZrBn$_2$-a,b**. Activating *rac*-**Lig^{1}ZrBn$_2$-a,b** with $[Ph_3C][B(C_6F_5)_4]$ in the presence of 1-hexene (1:1:1600) and toluene at 25 °C led to the formation of 0.47 g of poly(1-hexene) (35% conversion) in 10 minutes. The polymer (M_n = 67 kg/mol) exhibited a narrow molecular weight distribution (M_w/M_n = 1.91) indicative of a single-site polymerization catalyst. Activation with $B(C_6F_5)_3$ and $[PhNMe_2H][B(C_6F_5)_4]$ at 25 °C gave rise to poly(1-hexene)s with similar molecular weights and molecular weight distributions, but lower activity was observed. None of the molecular weight distributions were sufficiently narrow to indicate any potential living behavior, but we pressed on to screen *rac*-**Lig^{1}ZrBn$_2$-a,b** under the same conditions that gave living behavior for *rac*-

Lig^{1}HfBn$_2$-a,b. Interestingly, activation of *rac*-**Lig^{1}ZrBn$_2$-a,b** with $B(C_6F_5)_3$ at 0 °C in toluene (1-hexene:toluene = 1:5 V/V) led only to a trace of polymer in 90 minutes. However, increasing the concentration (1-hexene:toluene = 1:1 V/V) gave rise to the formation of 0.93 g of poly(1-hexene) (46% conversion) in 30 minutes. The polymer displayed an M_n of 105 kg/mol but the molecular weight distribution (M_w/M_n = 1.63) was too broad to indicate a living polymerization catalyst. Analysis of the poly(1-hexene) microstructure via $^{13}C\{^1H\}$ NMR spectroscopy revealed that the polymer was also regioregular and highly isotactic (see Appendix). In stark contrast to the polymerization behavior of *rac*-**Lig^{1}HfBn$_2$-a,b**/$B(C_6F_5)_3$ at 0 °C, the zirconium congener (*rac*-**Lig^{1}ZrBn$_2$-a,b**) displayed no characteristics of living 1-hexene polymerization behavior.

3.2.5 Propylene Polymerization Behavior

Having evaluated the 1-hexene polymerization behavior of *rac*-**Lig^{1}HfBn$_2$-a,b** and *rac*-**Lig^{1}ZrBn$_2$-a,b**, we proceeded to investigate the propylene polymerization behavior at 25 °C (Table 3.2). Activation of *rac*-**Lig^{1}HfBn$_2$-a,b** with $[Ph_3C][B(C_6F_5)_4]$ at 25 °C furnished polypropylene (PP) with an average turnover frequency (TOF) of 9,700 h^{-1} and the polymer possessed an M_n of 106 kg/mol (M_w/M_n = 1.88). Analysis of the PP microstructure by $^{13}C\{^1H\}$ NMR spectroscopy revealed that it was isotactic ($[m^4]$ = 78%) and regioregular with stereoerrors indicating an enantiomorphic site-control enchainment mechanism (*mmmr*:*mmrr*:*mrrm* pentads = 2:2:1, see Appendix). Similar molecular weights and molecular weight distributions were obtained upon activation with $B(C_6F_5)_3$ and $[PhNMe_2H][B(C_6F_5)_4]$ at 25 °C, with activity trends mirroring those observed for 1-hexene polymerization.

Table 3.2. Propylene polymerization data for *rac*-**Lig^{1}HfBn$_2$-a**,**b** and *rac*-**Lig^{1}ZrBn$_2$-a**,**b** at 25 °C.[a]

Cplx	Activator	Time (min)	Yield (g)	TOF (h^{-1})[b]	M_n (kg/mol)[c]	M_n^{theo} (kg/mol)[c]	M_w/M_n[c]	$[m^4]$[d]	T_g (°C)[e]	T_m (°C)[e]
rac-**Lig^{1}HfBn$_2$-a,b**	$[Ph_3C][B(C_6F_5)_4]$	10	0.68	9,700	106	68	1.88	0.78	-5.1	119.9
rac-**Lig^{1}HfBn$_2$-a,b**	$[PhNMe_2H][B(C_6F_5)_4]$	10	0.46	6,600	115	46	1.82	0.77	-3.8	121.9
rac-**Lig^{1}HfBn$_2$-a,b**	$B(C_6F_5)_3$	10	0.27	3,800	96	27	1.37	0.78	-6.1	124.1
rac-**Lig^{1}ZrBn$_2$-a,b**	$[Ph_3C][B(C_6F_5)_4]$	10	1.84	26,000	174	184	2.08	0.69	-7.1	102.0
rac-**Lig^{1}ZrBn$_2$-a,b**	$[PhNMe_2H][B(C_6F_5)_4]$	10	1.61	23,000	200	161	2.00	0.73	-8.2	102.4
rac-**Lig^{1}ZrBn$_2$-a,b**	$B(C_6F_5)_3$	10	0.84	12,000	241	84	1.99	0.74	-7.1	108.1

[a] General conditions: 10 μmol of the complex in toluene (5 mL) was added to a propylene-saturated solution of activator (25 mL of toluene; [Cplx]/[B] = 1.0) at 25 °C. [b] Average turnover frequency (TOF): mol propylene/(mol Cplx·h). [c] Determined using gel permeation chromatography in 1,2,4-$C_6H_3Cl_3$ at 140 °C versus polyethylene standards. [d] Determined by integration of the methyl region of the $^{13}C\{^1H\}$ NMR spectrum. [e] Determined using differential scanning calorimetry (second heating).

Table 3.3. Propylene polymerization data for *rac*-**Lig^{1}HfBn$_2$-a,b** and *rac*-**Lig^{1}ZrBn$_2$-a,b** at 0 °C.[a]

Cplx	Activator	Time (min)	Yield (g)	TOF (h^{-1})[b]	M_n (kg/mol)[c]	M_n^{theo} (kg/mol)[c]	M_w/M_n[c]	[m^4][d]	T_g (°C)[e]	T_m (°C)[e]
rac-**Lig^{1}HfBn$_2$-a,b**	$[Ph_3C][B(C_6F_5)_4]$	5	1.24	35,400	238	124	1.72	0.83	-3.7	130.5
rac-**Lig^{1}HfBn$_2$-a,b**[f]	$[PhNMe_2H][B(C_6F_5)_4]$	10	0.58	4,200	89	29	2.82	0.84	-4.6	134.1
rac-**Lig^{1}HfBn$_2$-a,b**[f]	$B(C_6F_5)_3$	10	0.44	3,200	95	22	1.48	0.84	-1.1	129.2
rac-**Lig^{1}ZrBn$_2$-a,b**	$[Ph_3C][B(C_6F_5)_4]$	2	2.56	183,000	396	256	2.14	0.77	-5.6	108.3
rac-**Lig^{1}ZrBn$_2$-a,b**	$[PhNMe_2H][B(C_6F_5)_4]$	5	2.04	58,000	478	204	2.32	0.75	-5.6	110.9
rac-**Lig^{1}ZrBn$_2$-a,b**[g]	$B(C_6F_5)_3$	20	2.22	5,300	217	74	1.17	0.76	-6.9	115.3

[a] General conditions: 10 μmol of the complex in toluene (5 mL) was added to a propylene-saturated solution of activator (25 mL of toluene; [Cplx]/[B] = 1.0) at 25 °C. [b] Average turnover frequency (TOF): mol propylene/(mol Cplx·h). [c] Determined using gel permeation chromatography in 1,2,4-$C_6H_3Cl_3$ at 140 °C versus polyethylene standards. [d] Determined by integration of the methyl region of the $^{13}C\{^1H\}$ NMR spectrum. [e] Determined using differential scanning calorimetry (second heating). [f] 20 μmol of the complex ([Cplx]/[B] = 1.0). [g] 30 μmol of the complex ([Cplx]/[B] = 1.0).

In light of the living behavior observed for 1-hexene polymerization at 0 °C, we investigated the propylene polymerization behavior of *rac*-**Lig^{1}HfBn$_2$-a,b** at 0 °C (Table 3.3). Activation of *rac*-**Lig^{1}HfBn$_2$-a,b** with $[Ph_3C][B(C_6F_5)_4]$ at 0 °C in the presence of propylene furnished isotactic polypropylene with a TOF of 35,400 h^{-1}. The higher activity can be attributed to the higher propylene concentration when the polymerization is conducted at 0 °C. The obtained polymer had an M_n of 238 kg/mol and M_w/M_n of 1.72 with an [m^4] = 83%. Interestingly, activation with $[PhNMe_2H][B(C_6F_5)_4]$ or $B(C_6F_5)_3$ at 0 °C resulted in much less active catalysts (TOF = 4,200 and 3,200 h^{-1} respectively) and gave iPP of much lower molecular weight (M_n = 89 and 95 kg/mol respectively). Furthermore, living behavior was not observed under any activation condition, which contrasts the living behavior observed for 1-hexene polymerization with *rac*-**Lig^{1}HfBn$_2$-a,b**/$B(C_6F_5)_3$ at 0 °C.

Investigation of propylene polymerization behavior with *rac*-**Lig^{1}ZrBn$_2$-a,b**/$[Ph_3C][B(C_6F_5)]$ at 25 °C resulted in a catalyst with a TOF of 26,000 h^{-1} and yielded isotactic polypropylene exhibiting an M_n of 174 kg/mol and M_w/M_n = 2.08. The iPP ([m^4] = 72%) was regioregular with stereoerrors indicating an enantiomorphic site-control enchainment mechanism. Activation with $B(C_6F_5)_3$ and $[PhNMe_2H][B(C_6F_5)_4]$ at 25 °C resulted in similar molecular weights and molecular weight distributions with activity trends reflecting those previously established. The effect of reaction temperature was investigated to find conditions for living propylene polymerization (Table 3.3). Activation of *rac*-**Lig^{1}ZrBn$_2$-a,b** with $[Ph_3C][B(C_6F_5)_4]$ at 0 °C in the presence of propylene provided a catalyst with a TOF of 183,000 h^{-1}. As before, the higher TOF at 0 °C can be attributed to the higher propylene concentration from condensed propylene in solution. Furthermore, it is unlikely that the polymerization

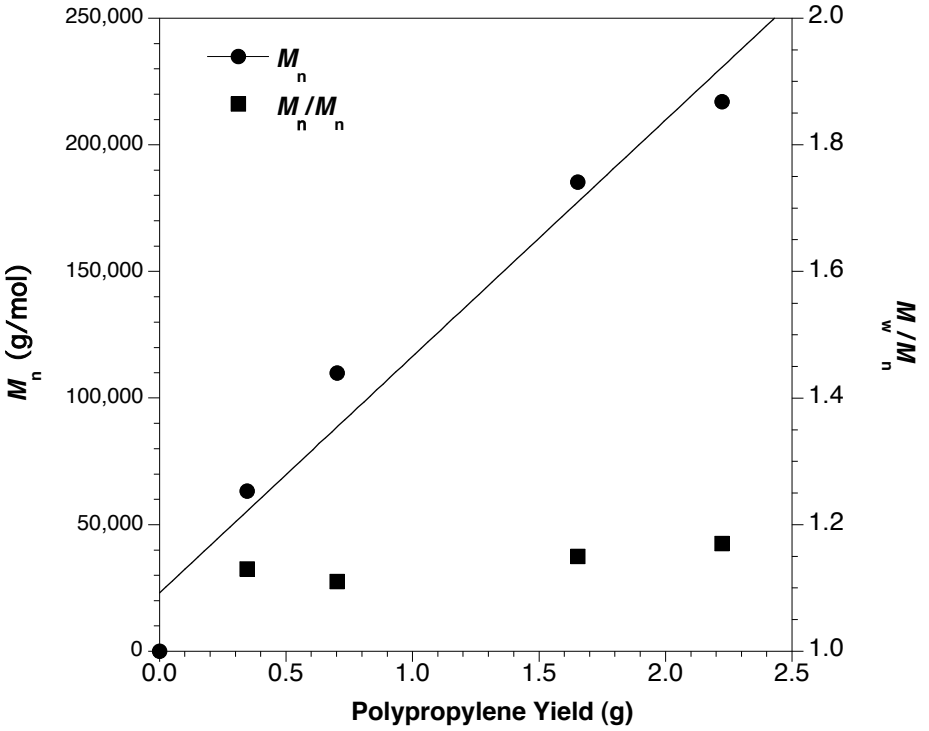

Figure 3.7. Plot of M_n (●) and M_w/M_n (■) versus polymer yield for propylene polymerization at 0 °C catalyzed by *rac*-**Lig^{1}ZrBn$_2$-a,b**/B(C_6F_5)$_3$. M_n and M_w/M_n values were determined by gel permeation chromatography in 1,2,4-$C_6H_3Cl_3$ at 140 °C (polyethylene standards).

temperature was maintained at 0 °C due to the extremely high activity of the catalyst. The polymer obtained had an M_n of 396 kg/mol and M_w/M_n = 2.14 with an [m^4] = 77%. Activation of *rac*-**Lig^{1}ZrBn$_2$-a,b** with [PhNMe$_2$H][B(C_6F_5)$_4$] at 0 °C afforded a very active catalyst (TOF = 58,300 h^{-1}) and the iPP obtained had an extremely high molecular weight (M_n = 478 kg/mol). However, the molecular weight distribution was broadened (M_w/M_n = 2.32) indicative of a non-living polymerization system. Interestingly, activation of *rac*-**Lig^{1}ZrBn$_2$-a,b** with B(C_6F_5)$_3$ at 0 °C gave a catalyst (TOF = 5,300 h^{-1}) that furnished iPP ([m^4] = 76%) with high molecular weight (M_n = 217 kg/mol) and a very narrow molecular weight distribution (M_w/M_n = 1.17), which indicates possible living behavior. To further demonstrate the living behavior of *rac*-

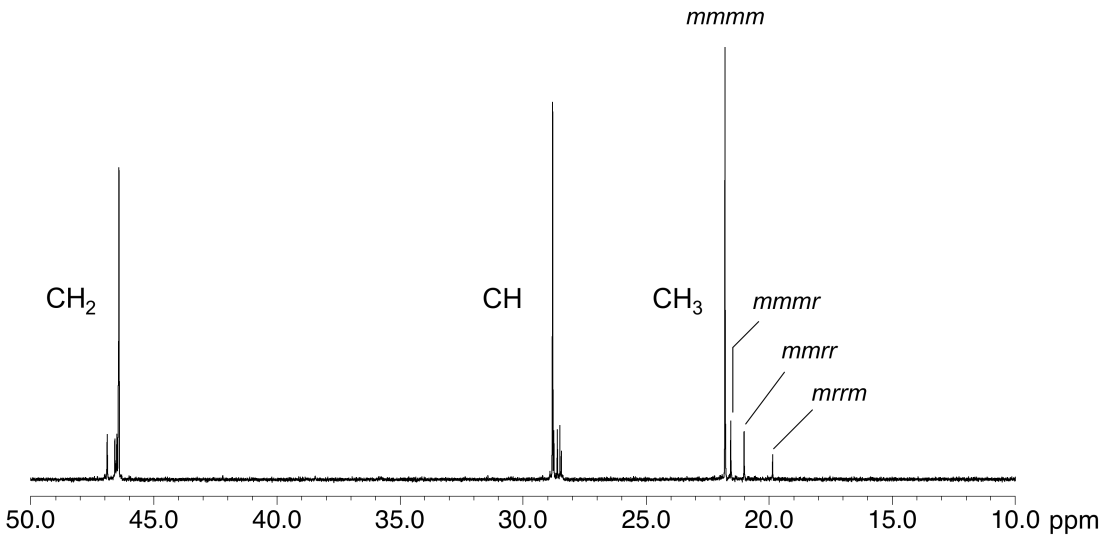

Figure 3.8. $^{13}C\{^1H\}$ NMR spectrum of iPP produced by *rac*-**Lig^{1}ZrBn$_2$-a,b**/$B(C_6F_5)_3$ at 0 °C (150 MHz, 1,1,2,2-$C_2D_2Cl_4$, 135 °C).

Lig^{1}ZrBn$_2$-a,b/$B(C_6F_5)_3$ at 0 °C, a linear increase in molecular weight versus polypropylene yield was shown (Figure 3.7). However, as was the case for living 1-hexene polymerization with *rac*-**Lig^{1}HfBn$_2$-a,b**/$B(C_6F_5)_3$, the obtained molecular weights were in all cases approximately four times higher than M_n^{theo} indicating that roughly 25% of the zirconium metal centers are active in the polymerization. Monitoring the reaction of *rac*-**Lig^{1}ZrBn$_2$-a,b** with $B(C_6F_5)_3$ in the absence of propylene by ^{19}F NMR spectroscopy reveals the initial formation of six main resonances (3 for each diastereomer) that progressively becomes more complex. This may suggest that catalyst decomposition competes with activation. It is also unclear if both diastereomers are active in the polymerization. Analysis of the polypropylene microstructure via $^{13}C\{^1H\}$ NMR spectroscopy revealed an enantiomorphic site-control enchainment mechanism (*mmmr*:*mmrr*:*mrrm* pentads = 2:2:1, Figure 3.8). Hence, *rac*-**Lig^{1}ZrBn$_2$-a,b**/$B(C_6F_5)_3$ represents a new catalyst for living and isoselective

propylene polymerization adding to the growing number of olefin polymerization catalysts that are capable of this behavior.[8,11,12,16,17,45-49] It is interesting to note that in both 1-hexene and propylene polymerizations, living behavior was only observed using $B(C_6F_5)_3$ as a cocatalyst. The observed loss of living behavior when the less-coordinating $[B(C_6F_5)_4]^-$ anion is employed may be due to a dramatic increase in the rate of propagation relative to the rate of initiation for the polymerization.[50]

3.2.6 Block Copolymer from Propylene and Ethylene

Despite the fact that a living polymerization system is capable of producing only one polymer chain per metal center, the real advantage lies in the ability to synthesize well-defined block copolymers yielding a near limitless number of materials. Random copolymers or physical blends of homopolymers typically give materials whose properties are in between those of each respective individual polymer. However, the mechanical properties of block copolymers are often superior to those of each respective homopolymer. This is often attributed to the ability of the different segments of some block copolymers to microphase separate into discrete domains and give rise to new morphologies.[51,52] One of the most attractive block copolymer targets are those containing iPP domains due to its highly desirable mechanical properties. In addition, iPP represents the vast majority of industrially produced polypropylenes in use today,[53] hence incorporation of these segments into block copolymers remains a highly sought after goal. To this end, a growing number of catalysts systems have been reported in the literature that are capable of furnishing block copolymers incorporating iPP segments.[6-9,11,12,45-48,54]

Owing to the living behavior, high activity, and relatively high isoselectivity for propylene polymerization catalyzed by *rac*-**Lig^{1}ZrBn$_2$-a,b**/B(C_6F_5)$_3$, we determined that it would make an ideal candidate for the synthesis of a block copolymer incorporating an iPP segment (Scheme 3.8). Polymerization of propylene was initiated at 0 °C for 4 minutes to form an iPP block (M_n = 49.8 kg/mol, M_w/M_n = 1.17). An overpressure of ethylene was added and copolymerized with unreacted propylene in solution for 10 minutes to produce a poly(ethylene-*co*-propylene) block. After quenching, the resultant iPP-*block*-PEP diblock copolymer had an M_n = 122 kg/mol and M_w/M_n = 1.20 with an ethylene fraction (F_e) of 33 mol% (Figure 3.9). To further illustrate the formation of a diblock copolymer, a representative GPC profile is shown in Scheme 3.8 where an aliquot was removed from the polymerization mixture following the formation of the first block and the resultant polymers were analyzed by gel permeation chromatography. The diblock copolymer had a melting temperature (T_m) of 114 °C and a glass transition temperature (T_g) of -55.8 °C, which is consistent with the formation of a block copolymer incorporating iPP and PEP segments.

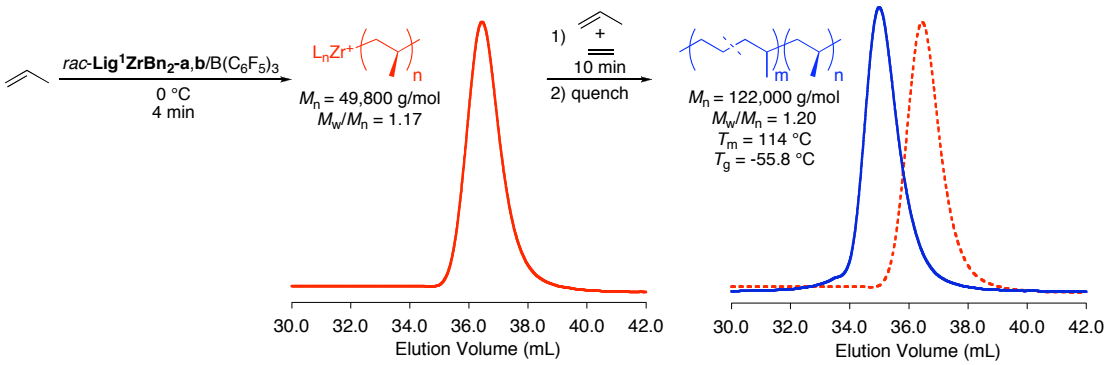

Scheme 3.8. Synthesis of iPP-*block*-PEP diblock copolymer.

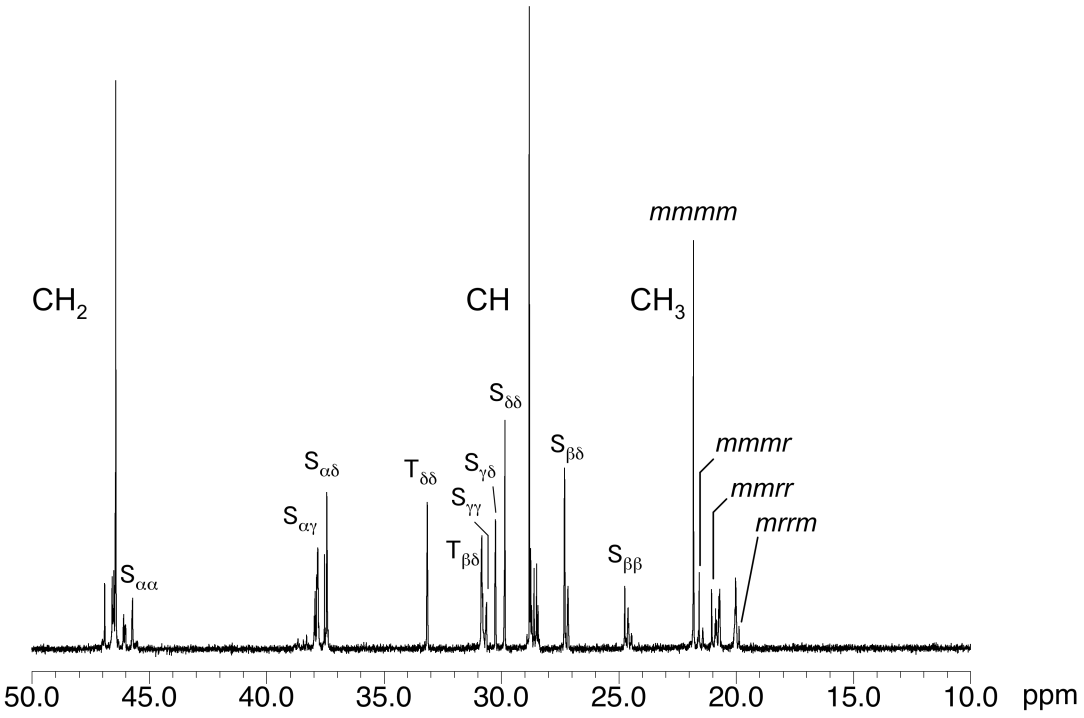

Figure 3.9. $^{13}C\{^1H\}$ NMR spectrum of iPP-*block*-PEP synthesized using *rac*-**Lig^{1}ZrBn$_2$-a,b**/$B(C_6F_5)_3$ at 0 °C (150 MHz, 1,1,2,2-$C_2D_2Cl_4$, 135 °C).

3.3 Conclusions

We set out to prepare new tridentate olefin polymerization catalysts supported by an sp^3-C donor through reaction and subsequent intramolecular 2,1-insertion of phenoxyamine vinyl-appended ligands with MBn_4 (M = Ti, Zr, Hf). Reaction of the ligand (**Lig^2**) with $TiBn_4$ gave a single diastereomer, *rac*-**Lig^{2}TiBn**, which can best be viewed as intermediate along the continuum between the titanium(II) alkene adduct and a titanium(IV) metallacyclopropane. While inactive for olefin polymerization, treatment of *rac*-**Lig^{2}TiBn** with ethylene results in pericyclic migratory insertion to afford a titanium metallacyclopentane complex as a racemic mixture of one diastereomer. Diastereomeric mixtures were obtained upon reaction of the

ligand (**Lig^1**) with $HfBn_4$ and $ZrBn_4$ yielding six-membered metallacycles *rac*-**Lig^{1}HfBn$_2$-a,b** and *rac*-**Lig^{1}ZrBn$_2$-a,b**, respectively, through migratory insertion of a benzyl group to the ligand-appended vinyl group on the neutral phenoxyamine metal tribenzyl precursors. Upon activation, these complexes formed highly active polymerization catalysts that isoselectively polymerized 1-hexene and propylene. Furthermore, *rac*-**Lig^{1}HfBn$_2$-a,b**/$B(C_6F_5)_3$ was living and isoselective for 1-hexene polymerization at 0 °C while living and isoselective propylene polymerization behavior was catalyzed by *rac*-**Lig^{1}ZrBn$_2$-a,b**/$B(C_6F_5)_3$ at 0 °C. Utilizing the living nature of this catalyst, an iPP-*block*-PEP diblock copolymer was synthesized via sequential monomer addition using *rac*-**Lig^{1}ZrBn$_2$-a,b**/$B(C_6F_5)_3$ at 0 °C. We are currently studying the source of isoselectivity in these systems and the nature of the active species in hopes of obtaining catalysts that are more isoselective while maintaining their living behavior and high activity.

3.4 Experimental

3.4.1 Complex Syntheses

General Methods. All manipulations of air- and/or water-sensitive compounds were carried out under dry nitrogen using a Braun UniLab drybox or standard Schlenk techniques. ^{1}H NMR spectra of ligands and complexes were recorded using Varian UnityInova (400, 500, or 600 MHz) spectrometers and were referenced versus residual non-deuterated solvent shifts. $^{13}C\{^1H\}$ NMR spectra of ligands and complexes were recorded on a Varian UnityInova (500 MHz) spectrometer equipped with a ^{1}H/BB switchable probe equipped with Z-axis pulsed field gradient. $^{13}C\{^1H\}$ NMR spectra of polymers were recorded using a Varian UnityInova (600 MHz)

spectrometer equipped with a 10 mm broadband probe operating at 135 °C and referenced versus residual non-deuterated solvent shifts. The gradient selected COSY, HSQCAD, gradient selected HMBCAD and ROESY spectra were recorded on a Varian UnityInova (600 MHz) spectrometer operating at 599.757 MHz for ^{1}H observation using a Varian inverse ^{1}H-{^{13}C,^{15}N} triple-resonance probehead with triple-axis gradients. NMR data were acquired with the pulse sequences supplied in Vnmrj 2.1B/Chempack 4.1 and were processed and analyzed using the MestReNova 5.3 software package (2008, Mestrelab Research S. L.). Gradient selected COSY spectra were acquired using the gCOSY sequence with a spectral width of 4.3–4.6 kHz. A total of 512 points were collected in the indirectly detected dimension with 1 scan and 4k points per increment. The resulting matrices were zero filled to 8k x 512 complex data points and 0° sinebell window functions were applied in both dimensions prior to Fourier transformation. ROESY spectra were acquired using the ROESY sequence with a spectral width of 4.3–4.6 kHz. A total of 200 complex points were collected in the indirectly detected dimension with 8 scans and 0.15 s acquisition time per increment. The resulting matrices were zero filled to 2k x 2k complex data points and unshifted Gaussian window functions were applied in both dimensions prior to Fourier transformation. The multiplicity-edited adiabatic HSQC spectrum was acquired with the HSQCAD sequence. Spectral widths were 4.3–4.6 kHz and 25–30 kHz in ^{1}H and ^{13}C dimensions, respectively. A total of 256 complex points were collected in the indirectly detected dimension with 4 scans and 0.15 s acquisition time per increment. The resulting matrices were zero filled to 2k x 2k complex data points and an unshifted Gaussian window function was applied in the ^{1}H dimension prior to Fourier transformation. Gradient selected adiabatic HMBC

spectra were acquired in phase sensitive mode with the gHMBCAD sequence optimized for 8 Hz couplings. Spectral widths were 4.3–4.6 kHz and 25–30 kHz in ^{1}H and ^{13}C dimensions, respectively. A total of 500-600 complex points were collected in the indirectly detected dimension with 4 scans and 2048 points per increment. The resulting matrices were zero filled to 2k x 4k complex data points and shifted sinebell window functions were applied in the ^{1}H dimension prior to Fourier transformation. The polymer samples were dissolved in 1,1,2,2-tetrachloroethane-d_2 in a 5 mm O.D. tube, and spectra were collected at 135 °C. For quantitative ^{13}C{^{1}H} analysis, the polymer samples were dissolved in 1,1,2,2-tetrachloroethane-d_2 in 10 mm O.D. tubes and the spectra were collected with inverse gated decoupling using the TYCO-25 decoupling sequence, a 30° excitation pulse width, 2.0 s acquisition time, and 10 s relaxation delay. Molecular weights (M_n and M_w) and polydispersities (M_w/M_n) were determined by high temperature gel permeation chromatography (GPC). Analyses were performed with a Waters Alliance GPCV 2000 GPC equipped with a Waters DRI detector and viscometer. The column set (four Waters HT 6E and one Waters HT2) was eluted with 1,2,4-trichlorobenzene containing 0.01 wt. % di-*tert*-butylhydroxytoluene (BHT) at 1.0 mL/min at 140 °C. Data were calibrated using monomodal polyethylene standards in the case of PP or monomodal polystyrene standards in the case of poly(1-hexene) (from Polymer Standards Service). Polymers were usually placed in a 140 °C oven for 24 h prior to molecular weight measurements. Polymer melting points (T_m) and glass transition temperatures (T_g) were measured by differential scanning calorimetry (DSC) using a TA Instruments Q1000 calorimeter equipped with an automated sampler. Analyses were performed in crimped aluminum pans under nitrogen and data were collected

from the second heating run at a heating rate of 10 °C/min from -100 to 200 °C, and processed with TA Q series software. Mass spectral analyses were conducted at the School of Chemical Sciences Mass Spectrometry Laboratory at the University of Illinois at Urbana-Champaign or they were acquired using a JEOL GCMate II mass spectrometer operating at 3000 resolving power for high resolution measurements in positive ion mode and an electron ionization potential of 70 eV. Samples were introduced via a GC inlet using an Agilent HP 6890N GC equipped with a 30 m (0.25 μm i.d.) HP-5ms capillary GC column. The carrier gas was helium with a flow rate of 1 mL/min. Samples were introduced into the GC using a split/splitless injector at 230 °C with a split ratio of 10:1.

Materials. Toluene and pentane were purified over columns of alumina and copper (Q5) prior to use. Diethyl ether (Et_2O) was purified over a column of alumina and degassed by three freeze-pump thaw cycles and stored under nitrogen. Benzene-d_6 was distilled from sodium benzophenone ketyl under nitrogen, degassed, and stored over 4Å molecular sieves in the glovebox under nitrogen. Propylene (Airgas, research purity) was purified over columns (40 cm inner diameter x 120 cm long) of BASF catalyst R3-12, BASF catalyst R3-11, and 4Å molecular sieves. 2-Bromostyrene, anhydrous *N*,*N*-dimethylformamide (DMF), ethyl acetate (EtOAc), hexanes, methylene chloride (CH_2Cl_2), magnesium sulfate ($MgSO_4$), methylamine (2.0 M in methanol), sodium borohydride ($NaBH_4$), paraformaldehyde, and 2,4-di-*tert*-butylphenol were purchased from Aldrich or Mallinkrodt and used as received. Tetrabenzylzirconium ($ZrBn_4$), magnesium turnings, tris(pentafluorophenyl)borane ($B(C_6F_5)_3$), trityl tetrakis(pentafluorophenyl)borate ($[Ph_3C][B(C_6F_5)_4]$), and *N*,*N*-

dimethylanilinium tetrakis(pentafluorophenyl)borate ([$PhNMe_2H$][$B(C_6F_5)_4$]) were purchased from Strem and used as received. 2-Vinylbenzaldehyde,[55] 2-(1-adamantyl)-4-methylphenol,[56] tetrabenzylhafnium ($HfBn_4$),[57] and tetrabenzyltitanium ($TiBn_4$)[58] were prepared from standard literature procedures.

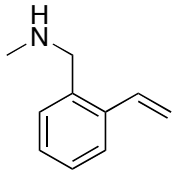

***N*-Methyl-1-(2-vinylphenyl)methanamine.** Following a modified procedure of Dale,[55] 2-vinylbenzaldehyde was prepared via Grignard formation of 2-bromostyrene (6.0 mL, 46 mmol) with magnesium turnings (1.5 g, 61 mmol) in Et_2O followed by reaction with DMF (5.4 mL, 70 mmol) to yield 4.2 g (68%) following column chromatography (2% EtOAc/hexanes). The 2-vinylbenzaldehyde (2.0 g, 15 mmol) was charged to a 100 mL round bottom flask containing a magnetic stir bar and methanol (15 mL). The reaction vessel was sealed with a rubber septum and methylamine (11 mL of a 2.0 M solution in methanol, 22 mmol) was added at room temperature via syringe. The reaction was stirred for one hour after which it was cooled to 0 °C and $NaBH_4$ (1.1 g, 29 mmol) was slowly added over ten minutes. The reaction was allowed to come to room temperature over two hours and water (50 mL) and CH_2Cl_2 (50 mL) were added. The organic layer was separated and the aqueous layer was extracted with CH_2Cl_2 (2 x 30 mL). The combined organics were washed with brine (50 mL), dried over $MgSO_4$, filtered, and concentrated via rotary evaporation. The residue was dried *in vacuo* to yield 2.09 g (94%) of a light yellow liquid. ^{1}H NMR (400 MHz, C_6D_6) δ 7.49 – 7.45 (m, 1H, Ar*H*), 7.25 –

7.18 (m, 1H, Ar*H*), 7.17 – 7.15 (m, 1H, Ar*H*), 7.14 – 7.07 (m, 2H, Ar*H* and C*H*=CH$_2$), 5.59 (dd, J = 17.5, 1.5, 1H, CH=C*H*$_2$), 5.18 (dd, J = 11.0, 1.5, 1H, CH=C*H*$_2$), 3.55 (s, 2H, ArC*H*$_2$), 2.21 (s, 3H, NHC*H*$_3$), 0.56 (s, 1H, N*H*CH$_3$). ^{13}C{^{1}H} NMR (125 MHz, C_6D_6) δ 138.38, 137.78, 135.48, 129.86, 128.18, 127.83, 126.35, 115.62, 54.47, 36.69. MS-EI (*m*/*z*): 147.1 (M^+). HRMS-EI (*m*/*z*): calcd for $C_{10}H_{13}N$, 147.1048; found, 147.1049.

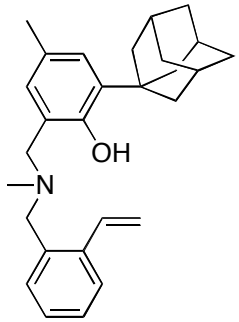

2-(1-Adamantyl)-4-methyl - 6 - ((methyl(2-vinylbenzyl)amino)methyl) phenol (Lig^1). A 20 mL scintillation vial was charged with 2-(1-adamantyl)-4-methylphenol (1.36 g, 5.61 mmol), *N*-methyl-1-(2-vinylphenyl)methanamine (0.820 g, 5.55 mmol), and paraformaldehyde (0.260 g, 8.59 mmol) in 8 mL of methanol. The vial was capped, sealed with electrical tape and heated at 65 °C for 48 hours. After cooling, the solvent was removed *in vacuo* and the residues were purified by flash chromatography (2% EtOAc/hexanes) to give 1.21 g (54%) of a colorless oil that solidified upon standing into a white solid. ^{1}H NMR (500 MHz, C_6D_6) δ 10.58 (s, 1H, O*H*), 7.39 (d, J = 7.1, 1H, Ar*H*), 7.13 (s, 1H, Ar*H*), 7.10 – 6.95 (m, 4H, Ar*H* and C*H*=CH$_2$), 6.62 (s, 1H, Ar*H*), 5.56 (dd, J = 17.3, 1.3, 1H, CH=C*H*$_2$), 5.29 (dd, J = 10.9, 1.3, 1H, CH=C*H*$_2$), 3.35 (s, 2H, ArC*H*$_2$NCH$_3$), 3.25 (s, 2H, ArC*H*$_2$NCH$_3$), 2.45 (d, J = 2.4, 6H, Ad-C*H*$_2$), 2.31 (s, 3H, ArC*H*$_3$), 2.14 (s, 3H, Ad-C*H*), 1.97 – 1.75 (m, 6H, Ad-C*H*$_2$), 1.81 (s, 3H, ArCH$_2$NC*H*$_3$). ^{13}C{^{1}H} NMR (125 MHz, C_6D_6) δ 155.45, 138.47, 137.26, 135.07,

134.95, 131.48, 128.68, 128.27, 127.87, 127.70, 127.58, 126.82, 122.78, 116.68, 62.50, 59.47, 41.30, 40.96, 38.02, 37.59, 30.11, 21.51. MS-ESI (*m*/*z*): 402.2 (M^+). HRMS-ESI (*m*/*z*): calcd for $C_{28}H_{36}NO$, 402.2797; found, 402.2800. Anal. calc. for $C_{28}H_{35}NO$: C, 83.74; H, 8.78; N, 3.49. Anal. found C, 83.70; H, 8.78; N, 3.34.

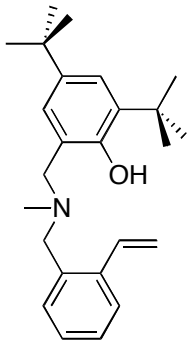

2,4-Di-*tert*-butyl – 6 - ((methyl(2-vinylbenzyl)amino)methyl) phenol (Lig^2). A 20 mL scintillation vial containing a magnetic stir bar was charged with 2,4-di-*tert*-butylphenol (0.85 g, 4.1 mmol), *N*-methyl-1-(2-vinylphenyl)methanamine (0.61 g, 4.1 mmol), paraformaldehyde (0.19 g, 6.2 mmol) and 8 mL methanol. The vial was capped, sealed with electrical tape and heated at 65 °C for 48 hours. Upon cooling to room temperature, the product crystallized to yield 0.80 g (53%) of a white crystalline solid after drying *in vacuo*. ^{1}H NMR (500 MHz, C_6D_6) δ 10.73 (s, 1H, O*H*), 7.51 (s, 1H, Ar*H*), 7.38 (d, J = 7.9, 1H, Ar*H*), 7.13 – 7.08 (m, 1H, Ar*H*), 7.07 – 7.00 (m, 2H, Ar*H*), 6.97 (dd, J = 17.7, 10.9, 1H, C*H*=CH_2), 6.93 (s, 1H, Ar*H*), 5.53 (dd, J = 17.3, 1.3, 1H, CH=CH_2), 5.26 (dd, J = 10.9, 1.3, 1H, CH=CH_2), 3.39 (s, 2H, NCH_2), 3.26 (s, 2H, NCH_2), 1.81 (s, 3H, NCH_3), 1.70 (s, 9H, ArCCH_3), 1.38 (s, 9H, ArCCH_3). ^{13}C{^{1}H} NMR (125 MHz, C_6D_6) δ 155.23, 141.16, 138.49, 136.42, 135.08, 134.92, 131.38, 128.68, 128.28, 126.82, 124.09, 123.61, 122.26, 116.70, 62.74, 59.41, 41.03, 35.71, 34.72, 32.37, 30.39. MS-ESI (*m*/*z*): 366.3 (M^+). HRMS-ESI (*m*/*z*): calcd for

$C_{25}H_{36}NO$, 366.2797; found, 366.2795. Anal. calc. for $C_{25}H_{35}NO$: C, 82.14; H, 9.65; N, 3.83. Anal. found C, 81.87; H, 9.81; N, 4.10.

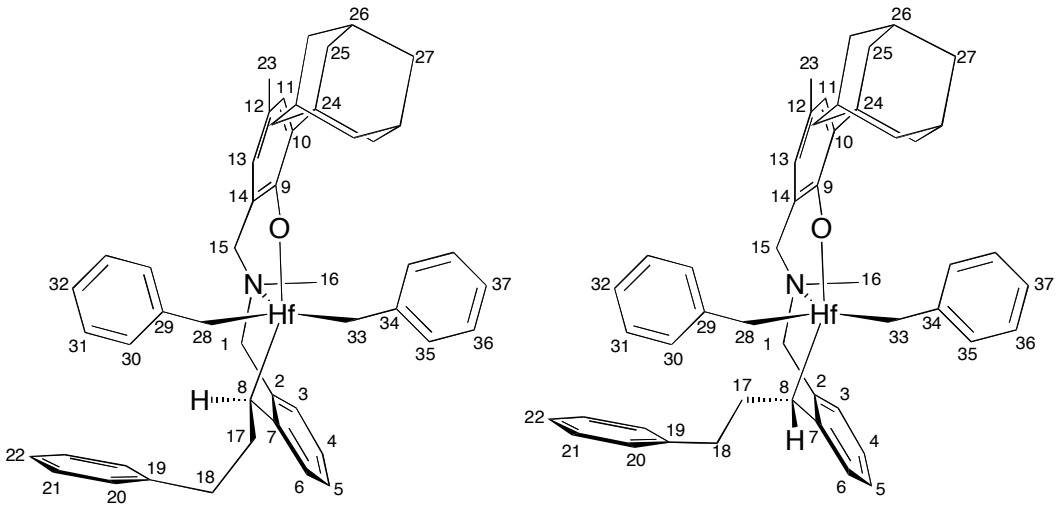

rac-**Lig^{1}HfBn$_2$-a** *rac*-**Lig^{1}HfBn$_2$-b**

Synthesis of *rac*-Lig^{1}HfBn$_2$-a,b. In a glovebox, a Schlenk adapted tube was charged with $HfBn_4$ (0.43 g, 0.78 mmol) in 5 mL of dry toluene. To this was charged 2-(1-adamantyl)-4-methyl-6-((methyl(2-vinylbenzyl)amino) methyl)phenol (0.31 g, 0.78 mmol) in 5 mL of dry toluene. The reaction vessel was sealed and heated at 60 °C for one hour. After cooling, the volatiles were removed *in vacuo* and the residues were taken up in dry pentane. The volatiles were removed again *in vacuo* and the residues were dried for 24 hours to yield 0.53 g (79%) of white powdery solid that was stored at -30 °C in the glovebox freezer. Single crystals of suitable quality for structural determination via X-ray crystallography were grown from slow diffusion of pentane into a saturated toluene solution at -30 °C over the course of several weeks. The ^{1}H and ^{13}C{^{1}H} NMR data are tabulated below in Table 3.4. The resonances were assigned with the aid of COSY, HMBCAD, HSCQAD, and ROESY NMR experiments.

Table 3.4. NMR Data for *rac*-**Lig^{1}HfBn$_2$-a,b**.

rac-**Lig^{1}HfBn$_2$-a**			*rac*-**Lig^{1}HfBn$_2$-b**		
Carbon atom #	^{1}H NMR δ	^{13}C{^{1}H} NMR δ	Carbon atom #	^{1}H NMR δ	^{13}C{^{1}H} NMR δ
1	3.63, 2.46	66.06	1	3.68, 2.69	66.76
2	-	128.19	2	-	127.96
3	6.72	130.16	3	6.86	129.13
4	6.85	119.94	4	6.87	119.69
5	7.44	129.57	5	7.40	129.94
6	7.18	122.32	6	7.16	122.58
7	-	147.74	7	-	146.15
8	1.33	84.21	8	1.48	84.93
9	-	157.24	9	-	156.47
10	-	137.38	10	-	137.40
11	7.10	127.76	11	7.05	127.82
12	-	nd	12	-	nd
13	6.37	127.50	13	6.22	127.70
14	-	125.26	14	-	125.56
15	2.29	63.58	15	2.93, 2.15	61.27
16	0.87	38.58	16	1.09	41.92
17	3.33, 3.05	30.89	17	3.23	31.48
18	3.15, 2.91	36.01	18	3.11, 2.84	35.87
19	-	142.79	19	-	142.86
20	7.20	129.36	20	7.11	129.39
21	7.19	128.41	21	7.22	128.32
22	7.12	125.83	22	7.11	125.72
23	2.27	20.88	23	2.24	20.80
24	-	36.70	24	-	36.51
25	2.45	41.09	25	2.33, 2.28	40.88
26	2.23	29.14	26	2.17	29.08
27	1.97, 1.88	37.22	27	1.88, 1.84	37.14
28	2.68, 2.64	80.20	28	2.65, 2.56	80.15
29	-	141.97	29	-	141.34
30	6.56	128.95	30	6.75	128.24
31	6.81	128.33	31	6.90	128.95
32	6.68	122.24	32	6.72	122.76
33	2.57, 2.20	81.53	33	2.28, 2.23	82.34
34	-	139.88	34	-	142.35
35	6.80	127.78	35	6.82	127.64
36	6.75	128.24	36	6.86	127.76
37	6.57	122.48	37	6.65	122.00

nd = could not be determined.

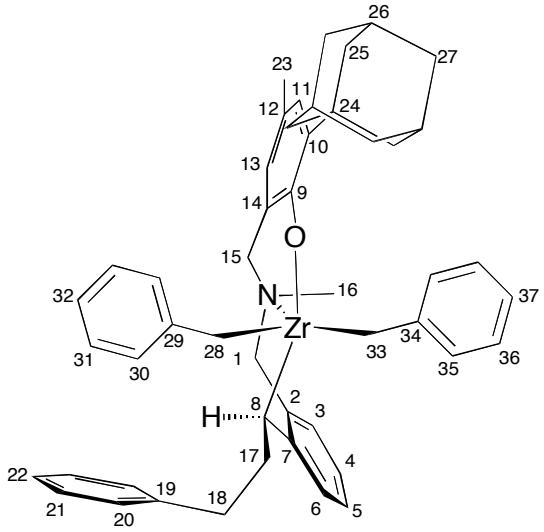

rac-**Lig^{1}ZrBn$_2$-a**

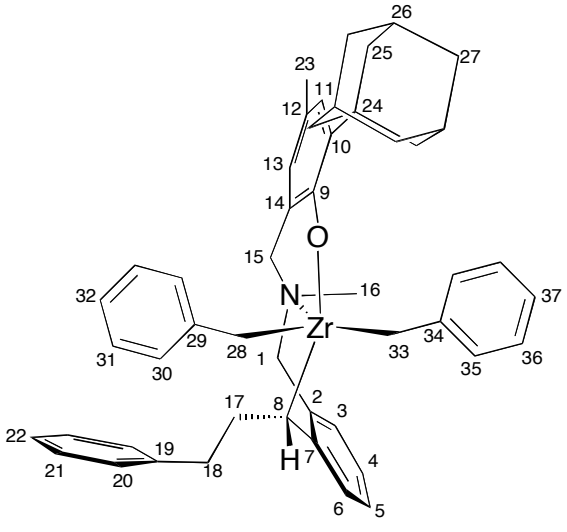

rac-**Lig^{1}ZrBn$_2$-b**

Synthesis of *rac*-Lig^{1}ZrBn$_2$-a,b. In a glovebox, a Schlenk adapted tube was charged with $ZrBn_4$ (0.46 g, 1.0 mmol) in 5 mL of dry toluene. To this was charged 2-(1-adamantyl)-4-methyl-6-((methyl(2-vinylbenzyl)amino)methyl) phenol (0.40 g, 1.0 mmol) in 5 mL of dry toluene. The reaction vessel was sealed and stirred for 30 minutes at room temperature. The volatiles were then removed *in vacuo* and the residues were taken up in dry pentane. The volatiles were removed again *in vacuo* and the residues were dried for 24 hours to yield 0.66 g (86%) of a thermally sensitive yellow-orange powdery solid that was stored at -30 °C in the glovebox freezer. Single crystals of suitable quality for structural determination via X-ray crystallography were grown from a saturated pentane solution at 20 °C over the course of several weeks. The ^{1}H and ^{13}C{^{1}H} NMR data obtained in toluene-d_8 at -10 °C are tabulated below in Table 3.5. The resonances were assigned with the aid of COSY, HMBCAD, HSQCAD, and ROESY NMR experiments.

Table 3.5. NMR Data for *rac*-**Lig^{1}ZrBn$_2$-a,b**.

rac-**Lig^{1}ZrBn$_2$-a**			*rac*-**Lig^{1}ZrBn$_2$-b**		
Carbon atom #	^{1}H NMR δ	^{13}C{^{1}H} NMR δ	Carbon atom #	^{1}H NMR δ	^{13}C{^{1}H} NMR δ
1	3.50, 2.39	65.83	1	3.58, 2.63	67.07
2	-	128.92	2	-	128.92
3	6.74	130.39	3	6.90	129.61
4	6.88	119.77	4	6.89	119.33
5	7.41	129.77	5	7.38	130.06
6	7.21	121.99	6	7.13	121.56
7	-	146.73	7	-	145.88
8	1.63	77.58	8	1.58	79.61
9	-	157.71	9	-	156.98
10	-	136.88	10	-	136.88
11	7.09	127.65	11	7.02	128.11
12	-	128.42	12	-	128.05
13	6.41	127.79	13	6.28	128.06
14	-	125.67	14	-	126.38
15	2.55, 2.41	63.49	15	3.25, 2.37	61.19
16	1.17	38.98	16	1.21	42.22
17	3.11, 2.91	31.72	17	3.10, 3.06	31.91
18	3.02, 2.83	35.61	18	2.99, 2.79	35.17
19	-	142.77	19	-	142.82
20	7.13	129.31	20	7.05	129.38
21	7.19	128.36	21	7.19	128.36
22	7.11	125.83	22	7.11	125.72
23	2.29	20.91	23	2.25	20.83
24	-	36.78	24	-	36.61
25	2.38, 2.34	41.00	25	2.27, 2.23	40.82
26	2.16	29.11	26	2.13	29.04
27	1.91, 1.83	37.21	27	1.85, 1.80	37.11
28	2.84, 2.57	71.41	28	2.64, 2.56	70.03
29	-	143.91	29	-	143.42
30	6.63	128.55	30	6.71	127.91
31	6.78	128.33	31	6.87	129.10
32	6.69	121.87	32	6.71	122.54
33	2.52, 2.37	71.09	33	2.44, 2.37	72.07
34	-	138.95	34	-	139.99
35	6.82	127.47	35	7.03	nd
36	6.90	129.73	36	7.04	nd
37	6.70	123.01	37	6.70	nd

nd = could not be determined.

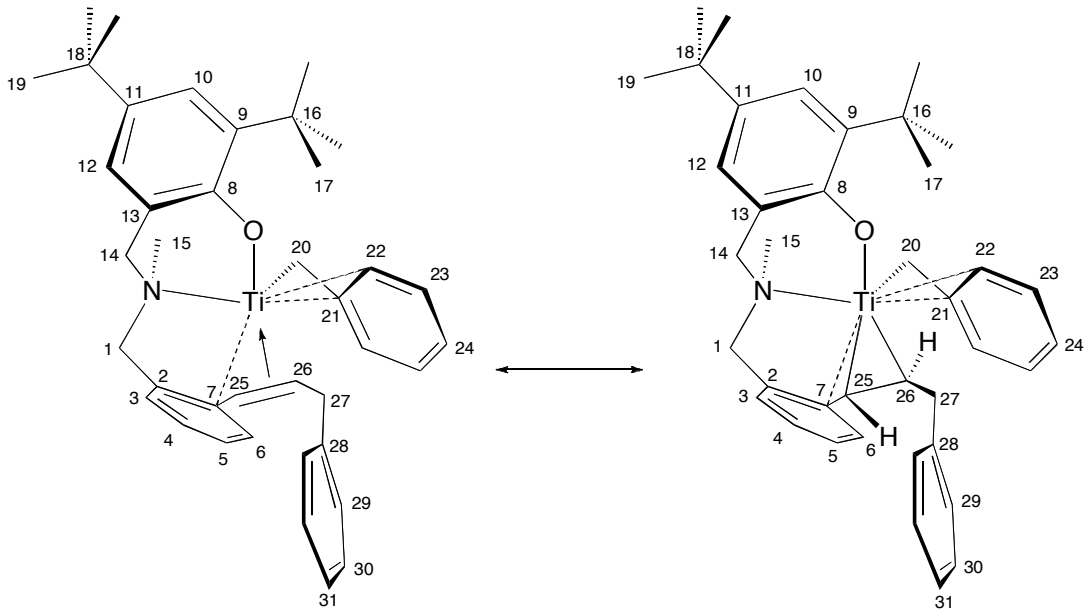

rac-**Lig^{2}TiBn**

Synthesis of *rac*-Lig^{2}TiBn. In a glovebox, a Schlenk adapted tube was charged with $TiBn_4$ (0.12 g, 0.29 mmol) in 3 mL of dry toluene. To this was charged 2,4-di-*tert*-butyl-6-((methyl(2-vinylbenzyl)amino)methyl)phenol (0.11 g, 0.29 mmol) in 3 mL of dry toluene. The reaction vessel was sealed and heated to 60 °C for one hour. After cooling, the volatiles were removed *in vacuo* and the residues were taken up in dry pentane. The volatiles were removed again *in vacuo* and the residues were dried for 24 hours to yield 0.11 g (63%) of a glassy black solid. Single crystals of suitable quality for structural determination via X-ray crystallography were grown from a saturated pentane solution at -30 °C over the course of several weeks. The ^1H and $^{13}C\{^1H\}$ NMR data obtained in C_6D_6 at room temperature are tabulated below in Table 3.6. The resonances were assigned with the aid of COSY, HMBCAD, and HSQCAD NMR experiments.

Table 3.6. NMR Data for *rac*-**Lig^{2}TiBn**.

	rac-**Lig^{2}TiBn**	
Carbon Atom #	^{1}H NMR δ	^{13}C{^{1}H} NMR δ
1	3.59, 2.42	64.10
2	-	137.91
3	6.70	128.74
4	6.88	123.73
5	7.12	130.19
6	6.82	133.36
7	-	133.32
8	-	160.42
9	-	135.29
10	7.60	124.65
11	-	141.62
12	7.07	124.82
13	-	124.29
14	4.42, 3.09	66.29
15	1.65	44.61
16	-	35.34
17	1.62	30.26
18	-	34.48
19	1.44	32.02
20	1.53	66.45
21	-	140.33
22	6.90	128.18
23	7.38	131.79
24	7.09	123.27
25	3.51	101.44
26	1.64	88.47
27	2.96, 2.76	40.26
28	-	145.83
29	7.27	128.46
30	7.18	128.47
31	7.06	125.53

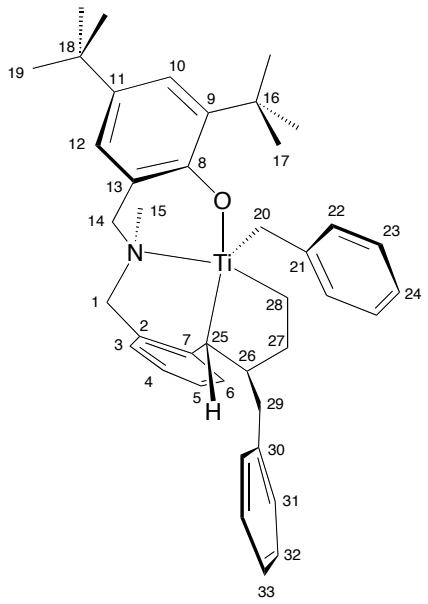

rac-**Lig^2(CH$_2$)$_2$TiBn**

Synthesis of *rac*-Lig^2(CH$_2$)$_2$TiBn. In a glovebox, a Schlenk adapted tube was charged with $TiBn_4$ (0.13 g, 0.32 mmol) in 3 mL of dry toluene. To this was charged 2,4-di-*tert*-butyl-6-((methyl(2-vinylbenzyl)amino)methyl)phenol (0.12 g, 0.32 mmol) in 3 mL of dry toluene. The reaction vessel was sealed and heated to 60 °C for one hour to afford a black solution *rac*-**Lig^{2}TiBn**. After cooling, the reaction was pressurized with 1 atm of ethylene causing an immediate color change to a dark red solution. The reaction was stirred overnight and the solution was filtered to remove residual polyethylene that had formed (~ 60 mg). The volatiles were then removed *in vacuo* and the residues were taken up in dry pentane. The volatiles were removed again *in vacuo* and the residues were dried for 24 hours to yield 0.12 g (61%) of a powdery dark red solid. The ^1H and $^{13}C\{^1H\}$ NMR data obtained in C_6D_6 at room temperature are tabulated below in Table 3.7. The resonances were assigned with the aid of COSY, HMBCAD, HSQCAD, and ROESY NMR experiments.

Table 3.7. NMR Data for *rac*-**Lig^2(CH$_2$)$_2$TiBn**.

rac-**Lig^2(CH$_2$)$_2$TiBn**		
Carbon atom #	^{1}H NMR δ	^{13}C{^{1}H} NMR δ
1	3.39, 2.47	65.55
2	-	132.11
3	6.77	129.75
4	6.97	121.40
5	7.51	131.33
6	7.81	126.75
7	-	145.19
8	-	160.42
9	-	136.66
10	7.53	124.05
11	-	142.23
12	6.82	124.41
13	-	123.98
14	3.81, 2.65	62.05
15	1.16	41.89
16	-	35.47
17	1.64	30.60
18	-	34.58
19	1.39	31.98
20	3.36, 3.19	87.58
21	-	145.72
22	6.34	126.76
23	6.87	128.31
24	6.63	122.23
25	2.52	102.48
26	3.97	46.80
27	2.59, 1.84	39.93
28	3.33, 1.66	95.56
29	3.14, 2.66	41.64
30	-	141.86
31	7.20	129.97
32	7.20	128.35
33	7.11	125.92

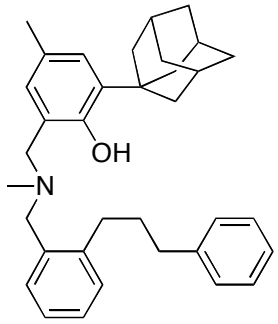

Methanolysis of *rac*-Lig^{1}HfBn$_2$-a,b or *rac*-Lig^{1}ZrBn$_2$-a,b. To a solution of *rac*-**Lig^{1}HfBn$_2$-a,b** or *rac*-**Lig^{1}ZrBn$_2$-a,b** (~25 mg) in C_6D_6 which had been stored in a J. Young NMR tube was added several drops of MeOH, the tube was shaken vigorously and the solution became colorless almost immediately. The volatiles were removed *in vacuo*. The residue was taken up in C_6D_6 and flashed through a small plug of Celite to isolate 2-(1-adamantyl)-4-methyl-6-((methyl(2-(3-phenylpropyl)benzyl)amino)methyl)phenol. ^{1}H NMR (400 MHz, C_6D_6) δ 10.82 (s, 1H, Ar-O*H*), 7.24 – 7.12 (m, 4H, Ar*H*), 7.12 – 7.04 (m, 4H, Ar*H*), 7.01 (t, J = 7.2, 2H, Ar*H*), 6.64 (s, 1H, Ar*H*), 3.34 (s, 2H, NCH_2), 3.19 (s, 2H, NCH_2), 2.64 – 2.56 (m, 2H, ArCH_2), 2.53 (t, J = 7.5, 2H, ArCH_2), 2.46 (s, 6H, Ad-CH_2), 2.32 (s, 3H, ArCH_3), 2.14 (s, 3, Ad-C*H*), 1.97 – 1.77 (m, 6H, Ad-CH_2), 1.85 (s, 3H, NCH_3), 1.74 (t, J = 7.7, 2H, ArCH$_2$CH_2CH$_2$Ar). ^{13}C{^{1}H} NMR (125 MHz, C_6D_6) δ 155.52, 142.78, 142.05, 137.25, 135.55, 131.33, 130.14, 129.22, 129.02, 128.68, 127.83, 127.73, 127.58, 126.68, 126.51, 122.87, 62.64, 59.27, 41.32, 41.06, 38.00, 37.61, 36.35, 33.66, 32.31, 30.11, 21.51. MS-ESI (*m*/*z*): 494.3 (M^+). HRMS-ESI (*m*/*z*): calcd for $C_{35}H_{44}NO$, 494.3423; found, 494.3416. Anal. calc. for $C_{35}H_{43}NO$: C, 85.14; H, 8.78; N, 2.84. Anal. found C, 84.90; H, 8.39; N, 2.56.

3.4.2 Polymer Syntheses

General Procedure for 1-Hexene Polymerization at 25 °C. In the glovebox, $B(C_6F_5)_3$ (5.1 mg, 10 μmol) was placed into a scintillation vial along with 9 mL of toluene and 2 mL of 1-hexene. To this solution was added *rac*-**Lig^{1}HfBn$_2$-a,b** (8.5 mg, 10 μmol) dissolved in 1 mL of toluene. The polymerization was allowed to proceed for 10 minutes after which time the vial was removed from the glovebox and the polymerization was terminated by the addition of MeOH. The volatiles were removed *in vacuo* to furnish poly(1-hexene) (0.30 g, 23%). The same procedure was followed for 1-hexene polymerization using $[Ph_3C][B(C_6F_5)_4]$ and $[PhNMe_2H][B(C_6F_5)_4]$ as activators and also for the analogous *rac*-**Lig^{1}ZrBn$_2$-a,b** complex.

Table 3.8. Living plot 1-hexene polymerization data for *rac*-**Lig^{1}HfBn$_2$-a,b**/$B(C_6F_5)_3$ at 0 °C.[a]

Entry	Time (min)	Yield (g)	Conv (%)	TOF (h^{-1})[b]	M_n (kg/mol)[c]	M_n^{theo} (kg/mol)[c]	M_w/M_n[c]
1	5	0.108	5.3	770	40.6	5.4	1.24
2	10	0.256	12.7	910	84.0	12.8	1.16
3	15	0.416	20.6	990	126	20.8	1.12
4	25	0.671	33.2	960	183	33.5	1.10
5	40	0.899	44.5	800	230	45.0	1.10

[a] General conditions: *rac*-**Lig^{1}HfBn$_2$-a,b** = 20 μmol, [Hf]/[$B(C_6F_5)_3$] = 1.0, 20 mL toluene, 3.0 mL 1–hexene. [b] Average turnover frequency (TOF): mol 1-hexene/(mol Hf·h). [c] Determined using gel permeation chromatography in 1,2,4-$C_6H_3Cl_3$ at 140 °C versus polystyrene standards.

General Procedure for 1-Hexene Polymerization at 0 °C. In the glovebox, $B(C_6F_5)_3$ (5.1 mg, 10 μmol) was placed into a Schlenk adapted tube

along with 19 mL of toluene and 3 mL of 1-hexene. The reaction was sealed, removed from the glovebox and equilibrated in an ice bath at 0 °C for 15 minutes. To this solution was added *rac*-**Lig^{1}HfBn$_2$-a,b** (8.5 mg, 10 μmol) dissolved in 1 mL of toluene in a gas tight syringe under an active nitrogen flow. The polymerization was allowed to proceed for the desired period of time after which time the polymerization was terminated by the addition of MeOH (Table 3.8). The volatiles were removed *in vacuo* to furnish poly(1-hexene). A similar procedure was followed for 1-hexene polymerization using the analogous *rac*-**Lig^{1}ZrBn$_2$-a,b** complex except the reaction was carried out in 3 mL of toluene.

General Procedure for Propylene Polymerization at 25 °C. In the glovebox, a 6 oz. flat-bottomed Lab-Crest pressure reaction vessel (Andrews Glass Co.) was charged with 25 mL of toluene and $B(C_6F_5)_3$ (5.1 mg, 10 μmol). The reactor was sealed, and the solution was saturated under a constant feed of propylene (30 psig) for 5 minutes with continuous stirring in a 25 °C water bath. Polymerization was initiated by injection of 5 mL of a solution of *rac*-**Lig^{1}HfBn$_2$-a,b** (8.5 mg, 10 μmol) dissolved in toluene. The polymerization was allowed to proceed under a constant feed of propylene for 10 minutes and terminated by the addition of MeOH with simultaneous venting and discontinuation of the propylene feed. The polymer was precipitated in copious MeOH and allowed to stir overnight; it was collected via filtration and dried to constant weight *in vacuo* at 60 °C. The same procedure was followed for propylene polymerization using $[Ph_3C][B(C_6F_5)_4]$ and $[PhNMe_2H][B(C_6F_5)_4]$ as activators and also for the analogous *rac*-**Lig^{1}ZrBn$_2$-a,b** complex.

Table 3.9. Living plot propylene polymerization data for *rac*-**Lig^{1}ZrBn$_2$-a,b**/$B(C_6F_5)_3$ at 0 °C.[a]

Entry	Time (min)	Yield (g)	TOF (h^{-1})[b]	M_n (kg/mol)[c]	M_n^{theo} (kg/mol)[c]	M_w/M_n[c]
1	4	0.346	4,100	63.3	11.5	1.13
2	8	0.703	4,200	110	23.4	1.11
3	16	1.654	4,900	185	55.1	1.15
4	20	2.224	5,300	217	74.1	1.17

[a] General conditions: 30 μmol of *rac*-**Lig^{1}ZrBn$_2$-a,b** in toluene (1.5 mL) was added to a propylene-saturated solution of activator (28.5 mL of toluene; $[Zr]/[B(C_6F_5)_3]$ = 1.0) at 0 °C. [b] Average turnover frequency (TOF): mol propylene/(mol Zr·h). [c] Determined using gel permeation chromatography in 1,2,4-$C_6H_3Cl_3$ at 140 °C versus polyethylene standards.

General Procedure for Propylene Polymerization at 0 °C. A stock solution of zirconium precatalyst was prepared by dilution of 200 μmol (153 mg) of *rac*-**Lig^{1}ZrBn$_2$-a,b** to 10 mL in a volumetric flask with toluene. A stock solution of $B(C_6F_5)_3$ (102 mg, 200 μmol) was prepared in an identical manner. In the glovebox, a 6 oz. flat-bottomed Lab-Crest pressure reaction vessel (Andrews Glass Co.) was charged with 27 mL of toluene and 1.5 mL of the $B(C_6F_5)_3$ solution. The reactor was sealed and equilibrated at 0 °C for 30 minutes. The solution was then saturated under a constant feed of propylene (30 psig) for 10 minutes with continuous stirring. Polymerization was initiated by injection of 1.5 mL of the *rac*-**Lig^{1}ZrBn$_2$-a,b** solution. The polymerization was allowed to proceed under a constant feed of propylene for the desired period of time and terminated by the addition of MeOH with simultaneous venting and discontinuation of the propylene feed (Table 3.9). The polymer was precipitated in copious MeOH and allowed to stir overnight; it was collected via filtration and dried to constant weight *in vacuo* at 60 °C. Similar

procedures were followed for propylene polymerization using $[Ph_3C][B(C_6F_5)_4]$ and $[PhNMe_2H][B(C_6F_5)_4]$ as activators and also for the analogous *rac*-**Lig^{1}HfBn$_2$-a,b** complex.

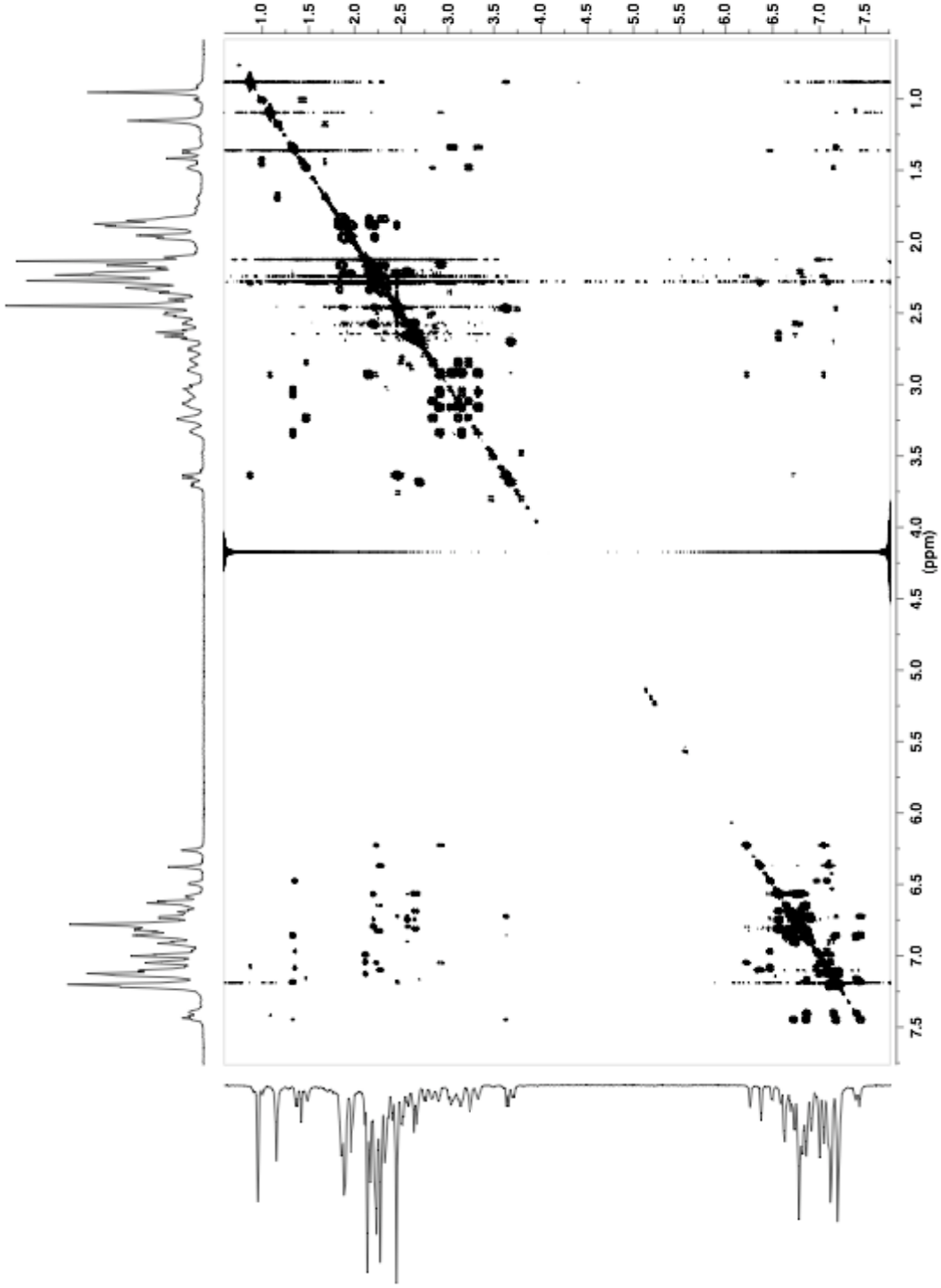

Figure 3.10. COSY spectrum of *rac*-**Lig^{1}HfBn$_2$-a,b** in toluene-d_8 at -10 °C.

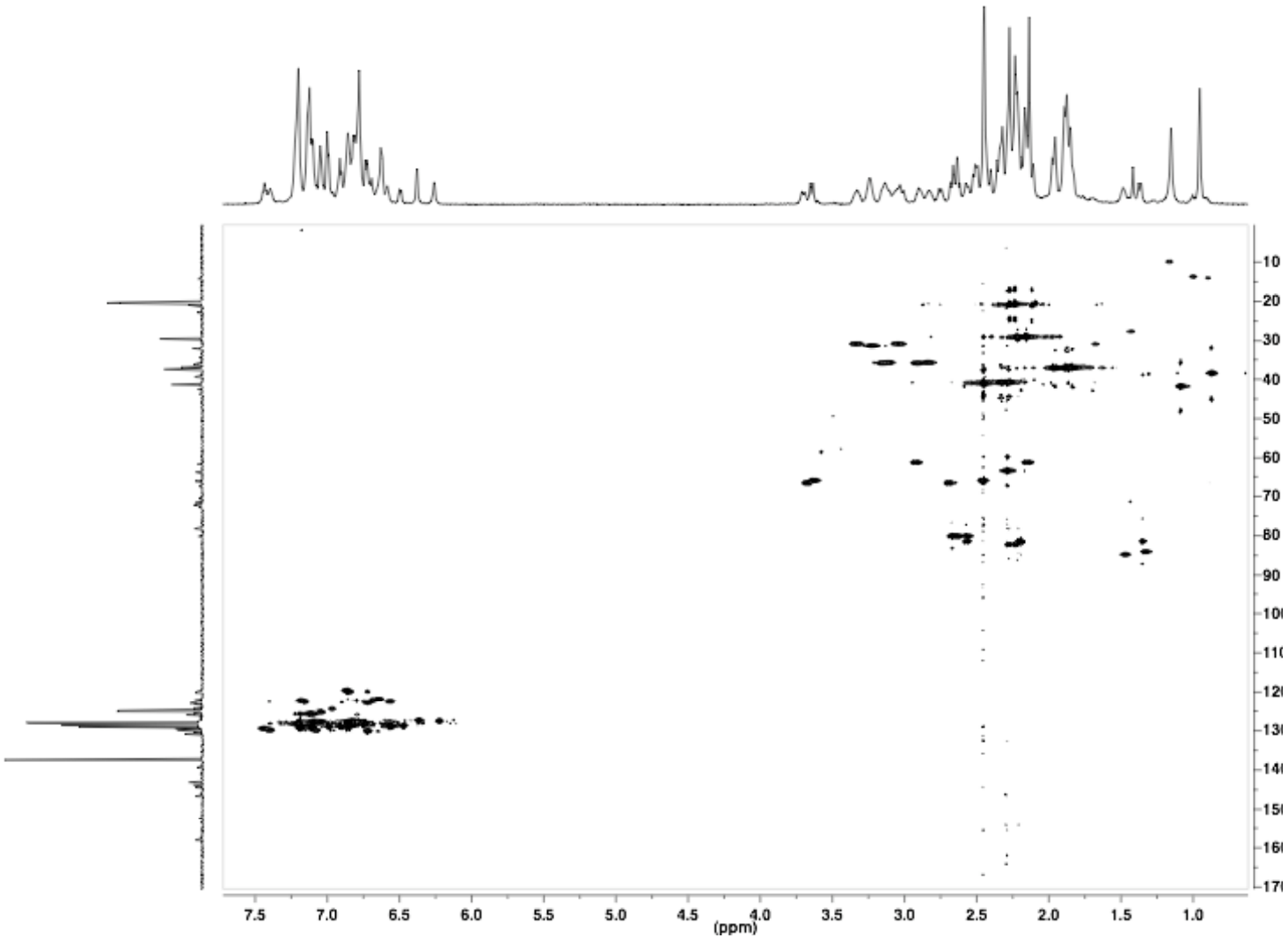

Figure 3.11. ^{1}H-^{13}C HSQC spectrum of *rac*-**Lig^{1}HfBn$_2$-a,b** in toluene-d_8 at -10 °C.

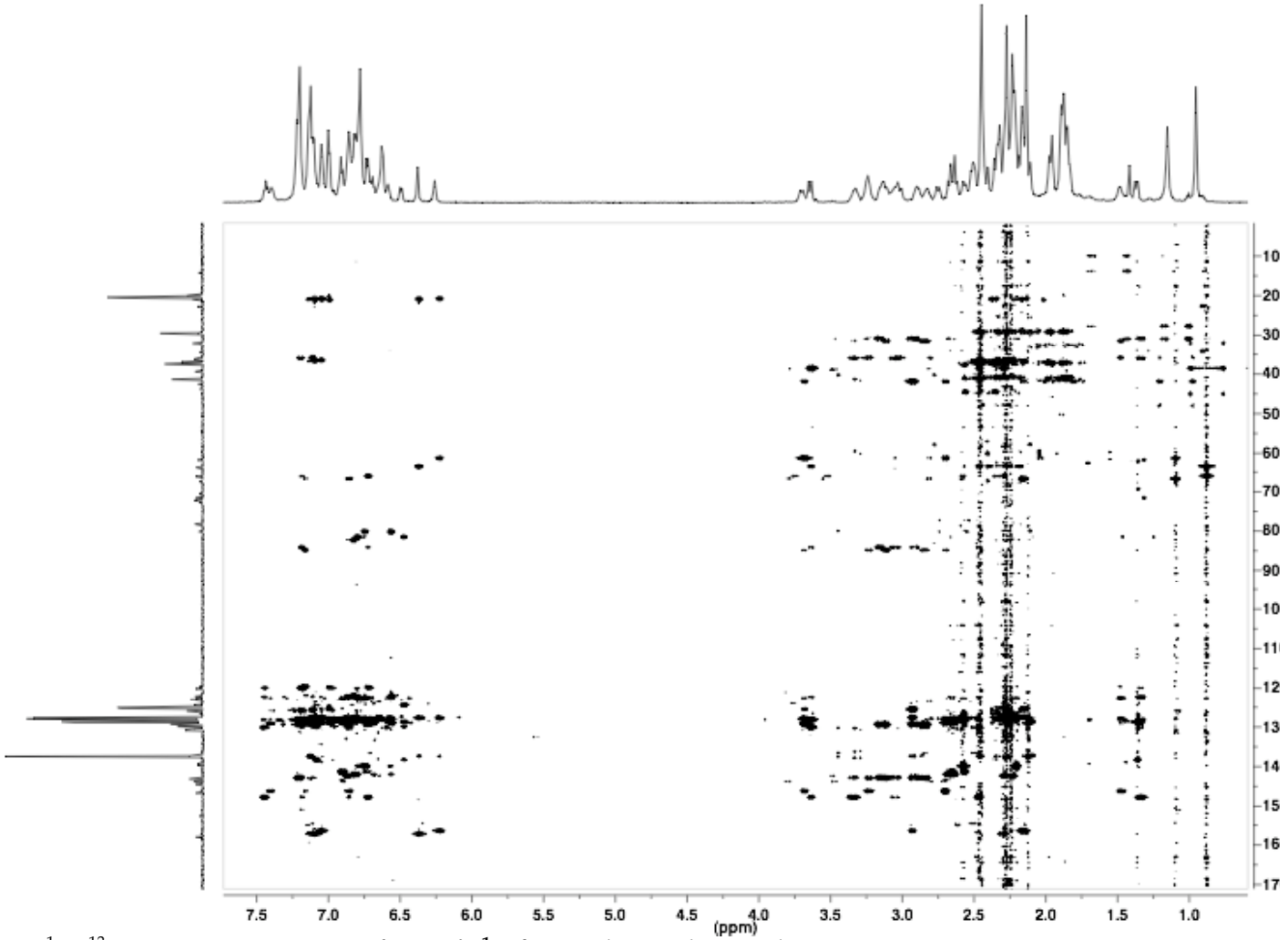

Figure 3.12. ^{1}H-^{13}C HMBC spectrum of *rac*-**Lig^{1}HfBn$_2$-a,b** in toluene-d_8 at -10 °C.

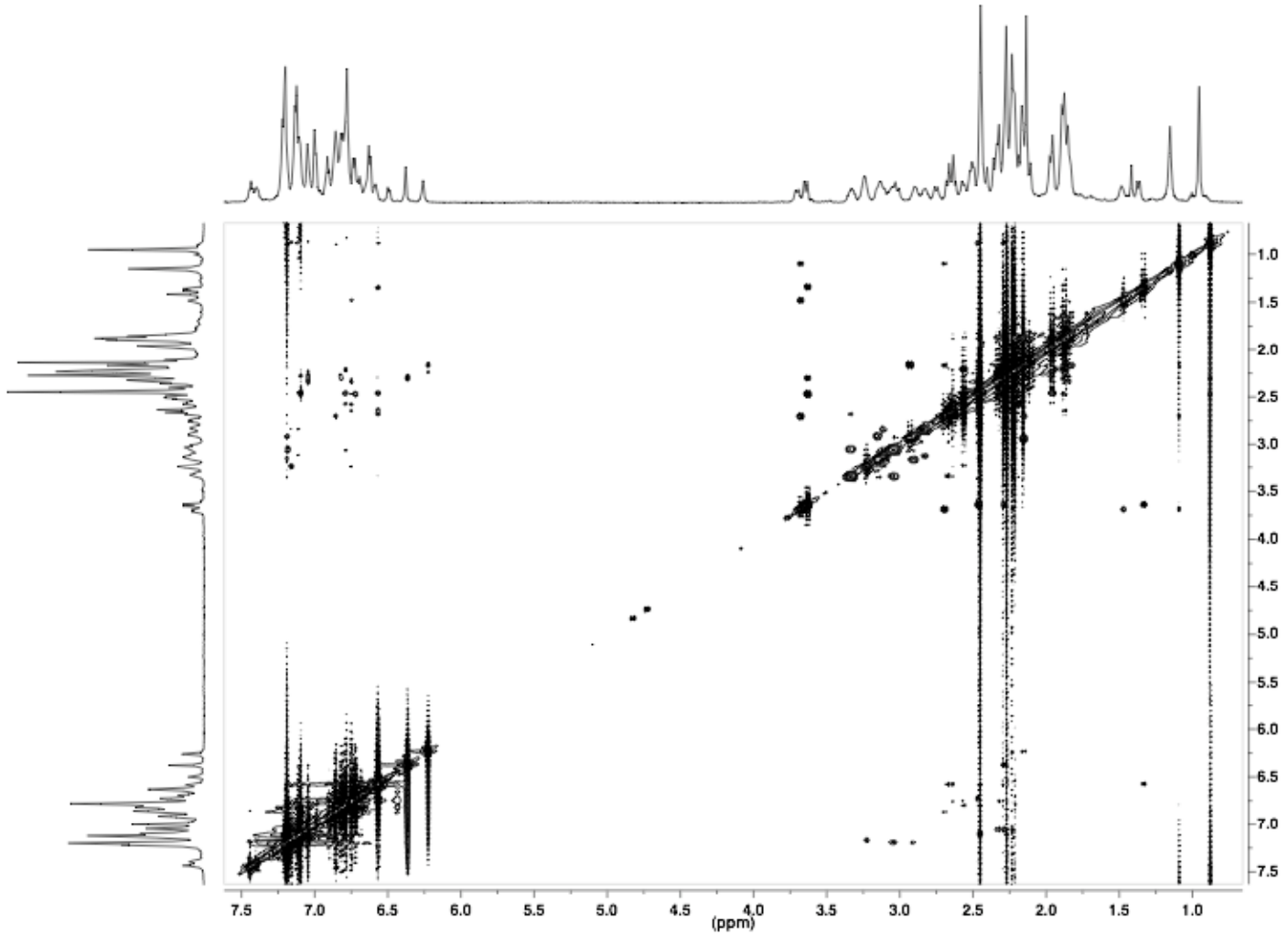

Figure 3.13. ROESY spectrum of *rac*-**Lig^{1}HfBn$_2$-a,b** in toluene-d_8 at -10 °C.

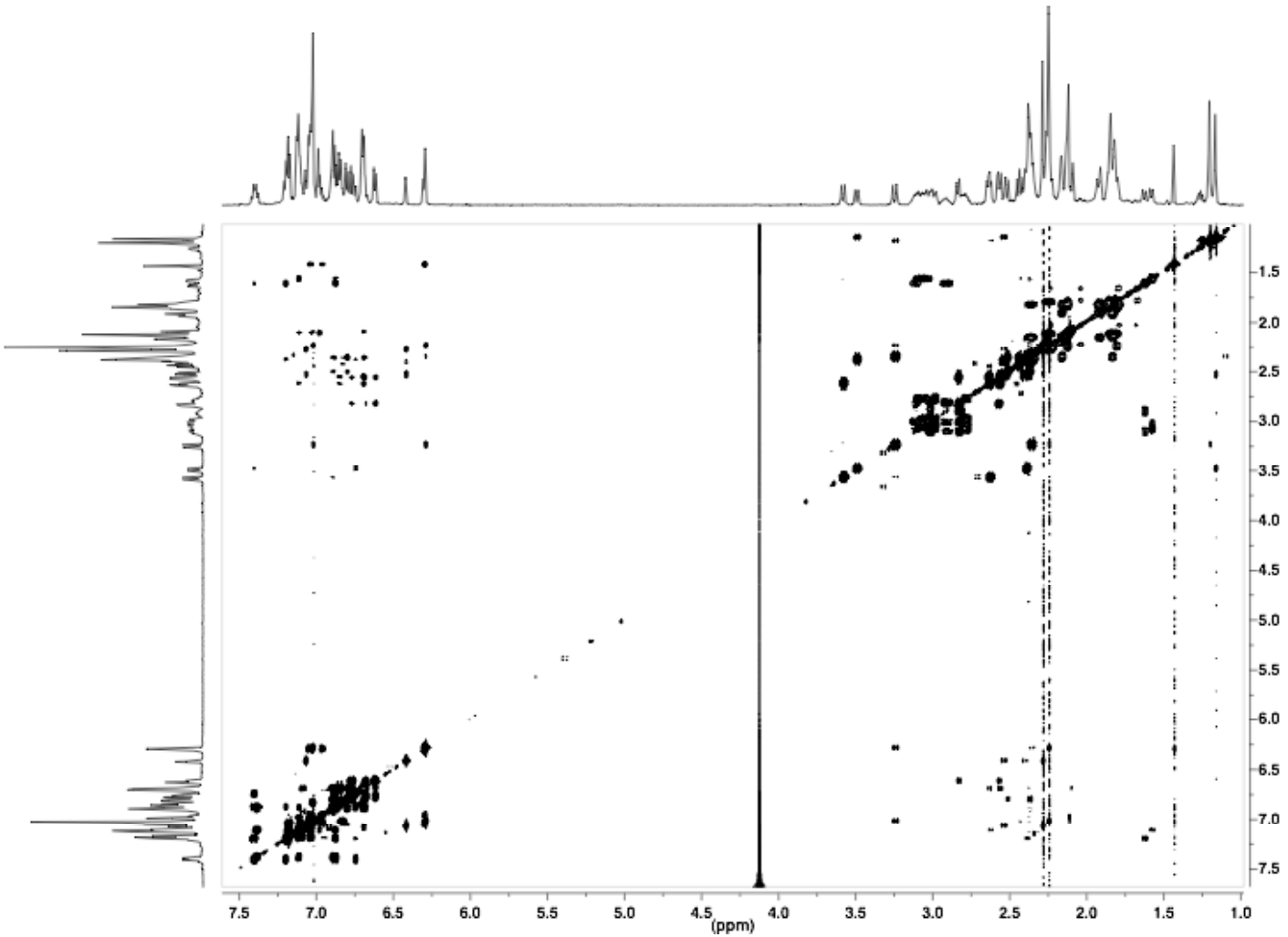

Figure 3.14. COSY spectrum of *rac*-**Lig^{1}ZrBn$_2$-a,b** in toluene-d_8 at -10 °C.

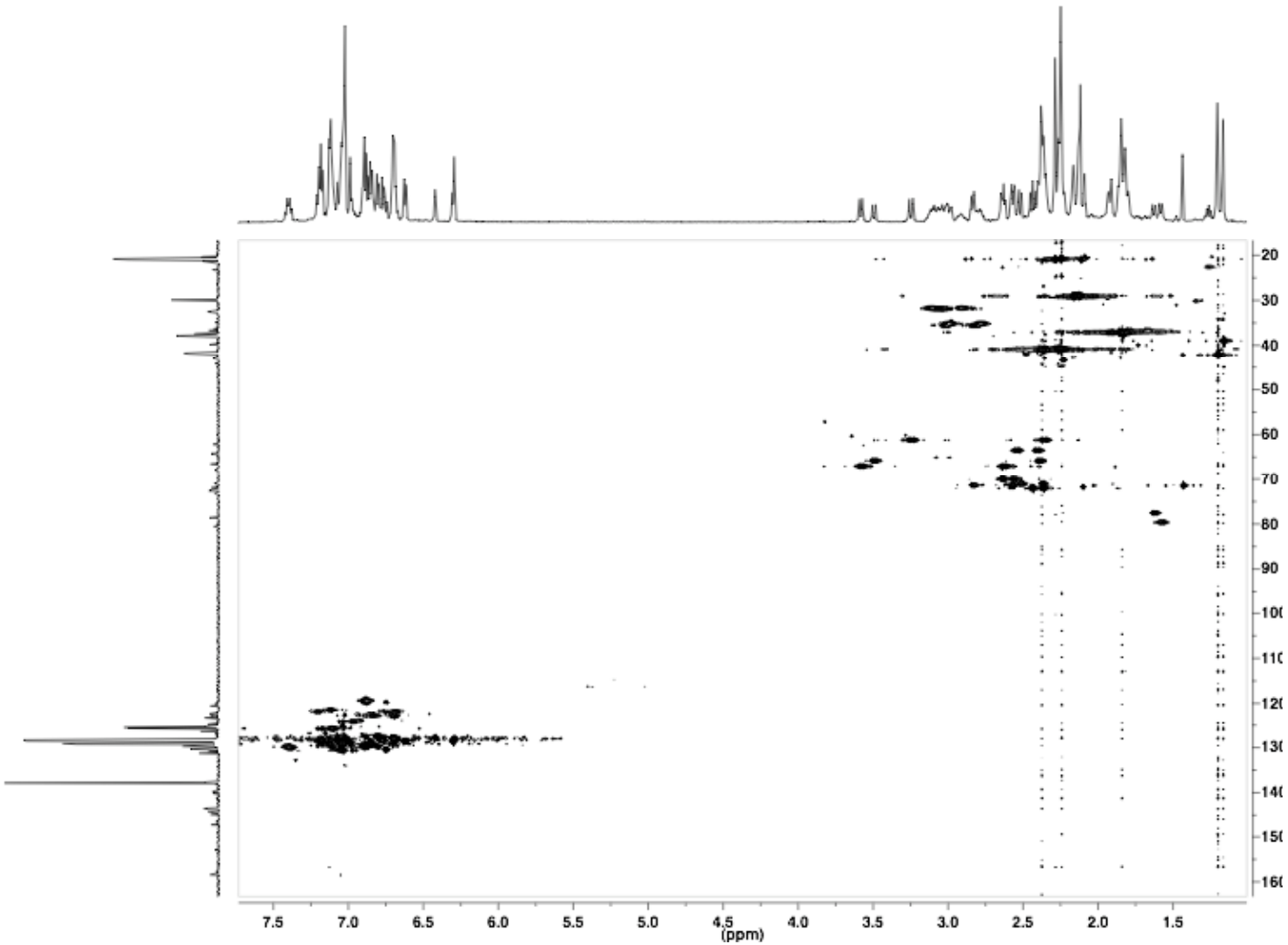

Figure 3.15. ^{1}H-^{13}C HSQC spectrum of *rac*-**Lig^{1}ZrBn$_{2}$-a,b** in toluene-d_8 at -10 °C.

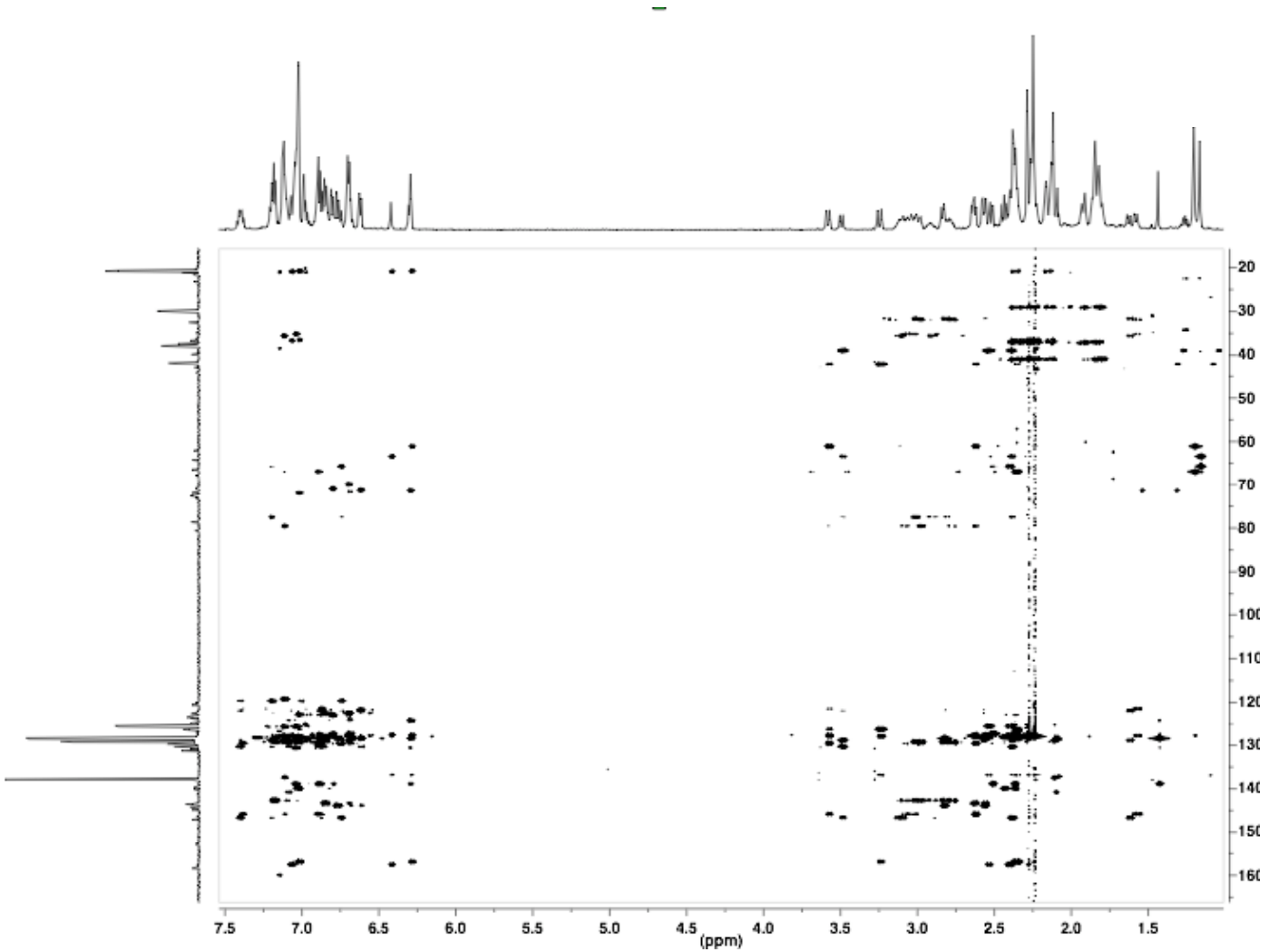

Figure 3.16. ^{1}H-^{13}C HMBC spectrum of *rac*-**Lig^{1}ZrBn$_2$-a,b** in toluene-d_8 at -10 °C.

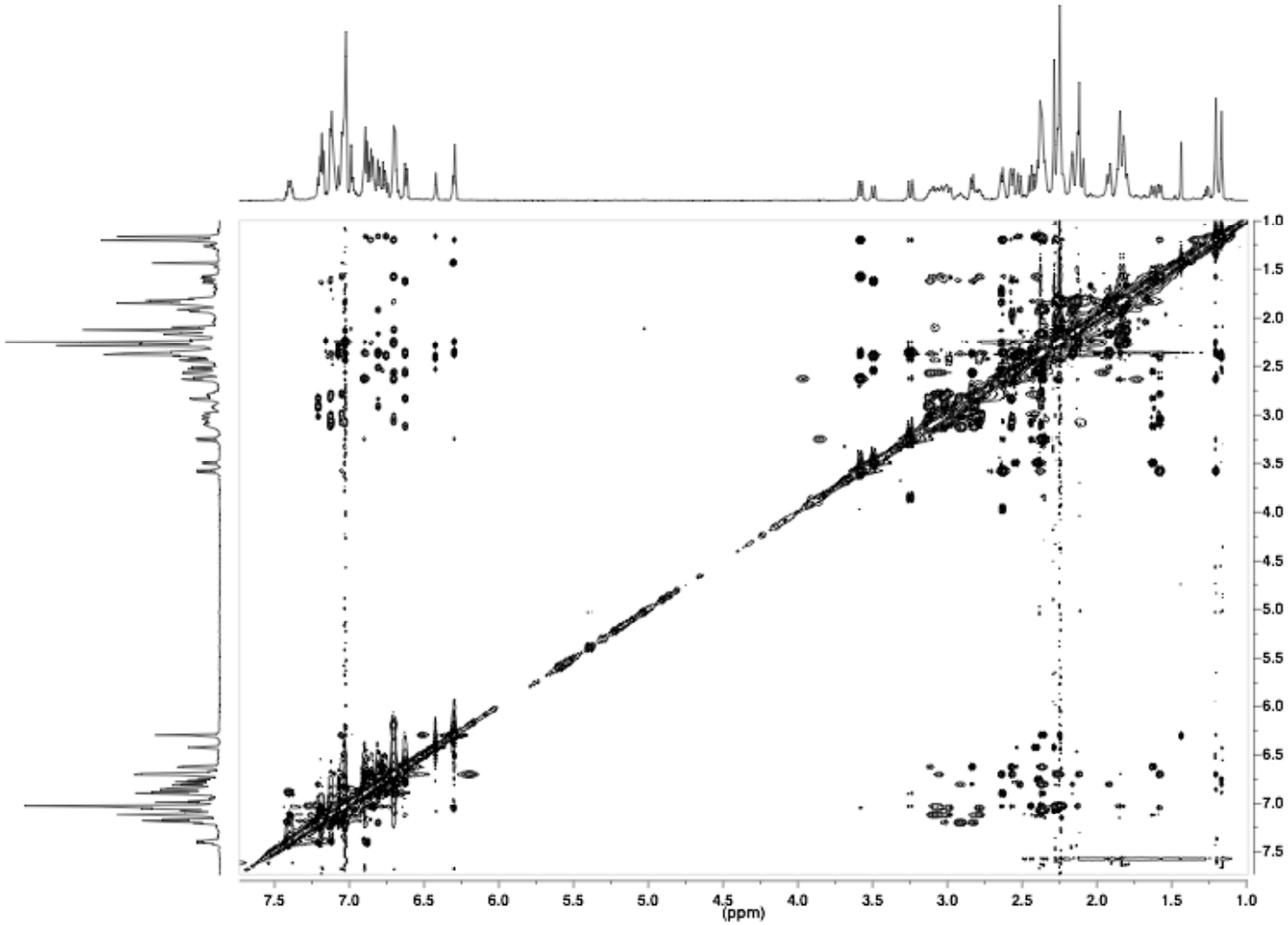

Figure 3.17. ROESY spectrum of *rac*-**Lig^{1}ZrBn$_2$-a,b** in toluene-d_8 at -10 °C.

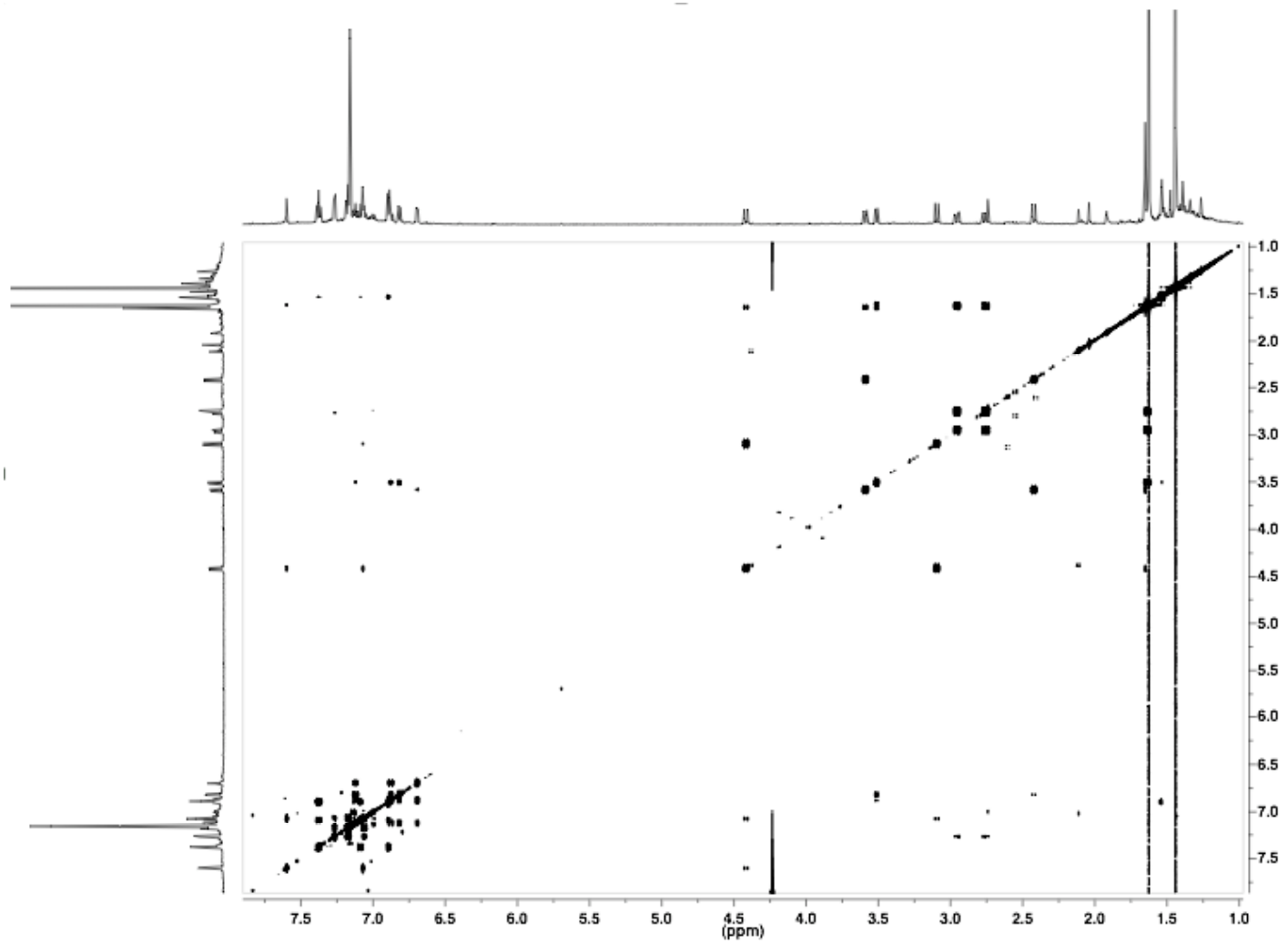

Figure 3.18. COSY spectrum of *rac*-**Lig^{2}TiBn** in C_6D_6 at 25 °C.

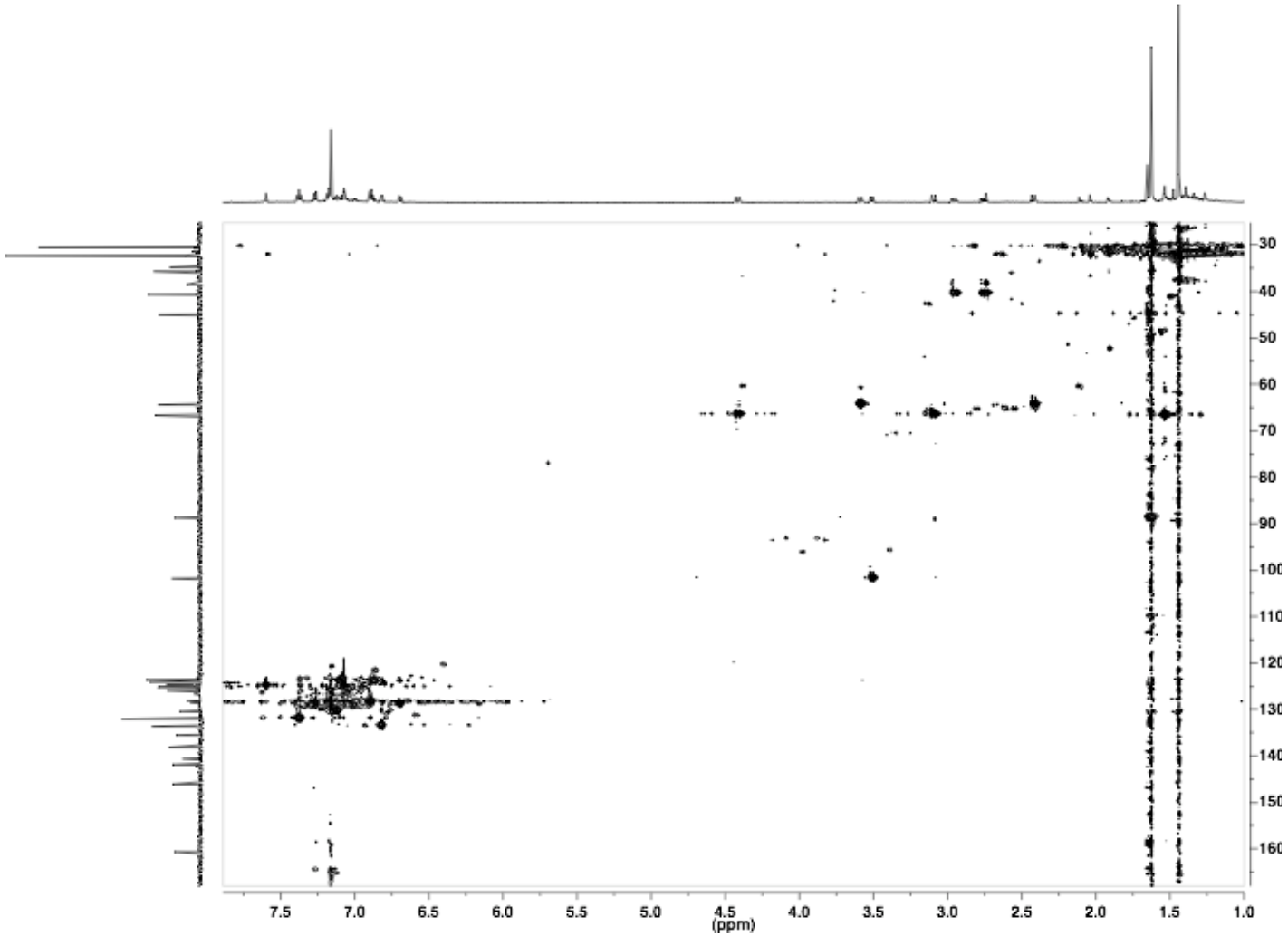

Figure 3.19. ^{1}H-^{13}C HSQC spectrum of *rac*-**Lig^{2}TiBn** in C_6D_6 at 25 °C.

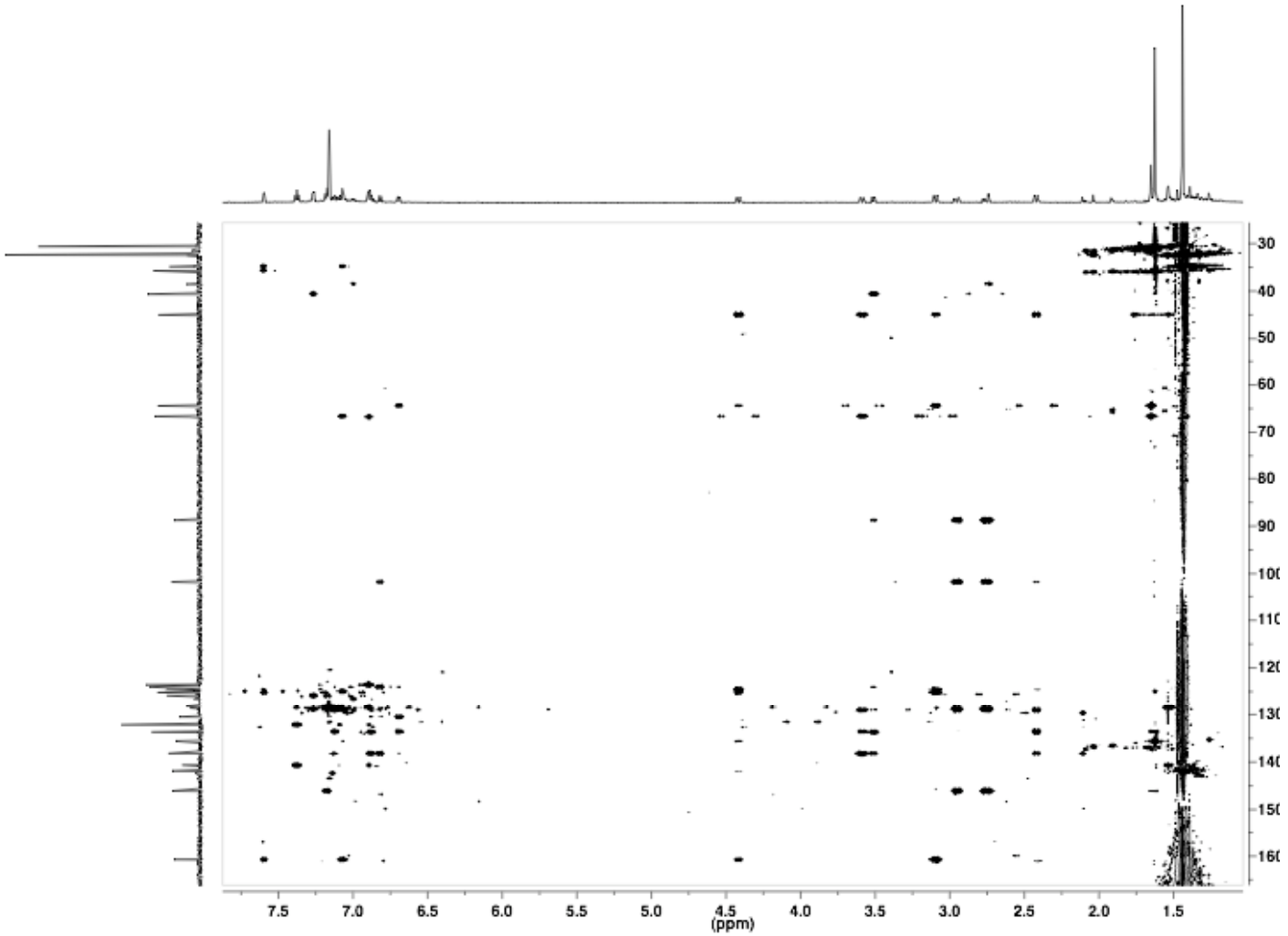

Figure 3.20. ^{1}H-^{13}C HMBC spectrum of *rac*-**Lig^{2}TiBn** in C_6D_6 at 25 °C.

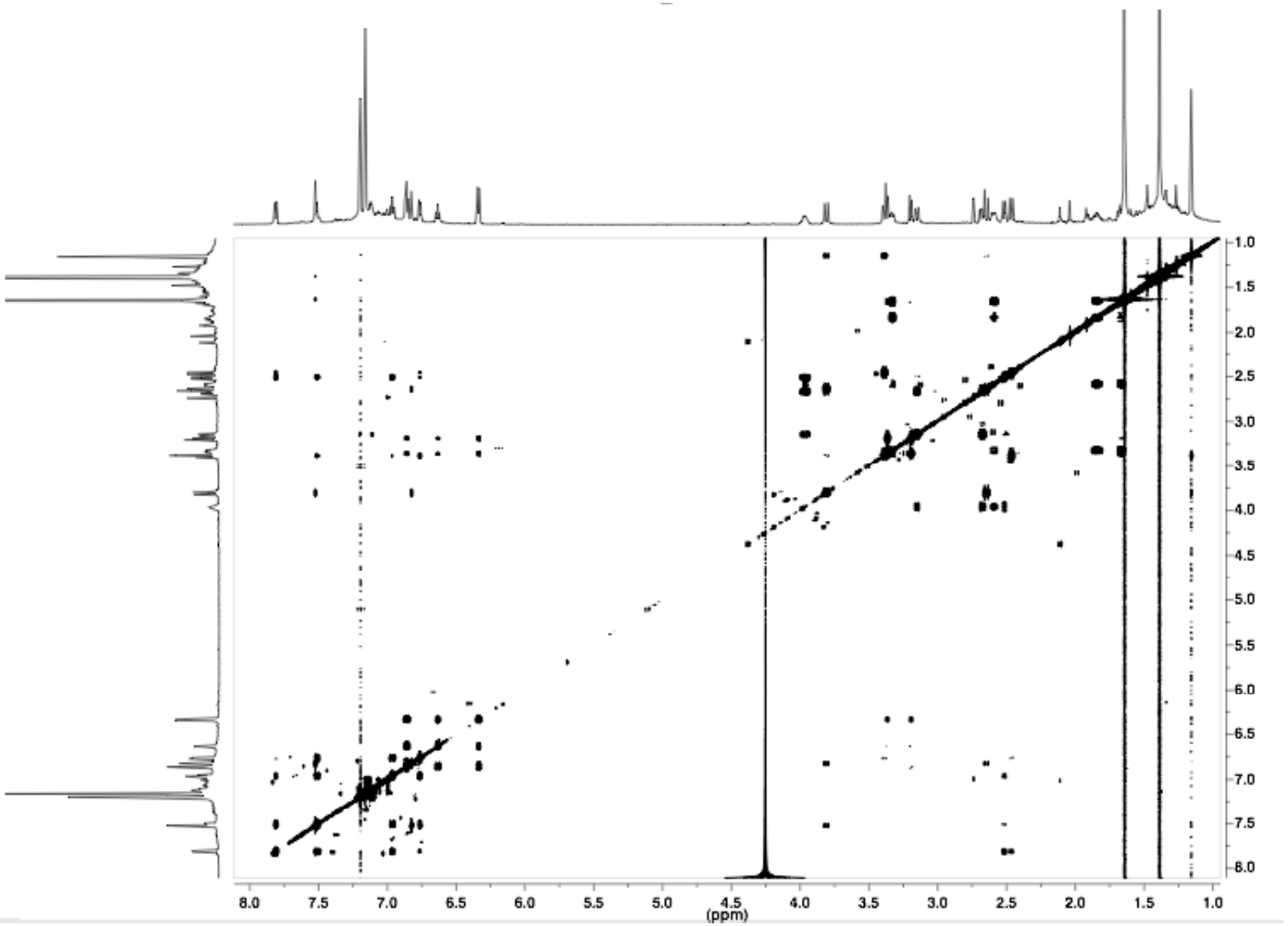

Figure 3.21. COSY spectrum of *rac*-**Lig^2(CH$_2$)$_2$TiBn** in C_6D_6 at 25 °C.

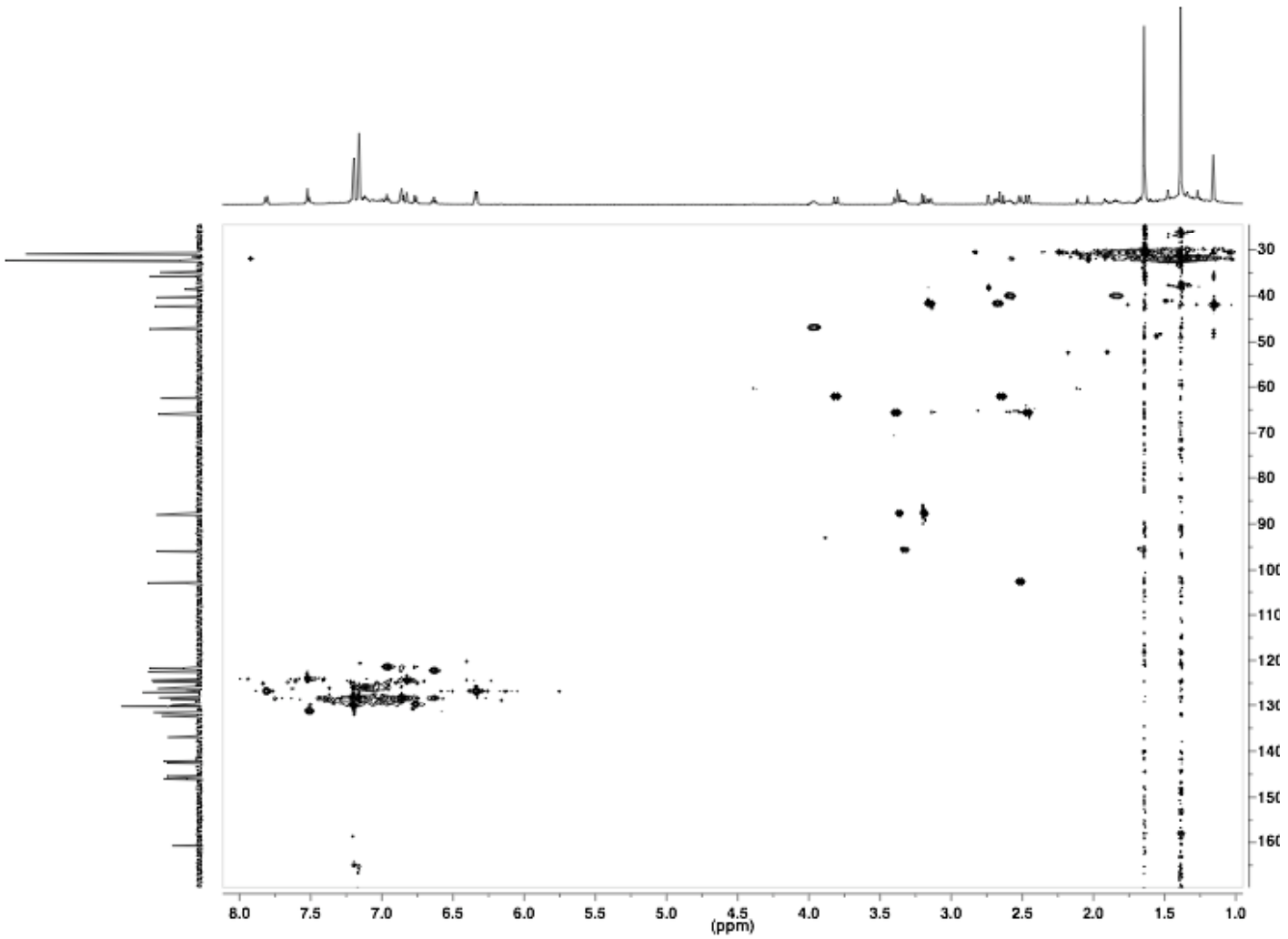

Figure 3.22. ^{1}H-^{13}C HSQC spectrum of *rac*-**Lig^{2}(CH$_2$)$_2$TiBn** in C_6D_6 at 25 °C.

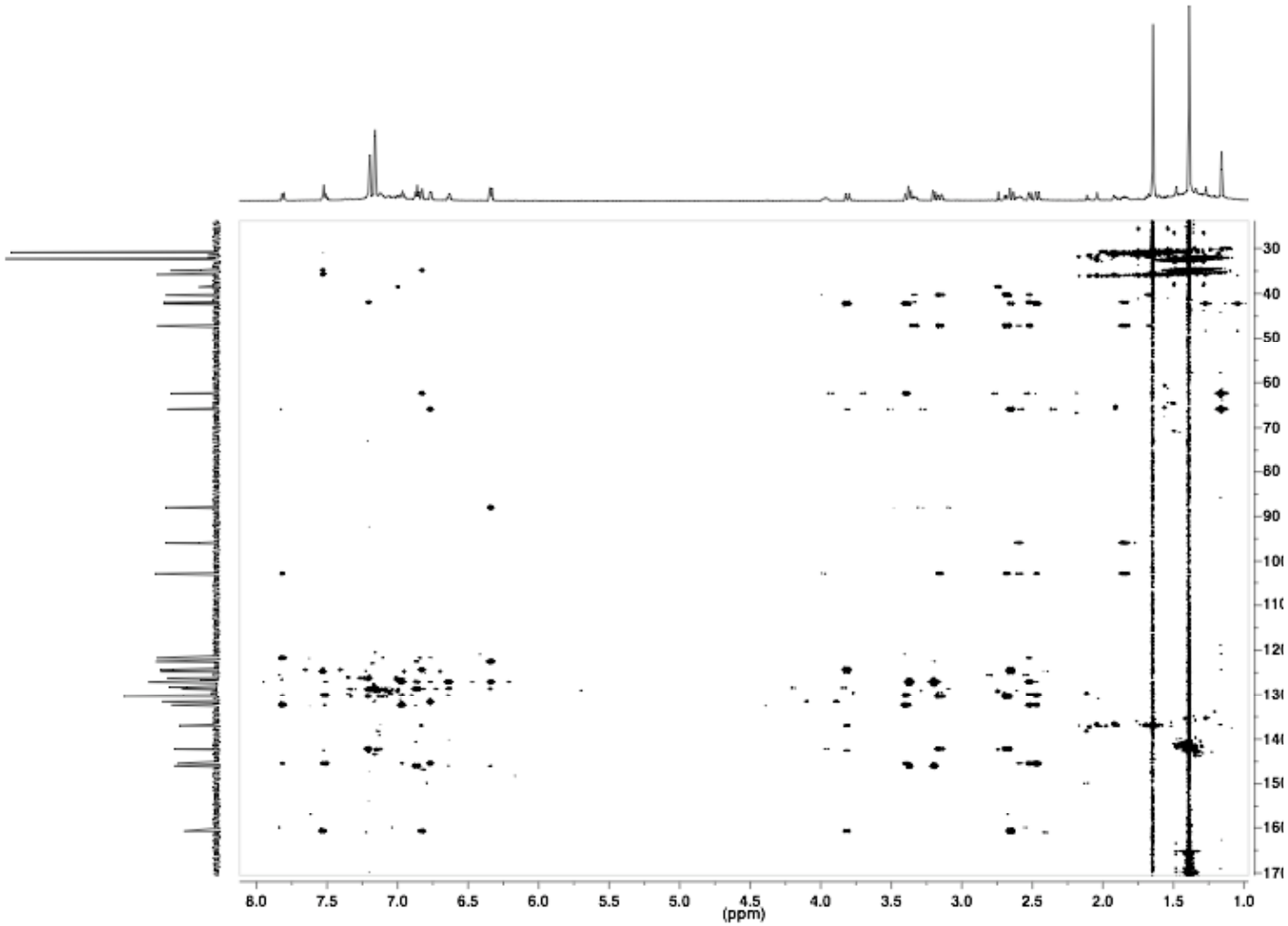

Figure 3.23. ^{1}H-^{13}C HMBC spectrum *rac*-**Lig^{2}(CH$_2$)$_2$TiBn** in C_6D_6 at 25 °C.

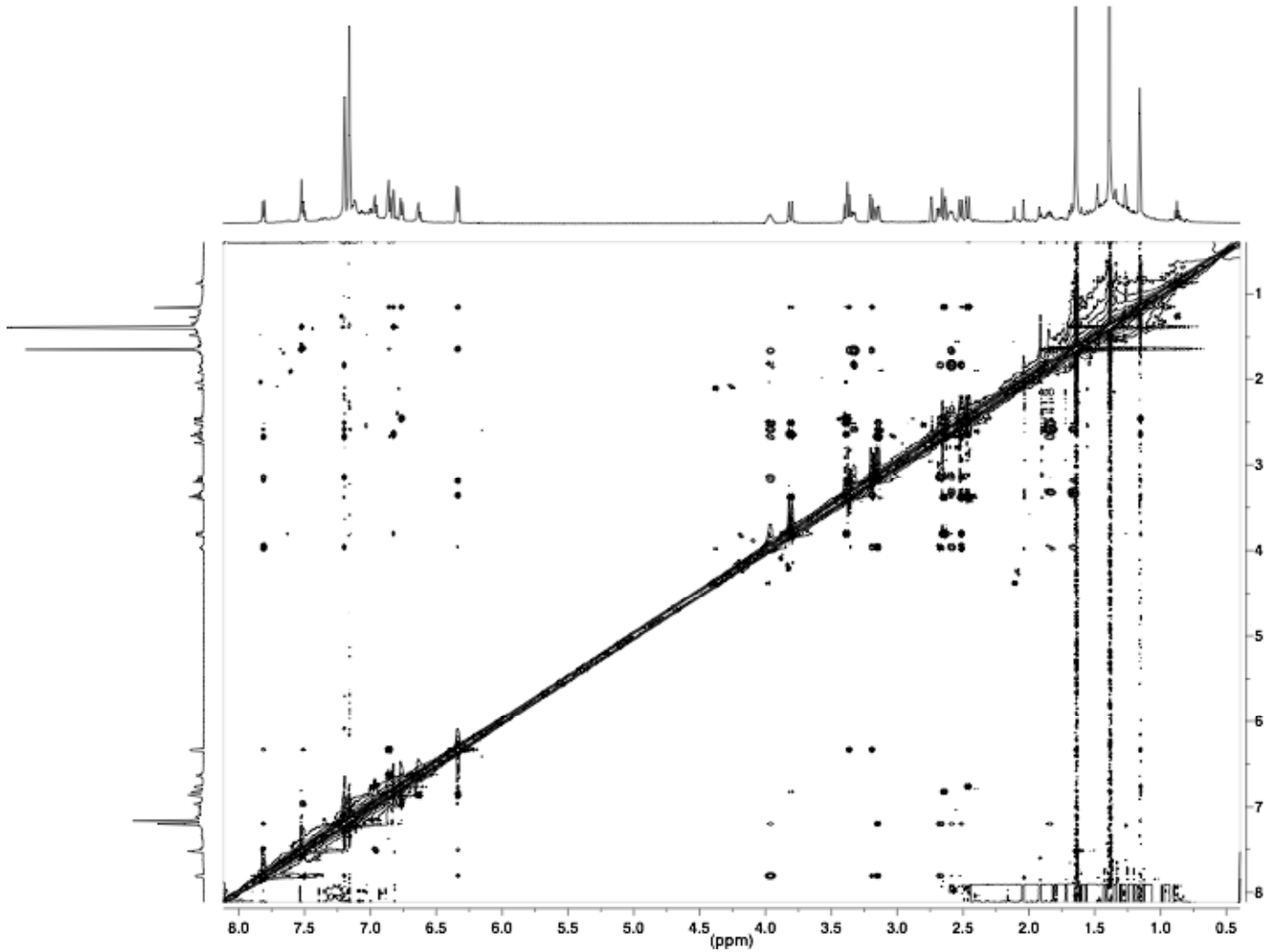

Figure 3.24. ROESY spectrum of *rac*-**Lig^2(CH$_2$)$_2$TiBn** in C_6D_6 at 50 °C.

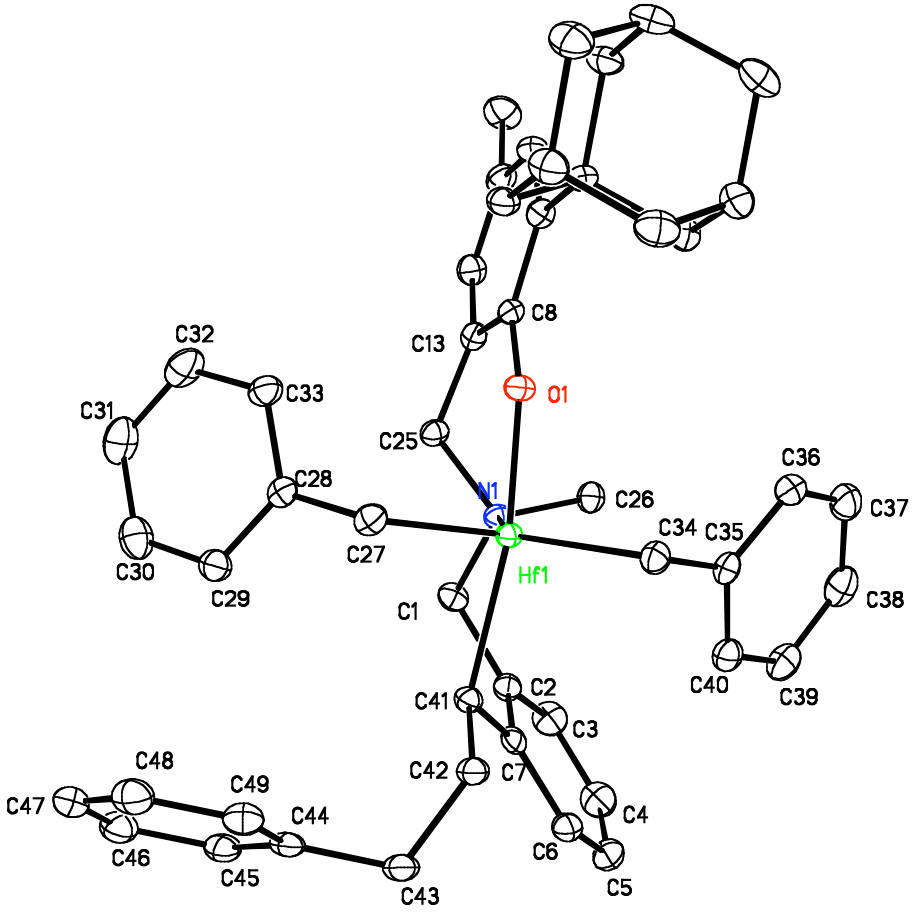

Figure 3.25. ORTEP diagram of *rac*-**Lig^{1}HfBn$_2$-a**. Thermal ellipsoids are drawn at the 40% probability level.

Table 3.10. Crystal data and structure refinement for *rac*-**Lig^{1}HfBn$_2$-a**.

Identification code	je9	
Empirical formula	$C_{49}H_{55}HfNO$	
Formula weight	852.43	
Temperature	173(2) K	
Wavelength	0.71073 Å	
Crystal system	Monoclinic	
Space group	P2(1)/c	
Unit cell dimensions	a = 14.5635(5) Å	α= 90°
	b = 25.1969(8) Å	β= 106.929(2)°
	c = 11.7742(4) Å	γ = 90°
Volume	4133.4(2) Å^3	
Z	4	
Density (calculated)	1.370 Mg/m^3	
Absorption coefficient	2.560 mm^{-1}	
F(000)	1744	
Crystal size	0.40 x 0.30 x 0.15 mm^3	
Theta range for data collection	1.98 to 29.75°	
Index ranges	-20<=h<=20, -34<=k<=35, -16<=l<=15	
Reflections collected	59156	
Independent reflections	11755 [R(int) = 0.0557]	
Completeness to theta = 29.75°	99.6 %	
Absorption correction	Semi-empirical from equivalents	
Max. and min. transmission	0.7001 and 0.4275	
Refinement method	Full-matrix least-squares on F^2	
Data / restraints / parameters	11755 / 0 / 471	
Goodness-of-fit on F^2	0.935	
Final R indices [I>2sigma(I)]	R1 = 0.0301, wR2 = 0.0669	
R indices (all data)	R1 = 0.0432, wR2 = 0.0709	
Largest diff. peak and hole	1.335 and -0.913 e.Å^{-3}	

Table 3.11. Atomic coordinates (x 10^4) and equivalent isotropic displacement parameters ($Å^2$ x 10^3) for *rac*-**Lig^{1}HfBn$_2$-a**. U(eq) is defined as one third of the trace of the orthogonalized U^{ij} tensor.

	x	y	z	U(eq)
Hf(1)	1294(1)	3672(1)	1539(1)	15(1)
O(1)	2673(1)	3554(1)	2252(1)	19(1)
N(1)	1410(1)	3680(1)	3564(2)	18(1)
C(1)	495(2)	3568(1)	3861(2)	21(1)
C(2)	-269(1)	3980(1)	3388(2)	21(1)
C(3)	-541(2)	4309(1)	4169(2)	29(1)
C(4)	-1240(2)	4689(1)	3776(2)	36(1)
C(5)	-1666(2)	4742(1)	2568(2)	32(1)
C(6)	-1399(2)	4417(1)	1783(2)	25(1)
C(7)	-693(1)	4025(1)	2153(2)	20(1)
C(8)	3395(1)	3442(1)	3248(2)	19(1)
C(9)	4370(2)	3461(1)	3284(2)	22(1)
C(10)	5031(2)	3369(1)	4390(2)	23(1)
C(11)	4776(2)	3274(1)	5415(2)	24(1)
C(12)	3812(2)	3240(1)	5324(2)	24(1)
C(13)	3117(1)	3314(1)	4247(2)	20(1)
C(14)	5529(2)	3219(1)	6603(2)	33(1)
C(15)	4685(2)	3581(1)	2182(2)	21(1)
C(16)	4229(1)	3185(1)	1175(2)	23(1)
C(17)	4519(2)	3318(1)	57(2)	27(1)
C(18)	5612(2)	3277(1)	344(2)	32(1)
C(19)	6080(2)	3670(1)	1323(2)	30(1)
C(20)	5768(2)	4233(1)	913(2)	32(1)
C(21)	4682(2)	4276(1)	631(2)	27(1)
C(22)	4203(2)	3879(1)	-340(2)	30(1)
C(23)	4379(2)	4146(1)	1735(2)	22(1)
C(24)	5776(2)	3545(1)	2427(2)	26(1)
C(25)	2082(1)	3237(1)	4147(2)	19(1)
C(26)	1821(2)	4186(1)	4126(2)	23(1)

Table 3.10. (Continued).

	x	y	z	U(eq)
C(27)	1153(2)	2927(1)	497(2)	23(1)
C(28)	1190(1)	2466(1)	1288(2)	18(1)
C(29)	361(2)	2219(1)	1391(2)	25(1)
C(30)	409(2)	1778(1)	2100(2)	33(1)
C(31)	1279(2)	1570(1)	2728(2)	36(1)
C(32)	2109(2)	1813(1)	2663(2)	34(1)
C(33)	2072(2)	2259(1)	1971(2)	25(1)
C(34)	1427(2)	4371(1)	436(2)	22(1)
C(35)	1477(2)	4809(1)	1280(2)	21(1)
C(36)	2341(2)	5066(1)	1890(2)	28(1)
C(37)	2367(2)	5450(1)	2733(2)	36(1)
C(38)	1546(2)	5594(1)	3005(2)	35(1)
C(39)	686(2)	5356(1)	2415(2)	30(1)
C(40)	657(2)	4972(1)	1569(2)	24(1)
C(41)	-342(1)	3688(1)	1341(2)	18(1)
C(42)	-896(2)	3745(1)	23(2)	22(1)
C(43)	-1913(2)	3503(1)	-368(2)	25(1)
C(44)	-1931(1)	2907(1)	-431(2)	21(1)
C(45)	-2214(2)	2603(1)	384(2)	25(1)
C(46)	-2235(2)	2055(1)	318(2)	30(1)
C(47)	-1979(2)	1800(1)	-575(2)	31(1)
C(48)	-1695(2)	2097(1)	-1391(2)	32(1)
C(49)	-1676(2)	2645(1)	-1327(2)	26(1)

Table 3.12. Bond lengths [Å] and angles [°] for *rac*-**Lig^{1}HfBn$_2$-a**.

Hf(1)-O(1)	1.9604(13)	C(18)-C(19)	1.522(3)
Hf(1)-C(27)	2.221(2)	C(19)-C(24)	1.523(3)
Hf(1)-C(34)	2.229(2)	C(19)-C(20)	1.525(3)
Hf(1)-C(41)	2.326(2)	C(20)-C(21)	1.523(3)
Hf(1)-N(1)	2.3411(17)	C(21)-C(23)	1.524(3)
O(1)-C(8)	1.357(2)	C(21)-C(22)	1.526(3)
N(1)-C(26)	1.481(2)	C(27)-C(28)	1.480(3)
N(1)-C(1)	1.500(3)	C(28)-C(29)	1.393(3)
N(1)-C(25)	1.511(2)	C(28)-C(33)	1.402(3)
C(1)-C(2)	1.504(3)	C(29)-C(30)	1.379(3)
C(2)-C(3)	1.380(3)	C(30)-C(31)	1.372(3)
C(2)-C(7)	1.409(3)	C(31)-C(32)	1.377(4)
C(3)-C(4)	1.376(3)	C(32)-C(33)	1.380(3)
C(4)-C(5)	1.382(3)	C(34)-C(35)	1.473(3)
C(5)-C(6)	1.374(3)	C(35)-C(40)	1.395(3)
C(6)-C(7)	1.399(3)	C(35)-C(36)	1.412(3)
C(7)-C(41)	1.478(3)	C(36)-C(37)	1.379(3)
C(8)-C(13)	1.389(3)	C(37)-C(38)	1.373(4)
C(8)-C(9)	1.408(3)	C(38)-C(39)	1.380(3)
C(9)-C(10)	1.395(3)	C(39)-C(40)	1.381(3)
C(9)-C(15)	1.527(3)	C(41)-C(42)	1.534(3)
C(10)-C(11)	1.384(3)	C(42)-C(43)	1.543(3)
C(11)-C(12)	1.379(3)	C(43)-C(44)	1.502(3)
C(11)-C(14)	1.512(3)	C(44)-C(45)	1.381(3)
C(12)-C(13)	1.386(3)	C(44)-C(49)	1.384(3)
C(13)-C(25)	1.490(3)	C(45)-C(46)	1.384(3)
C(15)-C(24)	1.534(3)	C(46)-C(47)	1.373(3)
C(15)-C(23)	1.538(3)	C(47)-C(48)	1.374(3)
C(15)-C(16)	1.545(3)	C(48)-C(49)	1.382(3)
C(16)-C(17)	1.532(3)		
C(17)-C(22)	1.518(3)	O(1)-Hf(1)-C(27)	91.51(7)
C(17)-C(18)	1.532(3)	O(1)-Hf(1)-C(34)	96.78(7)
		C(27)-Hf(1)-C(34)	110.82(8)
		O(1)-Hf(1)-C(41)	159.54(7)
		C(27)-Hf(1)-C(41)	91.79(7)

Table 3.12. (Continued).

C(34)-Hf(1)-C(41)	100.88(7)	C(11)-C(12)-C(13)	121.3(2)
O(1)-Hf(1)-N(1)	78.70(6)	C(12)-C(13)-C(8)	119.33(19)
C(27)-Hf(1)-N(1)	122.50(7)	C(12)-C(13)-C(25)	120.53(19)
C(34)-Hf(1)-N(1)	126.49(6)	C(8)-C(13)-C(25)	120.09(17)
C(41)-Hf(1)-N(1)	82.51(6)	C(9)-C(15)-C(24)	112.27(17)
C(8)-O(1)-Hf(1)	147.27(13)	C(9)-C(15)-C(23)	110.22(17)
C(26)-N(1)-C(1)	109.19(16)	C(24)-C(15)-C(23)	107.49(17)
C(26)-N(1)-C(25)	108.07(15)	C(9)-C(15)-C(16)	110.86(17)
C(1)-N(1)-C(25)	104.94(15)	C(24)-C(15)-C(16)	107.22(17)
C(26)-N(1)-Hf(1)	111.20(12)	C(23)-C(15)-C(16)	108.64(16)
C(1)-N(1)-Hf(1)	115.49(12)	C(17)-C(16)-C(15)	110.69(17)
C(25)-N(1)-Hf(1)	107.51(12)	C(22)-C(17)-C(16)	109.54(18)
N(1)-C(1)-C(2)	113.32(17)	C(22)-C(17)-C(18)	109.46(19)
C(3)-C(2)-C(7)	120.95(19)	C(16)-C(17)-C(18)	108.90(17)
C(3)-C(2)-C(1)	119.53(18)	C(19)-C(18)-C(17)	109.30(19)
C(7)-C(2)-C(1)	119.52(18)	C(18)-C(19)-C(24)	109.55(19)
C(4)-C(3)-C(2)	121.4(2)	C(18)-C(19)-C(20)	109.83(19)
C(5)-C(4)-C(3)	118.7(2)	C(24)-C(19)-C(20)	109.20(19)
C(6)-C(5)-C(4)	120.3(2)	C(21)-C(20)-C(19)	109.23(18)
C(5)-C(6)-C(7)	122.5(2)	C(20)-C(21)-C(23)	109.87(17)
C(6)-C(7)-C(2)	116.14(19)	C(20)-C(21)-C(22)	109.62(19)
C(6)-C(7)-C(41)	124.42(18)	C(23)-C(21)-C(22)	108.41(18)
C(2)-C(7)-C(41)	119.35(18)	C(17)-C(22)-C(21)	110.38(18)
O(1)-C(8)-C(13)	115.80(18)	C(21)-C(23)-C(15)	111.27(18)
O(1)-C(8)-C(9)	122.71(18)	C(19)-C(24)-C(15)	111.70(17)
C(13)-C(8)-C(9)	121.49(18)	C(13)-C(25)-N(1)	116.45(16)
C(10)-C(9)-C(8)	116.01(19)	C(28)-C(27)-Hf(1)	109.61(13)
C(10)-C(9)-C(15)	122.00(19)	C(29)-C(28)-C(33)	117.18(19)
C(8)-C(9)-C(15)	121.99(17)	C(29)-C(28)-C(27)	122.08(18)
C(11)-C(10)-C(9)	123.7(2)	C(33)-C(28)-C(27)	120.74(19)
C(12)-C(11)-C(10)	117.94(18)	C(30)-C(29)-C(28)	121.3(2)
C(12)-C(11)-C(14)	120.9(2)	C(31)-C(30)-C(29)	120.7(2)
C(10)-C(11)-C(14)	121.1(2)	C(30)-C(31)-C(32)	119.1(2)
		C(31)-C(32)-C(33)	120.8(2)
		C(32)-C(33)-C(28)	120.8(2)

Table 3.12. (Continued).

C(35)-C(34)-Hf(1)	101.17(13)
C(40)-C(35)-C(36)	116.1(2)
C(40)-C(35)-C(34)	120.56(19)
C(36)-C(35)-C(34)	123.2(2)
C(37)-C(36)-C(35)	121.4(2)
C(38)-C(37)-C(36)	120.7(2)
C(37)-C(38)-C(39)	119.5(2)
C(40)-C(39)-C(38)	120.0(2)
C(39)-C(40)-C(35)	122.3(2)
C(7)-C(41)-C(42)	114.93(17)
C(7)-C(41)-Hf(1)	118.83(13)
C(42)-C(41)-Hf(1)	108.95(14)
C(41)-C(42)-C(43)	116.19(18)
C(44)-C(43)-C(42)	114.27(17)
C(45)-C(44)-C(49)	117.8(2)
C(45)-C(44)-C(43)	121.59(19)
C(49)-C(44)-C(43)	120.6(2)
C(44)-C(45)-C(46)	121.4(2)
C(47)-C(46)-C(45)	120.3(2)
C(48)-C(47)-C(46)	118.9(2)
C(47)-C(48)-C(49)	120.8(2)
C(48)-C(49)-C(44)	120.8(2)

Table 3.13. Anisotropic displacement parameters ($Å^2 x\ 10^3$) for *rac*-**Lig^{1}HfBn$_2$-a**. The anisotropic displacement factor exponent takes the form: $-2p^2[h^2\ a^{*2}U^{11} + ...\ + 2\ h\ k\ a^*\ b^*\ U^{12}\ ]$

	U^{11}	U^{22}	U^{33}	U^{23}	U^{13}	U^{12}
Hf(1)	14(1)	16(1)	16(1)	1(1)	5(1)	1(1)
O(1)	15(1)	24(1)	18(1)	3(1)	5(1)	1(1)
N(1)	16(1)	20(1)	18(1)	1(1)	6(1)	1(1)
C(1)	20(1)	26(1)	20(1)	2(1)	10(1)	-2(1)
C(2)	19(1)	21(1)	27(1)	0(1)	10(1)	0(1)
C(3)	30(1)	33(1)	29(1)	-7(1)	17(1)	0(1)
C(4)	32(1)	33(1)	47(1)	-15(1)	19(1)	2(1)
C(5)	26(1)	23(1)	50(1)	-4(1)	15(1)	5(1)
C(6)	19(1)	22(1)	33(1)	-3(1)	7(1)	1(1)
C(7)	16(1)	18(1)	28(1)	-1(1)	10(1)	-4(1)
C(8)	16(1)	16(1)	22(1)	0(1)	3(1)	1(1)
C(9)	21(1)	19(1)	25(1)	-2(1)	8(1)	1(1)
C(10)	17(1)	25(1)	25(1)	2(1)	2(1)	2(1)
C(11)	24(1)	23(1)	23(1)	2(1)	1(1)	4(1)
C(12)	26(1)	24(1)	22(1)	3(1)	8(1)	0(1)
C(13)	21(1)	17(1)	23(1)	2(1)	7(1)	1(1)

Table 3.13. (Continued).

	U^{11}	U^{22}	U^{33}	U^{23}	U^{13}	U^{12}
C(14)	27(1)	42(1)	24(1)	3(1)	-3(1)	-2(1)
C(15)	15(1)	21(1)	24(1)	1(1)	3(1)	3(1)
C(16)	17(1)	23(1)	29(1)	-6(1)	8(1)	0(1)
C(17)	23(1)	32(1)	26(1)	-6(1)	7(1)	-2(1)
C(18)	28(1)	39(1)	33(1)	-4(1)	15(1)	0(1)
C(19)	16(1)	43(1)	33(1)	-2(1)	9(1)	-1(1)
C(20)	25(1)	41(1)	32(1)	2(1)	12(1)	-9(1)
C(21)	25(1)	26(1)	32(1)	4(1)	10(1)	-2(1)
C(22)	26(1)	41(1)	25(1)	1(1)	10(1)	1(1)
C(23)	22(1)	20(1)	24(1)	0(1)	6(1)	0(1)
C(24)	16(1)	32(1)	29(1)	-2(1)	4(1)	-1(1)
C(25)	19(1)	21(1)	18(1)	4(1)	6(1)	3(1)
C(26)	26(1)	20(1)	23(1)	-2(1)	8(1)	-1(1)
C(27)	23(1)	22(1)	22(1)	0(1)	6(1)	3(1)
C(28)	21(1)	19(1)	14(1)	-4(1)	4(1)	2(1)
C(29)	22(1)	25(1)	26(1)	-6(1)	7(1)	0(1)
C(30)	40(1)	30(1)	33(1)	-2(1)	17(1)	-7(1)
C(31)	56(2)	27(1)	23(1)	7(1)	10(1)	0(1)
C(32)	40(1)	32(1)	23(1)	2(1)	-4(1)	10(1)
C(33)	23(1)	25(1)	25(1)	-3(1)	2(1)	4(1)
C(34)	24(1)	19(1)	22(1)	3(1)	6(1)	0(1)
C(35)	25(1)	17(1)	23(1)	5(1)	6(1)	2(1)
C(36)	23(1)	22(1)	37(1)	1(1)	4(1)	1(1)
C(37)	33(1)	25(1)	41(1)	0(1)	-2(1)	-4(1)
C(38)	47(2)	24(1)	32(1)	-1(1)	8(1)	4(1)
C(39)	37(1)	27(1)	28(1)	5(1)	13(1)	7(1)
C(40)	26(1)	23(1)	24(1)	6(1)	7(1)	1(1)
C(41)	15(1)	20(1)	20(1)	2(1)	5(1)	-1(1)
C(42)	16(1)	23(1)	25(1)	3(1)	5(1)	2(1)
C(43)	17(1)	28(1)	26(1)	-2(1)	2(1)	4(1)
C(44)	13(1)	27(1)	23(1)	-4(1)	3(1)	3(1)
C(45)	17(1)	31(1)	28(1)	-3(1)	8(1)	3(1)
C(46)	20(1)	33(1)	37(1)	6(1)	10(1)	0(1)

Table 3.13. (Continued).

	U^{11}	U^{22}	U^{33}	U^{23}	U^{13}	U^{12}
C(47)	20(1)	29(1)	39(1)	-2(1)	1(1)	0(1)
C(48)	26(1)	37(1)	29(1)	-10(1)	3(1)	4(1)
C(49)	22(1)	34(1)	22(1)	1(1)	4(1)	2(1)

Table 3.14. Hydrogen coordinates (x 10^4) and isotropic displacement parameters (Å^{2}x 10^3) for *rac*-**Lig^{1}HfBn$_2$-a**.

	x	y	z	U(eq)
H(1A)	634	3549	4734	25
H(1B)	246	3218	3531	25
H(3A)	-239	4272	4997	35
H(4A)	-1427	4910	4323	43
H(5A)	-2144	5005	2280	38
H(6A)	-1704	4459	957	30
H(10A)	5694	3373	4442	28
H(12A)	3621	3164	6012	28
H(14A)	5220	3119	7209	50
H(14B)	5866	3557	6820	50
H(14C)	5990	2943	6551	50
H(16A)	4442	2820	1439	27
H(16B)	3521	3197	991	27
H(17A)	4207	3062	-590	32
H(18A)	5822	2911	606	39
H(18B)	5809	3356	-375	39
H(19A)	6794	3641	1516	36
H(20A)	6081	4489	1544	38
H(20B)	5965	4318	197	38
H(21A)	4473	4644	358	33
H(22A)	3497	3907	-522	36
H(22B)	4379	3963	-1071	36
H(23A)	3673	4179	1547	27
H(23B)	4674	4405	2369	27
H(24A)	6091	3797	3066	31

Table 3.14. (Continued).

	x	y	z	U(eq)
H(24B)	5993	3183	2706	31
H(25A)	2022	3182	4955	23
H(25B)	1863	2906	3692	23
H(26A)	1374	4477	3801	34
H(26B)	2433	4253	3964	34
H(26C)	1926	4164	4986	34
H(27A)	536	2927	-143	27
H(27B)	1680	2902	126	27
H(29A)	-249	2357	964	29
H(30A)	-166	1617	2154	40
H(31A)	1309	1262	3202	43
H(32A)	2714	1673	3099	41
H(33A)	2651	2429	1957	30
H(34A)	2016	4351	180	26
H(34B)	861	4405	-272	26
H(36A)	2918	4972	1716	34
H(37A)	2958	5616	3130	43
H(38A)	1571	5856	3594	41
H(39A)	114	5457	2592	35
H(40A)	59	4813	1170	29
H(41A)	-488	3318	1544	22
H(42A)	-513	3577	-450	26
H(42B)	-948	4127	-177	26
H(43A)	-2262	3618	195	30
H(43B)	-2261	3646	-1160	30
H(45A)	-2398	2775	1003	30
H(46A)	-2427	1854	893	36
H(47A)	-1999	1424	-627	37
H(48A)	-1509	1924	-2006	38
H(49A)	-1486	2844	-1906	32

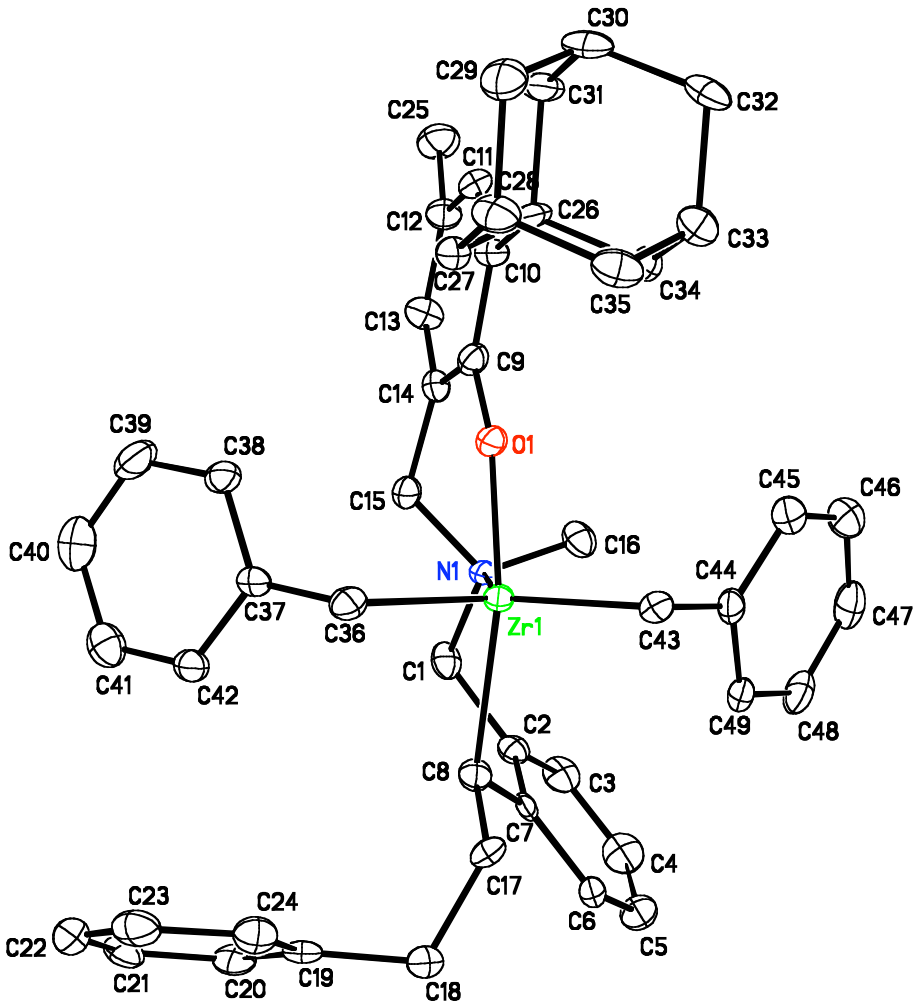

Figure 3.26. ORTEP diagram of *rac*-**Lig^{1}ZrBn$_2$-a**. Thermal ellipsoids are drawn at the 40% probability level.

Table 3.15. Crystal data and structure refinement for *rac*-**Lig^{1}ZrBn$_2$-a**.

Identification code	je13	
Empirical formula	$C_{49}H_{55}NOZr$	
Formula weight	765.16	
Temperature	173(2) K	
Wavelength	0.71073 Å	
Crystal system	Monoclinic	
Space group	P2(1)/c	
Unit cell dimensions	a = 14.6133(12) Å	α= 90°
	b = 25.2865(18) Å	β= 106.807(2)°
	c = 11.8357(9) Å	γ = 90°
Volume	4186.7(6) Å^3	
Z	4	
Density (calculated)	1.214 Mg/m^3	
Absorption coefficient	0.298 mm^{-1}	
F(000)	1616	
Crystal size	0.15 x 0.03 x 0.02 mm^3	
Theta range for data collection	1.66 to 23.26°	
Index ranges	-16<=h<=16, -25<=k<=28, -13<=l<=13	
Reflections collected	28357	
Independent reflections	6013 [R(int) = 0.1242]	
Completeness to theta = 23.26°	100.0 %	
Absorption correction	Semi-empirical from equivalents	
Max. and min. transmission	0.9941 and 0.9567	
Refinement method	Full-matrix least-squares on F^2	
Data / restraints / parameters	6013 / 0 / 469	
Goodness-of-fit on F^2	0.954	
Final R indices [I>2sigma(I)]	R1 = 0.0591, wR2 = 0.1224	
R indices (all data)	R1 = 0.1054, wR2 = 0.1389	
Largest diff. peak and hole	0.415 and -0.485 e.Å^{-3}	

Table 3.16. Atomic coordinates (x 10^4) and equivalent isotropic displacement parameters ($Å^2$x 10^3) for *rac*-**Lig^{1}ZrBn$_2$-a**. U(eq) is defined as one third of the trace of the orthogonalized U^{ij} tensor.

	x	y	z	U(eq)
Zr(1)	3697(1)	3677(1)	3485(1)	19(1)
O(1)	2315(2)	3556(1)	2754(2)	22(1)
N(1)	3578(2)	3680(1)	1436(3)	19(1)
C(1)	4496(3)	3570(2)	1136(4)	26(1)
C(2)	5263(3)	3980(2)	1614(4)	22(1)
C(3)	5538(3)	4308(2)	843(4)	30(1)
C(4)	6234(3)	4696(2)	1237(4)	41(1)
C(5)	6658(3)	4740(2)	2435(4)	37(1)
C(6)	6392(3)	4415(2)	3226(4)	27(1)
C(7)	5680(3)	4024(2)	2832(4)	21(1)
C(8)	5341(3)	3690(2)	3658(4)	23(1)
C(9)	1597(3)	3445(2)	1752(4)	22(1)
C(10)	622(3)	3461(2)	1719(4)	25(1)
C(11)	-32(3)	3368(2)	626(4)	26(1)
C(12)	223(3)	3264(2)	-391(4)	28(1)
C(13)	1185(3)	3234(2)	-313(4)	32(1)
C(14)	1874(3)	3316(2)	757(4)	25(1)
C(15)	2917(3)	3240(2)	867(4)	26(1)
C(16)	3167(3)	4190(2)	873(4)	29(1)
C(17)	5888(3)	3742(2)	4974(4)	23(1)
C(18)	6901(3)	3502(2)	5380(4)	30(1)
C(19)	6921(3)	2902(2)	5442(4)	24(1)
C(20)	7203(3)	2596(2)	4614(4)	27(1)
C(21)	7226(3)	2050(2)	4691(4)	32(1)
C(22)	6978(3)	1796(2)	5581(4)	35(1)
C(23)	6702(3)	2098(2)	6409(4)	35(1)
C(24)	6663(3)	2648(2)	6338(4)	28(1)
C(25)	-530(3)	3218(2)	-1582(4)	40(1)
C(26)	310(3)	3582(2)	2826(4)	24(1)
C(27)	764(3)	3191(2)	3847(4)	26(1)

Table 3.16. (Continued).

	x	y	z	U(eq)
C(28)	458(3)	3319(2)	4941(4)	31(1)
C(29)	-620(3)	3275(2)	4651(4)	35(1)
C(30)	-1080(3)	3673(2)	3678(4)	35(1)
C(31)	-793(3)	3546(2)	2577(4)	31(1)
C(32)	-787(3)	4237(2)	4095(4)	34(1)
C(33)	308(3)	4275(2)	4373(4)	33(1)
C(34)	614(3)	4146(2)	3259(4)	27(1)
C(35)	782(3)	3878(2)	5336(4)	33(1)
C(36)	3845(3)	2913(2)	4515(4)	27(1)
C(37)	3798(3)	2462(2)	3707(3)	19(1)
C(38)	2928(3)	2254(2)	3031(4)	27(1)
C(39)	2885(3)	1812(2)	2343(4)	40(1)
C(40)	3720(4)	1568(2)	2277(4)	41(1)
C(41)	4591(3)	1779(2)	2911(4)	36(1)
C(42)	4632(3)	2211(2)	3604(4)	27(1)
C(43)	3555(3)	4379(2)	4599(4)	27(1)
C(44)	3508(3)	4813(2)	3734(4)	23(1)
C(45)	2647(3)	5072(2)	3119(4)	35(1)
C(46)	2622(3)	5449(2)	2263(5)	43(2)
C(47)	3443(3)	5585(2)	1992(4)	37(1)
C(48)	4303(3)	5349(2)	2580(4)	34(1)
C(49)	4325(3)	4972(2)	3425(4)	28(1)

Table 3.17. Bond lengths [Å] and angles [°] for *rac*-**Lig^{1}ZrBn$_2$-a**.

Zr(1)-O(1)	1.977(2)
Zr(1)-C(43)	2.257(4)
Zr(1)-C(36)	2.260(4)
Zr(1)-C(8)	2.351(4)
Zr(1)-N(1)	2.381(3)
O(1)-C(9)	1.366(4)
N(1)-C(16)	1.495(5)
N(1)-C(15)	1.500(5)
N(1)-C(1)	1.509(5)
C(1)-C(2)	1.511(6)
C(2)-C(3)	1.377(6)
C(2)-C(7)	1.398(6)
C(3)-C(4)	1.393(6)
C(4)-C(5)	1.378(6)
C(5)-C(6)	1.383(6)
C(6)-C(7)	1.414(5)
C(7)-C(8)	1.482(6)
C(8)-C(17)	1.538(5)
C(9)-C(14)	1.390(6)
C(9)-C(10)	1.415(5)
C(10)-C(11)	1.388(5)
C(10)-C(26)	1.537(6)
C(11)-C(12)	1.384(6)
C(12)-C(13)	1.385(6)
C(12)-C(25)	1.521(6)
C(13)-C(14)	1.387(6)
C(14)-C(15)	1.504(5)
C(17)-C(18)	1.544(5)
C(18)-C(19)	1.518(6)
C(19)-C(24)	1.383(6)
C(19)-C(20)	1.400(6)
C(20)-C(21)	1.384(6)
C(21)-C(22)	1.369(6)
C(22)-C(23)	1.391(7)
C(23)-C(24)	1.393(6)
C(26)-C(34)	1.537(6)
C(26)-C(31)	1.556(5)
C(26)-C(27)	1.554(6)
C(27)-C(28)	1.523(6)
C(28)-C(29)	1.516(6)
C(28)-C(35)	1.521(6)
C(29)-C(30)	1.531(6)
C(30)-C(31)	1.514(6)
C(30)-C(32)	1.529(6)
C(32)-C(33)	1.541(6)
C(33)-C(35)	1.527(6)
C(33)-C(34)	1.545(6)
C(36)-C(37)	1.478(6)
C(37)-C(38)	1.395(5)
C(37)-C(42)	1.410(6)
C(38)-C(39)	1.373(6)
C(39)-C(40)	1.391(7)
C(40)-C(41)	1.384(6)
C(41)-C(42)	1.357(6)
C(43)-C(44)	1.489(6)
C(44)-C(49)	1.405(6)
C(44)-C(45)	1.418(6)
C(45)-C(46)	1.384(7)
C(46)-C(47)	1.373(7)
C(47)-C(48)	1.383(6)
C(48)-C(49)	1.375(6)
O(1)-Zr(1)-C(43)	97.02(13)
O(1)-Zr(1)-C(36)	91.72(13)
C(43)-Zr(1)-C(36)	111.58(16)
O(1)-Zr(1)-C(8)	158.22(13)
C(43)-Zr(1)-C(8)	101.70(15)

Table 3.17. (Continued).

C(36)-Zr(1)-C(8)	91.65(15)
O(1)-Zr(1)-N(1)	77.91(11)
C(43)-Zr(1)-N(1)	126.91(14)
C(36)-Zr(1)-N(1)	121.31(14)
C(8)-Zr(1)-N(1)	81.97(12)
C(9)-O(1)-Zr(1)	147.4(3)
C(16)-N(1)-C(15)	108.4(3)
C(16)-N(1)-C(1)	108.9(3)
C(15)-N(1)-C(1)	105.1(3)
C(16)-N(1)-Zr(1)	111.0(2)
C(15)-N(1)-Zr(1)	107.6(2)
C(1)-N(1)-Zr(1)	115.5(2)
N(1)-C(1)-C(2)	113.5(3)
C(3)-C(2)-C(7)	120.8(4)
C(3)-C(2)-C(1)	119.5(4)
C(7)-C(2)-C(1)	119.7(4)
C(2)-C(3)-C(4)	121.8(4)
C(5)-C(4)-C(3)	118.0(4)
C(6)-C(5)-C(4)	121.2(4)
C(5)-C(6)-C(7)	121.1(4)
C(2)-C(7)-C(6)	117.1(4)
C(2)-C(7)-C(8)	120.4(3)
C(6)-C(7)-C(8)	122.4(4)
C(7)-C(8)-C(17)	116.3(3)
C(7)-C(8)-Zr(1)	118.6(3)
C(17)-C(8)-Zr(1)	107.9(3)
O(1)-C(9)-C(14)	116.4(4)
O(1)-C(9)-C(10)	122.2(4)
C(14)-C(9)-C(10)	121.4(4)
C(11)-C(10)-C(9)	116.0(4)
C(11)-C(10)-C(26)	122.3(4)
C(9)-C(10)-C(26)	121.7(4)
C(12)-C(11)-C(10)	123.8(4)
C(11)-C(12)-C(13)	118.5(4)
C(11)-C(12)-C(25)	121.0(4)
C(13)-C(12)-C(25)	120.4(4)
C(14)-C(13)-C(12)	120.5(4)
C(13)-C(14)-C(9)	119.8(4)
C(13)-C(14)-C(15)	120.6(4)
C(9)-C(14)-C(15)	119.5(4)
N(1)-C(15)-C(14)	116.7(3)
C(8)-C(17)-C(18)	116.9(4)
C(19)-C(18)-C(17)	114.3(3)
C(24)-C(19)-C(20)	118.8(4)
C(24)-C(19)-C(18)	119.7(4)
C(20)-C(19)-C(18)	121.6(4)
C(21)-C(20)-C(19)	120.8(4)
C(22)-C(21)-C(20)	120.7(4)
C(21)-C(22)-C(23)	118.7(5)
C(22)-C(23)-C(24)	121.4(5)
C(19)-C(24)-C(23)	119.6(4)
C(10)-C(26)-C(34)	109.9(3)
C(10)-C(26)-C(31)	111.9(3)
C(34)-C(26)-C(31)	107.5(3)
C(10)-C(26)-C(27)	111.8(3)
C(34)-C(26)-C(27)	108.3(3)
C(31)-C(26)-C(27)	107.2(3)
C(28)-C(27)-C(26)	111.2(3)
C(29)-C(28)-C(27)	109.4(4)
C(29)-C(28)-C(35)	110.3(4)
C(27)-C(28)-C(35)	108.5(4)
C(28)-C(29)-C(30)	108.9(4)
C(31)-C(30)-C(29)	109.7(4)
C(31)-C(30)-C(32)	110.8(4)
C(29)-C(30)-C(32)	110.5(4)
C(30)-C(31)-C(26)	110.7(3)
C(30)-C(32)-C(33)	107.7(3)
C(35)-C(33)-C(32)	109.7(4)
C(35)-C(33)-C(34)	108.5(4)

Table 3.17. (Continued).

C(32)-C(33)-C(34)	110.1(4)
C(26)-C(34)-C(33)	110.7(3)
C(28)-C(35)-C(33)	110.4(4)
C(37)-C(36)-Zr(1)	109.4(3)
C(38)-C(37)-C(42)	116.6(4)
C(38)-C(37)-C(36)	121.7(4)
C(42)-C(37)-C(36)	121.6(4)
C(39)-C(38)-C(37)	121.6(4)
C(38)-C(39)-C(40)	120.3(4)
C(41)-C(40)-C(39)	118.9(5)
C(42)-C(41)-C(40)	120.7(4)
C(41)-C(42)-C(37)	121.8(4)
C(44)-C(43)-Zr(1)	99.9(3)
C(49)-C(44)-C(45)	115.5(4)
C(49)-C(44)-C(43)	121.1(4)
C(45)-C(44)-C(43)	123.4(4)
C(46)-C(45)-C(44)	121.7(4)
C(47)-C(46)-C(45)	120.3(4)
C(46)-C(47)-C(48)	120.1(5)
C(49)-C(48)-C(47)	119.5(4)
C(48)-C(49)-C(44)	122.9(4)

Table 3.18. Anisotropic displacement parameters ($Å^2 x\ 10^3$) for *rac*-**Lig^{1}ZrBn$_2$-a**. The anisotropic displacement factor exponent takes the form: $-2p^2[\ h^2\ a^{*2}U^{11} + ...\ + 2\ h\ k\ a^*\ b^*\ U^{12}\ ]$

	U^{11}	U^{22}	U^{33}	U^{23}	U^{13}	U^{12}
Zr(1)	15(1)	19(1)	24(1)	-1(1)	8(1)	-1(1)
O(1)	20(1)	21(2)	24(2)	-6(1)	5(1)	-1(1)
N(1)	13(2)	19(2)	24(2)	-5(2)	5(2)	0(2)
C(1)	32(2)	23(3)	27(3)	-3(2)	16(2)	4(2)
C(2)	18(2)	25(3)	24(3)	1(2)	10(2)	2(2)
C(3)	29(2)	36(3)	32(3)	4(2)	21(2)	4(2)
C(4)	34(3)	38(3)	63(4)	16(3)	32(3)	-4(2)
C(5)	26(2)	29(3)	58(4)	5(3)	17(3)	-7(2)
C(6)	20(2)	17(2)	43(3)	-2(2)	8(2)	2(2)
C(7)	15(2)	12(2)	39(3)	4(2)	10(2)	5(2)
C(8)	20(2)	23(2)	31(3)	0(2)	13(2)	0(2)
C(9)	23(2)	20(2)	22(3)	-2(2)	3(2)	-3(2)
C(10)	16(2)	26(3)	31(3)	-3(2)	6(2)	-2(2)
C(11)	20(2)	24(3)	33(3)	-3(2)	5(2)	-5(2)
C(12)	22(2)	30(3)	27(3)	0(2)	1(2)	0(2)
C(13)	24(2)	37(3)	33(3)	1(2)	7(2)	3(2)

Table 3.18. (Continued).

	U^{11}	U^{22}	U^{33}	U^{23}	U^{13}	U^{12}
C(14)	23(2)	19(2)	31(3)	-5(2)	6(2)	2(2)
C(15)	25(2)	20(3)	32(3)	-8(2)	9(2)	-1(2)
C(16)	29(2)	29(3)	33(3)	3(2)	15(2)	6(2)
C(17)	20(2)	23(2)	26(3)	-2(2)	6(2)	-9(2)
C(18)	21(2)	27(3)	38(3)	1(2)	3(2)	-1(2)
C(19)	10(2)	32(3)	27(3)	-1(2)	1(2)	-2(2)
C(20)	16(2)	38(3)	30(3)	5(2)	12(2)	-4(2)
C(21)	16(2)	36(3)	45(3)	-5(2)	8(2)	8(2)
C(22)	27(2)	26(3)	47(3)	5(3)	5(2)	-2(2)
C(23)	26(2)	44(3)	29(3)	15(2)	0(2)	-4(2)
C(24)	26(2)	36(3)	21(3)	-2(2)	5(2)	0(2)
C(25)	30(3)	46(3)	37(3)	-7(3)	0(2)	-4(2)
C(26)	14(2)	30(3)	29(3)	-8(2)	7(2)	-7(2)
C(27)	20(2)	22(3)	36(3)	2(2)	9(2)	0(2)
C(28)	25(2)	40(3)	32(3)	12(2)	14(2)	1(2)
C(29)	32(3)	37(3)	41(3)	0(2)	19(2)	-5(2)
C(30)	16(2)	50(3)	43(3)	3(3)	15(2)	-3(2)
C(31)	15(2)	38(3)	39(3)	3(2)	6(2)	0(2)
C(32)	20(2)	43(3)	43(3)	2(2)	15(2)	10(2)
C(33)	29(2)	34(3)	38(3)	-2(2)	14(2)	3(2)
C(34)	25(2)	17(2)	42(3)	3(2)	15(2)	0(2)
C(35)	24(2)	49(3)	28(3)	0(2)	10(2)	3(2)
C(36)	21(2)	27(3)	35(3)	4(2)	10(2)	-3(2)
C(37)	18(2)	24(2)	13(2)	9(2)	2(2)	0(2)
C(38)	22(2)	26(3)	30(3)	7(2)	1(2)	-3(2)
C(39)	36(3)	35(3)	42(3)	-4(3)	2(3)	-15(2)
C(40)	64(3)	32(3)	31(3)	2(2)	20(3)	1(3)
C(41)	41(3)	34(3)	34(3)	6(2)	14(2)	6(2)
C(42)	21(2)	26(3)	33(3)	11(2)	6(2)	0(2)
C(43)	20(2)	24(3)	34(3)	-7(2)	4(2)	-2(2)
C(44)	26(2)	16(2)	30(3)	-5(2)	11(2)	0(2)
C(45)	29(3)	26(3)	50(3)	-4(2)	14(2)	0(2)
C(46)	36(3)	30(3)	54(4)	2(3)	-1(3)	6(2)

Table 3.18. (Continued).

	U^{11}	U^{22}	U^{33}	U^{23}	U^{13}	U^{12}
C(47)	55(3)	20(3)	35(3)	2(2)	9(3)	-1(2)
C(48)	43(3)	20(3)	44(3)	-5(2)	21(2)	-10(2)
C(49)	25(2)	16(3)	43(3)	-6(2)	11(2)	-2(2)

Table 3.19. Hydrogen coordinates (x 10^4) and isotropic displacement parameters (Å^{-}x 10^3) for *rac*-**Lig^{1}ZrBn$_2$-a**.

	x	y	z	U(eq)
H(1A)	4357	3555	267	31
H(1B)	4742	3220	1456	31
H(3A)	5245	4269	19	36
H(4A)	6411	4924	697	50
H(5A)	7142	4998	2723	44
H(6A)	6694	4455	4048	32
H(8A)	5482	3320	3454	28
H(11A)	-693	3376	573	31
H(13A)	1375	3157	-998	38
H(15A)	3134	2912	1325	31
H(15B)	2981	3182	66	31
H(16A)	3125	4181	31	43
H(16B)	3580	4483	1254	43
H(16C)	2527	4239	964	43
H(17A)	5500	3575	5437	28
H(17B)	5938	4123	5176	28
H(18A)	7259	3617	4829	36
H(18B)	7238	3644	6170	36
H(20A)	7380	2766	3992	32
H(21A)	7417	1849	4119	39
H(22A)	6995	1421	5632	42
H(23A)	6537	1926	7035	42
H(24A)	6460	2848	6903	34

Table 3.19. (Continued).

	x	y	z	U(eq)
H(25A)	-217	3146	-2195	59
H(25B)	-890	3549	-1761	59
H(25C)	-968	2927	-1556	59
H(27A)	566	2825	3586	31
H(27B)	1469	3210	4042	31
H(28A)	766	3064	5585	38
H(29A)	-822	3350	5364	42
H(29B)	-826	2912	4381	42
H(30A)	-1791	3643	3489	42
H(31A)	-1107	3797	1942	37
H(31B)	-1011	3185	2305	37
H(32A)	-984	4318	4809	41
H(32B)	-1100	4494	3471	41
H(33A)	522	4641	4648	39
H(34A)	317	4402	2627	32
H(34B)	1317	4179	3441	32
H(35A)	1485	3902	5512	40
H(35B)	611	3963	6066	40
H(36A)	4463	2909	5143	33
H(36B)	3324	2885	4892	33
H(38A)	2350	2423	3046	33
H(39A)	2282	1673	1911	48
H(40A)	3694	1261	1805	49
H(41A)	5167	1619	2861	43
H(42A)	5238	2347	4032	33
H(43A)	2965	4360	4849	32
H(43B)	4116	4416	5302	32
H(45A)	2073	4984	3300	42
H(46A)	2034	5614	1862	52
H(47A)	3421	5842	1400	45
H(48A)	4873	5447	2402	41
H(49A)	4920	4811	3816	33

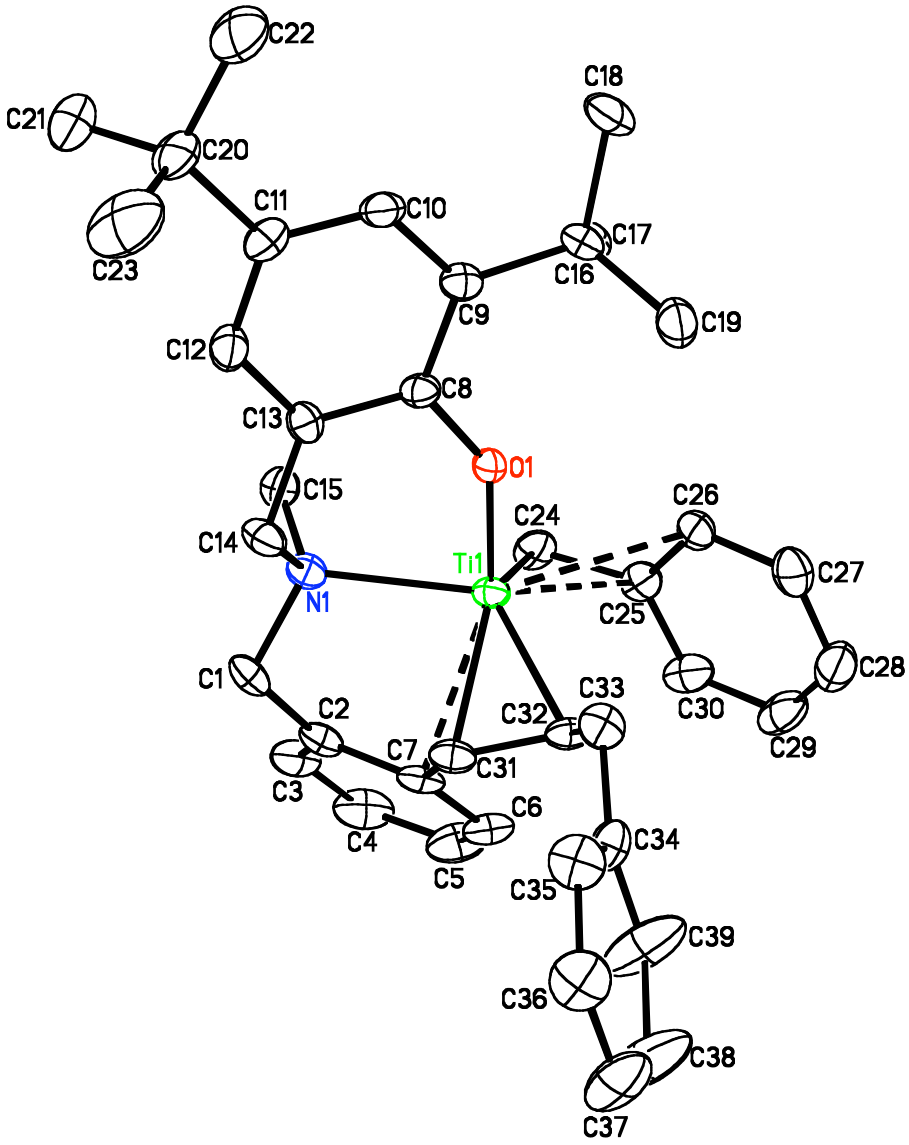

Figure 3.27. ORTEP diagram of *rac*-**Lig^{2}TiBn**. Thermal ellipsoids are drawn at the 40% probability level.

Table 3.20. Crystal data and structure refinement for *rac*-**Lig^{2}TiBn**.

Identification code	je11	
Empirical formula	$C_{39}H_{46}NOTi$	
Formula weight	592.67	
Temperature	173(2) K	
Wavelength	0.71073 Å	
Crystal system	Monoclinic	
Space group	P2(1)/c	
Unit cell dimensions	a = 11.0966(11) Å	α= 90°
	b = 28.554(3) Å	β= 112.514(5)°
	c = 11.2687(11) Å	γ = 90°
Volume	3298.4(6) Å^3	
Z	4	
Density (calculated)	1.193 Mg/m^3	
Absorption coefficient	0.290 mm^{-1}	
F(000)	1268	
Crystal size	0.20 x 0.10 x 0.05 mm^3	
Theta range for data collection	1.99 to 24.71°	
Index ranges	-13<=h<=13, -25<=k<=33, -13<=l<=13	
Reflections collected	23361	
Independent reflections	5591 [R(int) = 0.0557]	
Completeness to theta = 24.71°	99.5 %	
Absorption correction	Semi-empirical from equivalents	
Max. and min. transmission	0.9857 and 0.9443	
Refinement method	Full-matrix least-squares on F^2	
Data / restraints / parameters	5591 / 0 / 379	
Goodness-of-fit on F^2	1.114	
Final R indices [I>2sigma(I)]	R1 = 0.0830, wR2 = 0.2210	
R indices (all data)	R1 = 0.1131, wR2 = 0.2342	
Largest diff. peak and hole	1.054 and -0.488 e.Å^{-3}	

Table 3.21. Atomic coordinates (x 10^4) and equivalent isotropic displacement parameters (Å^{2}x 10^3) for *rac*-**Lig^{2}TiBn**. U(eq) is defined as one third of the trace of the orthogonalized U^{ij} tensor.

	x	y	z	U(eq)
Ti(1)	4025(1)	822(1)	2312(1)	23(1)
O(1)	4615(3)	1429(1)	2720(3)	25(1)
N(1)	6128(3)	690(1)	2624(3)	26(1)
C(1)	6282(5)	244(2)	1985(5)	33(1)
C(2)	5225(5)	-92(2)	1903(4)	31(1)
C(3)	5471(5)	-523(2)	2535(5)	41(1)
C(4)	4447(6)	-809(2)	2477(5)	48(2)
C(5)	3188(6)	-676(2)	1812(5)	49(2)
C(6)	2913(5)	-252(2)	1155(5)	37(1)
C(7)	3913(5)	44(2)	1149(4)	30(1)
C(8)	5655(4)	1719(2)	2954(4)	25(1)
C(9)	5694(4)	2164(2)	3489(4)	27(1)
C(10)	6758(4)	2449(2)	3581(5)	30(1)
C(11)	7774(4)	2308(2)	3258(5)	31(1)
C(12)	7742(4)	1850(2)	2832(5)	32(1)
C(13)	6697(4)	1557(2)	2658(4)	26(1)
C(14)	6644(4)	1079(2)	2072(5)	31(1)
C(15)	6886(5)	652(2)	4006(5)	35(1)
C(16)	4633(5)	2326(2)	3944(5)	34(1)
C(17)	4615(5)	1997(2)	5024(5)	39(1)
C(18)	4905(5)	2821(2)	4545(6)	50(2)
C(19)	3296(5)	2337(2)	2818(5)	39(1)
C(20)	8906(5)	2640(2)	3338(5)	40(1)
C(21)	10190(5)	2442(2)	4238(6)	54(2)
C(22)	8725(6)	3124(2)	3818(7)	63(2)
C(23)	8936(7)	2694(3)	2005(6)	73(2)
C(24)	3750(4)	495(2)	3926(4)	33(1)
C(25)	2388(4)	631(2)	3279(4)	32(1)
C(26)	2061(4)	1104(2)	2998(4)	33(1)
C(27)	840(5)	1243(2)	2159(5)	41(1)
C(28)	-110(5)	919(2)	1570(5)	46(2)

Table 3.21. (Continued).

	x	y	z	U(eq)
C(29)	158(5)	453(2)	1874(5)	49(2)
C(30)	1379(5)	300(2)	2695(5)	40(1)
C(31)	3673(5)	502(2)	515(4)	28(1)
C(32)	2556(4)	779(2)	404(4)	27(1)
C(33)	2280(5)	1212(2)	-445(5)	34(1)
C(34)	1713(4)	1115(2)	-1869(5)	32(1)
C(35)	2029(5)	1381(2)	-2712(5)	42(1)
C(36)	1549(5)	1289(2)	-4020(5)	48(2)
C(37)	730(6)	925(2)	-4523(5)	58(2)
C(38)	415(7)	644(3)	-3701(6)	83(3)
C(39)	890(6)	743(3)	-2394(5)	72(2)

Table 3.22. Bond lengths [Å] and angles [°] for *rac*-**Lig^{2}TiBn**.

Ti(1)-O(1)	1.848(3)	C(4)-C(5)	1.362(8)
Ti(1)-C(31)	2.118(4)	C(5)-C(6)	1.389(7)
Ti(1)-C(32)	2.148(4)	C(6)-C(7)	1.397(7)
Ti(1)-C(24)	2.167(5)	C(7)-C(31)	1.465(6)
Ti(1)-N(1)	2.255(4)	C(8)-C(9)	1.398(6)
Ti(1)-C(25)	2.510(5)	C(8)-C(13)	1.399(6)
Ti(1)-C(7)	2.560(5)	C(9)-C(10)	1.405(7)
Ti(1)-C(26)	2.699(5)	C(9)-C(16)	1.525(7)
O(1)-C(8)	1.362(5)	C(10)-C(11)	1.372(7)
N(1)-C(15)	1.464(6)	C(11)-C(12)	1.388(7)
N(1)-C(14)	1.490(6)	C(11)-C(20)	1.549(7)
N(1)-C(1)	1.505(6)	C(12)-C(13)	1.381(6)
C(1)-C(2)	1.491(7)	C(13)-C(14)	1.509(6)
C(2)-C(3)	1.394(7)	C(16)-C(19)	1.540(7)
C(2)-C(7)	1.429(6)	C(16)-C(17)	1.543(7)
C(3)-C(4)	1.381(8)	C(16)-C(18)	1.546(7)
		C(20)-C(21)	1.507(7)
		C(20)-C(23)	1.524(9)

Table 3.22. (Continued).

C(20)-C(22)	1.525(8)
C(24)-C(25)	1.456(6)
C(25)-C(26)	1.403(7)
C(25)-C(30)	1.419(7)
C(26)-C(27)	1.381(6)
C(27)-C(28)	1.368(7)
C(28)-C(29)	1.378(8)
C(29)-C(30)	1.386(7)
C(31)-C(32)	1.436(7)
C(32)-C(33)	1.521(6)
C(33)-C(34)	1.508(7)
C(34)-C(35)	1.363(7)
C(34)-C(39)	1.376(8)
C(35)-C(36)	1.387(7)
C(36)-C(37)	1.354(8)
C(37)-C(38)	1.369(9)
C(38)-C(39)	1.390(9)
O(1)-Ti(1)-C(31)	124.12(16)
O(1)-Ti(1)-C(32)	111.27(16)
C(31)-Ti(1)-C(32)	39.33(18)
O(1)-Ti(1)-C(24)	110.22(17)
C(31)-Ti(1)-C(24)	125.66(19)
C(32)-Ti(1)-C(24)	121.28(18)
O(1)-Ti(1)-N(1)	82.60(13)
C(31)-Ti(1)-N(1)	82.97(16)
C(32)-Ti(1)-N(1)	119.33(16)
C(24)-Ti(1)-N(1)	105.52(16)
O(1)-Ti(1)-C(25)	110.06(15)
C(31)-Ti(1)-C(25)	114.93(17)
C(32)-Ti(1)-C(25)	91.38(17)
C(24)-Ti(1)-C(25)	35.33(16)
N(1)-Ti(1)-C(25)	140.71(15)
O(1)-Ti(1)-C(7)	152.26(15)
C(31)-Ti(1)-C(7)	34.91(16)
C(32)-Ti(1)-C(7)	64.44(16)
C(24)-Ti(1)-C(7)	93.52(18)
N(1)-Ti(1)-C(7)	77.21(15)
C(25)-Ti(1)-C(7)	97.58(17)
O(1)-Ti(1)-C(26)	84.12(14)
C(31)-Ti(1)-C(26)	121.93(16)
C(32)-Ti(1)-C(26)	85.24(16)
C(24)-Ti(1)-C(26)	59.94(17)
N(1)-Ti(1)-C(26)	155.02(14)
C(25)-Ti(1)-C(26)	30.98(16)
C(7)-Ti(1)-C(26)	121.29(16)
C(8)-O(1)-Ti(1)	144.3(3)
C(15)-N(1)-C(14)	110.1(4)
C(15)-N(1)-C(1)	108.8(4)
C(14)-N(1)-C(1)	107.4(4)
C(15)-N(1)-Ti(1)	108.5(3)
C(14)-N(1)-Ti(1)	110.5(3)
C(1)-N(1)-Ti(1)	111.6(3)
C(2)-C(1)-N(1)	110.1(4)
C(3)-C(2)-C(7)	119.9(5)
C(3)-C(2)-C(1)	122.7(4)
C(7)-C(2)-C(1)	117.4(4)
C(4)-C(3)-C(2)	120.0(5)
C(5)-C(4)-C(3)	120.9(5)
C(4)-C(5)-C(6)	120.4(5)
C(5)-C(6)-C(7)	121.0(5)
C(6)-C(7)-C(2)	117.6(4)
C(6)-C(7)-C(31)	123.0(4)
C(2)-C(7)-C(31)	119.1(4)
C(6)-C(7)-Ti(1)	113.9(3)
C(2)-C(7)-Ti(1)	95.3(3)
C(31)-C(7)-Ti(1)	55.8(2)
O(1)-C(8)-C(9)	121.3(4)
O(1)-C(8)-C(13)	117.9(4)

Table 3.22. (Continued).

C(9)-C(8)-C(13)	120.7(4)
C(8)-C(9)-C(10)	116.4(4)
C(8)-C(9)-C(16)	121.4(4)
C(10)-C(9)-C(16)	122.3(4)
C(11)-C(10)-C(9)	124.2(5)
C(10)-C(11)-C(12)	117.0(4)
C(10)-C(11)-C(20)	122.4(5)
C(12)-C(11)-C(20)	120.6(4)
C(13)-C(12)-C(11)	121.9(5)
C(12)-C(13)-C(8)	119.4(4)
C(12)-C(13)-C(14)	120.0(4)
C(8)-C(13)-C(14)	120.5(4)
N(1)-C(14)-C(13)	116.6(4)
C(9)-C(16)-C(19)	110.7(4)
C(9)-C(16)-C(17)	108.9(4)
C(19)-C(16)-C(17)	111.3(4)
C(9)-C(16)-C(18)	112.2(4)
C(19)-C(16)-C(18)	107.9(4)
C(17)-C(16)-C(18)	105.7(4)
C(21)-C(20)-C(23)	109.3(5)
C(21)-C(20)-C(22)	108.7(5)
C(23)-C(20)-C(22)	108.2(5)
C(21)-C(20)-C(11)	110.3(4)
C(23)-C(20)-C(11)	109.1(4)
C(22)-C(20)-C(11)	111.2(4)
C(25)-C(24)-Ti(1)	85.3(3)
C(26)-C(25)-C(30)	116.4(4)
C(26)-C(25)-C(24)	119.8(4)
C(30)-C(25)-C(24)	122.7(5)
C(26)-C(25)-Ti(1)	82.0(3)
C(30)-C(25)-Ti(1)	121.2(3)
C(24)-C(25)-Ti(1)	59.4(2)
C(27)-C(26)-C(25)	122.2(5)
C(27)-C(26)-Ti(1)	125.3(3)
C(25)-C(26)-Ti(1)	67.0(3)
C(28)-C(27)-C(26)	120.6(5)
C(27)-C(28)-C(29)	118.6(5)
C(28)-C(29)-C(30)	122.2(5)
C(29)-C(30)-C(25)	119.8(5)
C(32)-C(31)-C(7)	121.7(4)
C(32)-C(31)-Ti(1)	71.5(3)
C(7)-C(31)-Ti(1)	89.3(3)
C(31)-C(32)-C(33)	117.6(4)
C(31)-C(32)-Ti(1)	69.2(2)
C(33)-C(32)-Ti(1)	118.5(3)
C(34)-C(33)-C(32)	114.8(4)
C(35)-C(34)-C(39)	115.8(5)
C(35)-C(34)-C(33)	121.6(4)
C(39)-C(34)-C(33)	122.5(5)
C(34)-C(35)-C(36)	122.6(5)
C(37)-C(36)-C(35)	120.8(5)
C(36)-C(37)-C(38)	118.1(6)
C(37)-C(38)-C(39)	120.3(6)
C(34)-C(39)-C(38)	122.2(6)

Table 3.23. Anisotropic displacement parameters ($Å^2 x\ 10^3$) for *rac*-**Lig²TiBn**. The anisotropic displacement factor exponent takes the form: $-2p^2[\ h^2\ a^{*2}U^{11} + ...\ + 2\ h\ k\ a^*\ b^*\ U^{12}\ ]$

	U^{11}	U^{22}	U^{33}	U^{23}	U^{13}	U^{12}
Ti(1)	27(1)	23(1)	19(1)	-3(1)	10(1)	-3(1)
O(1)	22(1)	25(2)	32(2)	-7(1)	14(1)	-4(1)
N(1)	33(2)	21(2)	26(2)	0(2)	12(2)	1(2)
C(1)	42(2)	26(3)	34(2)	-2(2)	20(2)	11(2)
C(2)	45(3)	22(3)	29(2)	-5(2)	16(2)	3(2)
C(3)	55(3)	32(3)	30(3)	-3(2)	9(2)	5(3)
C(4)	78(4)	22(3)	36(3)	6(2)	13(3)	-1(3)
C(5)	66(4)	28(3)	42(3)	1(2)	9(3)	-18(3)
C(6)	45(3)	31(3)	26(2)	-6(2)	4(2)	-10(2)
C(7)	46(3)	23(3)	17(2)	-6(2)	10(2)	-1(2)
C(8)	27(2)	21(2)	26(2)	-3(2)	11(2)	-6(2)
C(9)	31(2)	23(2)	25(2)	1(2)	9(2)	0(2)
C(10)	30(2)	25(3)	30(2)	-6(2)	4(2)	-2(2)
C(11)	27(2)	31(3)	33(3)	1(2)	8(2)	-7(2)
C(12)	26(2)	33(3)	39(3)	1(2)	15(2)	0(2)
C(13)	28(2)	28(3)	26(2)	1(2)	14(2)	2(2)
C(14)	43(2)	22(3)	37(2)	-7(2)	26(2)	-6(2)
C(15)	30(2)	37(3)	37(3)	-3(2)	9(2)	3(2)
C(16)	36(2)	29(3)	38(3)	-13(2)	14(2)	1(2)
C(17)	45(3)	44(3)	35(3)	-14(2)	23(2)	-5(2)
C(18)	54(3)	35(3)	70(4)	-24(3)	33(3)	-3(3)
C(19)	33(2)	37(3)	52(3)	-2(2)	22(2)	2(2)
C(20)	33(2)	41(3)	48(3)	-5(2)	19(2)	-15(2)
C(21)	33(3)	66(4)	63(4)	-9(3)	18(3)	-10(3)
C(22)	47(3)	43(4)	102(5)	-12(3)	31(3)	-18(3)
C(23)	75(4)	78(5)	69(4)	1(4)	33(3)	-38(4)
C(24)	33(2)	45(3)	18(2)	3(2)	7(2)	-2(2)
C(25)	33(2)	45(3)	23(2)	-1(2)	17(2)	-7(2)
C(26)	31(2)	46(3)	25(2)	-5(2)	16(2)	1(2)
C(27)	38(2)	49(3)	44(3)	-1(2)	26(2)	2(2)
C(28)	31(3)	62(4)	42(3)	1(3)	12(2)	1(3)

Table 3.23. (Continued).

	U^{11}	U^{22}	U^{33}	U^{23}	U^{13}	U^{12}
C(29)	35(3)	73(4)	41(3)	-11(3)	17(2)	-24(3)
C(30)	46(3)	46(3)	32(3)	-6(2)	19(2)	-18(2)
C(31)	40(2)	25(3)	19(2)	-1(2)	11(2)	-3(2)
C(32)	34(2)	26(3)	16(2)	-1(2)	5(2)	-3(2)
C(33)	39(2)	26(3)	36(3)	4(2)	15(2)	1(2)
C(34)	26(2)	33(3)	32(2)	12(2)	7(2)	4(2)
C(35)	50(3)	35(3)	43(3)	7(2)	22(2)	-4(2)
C(36)	56(3)	54(4)	37(3)	12(3)	21(2)	-1(3)
C(37)	48(3)	91(5)	23(3)	14(3)	1(2)	-12(3)
C(38)	75(4)	122(6)	33(3)	11(4)	0(3)	-56(4)
C(39)	68(4)	109(5)	24(3)	18(3)	2(3)	-51(4)

Table 3.24. Hydrogen coordinates (x 10^4) and isotropic displacement parameters (Å^{2}x 10^3) for *rac*-**Lig^{2}TiBn**.

	x	y	z	U(eq)
H(1A)	6245	314	1111	39
H(1B)	7142	102	2484	39
H(3A)	6345	-619	3006	50
H(4A)	4622	-1102	2906	57
H(5A)	2494	-874	1797	59
H(6A)	2030	-162	704	44
H(10A)	6775	2760	3887	36
H(12A)	8459	1735	2656	38
H(14A)	6927	1028	1385	37
H(15A)	7804	594	4158	53
H(15B)	6550	392	4357	53
H(15C)	6812	944	4429	53
H(17A)	4446	1675	4697	59
H(17B)	3927	2096	5313	59
H(17C)	5462	2010	5746	59
H(18A)	4928	3047	3899	76
H(18B)	5747	2822	5274	76

Table 3.24. (Continued).

	x	y	z	U(eq)
H(18C)	4213	2908	4842	76
H(19A)	3100	2026	2420	59
H(19B)	3316	2567	2179	59
H(19C)	2621	2425	3137	59
H(21A)	10898	2655	4281	81
H(21B)	10334	2136	3923	81
H(21C)	10174	2407	5097	81
H(22A)	9454	3326	3859	95
H(22B)	8702	3096	4675	95
H(22C)	7904	3260	3227	95
H(23A)	9651	2904	2050	109
H(23B)	8106	2826	1419	109
H(23C)	9070	2387	1687	109
H(24A)	3902	153	3992	40
H(24B)	4210	653	4760	40
H(26A)	2384	1302	3790	39
H(27A)	659	1567	1988	49
H(28A)	-938	1014	964	55
H(29A)	-517	229	1508	59
H(30A)	1539	-25	2865	48
H(31A)	4214	598	23	34
H(32A)	1765	595	331	32
H(33A)	1666	1416	-235	40
H(33B)	3104	1389	-236	40
H(35A)	2602	1639	-2390	50
H(36A)	1798	1484	-4570	58
H(37A)	384	867	-5421	69
H(38A)	-131	379	-4025	99
H(39A)	639	549	-1846	86

REFERENCES

(1) Coates, G. W. *Chem. Rev.* **2000**, *100*, 1223-1252.

(2) Resconi, L.; Cavallo, L.; Fait, A.; Piemontesi, F. *Chem. Rev.* **2000**, *100*, 1253-1345.

(3) Britovsek, G. J. P.; Gibson, V. C.; Wass, D. F. *Angew. Chem., Int. Ed.* **1999**, *38*, 428-447.

(4) Gibson, V. C.; Spitzmesser, S. K. *Chem. Rev.* **2003**, *103*, 283-315.

(5) Coates, G. W.; Hustad, P. D.; Reinartz, S. *Angew. Chem., Int. Ed.* **2002**, *41*, 2236-2257.

(6) Domski, G. J.; Rose, J. M.; Coates, G. W.; Bolig, A. D.; Brookhart, M. *Prog. Polym. Sci.* **2007**, *32*, 30-92.

(7) Edson, J. B.; Domski, G. J.; Rose, J. M.; Bolig, A. D.; Brookhart, M.; Coates, G. W. *Controlled and Living Polymerizations: From Mechanisms to Applications*; Wiley-VCH, 2009.

(8) Harney, M. B.; Zhang, Y. H.; Sita, L. R. *Angew. Chem., Int. Ed.* **2006**, *45*, 2400-2404.

(9) Hotta, A.; Cochran, E.; Ruokolainen, J.; Khanna, V.; Fredrickson, G. H.; Kramer, E. J.; Shin, Y.-W.; Shimizu, F.; Cherian, A. E.; Rose, J. M.; Coates, G. W. *Proc. Natl. Acad. Sci. USA.* **2006**, *42*, 15327-15332.

(10) Coffin, R. C.; Diamanti, S. J.; Hotta, A.; Khanna, V.; Kramer, E. J.; Fredrickson, G. H.; Bazan, G. C. *Chem. Commun.* **2007**, 3550-3552.

(11) Edson, J. B.; Wang, Z. G.; Kramer, E. J.; Coates, G. W. *J. Am. Chem. Soc.* **2008**, *130*, 4968-4977.

(12) Rose, J. M.; Deplace, F.; Lynd, N. A.; Wang, Z.; Hotta, A.; Lobkovsky, E. B.; Kramer, E. J.; Coates, G. W. *Macromolecules* **2008**, *41*, 9548-9555.

(13) Boussie, T. R.; Diamond, G. M.; Goh, C.; Hall, K. A.; LaPointe, A. M.; Leclerc, M. K.; Murphy, V.; Shoemaker, J. A. W.; Turner, H.; Rosen, R. K.; Stevens, J. C.; Alfano, F.; Busico, V.; Cipullo, R.; Talarico, G. *Angew. Chem., Int. Ed.* **2006**, *45*, 3278-3283.

(14) Froese, R. D. J.; Hustad, P. D.; Kuhlman, R. L.; Wenzel, T. T. *J. Am. Chem. Soc.* **2007**, *129*, 7831-7840.

(15) Zuccaccia, C.; Macchioni, A.; Busico, V.; Cipullo, R.; Talarico, G.; Alfano, F.; Boone, H. W.; Frazier, K. A.; Hustad, P. D.; Stevens, J. C.; Vosejpka, P. C.; Abboud, K. A. *J. Am. Chem. Soc.* **2008**, *130*, 10354-10368.

(16) Domski, G. J.; Lobkovsky, E. B.; Coates, G. W. *Macromolecules* **2007**, *40*, 3510-3513.

(17) Domski, G. J.; Edson, J. B.; Keresztes, I.; Lobkovsky, E. B.; Coates, G. W. *Chem. Commun.* **2008**, *46*, 6137-6139.

(18) Tshuva, E. Y.; Versano, M.; Goldberg, I.; Kol, M.; Weitman, H.; Goldschmidt, Z. *Inorg. Chem. Commun.* **1999**, *2*, 371-373.

(19) Tshuva, E. Y.; Goldberg, I.; Kol, M. *J. Am. Chem. Soc.* **2000**, *122*, 10706-10707.

(20) Tshuva, E. Y.; Goldberg, I.; Kol, M.; Goldschmidt, Z. *Inorg. Chem. Commun.* **2000**, *3*, 611-614.

(21) Tshuva, E. Y.; Goldberg, I.; Kol, M.; Weitman, H.; Goldschmidt, Z. *Chem. Commun.* **2000**, 379-380.

(22) Tshuva, E. Y.; Gendeziuk, N.; Kol, M. *Tetrahedron Lett.* **2001**, *42*, 6405-6407.

(23) Attar, S.; Nelson, J. H.; Fischer, J.; Decian, A.; Sutter, J. P.; Pfeffer, M. *Organometallics* **1995**, *14*, 4559-4569.

(24) Negishi, E.; Cederbaum, F. E.; Takahashi, T. *Tetrahedron Lett.* **1986**, *27*, 2829-2832.

(25) Buchwald, S. L.; Watson, B. T.; Huffman, J. C. *J. Am. Chem. Soc.* **1987**, *109*, 2544-2546.

(26) Wiecko, M.; Girnt, D.; Rastatter, M.; Panda, T. K.; Roesky, P. W. *Dalton Trans.* **2005**, 2147-2150.

(27) Hill, J. E.; Fanwick, P. E.; Rothwell, I. P. *Organometallics* **1992**, *11*, 1771-1773.

(28) Thorn, M. G.; Hill, J. E.; Waratuke, S. A.; Johnson, E. S.; Fanwick, P. E.; Rothwell, I. P. *J. Am. Chem. Soc.* **1997**, *119*, 8630-8641.

(29) Cohen, S. A.; Auburn, P. R.; Bercaw, J. E. *J. Am. Chem. Soc.* **1983**, *105*, 1136-1143.

(30) Cohen, S. A.; Bercaw, J. E. *Organometallics* **1985**, *4*, 1006-1014.

(31) Albright, T. A.; Hoffmann, R.; Thibeault, J. C.; Thorn, D. L. *J. Am. Chem. Soc.* **1979**, *101*, 3801-3812.

(32) Dewar, M. J. S.; Ford, G. P. *J. Am. Chem. Soc.* **1979**, *101*, 783-791.

(33) Kulinkovich, O. G. *Pure Appl. Chem.* **2000**, *72*, 1715-1719.

(34) Kulinkovich, O. G.; de Meijere, A. *Chem. Rev.* **2000**, *100*, 2789-2834.

(35) Sato, F.; Urabe, H.; Okamoto, S. *Chem. Rev.* **2000**, *100*, 2835-2886.

(36) Hill, J. E.; Fanwick, P. E.; Rothwell, I. P. *Organometallics* **1991**, *10*, 15-16.

(37) Jayaratne, K. C.; Sita, L. R. *J. Am. Chem. Soc.* **2000**, *122*, 958-959.

(38) Zhang, Y. H.; Sita, L. R. *Chem. Commun.* **2003**, 2358-2359.

(39) Kissounko, D. A.; Zhang, Y. H.; Harney, M. B.; Sita, L. R. *Adv. Synth. Cat.* **2005**, *347*, 426-432.

(40) Segal, S.; Goldberg, I.; Kol, M. *Organometallics* **2005**, *24*, 200-202.

(41) Sudhakar, P.; Sundararajan, G. *Macromol. Rapid. Commun.* **2005**, *26*, 1854-1859.

(42) Ward, B. D.; Bellemin-Laponnaz, S.; Gade, L. H. *Angew. Chem., Int. Ed.* **2005**, *44*, 1668-1671.

(43) Yasumoto, T.; Yamagata, T.; Mashima, K. *Organometallics* **2005**, *24*, 3375-3377.

(44) Sudhakar, P. *J. Polym. Sci. Part A: Polym. Chem.* **2007**, *45*, 5470-5479.

(45) Busico, V.; Cipullo, R.; Friederichs, N.; Ronca, S.; Togrou, M. *Macromolecules* **2003**, *36*, 3806-3808.

(46) Busico, V.; Cipullo, R.; Friederichs, N.; Ronca, S.; Talarico, G.; Togrou, M.; Wang, B. *Macromolecules* **2004**, *37*, 8201-8203.

(47) Mason, A. F.; Coates, G. W. *J. Am. Chem. Soc.* **2004**, *126*, 16326-16327.

(48) Cherian, A. E.; Rose, J. M.; Lobkovsky, E. B.; Coates, G. W. *J. Am. Chem. Soc.* **2005**, *127*, 13770-13771.

(49) Zhang, W.; Sita, L. R. *Adv. Synth. Cat.* **2008**, *350*, 439-447.

(50) Chen, E. Y. X.; Marks, T. J. *Chem. Rev.* **2000**, *100*, 1391-1434.

(51) Bates, F. S. *Science* **1991**, *251*, 898-905.

(52) Ruzette, A. V.; Leibler, L. *Nat. Mater.* **2005**, *4*, 19-31.

(53) Karian, H. G. In *Handbook of Polypropylene and Polypropylene Composites*; Marcel Dekker Inc.: New York, 2003.

(54) Coates, G. W.; Waymouth, R. M. *Science* **1995**, *267*, 217-219.

(55) Dale, W. J.; Starr, L.; Strobel, C. W. *J. Org. Chem.* **1961**, *26*, 2225-2227.

(56) Gademann, K.; Chavez, D. E.; Jacobsen, E. N. *Angew. Chem., Int. Ed.* **2002**, *41*, 3059-3061.

(57) Rodriguez, G.; Cano, D. A.; McConville, D. H.; Rix, F. C. United States Patent 7,067,686, **2006**

(58) Zucchini, U.; Albizzat E.; Giannini, U. *J. Organomet. Chem.* **1971**, *26*, 357-372.

Chapter 4

Cyclopolymerization of Nonconjugated Dienes with Tridentate Phenoxyamine Zirconium and Hafnium Complexes Supported by an sp^3-C Donor: Isotactic Enchainment and Diastereoselective Cis-Ring Closure

4.1 Introduction

The control over polymer microstructure can have dramatic influences on the physical properties of the material. With the advent of homogeneous stereospecific olefin polymerization catalysts,[1,2] the control over polyolefin microstructure can now be rationalized by the appropriate choice of a metallocene[2] or non-metallocene[3,4] transition metal catalyst precursor. While the stereospecific polymerization of vinyl-monomers can give rise to only two microstructures of maximum order (i.e. isotactic and syndiotactic), the cyclopolymerization of dienes can give rise to four microstructures of maximum order.[5] These four microstructures for the cyclopolymerization of 1,5-hexadiene to poly(methylene-1,3-cyclopentane) (PMCP) and 1,6-heptadiene to poly(methylene-1,3-cyclohexane) (PMCH) are depicted in Figure 4.1

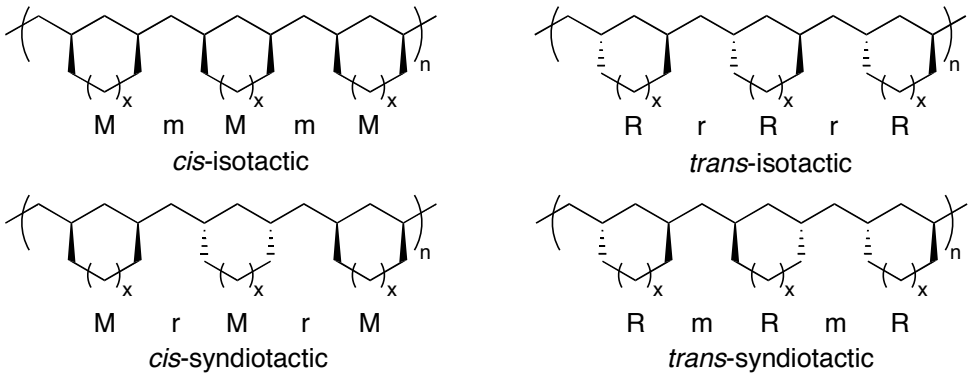

Figure 4.1. Microstructures of maximum order for PMCP ($x = 0$) and PMCH ($x = 1$).

Because cyclopolymers include both *cis* and *trans* stereochemistry of the rings and the relative stereochemistry between the rings, the microstructure is significantly more complicated than linear polymers derived from simple vinyl-monomers. Due to its relatively lower cost, the cyclopolymerization of

1,5-hexadiene has been extensively more studied than the cyclopolymerization of 1,6-heptadiene Coates and Waymouth have carried out a full microstructural analysis of PMCP derived from the cyclopolymerization of 1,5-hexadiene.[6] The formation of PMCP from 1,5-hexadiene is assumed to proceed via a two-step reaction mechanism; olefin insertion followed by cyclization. The tacticity is described as the relative stereochemistry of the first stereocenter of every ring, which is independent of the *cis*/*trans* stereochemistry. Thus, the tacticity of the polymer is influenced by the enantiofacial selectivity of the catalyst on the first insertion step whereas the *cis*/*trans* stereochemistry of the ring is determined by the diastereoselectivity of the cyclization step.

Cyclopolymerization of 1,5-hexadiene was first reported by Marvel and Stille[7] and was later investigated by Makowski[8] and Cheng[9] using heterogeneous catalysts derived from $TiCl_4$ and $TiCl_3$ in conjunction with alkyl aluminum compounds. More recently the use of homogeneous catalysts derived from metallocenes activated with methyl aluminoxane (MAO) have been described by Resconi and Waymouth.[10,11] Since these initial reports, the cyclopolymerization of 1,5-hexadiene has been extensively studied. Depending on the catalyst system employed,[12] PMCP with different microstructures have been reported. These include: random-atactic,[10] random-isotactic,[8] *cis*-atactic,[10,11] *trans*-atactic[10,11] and *trans*-isotactic.[6,13-16] Of the microstructures reported for PMCP, only one microstructure of maximum order (*trans*-isotactic) has been reported to date.

We previously reported the synthesis of metallacycle tridentate phenoxyamine zirconium and hafnium complexes supported by an sp^3-C donor (*rac*-**Lig^{1}ZrBn$_2$-a,b** and *rac*-**Lig^{1}HfBn$_2$-a,b**, Scheme 1).[17] Upon activation,

these complexes facilitate the living polymerization[18-20] of 1-hexene (*rac*-**Lig^{1}HfBn$_2$-a,b**) and propylene (*rac*-**Lig^{1}ZrBn$_2$-a,b**) in an isoselective manner. Due to the relative high isoselectivity for olefin polymerization of both *rac*-**Lig^{1}ZrBn$_2$-a,b** and *rac*-**Lig^{1}HfBn$_2$-a,b** catalysts, which bear a bulky adamantyl group, we reasoned that these sterically encumbered complexes may favor a twist-boat conformation in the cyclization step and give rise to a *cis*-isotactic PMCP microstructure. Herein we report the results for cyclopolymerization of 1,5-hexadiene and 1,6-heptadiene with *rac*-**Lig^{1}ZrBn$_2$-a,b** and *rac*-**Lig^{1}HfBn$_2$-a,b** (Scheme 1).

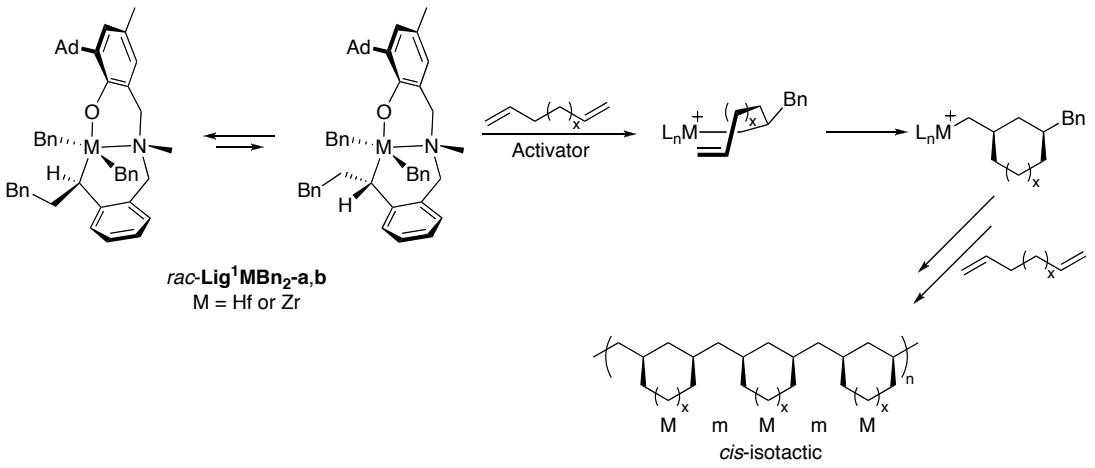

Scheme 4.1. Cyclopolymerization of 1,5-hexadiene (x = 0) and 1,6-heptadiene (x = 1) to *cis*-isotactic PMCP and PMCH by *rac*-**Lig^{1}ZrBn$_2$-a,b** and *rac*-**Lig^{1}HfBn$_2$-a,b**.

4.2 Results and Discussion

4.2.1 1,5-Hexadiene Cyclopolymerization Catalysts

Before discussion on polymerization behavior of catalysts derived from *rac*-**Lig^{1}ZrBn$_2$-a,b** and *rac*-**Lig^{1}HfBn$_2$-a,b**, a brief overview of the history of catalysts used for the cyclopolymerization of 1,5-hexadiene would be beneficial. The cyclopolymerization of 1,5-hexadiene was first reported using

heterogeneous catalysts. Marvel and Stille[7] first reported on the cyclopolymerization of 1,5-hexadiene using catalysts derived from $TiCl_4$ in combination with $^{i}Bu_3Al$ or Et_3Al. Makowski[8] later reported on this system and both groups noted incomplete cyclization and low activities. Cheng and co-workers[9] more recently reported on the use of $TiCl_3/Et_2AlCl$ for the cyclopolymerization of 1,5-hexadiene. Analysis of the polymer microstructure

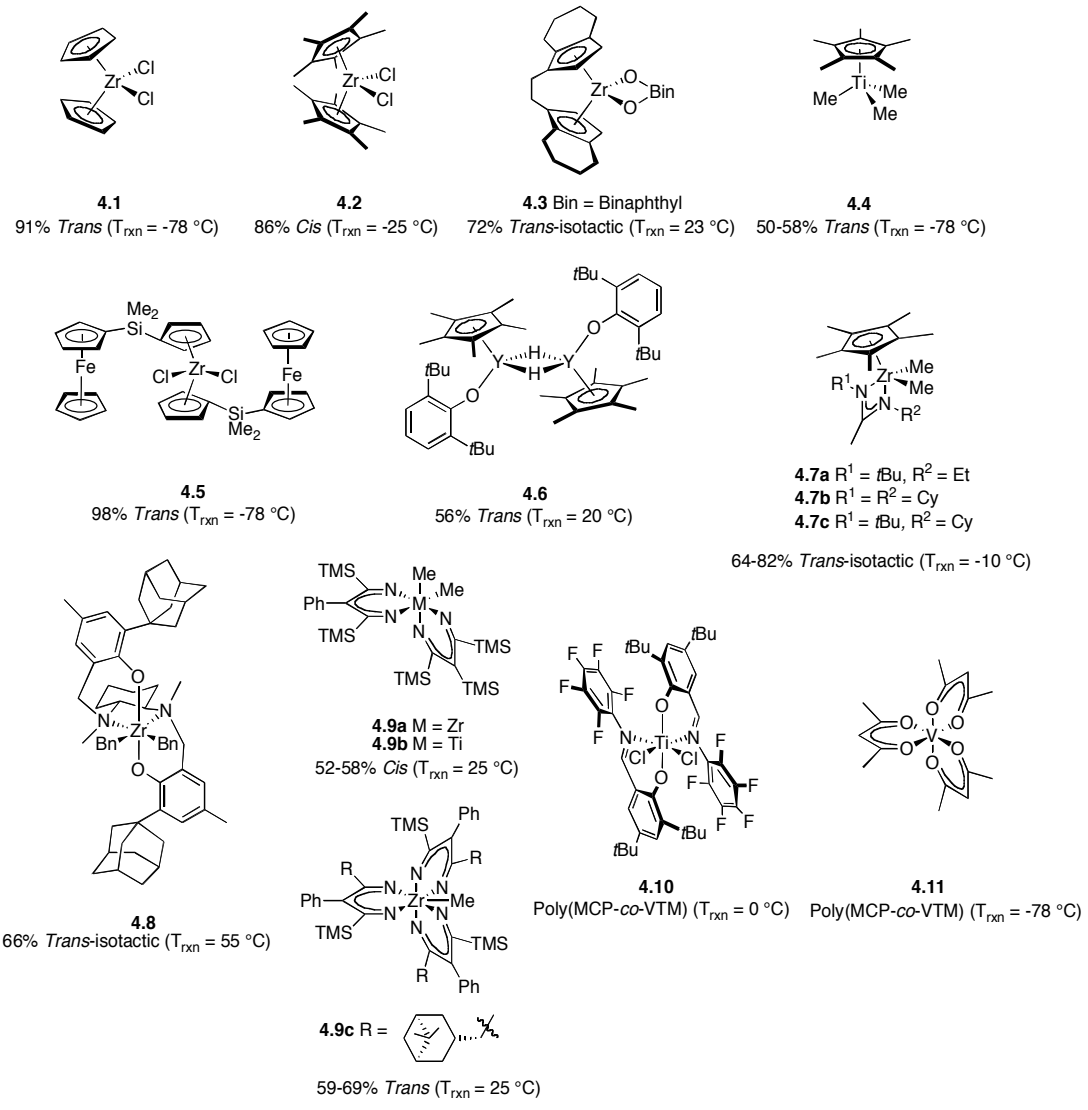

Figure 4.2. Catalysts used for the cyclopolymerization of 1,5-hexadiene.

by ^{13}C NMR spectroscopy revealed complete cyclization and a 1:1 ratio of *cis*- and *trans*-cyclopentane rings in the polymer. Further investigation into the cyclopolymerization of 1,5-hexadiene would center on the use of homogeneous catalysts.

Resconi and Waymouth reported on the first use of metallocene catalysts ($CpZrCl_2$ (**4.1**) and $Cp^*_2ZrCl_2$ (**4.2**), Figure 4.2) activated with MAO for the cyclopolymerization of 1,5-hexadiene. Polymerization of 1,5-hexadiene at room temperature or below with **4.1**/MAO affords PMCP with a high selectivity for *trans*-cyclopentane rings. In contrast, polymerization of 1,5-hexadiene with **4.2**/MAO furnishes PMCP with a predominance of *cis*-cyclopentane rings. The difference in selectivity is attributed to the preference of the growing polymer chain to adopt a pseudo-chair transition state in the cyclization step for **4.1,** which leads to a trans ring. The more sterically encumbered **4.2** forces the polymer chain to adopt a twist-boat conformation in the transition state that leads to the formation of a cis ring. Both catalysts showed no selectivity for the insertion step thus leading to atactic polymers.[10,11]

The first enantioselective cyclopolymerization of 1,5-hexadiene was reported by Coates and Waymouth.[13] Using an optically pure catalyst derived from (-)-(*R*)-ethylenebis(tetrahydroindenyl)zirconium (*R*)-binaphtholate (**4.3**, Figure 4.2) and MAO, optically active PMCP was obtained that showed a positive molar optical rotation. Cyclopolymerization of 1,5-hexadiene with the opposite enantiomer afforded PMCP with an opposite and equal molar optical rotation value. The optically active polymers contained approximately 68% trans rings. Of the four possible microstructures of maximum order (Figure 4.1), only *trans*-isotactic PMCP is chiral. Based on this, the observation of

optical activity provides proof that the polymers obtained had an isotactic microstructure. This observation was later supported by a full microstructural analysis of the PMCP revealing an enantiofacial selectivity of 91%.[6]

Other metallocene derivatives have also been studied for the cyclopolymerization of 1,5-hexadiene. Baird and co-workers reported on the use of Cp^*TiMe_3 (**4.4**, Figure 4.2) activated with $B(C_6F_5)_3$ in the presence of 1,5-hexadiene that resulted in PMCP of high molecular weight (M_w = 400 – 500 kg/mol) and broad polydispersities (M_w/M_n = 4 – 5).[21] Analysis of the polymers by $^{13}C\{^1H\}$ NMR spectroscopy revealed the PMCP generally contained *trans*:*cis* ratios of 1.4:1 to 1:1. However, the resonances were sufficiently broadened that no tacticity information could be obtained. Mukaiyama and co-workers reported on a C_2-symmetric heterotrinuclear zirconium iron metallocene complex (**4.5**, Figure 4.2).[22] Upon activation with MAO in the presence of 1,5-hexadiene, PMCP was obtained with greater than 91% *trans*-cyclopentane rings. However, no information regarding the tacticity of the polymer was reported. Schaverien has reported on the use of a dimeric yttrium hydride catalyst supported by Cp* and aryloxide ligands (**4.6**, Figure 4.2) for the cyclopolymerization of 1,5-hexadiene.[23] Reaction of **4.6** with neat 1,5-hexadiene afforded PMCP containing a slight selectivity for *trans*-cyclopentane rings (*trans*:*cis* ratio 1.0:0.8). Again, no information regarding the tacticity was disclosed.

The use of non-metallocene catalysts for the cyclopolymerization of 1,5-hexadiene has been the focus of more recent reports. In 2000 Sita and co-workers reported the use of amidinate-based zirconium catalysts (**4.7a-c**, Figure 4.2) activated with $[PhNMe_2H][B(C_6F_5)_4]$ for the cyclopolymerization of 1,5-hexadiene.[14] All the catalysts showed selectivity for the formation of *trans*-

cyclopentane rings with an increase in steric bulk (**4.7c**) resulting in an increase in *trans* content. The structure of the catalyst was found to influence the isotactic content of the PMCP with **4.7a** giving the highest degree of isoselectivity. Furthermore, these catalyst systems were found to be living[18-20] enabling the formation of block copolymers with PMCP and poly(1-hexene) blocks that undergo microphase separation

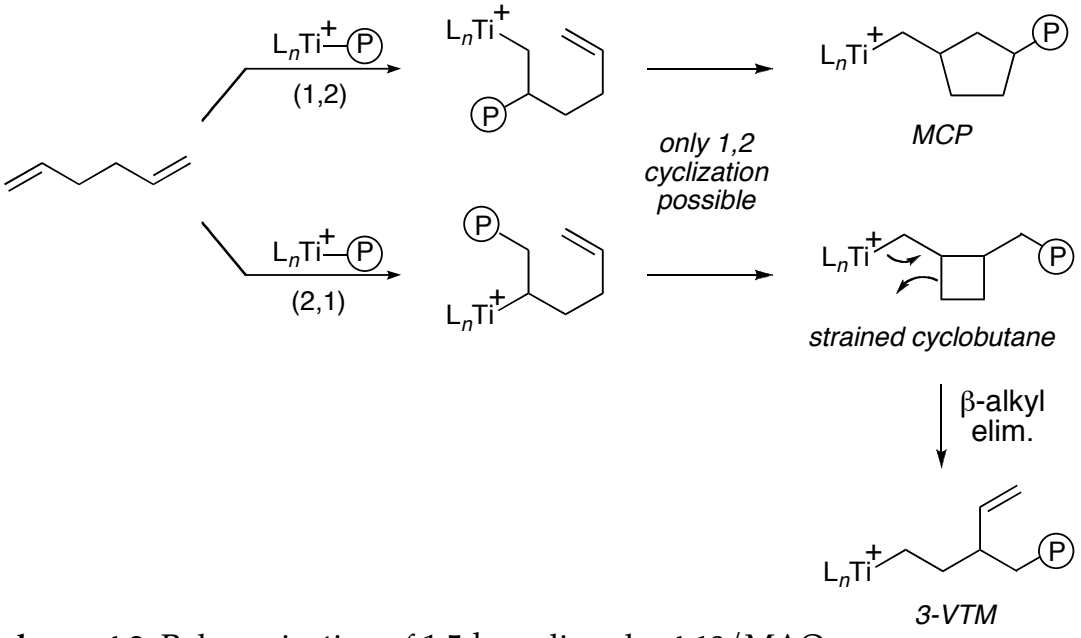

Scheme 4.2. Polymerization of 1,5-hexadiene by **4.10**/MAO.

Kol and co-workers have recently reported on the synthesis of diastereomerically pure zirconium complexes supported by chiral Salan ligands (**4.8**, Figure 4.2) for the cyclopolymerization of 1,5-hexadiene.[15,16] Activation of **4.8** with $B(C_6F_5)_3$ in the presence of 1,5-hexadiene furnished PMCP with *trans*-isotactic rings. The polymers were found to be optically active and use of the other diastereomer of **4.8** produced polymers with opposite optical rotation values.

Eisen and co-workers reported on the reactivity of group IV benzamidinate complexes (**4.9a-c**, Figure 4.2) activated with MAO towards 1,5-hexadiene. The PMCP obtained from **4.9a,b**/MAO showed a *cis*:*trans* ring ratio of 1.0:1.0 while **4.9c**/MAO displayed a higher preference for *trans* ring closure (59-69%). For **4.9c**/MAO a high degree of R*m*R tetrads were observed, which would indicate selectivity for the formation of *trans*-syndiotactic PMCP. However, the authors claim that **4.9c**/MAO catalyzes the highly *isoselective* polymerization of propylene (*mmmm* > 99.9%), which casts doubt on the assignment of the PMCP containing a high degree of syndiotacticity.

Exquisite control over the polymer microstructure in the polymerization of vinyl-monomers by Ziegler-Natta catalysts has been achieved with a wide variety of catalysts throughout the past several decades. Yet, in the polymerization of dienes such as 1,5-hexadiene, only one of the possible four microstructures of maximum order have been reported to date. Highly isotactic catalysts for the polymerization of vinyl-monomers tend to give *trans*-isotactic PMCP due to the lower energy pseudo-chair conformational transition state for ring closure.[12] Few syndioselective catalysts have been investigated in the polymerization of 1,5-hexadiene. However, of those reported for the polymerization of 1,5-hexadiene, an entirely different microstructure is obtained. For example, Hustad and Coates reported on the polymerization of 1,5-hexadiene with a fluorinated bis(phenoxyimine) titanium complex (**4.10**, Figure 4.2) activated with MAO.[24] The polymer was found to contain methylene-1,3-cyclopentane (MCP) units (63%) as well as 3-vinyl tetramethylene (VTM) units (37%). Doi and co-workers reported that syndioselective $V(acac)_3$ (**4.11**, Figure 4.2) catalysts produce nearly identical poly(1,5-hexadiene).[25] The formation of MCP units is easily explained from

1,2-insertion followed by 1,2-cyclization. However, an initial 2,1-insertion of 1,5-hexadiene followed by a 1,2-cyclization forms a strained cyclobutane species. After a β-alkyl elimination, the 3-VTM unit is generated (Scheme 4.2). Thus, microstructures of *cis*- or *trans*-syndiotactic PMCP remain elusive. To date the formation of *cis*-isotactic PMCP has remained elusive as well. This may be due to a higher energy twist-boat conformational transition state for ring closure in the cyclization step. Modeling has suggested that more sterically encumbered ligands tend to disfavor the pseudo-chair conformation with respect to the twist-boat conformation to give rise to *cis*-specific ring closure.[12] We reasoned that use of the isospecific *rac*-**Lig^{1}ZrBn$_2$-a,b** and *rac*-**Lig^{1}HfBn$_2$-a,b** catalysts bearing bulky adamantyl groups may be sterically encumbered enough to disfavor the pseudo-chair conformation and give rise to a previously unreported *cis*-isotactic PMCP microstructure.

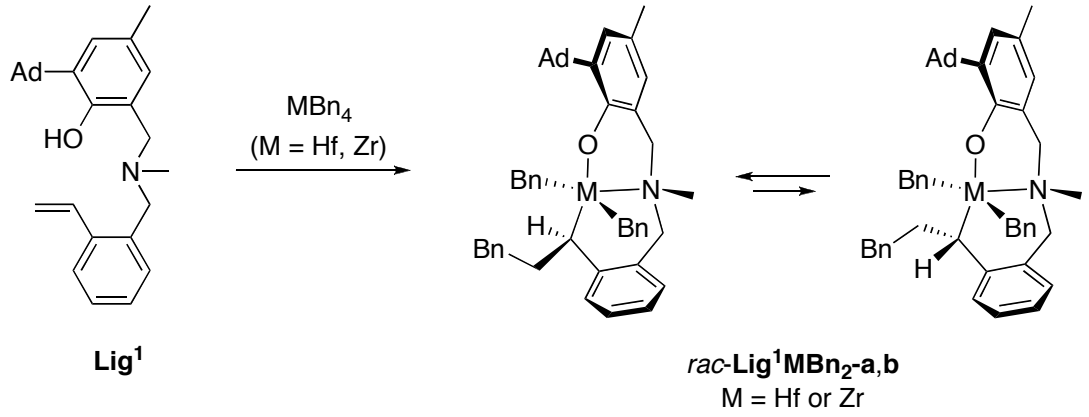

Scheme 4.3. Synthesis of *rac*-**Lig^{1}ZrBn$_2$-a,b** and *rac*-**Lig^{1}HfBn$_2$-a,b**.

4.2.2 Synthesis of *rac*-Lig^{1}ZrBn$_2$-a,b and *rac*-Lig^{1}HfBn$_2$-a,b

The tridentate phenoxyamine derivatives of zirconium and hafnium were synthesized as previously described and reported in Chapter 3.[17] The reaction of a vinyl-appended phenoxyamine ligand featuring a 1-adamantyl

substituent (**Lig^1**) with $ZrBn_4$ and $HfBn_4$ in toluene afforded *rac*-**Lig^{1}ZrBn$_2$-a,b** and *rac*-**Lig^{1}HfBn$_2$-a,b** as a mixture of diastereomers (55:45 ratio of a:b, Scheme 4.3) in quantitative yield.

4.2.3 1,5-Hexadiene Polymerization Behavior

The polymerization of 1,5-hexadiene was carried out using *rac*-**Lig^{1}ZrBn$_2$-a,b** and *rac*-**Lig^{1}HfBn$_2$-a,b** activated with boron based co-catalysts (Table 4.1). Addition of *rac*-**Lig^{1}HfBn$_2$-a,b** to a solution of $[Ph_3C][B(C_6F_5)_4]$ and 1,5-hexadiene (1:1:1685) in toluene at 25 °C led to the formation of 0.73 g of PMCP (53% conversion) in 10 minutes. The reaction was quite exothermic and the solution was noted to stop stirring within 30 – 60 seconds, which may indicate some potential crosslinking. However, the obtained polymer was soluble in 1,2,4-trichlorobenzene at 135 °C enabling analysis of the molecular weight by gel permeation chromatography. The polymer possessed a molecular weight (M_n) of 322 kg/mol and a relatively narrow molecular weight distribution (M_w/M_n = 1.48). Similar molecular weights and molecular weight distributions were obtained upon activation with $B(C_6F_5)_3$ and $[PhNMe_2H][B(C_6F_5)_4]$ at 25 °C, albeit with lower activity. The catalyst system *rac*-**Lig^{1}HfBn$_2$-a,b**/$B(C_6F_5)_3$ has been previously shown to be living for 1-hexene polymerization at 0 °C.[17] A similar molecular weight distribution of the PMCP prepared using *rac*-**Lig^{1}HfBn$_2$-a,b/**$B(C_6F_5)_3$ at 25 °C was obtained (M_w/M_n = 1.35) in comparison to that reported for 1-hexene polymerization, which prompted us to investigate the polymerization behavior of this catalyst at lower reaction temperatures. Activation of *rac*-**Lig^{1}HfBn$_2$-a,b** with $B(C_6F_5)_3$ at 0 °C in toluene resulted in the formation of 0.33 g of PMCP (16% conversion) in 10 minutes. The obtained polymer had an M_n of 211 kg/mol,

Table 4.1. 1,5-Hexadiene polymerization data for *rac*-**Lig^{1}HfBn$_2$-a,b** and *rac*-**Lig^{1}ZrBn$_2$-a,b**.[a]

Cplx	Activator	Time (min)	Temp (°C)	Yield (g)	TOF (h^{-1})[b]	M_n (kg/mol)[c]	M_n^{theo} (kg/mol)[c]	M_w/M_n[c]	*cis* %[d]	α[e]
rac-**Lig^{1}HfBn$_2$-a,b**	$[Ph_3C][B(C_6F_5)_4]$	10	25	0.73	5,300	322	73	1.48	70	0.93
rac-**Lig^{1}HfBn$_2$-a,b**	$[PhNMe_2H][B(C_6F_5)_4]$	10	25	0.61	4,500	358	61	1.46	72	0.96
rac-**Lig^{1}HfBn$_2$-a,b**	$B(C_6F_5)_3$	10	25	0.52	3,800	341	52	1.35	72	0.94
rac-**Lig^{1}HfBn$_2$-a,b**[f]	$B(C_6F_5)_3$	10	0	0.33	1,200	211	17	1.66	74	0.95
rac-**Lig^{1}ZrBn$_2$-a,b**	$[Ph_3C][B(C_6F_5)_4]$	10	25	0.69	5,100	366	69	2.21	59	nd
rac-**Lig^{1}ZrBn$_2$-a,b**	$[PhNMe_2H][B(C_6F_5)_4]$	10	25	0.44	3,200	422	44	1.66	63	0.91
rac-**Lig^{1}ZrBn$_2$-a,b**	$B(C_6F_5)_3$	10	25	0.38	2,800	410	38	1.60	63	nd
rac-**Lig^{1}ZrBn$_2$-a,b**[f]	$B(C_6F_5)_3$	10	0	0.75	2,700	280	38	1.51	66	nd

[a] General conditions: 10 μmol of the complex in toluene (1 mL) was added to a 1,5-hexadiene (2 mL) solution of activator (9 mL of toluene; [Cplx]/[B] = 1.0) at 25 °C. [b] Average turnover frequency (TOF): mol 1,5-hexadiene/(mol Cplx·h). [c] Determined using gel permeation chromatography in 1,2,4-$C_6H_3Cl_3$ at 140 °C versus polystyrene standards. [d] Determined by integration of the $C_{4,5}$ region of the $^{13}C\{^1H\}$ NMR spectrum. [e] enantioselectivity factor (α): calculated according to ref 6. [f] 20 μmol of the complex ([Cplx]/[B] = 1.0); 3 mL 1,5-hexadiene, 3 mL toluene. nd = resonances too broad for quantitative tacticity determination.

however, the molecular weight distribution (M_w/M_n = 1.66) was too broad to indicate a living polymerization catalyst.

We moved on to investigate the 1,5-hexadiene polymerization behavior of *rac*-**Lig^{1}ZrBn$_2$-a,b**. Activating *rac*-**Lig^{1}ZrBn$_2$-a,b** with [Ph_3C][$B(C_6F_5)_4$] in the presence of 1,5-hexadiene (1:1:1685) and toluene at 25 °C led to the formation of 0.69 g of PMCP (50% conversion) in 10 minutes. Again, the reaction was noted to be very exothermic and the solution stopped stirring within 30 – 60 seconds. The polymer (M_n = 366 kg/mol) exhibited a narrow molecular weight distribution (M_w/M_n = 2.21) indicative of a single-site polymerization catalyst. Activation with $B(C_6F_5)_3$ and [$PhNMe_2H$][$B(C_6F_5)_4$] at 25 °C gave rise to PMCPs with similar molecular weights and molecular weight distributions, but activity trends mirrored those of *rac*-**Lig^{1}HfBn$_2$-a,b**. None of the molecular weight distributions were sufficiently narrow to indicate any potential living behavior. However, *rac*-**Lig^{1}ZrBn$_2$-a,b**/$B(C_6F_5)_3$ has been shown to be living for propylene polymerization at 0 °C.[17] Thus, we decided to screen *rac*-**Lig^{1}ZrBn$_2$-a,b**/$B(C_6F_5)_3$ under those same activation conditions to compare the results as obtained from the polymerization of propylene. Activation of *rac*-**Lig^{1}ZrBn$_2$-a,b** with $B(C_6F_5)_3$ at 0 °C in toluene resulted in the formation of 0.75 g of PMCP (36% conversion) in 10 minutes under rather concentrated conditions (toluene:1,5-hexadiene = 1:1 V/V). The polymer displayed an M_n of 280 kg/mol but the molecular weight distribution (M_w/M_n = 1.51) was again too broadened to indicate a living polymerization catalyst. While *rac*-**Lig^{1}HfBn$_2$-a,b**/$B(C_6F_5)_3$ has been shown to be living for 1-hexene polymerization at 0 °C and living propylene polymerization is catalyzed by *rac*-**Lig^{1}ZrBn$_2$-a,b**/$B(C_6F_5)_3$ at 0 °C,[17] neither catalyst system promotes the living polymerization of 1,5-hexadiene.

4.2.4 Microstructure of Poly(Methylene-1,3-Cyclopentane)

Microstructural analysis of the PMCPs was accomplished by using $^{13}C\{^1H\}$ NMR spectroscopy. A typical $^{13}C\{^1H\}$ NMR spectrum for PMCP produced by *rac*-**Lig^{1}HfBn$_2$-a,b**/$B(C_6F_5)_3$ at 0 °C is presented in Figure 4.3. Resonances in the region of 30 – 45 ppm correspond to PMCP carbons as shown. Resonances were assigned with the same notation used by Coates and Waymouth.[6] The capital letters (M for meso, R for racemic) denote relative stereochemistry within the rings and lower case letters (*m* and *r*) refer to the relative stereochemistry between the rings (Figure 4.1). The small letter *x* denotes either *m* or *r* stereochemistry. Assignment of the *cis*:*trans* ratio can be accomplished on the basis of the relative intensities of resonances at δ 32.3 and 33.5 ppm in the $^{13}C\{^1H\}$ NMR spectra (Figure 4.4), corresponding to ring carbons C_4 and C_5 of the *cis* and *trans* repeating units respectively. For comparison, the $^{13}C\{^1H\}$ NMR spectrum of *trans*-atactic PMCP prepared with achiral Cp_2ZrCl_2/MAO is included.

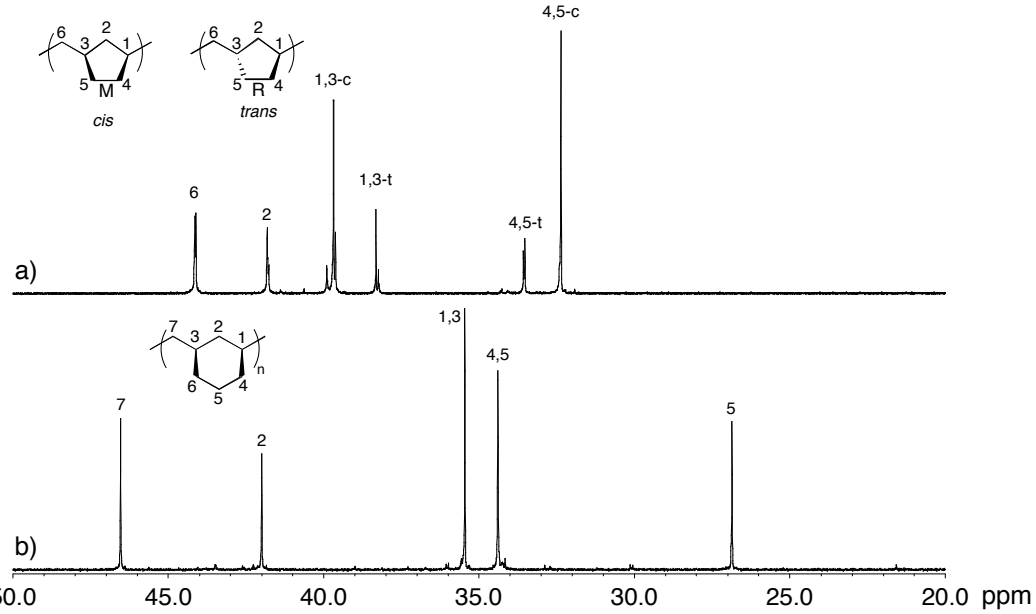

Figure 4.3. $^{13}C\{^1H\}$ NMR spectra for a) PMCP and b) PMCH prepared with *rac*-**Lig^{1}HfBn$_2$-a,b**/$B(C_6F_5)_3$ at 0 °C (150 MHz, 1,1,2,2-$C_2D_2Cl_4$, 135 °C).

Many of the PMCPs produced from *rac*-**Lig^{1}ZrBn$_2$-a,b** would only swell in 1,1,2,2-tetrachloroethane-d_2 at 135 °C enabling only the *cis*:*trans* ratio to be determined. The PMCPs produced from *rac*-**Lig^{1}ZrBn$_2$-a,b** and *rac*-**Lig^{1}HfBn$_2$-a,b** generally contained *cis*:*trans* ratios of 1.4:1.0 to 2.9:1.0, with catalysts derived from *rac*-**Lig^{1}HfBn$_2$-a,b** showing a higher propensity towards *cis*-ring closure. These ratios correspond to a moderate *cis*-preference of $\sigma = 0.59 - 0.74$ (Table 4.1). The tacticity of PMCP is influenced by the enantiofacial selectivity in the 1,5-hexadiene insertion step. Because both *rac*-**Lig^{1}ZrBn$_2$-a,b** and *rac*-**Lig^{1}HfBn$_2$-a,b** promote the isoselective polymerization of propylene (*mmmm* =

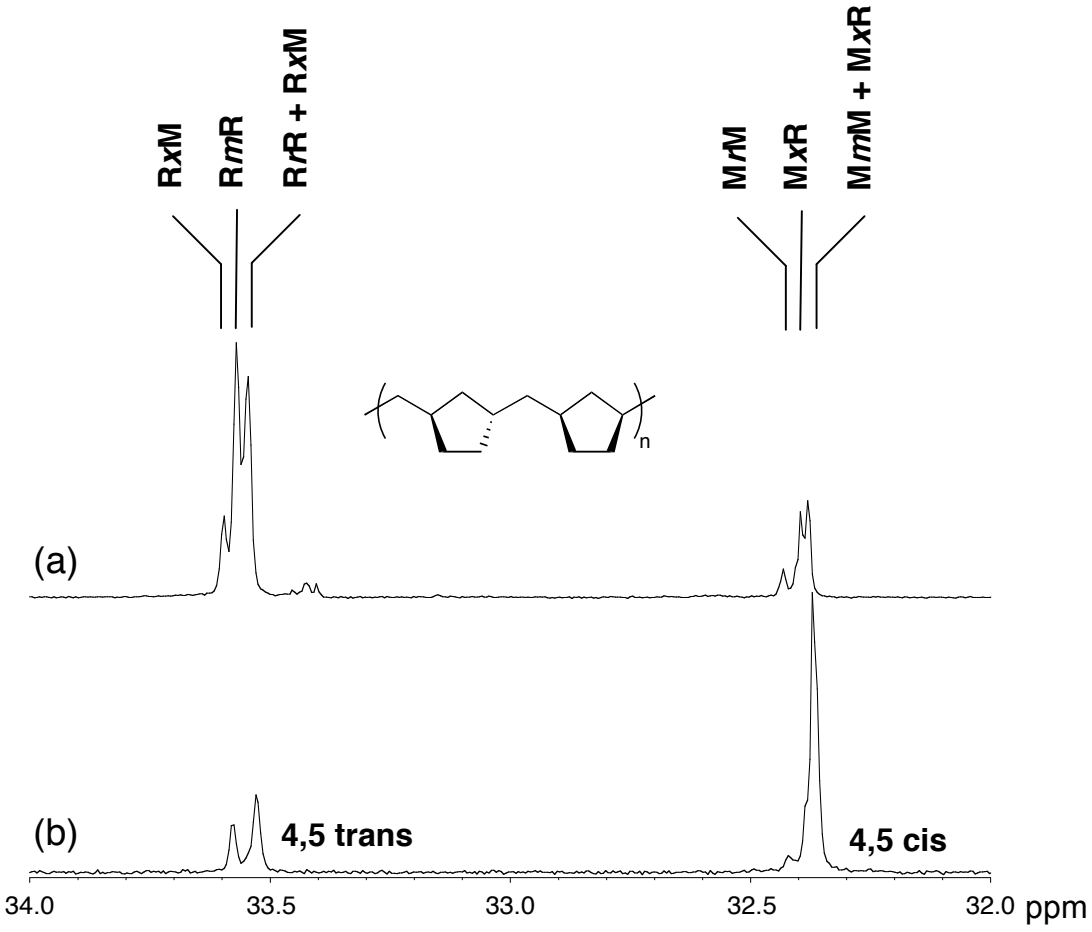

Figure 4.4. $^{13}C\{^1H\}$ NMR spectra of $C_{4,5}$ for PMCP prepared with (a) Cp_2ZrCl_2/MAO and (b) *rac*-**Lig^{1}HfBn$_2$-a,b**/$B(C_6F_5)_3$ at 25 °C (150 MHz, 1,1,2,2-$C_2D_2Cl_4$, 135 °C).

0.69 – 0.77 and 0.77 – 0.84, respectively),[25] the polymerization of 1,5-hexadiene is expected to proceed with isotactic enantioselectivity. Due to close overlap of the $^{13}C\{^1H\}$ NMR resonances for the various tetrads, the experimental tetrad distribution was evaluated by deconvolution of the spectra and variation of the enatioselectivity factor (α) until an optimum fit was obtained.[6] On $^{13}C\{^1H\}$ NMR analysis of soluble samples, it was possible to assign an enantiofacial selectivity of a = 0.91 to 0.96, with the 1,5-hexadiene polymerization catalyzed by *rac*-**Lig^{1}HfBn$_2$-a,b**/$B(C_6F_5)_3$ at 0 °C displaying the highest *cis*-preference (σ = 0.74) with an isospecificity factor of α = 0.95. This enantiofacial selectivity correlates well to polymerization of propylene under the same conditions (*mmmm* = 0.84, a = 0.97).[25]

As can be concluded from Table 4.2, the PMCP synthesized from complexes *rac*-**Lig^{1}ZrBn$_2$-a,b** and *rac*-**Lig^{1}HfBn$_2$-a,b** contain a high proportion of M*m*M resonances and represent a new, previously unreported microstructure with a predominance of *cis*-isotactic rings. $^{13}C\{^1H\}$ NMR resonances representing R*m*R and M*r*M tetrads were not observed. While PMCPs have been synthesized with a high degree of *cis*-cyclopentane rings,[10,11] a total lack of enantiofacial selectivity was observed. Furthermore, PMCPs have been reported with a high selectivity for isotactic enchainment, however, they all contain a predominance of *trans*-cyclopentane rings.[6,13-16] Thus, this work represents the first report of a relatively highly maximum ordered *cis*-isotactic microstructure for PMCP.

Table 4.2. $^{13}C\{^{1}H\}$ NMR data for carbons 4 and 5 of PMCP produced by *rac*-**Lig^{1}HfBn$_2$-a**,**b** and *rac*-**Lig^{1}ZrBn$_2$-a**,**b**.[a]

Cplx	Activator	Temp (°C)	M*m*M + M*x*R (%)	M*x*R (%)	M*r*M (%)	R*r*R + R*x*M (%)	R*m*R (%)	R*x*M (%)
rac-**Lig^{1}HfBn$_2$-a,b**	$[Ph_3C][B(C_6F_5)_4]$	25	54.7	6.7	3.4	18.2	2.7	14.3
rac-**Lig^{1}HfBn$_2$-a,b**	$[PhNMe_2H][B(C_6F_5)_4]$	25	57.8	7.5	4.0	19.0	0.8	10.9
rac-**Lig^{1}HfBn$_2$-a,b**	$B(C_6F_5)_3$	25	54.1	6.6	4.3	20.6	2.1	12.3
rac-**Lig^{1}HfBn$_2$-a,b**	$B(C_6F_5)_3$	0	59.6	7.5	5.1	17.3	0.3	10.2
rac-**Lig^{1}ZrBn$_2$-a,b**	$[Ph_3C][B(C_6F_5)_4]$	25	nd	nd	nd	nd	nd	nd
rac-**Lig^{1}ZrBn$_2$-a,b**	$[PhNMe_2H][B(C_6F_5)_4]$	25	46.2	17.8	3.1	16.3	6.6	10.0
rac-**Lig^{1}ZrBn$_2$-a,b**	$B(C_6F_5)_3$	25	nd	nd	nd	nd	nd	nd
rac-**Lig^{1}ZrBn$_2$-a,b**	$B(C_6F_5)_3$	0	nd	nd	nd	nd	nd	nd

[a] Tetrads calculated according to ref 6. nd = $^{13}C\{^{1}H\}$ NMR resonances were too broad for tacticity assignment to be quantified.

4.2.5 1,6-Heptadiene Polymerization Behavior

Owing to the relatively high *cis*-isotactic content of the PMCP produced by *rac*-**Lig^{1}HfBn$_2$-a**,**b**/B(C_6F_5)$_3$ at 0 °C (σ = 0.74, α = 0.95), we proceeded to investigate this system for the cyclopolymerization of 1,6-heptadiene. It has been shown that an increase in the diene length results in an increase in the *cis* ring content of the cyclopolymers.[26] Cyclopolymerization of 1,6-heptadiene with *rac*-**Lig^{1}HfBn$_2$-a**,**b**/B(C_6F_5)$_3$ at 0 °C in toluene resulted in the formation of 0.11g (15% conversion) of poly(methylene-1,3-cyclohexane) in 20 minutes. The PMCH had an M_n of 87 kg mol^{-1} and M_w/M_n = 1.38. Inspection of the thermal properties of the PMCH revealed a glass transition temperature (T_g) of 103.1 °C and no melting transition up to 380 °C. Analysis of the PMCH microstructure by $^{13}C\{^1H\}$ NMR spectroscopy revealed the presence of only 5 resonances that correspond to >97% *cis* ring content (Figure 4.3). This is the first synthesis of a nearly perfect *cis*-isotactic microstructure for PMCH.

4.3 Conclusions

We set out to explore the 1,5-hexadiene cyclopolymerization behavior for catalysts derived from *rac*-**Lig^{1}HfBn$_2$-a**,**b** and *rac*-**Lig^{1}ZrBn$_2$-a**,**b**. Upon activation, these complexes formed highly active cyclopolymerization catalysts for 1,5-hexadiene furnishing PMCP with a predominance of *cis*-cyclopentane rings (*cis*:*trans* ratio = 1.4:1.0 to 2.9:1.0). Catalysts derived from *rac*-**Lig^{1}HfBn$_2$-a**,**b** showed a higher propensity towards *cis*-ring closure than those derived from *rac*-**Lig^{1}ZrBn$_2$-a**,**b**. Furthermore, we demonstrated that the enantiofacial selectivity for the insertion step of 1,5-hexadiene polymerization proceeded with a relative high selectivity for isotactic enchainment. The obtained PMCPs represent the first report of a highly *cis*-isotactic

microstructure. Cyclopolymerization of 1,6-heptadiene with *rac*-**Lig^{1}HfBn$_2$-a,b**/B(C_6F_5)$_3$ produced PMCH with a nearly perfect *cis*-isotactic microstructure. We are currently studying the use of these catalysts for the cyclopolymerization of other nonconjugated dienes in the hopes of obtaining polymers possessing new microstructures.

4.4 Experimental

4.4.1 Complex Syntheses

General Methods. All manipulations of air- and/or water-sensitive compounds were carried out under dry nitrogen using a Braun UniLab drybox or standard Schlenk techniques. $^{13}C\{^1H\}$ NMR spectra of polymers were recorded using a Varian UnityInova (600 MHz) spectrometer equipped with a 10 mm broadband probe operating at 135 °C and referenced versus residual non-deuterated solvent shifts. The polymer samples were dissolved in 1,1,2,2-tetrachloroethane-d_2 in a 5 mm O.D. tube, and spectra were collected at 135 °C. For quantitative $^{13}C\{^1H\}$ analysis, the polymer samples were dissolved in 1,1,2,2-tetrachloroethane-d_2 in 10 mm O.D. tubes and the spectra were collected with inverse gated decoupling using the TYCO-25 decoupling sequence, a 30° excitation pulse width, 2.0 s acquisition time, and 10 s relaxation delay. Molecular weights (M_n and M_w) and polydispersities (M_w/M_n) were determined by high temperature gel permeation chromatography (GPC). Analyses were performed with a Waters Alliance GPCV 2000 GPC equipped with a Waters DRI detector and viscometer. The column set (four Waters HT 6E and one Waters HT2) was eluted with 1,2,4-trichlorobenzene containing 0.01 wt. % di-*tert*-butylhydroxytoluene (BHT) at 1.0 mL/min at 140 °C. Data were calibrated using monomodal polystyrene

standards (from Polymer Standards Service). Polymers were usually placed in a 140 °C oven for 24 h prior to molecular weight measurements. Polymer melting points (T_m) and glass transition temperatures (T_g) were measured by differential scanning calorimetry (DSC) using a TA Instruments Q1000 calorimeter equipped with an automated sampler. Analyses were performed in crimped aluminum pans under nitrogen and data were collected from the second heating run at a heating rate of 10 °C/min from -100 to 200 °C, and processed with TA Q series software.

Materials. Toluene was purified over columns of alumina and copper (Q5) prior to use. Tris(pentafluorophenyl)borane ($B(C_6F_5)_3$), trityl tetrakis(pentafluorophenyl)borate ($[Ph_3C][B(C_6F_5)_4]$), and *N*,*N*-dimethylanilinium tetrakis(pentafluorophenyl)borate ($[PhNMe_2H][B(C_6F_5)_4]$) were purchased from Strem and used as received. 1,5-Hexadiene was fractionally distilled and the middle fraction was dried over 4Å molecular sieves for several days and then vacuum transferred and degassed using three freeze/pump/thaw cycles. The complexes *rac*-**Lig^{1}HfBn$_2$-a**,**b** and *rac*-**Lig^{1}ZrBn$_2$-a**,**b** were prepared as previously published and described in Chapter 3.[17]

4.4.2 Polymer Syntheses

General Procedure for 1,5-Hexadiene Polymerization at 25 °C. In the glovebox, $B(C_6F_5)_3$ (5.1 mg, 10 μmol) was placed into a scintillation vial along with 9 mL of toluene and 2 mL of 1,5-hexadiene. To this solution was added *rac*-**Lig^{1}HfBn$_2$-a,b** (8.5 mg, 10 μmol) dissolved in 1 mL of toluene. The polymerization was allowed to proceed for 10 minutes after which time the vial was removed from the glovebox and the polymerization was terminated

by the addition of MeOH. The volatiles were removed *in vacuo* to furnish poly(methylene-1,3-cyclopentane) (0.52 g, 38%). The same procedure was followed for 1,5-hexadiene polymerization using $[Ph_3C][B(C_6F_5)_4]$ and $[PhNMe_2H][B(C_6F_5)_4]$ as activators and also for the analogous *rac*-**Lig^{1}ZrBn$_2$-a,b** complex.

General Procedure for 1,5-Hexadiene Polymerization at 0 °C. In the glovebox, $B(C_6F_5)_3$ (10.2 mg, 20 μmol) was placed into a Schlenk adapted tube along with 2 mL of toluene and 3 mL of 1,5-hexadiene. The reaction was sealed, removed from the glovebox and equilibrated in an ice bath at 0 °C for 15 minutes. To this solution was added *rac*-**Lig^{1}HfBn$_2$-a,b** (17.0 mg, 20 μmol) dissolved in 1 mL of toluene in a gas tight syringe under an active nitrogen flow. The polymerization was allowed to proceed for the desired period of time after which time the polymerization was terminated by the addition of MeOH (Table 4.1). The volatiles were removed *in vacuo* to furnish poly(methylene-1,3-cyclopentane). A similar procedure was followed for 1,5-hexadiene polymerization using the analogous *rac*-**Lig^{1}ZrBn$_2$-a,b** complex.

REFERENCES

(1) Coates, G. W. *Chem. Rev.* **2000**, *100*, 1223-1252.

(2) Resconi, L.; Cavallo, L.; Fait, A.; Piemontesi, F. *Chem. Rev.* **2000**, *100*, 1253-1345.

(3) Britovsek, G. J. P.; Gibson, V. C.; Wass, D. F. *Angew. Chem., Int. Ed.* **1999**, *38*, 428-447.

(4) Gibson, V. C.; Spitzmesser, S. K. *Chem. Rev.* **2003**, *103*, 283-315.

(5) Farina, M. *Top. Stereochem.* **1987**, *17*, 1-111.

(6) Coates, G. W.; Waymouth, R. M. *J. Am. Chem. Soc.* **1993**, *115*, 91-98.

(7) Marvel, C. S.; Stille, J. K. *J. Am. Chem. Soc.* **1958**, *80*, 1740-1744.

(8) Makowski, H. S.; Wilchinsky, Z. W.; Shim, B. K. C. *J. Polym. Sci., Part A* **1964**, *2*, 1549.

(9) Cheng, H. N.; Khasat, N. P. *J. Appl. Polym. Sci.* **1988**, *35*, 825-829.

(10) Resconi, L.; Waymouth, R. M. *J. Am. Chem. Soc.* **1990**, *112*, 4953-4954.

(11) Resconi, L.; Coates, G. W.; Mogstad, A.; Waymouth, R. M. *J. Macromol. Sci., Chem.* **1991**, *A28*, 1225-1234.

(12) Cavallo, L.; Guerra, G.; Corradini, P.; Resconi, L.; Waymouth, R. M. *Macromolecules* **1993**, *26*, 260-267.

(13) Coates, G. W.; Waymouth, R. M. *J. Am. Chem. Soc.* **1991**, *113*, 6270-6271.

(14) Jayaratne, K. C.; Keaton, R. J.; Henningsen, D. A.; Sita, L. R. *J. Am. Chem. Soc.* **2000**, *122*, 10490-10491.

(15) Yeori, A.; Goldberg, I.; Shuster, M.; Kol, M. *J. Am. Chem. Soc.* **2006**, *128*, 13062-13063.

(16) Yeori, A.; Goldberg, I.; Kol, M. *Macromolecules* **2007**, *40*, 8521-8523.

(17) Edson, J. B.; Keresztes, I.; Lobkovsky, E. B.; Coates, G. W. *ChemCatChem* **2009**, *1*, Accepted.

(18) Coates, G. W.; Hustad, P. D.; Reinartz, S. *Angew. Chem., Int. Ed.* **2002**, *41*, 2236-2257.

(19) Domski, G. J.; Rose, J. M.; Coates, G. W.; Bolig, A. D.; Brookhart, M. *Prog. Polym. Sci.* **2007**, *32*, 30-92.

(20) Edson, J. B.; Domski, G. J.; Rose, J. M.; Bolig, A. D.; Brookhart, M.; Coates, G. W. In *Controlled and Living Polymerizations: From Mechanisms to Applications*; Wiley-VCH, Weinheim, **2009**, 167-239.

(21) Jeremic, D.; Wang, Q. Y.; Quyoum, R.; Baird, M. C. *J. Organomet. Chem.* **1995**, *497*, 143-147.

(22) Mitani, M.; Oouchi, K.; Hayakawa, M.; Yamada, T.; Mukaiyama, T. *Chem. Lett.* **1995**, 905-906.

(23) Schaverien, C. J. *Organometallics* **1994**, *13*, 69-82.

(24) Hustad, P. D.; Coates, G. W. *J. Am. Chem. Soc.* **2002**, *124*, 11578-11579.

(25) Doi, Y.; Tokuhiro, N.; Soga, K. *Makromol. Chem., Macromol. Chem. Phys.* **1989**, *190*, 643-651.

(26) Coates, G. W.; Waymouth, R. M. *J. Mol. Cat.* **1992**, *76*, 189-194.